APPENDIX A: TEMPERATURE TECHNICAL ANALYSIS

Supporting Documentation for the Tualatin Subbasin Temperature TMDL

This page is left blank intentionally.

Appendix A

Temperature Technical Analysis
Supporting Documentation for the Tualatin Subbasin Temperature TMDL

Table of Contents

This page is left blank intentionally.

Appendix A

TEMPERATURE TECHNICAL ANALYSIS
STREAM HEATING PROCESSES – BACKGROUND INFORMATION

Riparian vegetation, stream morphology, hydrology, climate, and geographic location influence stream temperature. While climate and geographic location are outside of human control, riparian condition, channel morphology and hydrology are affected by land use activities. Specifically, the elevated summertime stream temperatures attributed to anthropogenic sources in the Tualatin River subbasin result from the following:

- ✓ Riparian vegetation disturbance reduces stream surface shading via decreased riparian vegetation height, width and/or density, thus increasing the amount of solar radiation reaching the stream surface; and
- ✓ Point source discharge.

In addition, the following conditions can effect stream temperatures in the Tualatin River subbasin:

- ✓ Reduced summertime base flows from instream withdrawals;
- ✓ Localized channel widening (increased wetted width to depth ratios) increases the stream surface area exposed to energy processes, namely solar radiation; and
- ✓ Localized near-stream disturbance zone[*] (NSDZ) widening decreases potential shading effectiveness of shade-producing near-stream vegetation.

Human activities that contribute to degraded water quality conditions in the Tualatin River subbasin include timber harvest, agriculture activities, road location, and rural/urban residential development related riparian disturbances. The relationships between percent effective shade, channel morphology, hydrology and stream temperature are illustrated in **Figure A-1**.

---

[*] The term "near-stream disturbance zone" is defined for the purposes of the Tualatin River sub-basin TMDL as a GIS estimate of bankfull width.

Figure A-1. Stream Heating Processes in the Tualatin River Subbasin
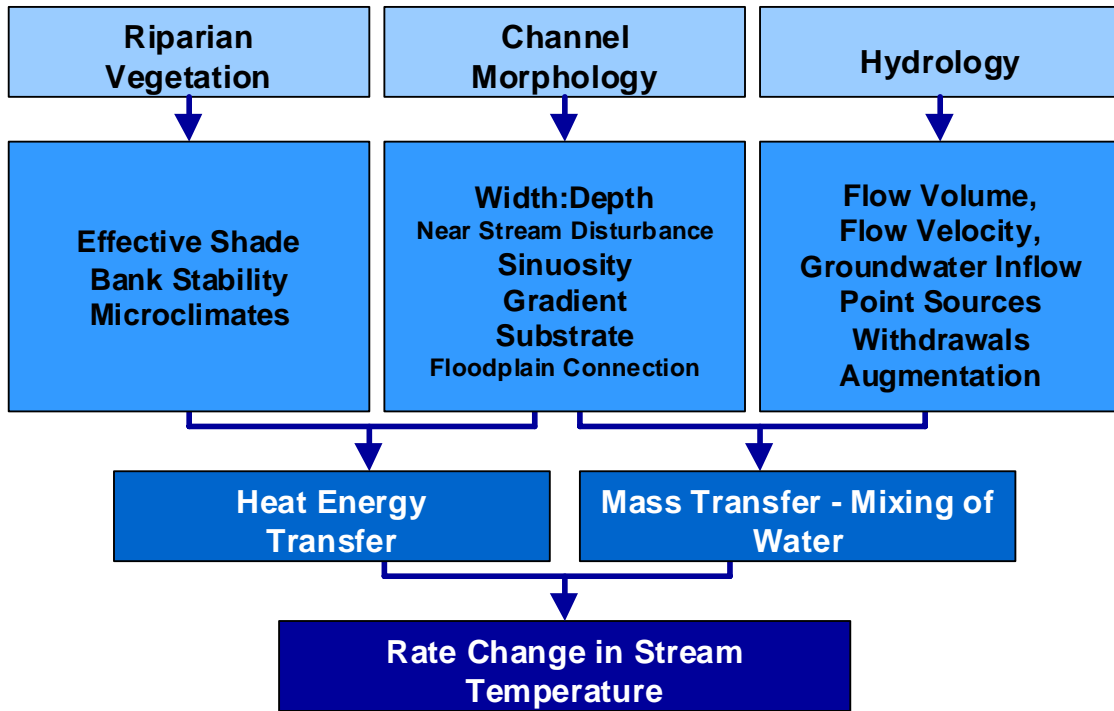
RIPARIAN VEGETATION

The Dynamics of Shade

Stream surface shade is a function of several landscape and stream geometric relationships. Some of the factors that influence shade are listed in **Table A-1**. Geometric relationships important for understanding the mechanics of shade are displayed in **Figure A-2**. In the Northern Hemisphere, the earth tilts on its axis toward the sun during summertime months allowing longer day length and higher solar altitude, both of which are functions of solar declination (i.e.,, a measure of the earth's tilt toward the sun). Geographic position (i.e.,, latitude and longitude) fixes the stream to a position on the globe, while aspect provides the stream/riparian orientation. Riparian height, width and density describe the physical barriers between the stream and sun that can attenuate and scatter incoming solar radiation (i.e.,, produce shade). The solar position has a vertical component (i.e.,, altitude) and a horizontal component (i.e.,, azimuth) that are both functions of time/date (i.e.,, solar declination) and the earth's rotation (i.e.,, hour angle). While the interaction of these shade variables may seem complex, the math that describes them is relatively straightforward geometry.

Table A-1. Factors that Influence Stream Surface Shade	
Description	*Measure*
Season/Time	Date/Time
Stream Characteristics	Aspect, Near-Stream Disturbance Zone Width
Geographic Position	Latitude, Longitude
Vegetative Characteristics	Buffer Height, Buffer Width, Buffer Density
Solar Position	Solar Altitude, Solar Azimuth

Figure A-2. Geometric Relationships that Affect Stream Surface Shade

Solar Altitude and **Solar Azimuth** are two basic measurements of the sun's position. When a stream's orientation, geographic position, riparian condition and solar position are known, shading characteristics can be simulated.

Solar Altitude measures the <u>vertical</u> component of the sun's position
Solar Azimuth measures the <u>horizontal</u> component of the sun's position
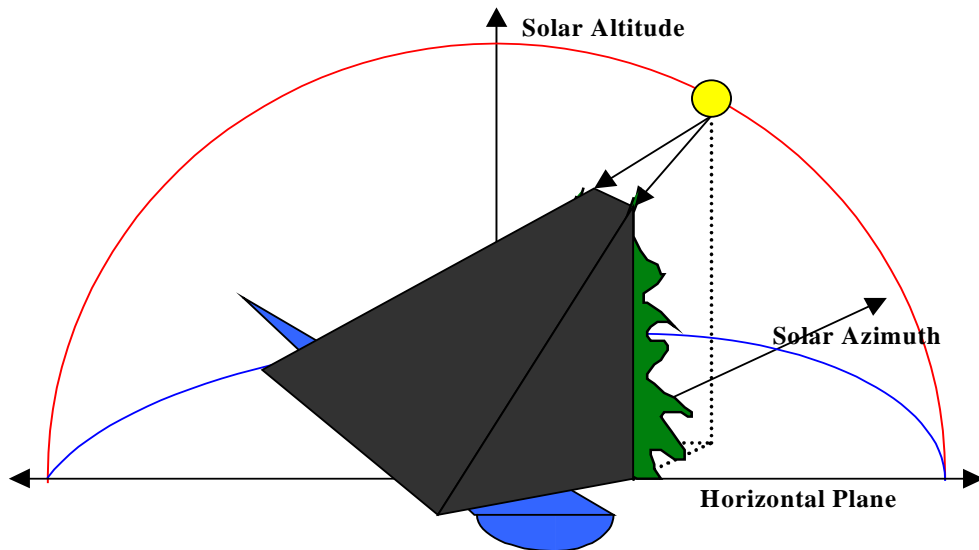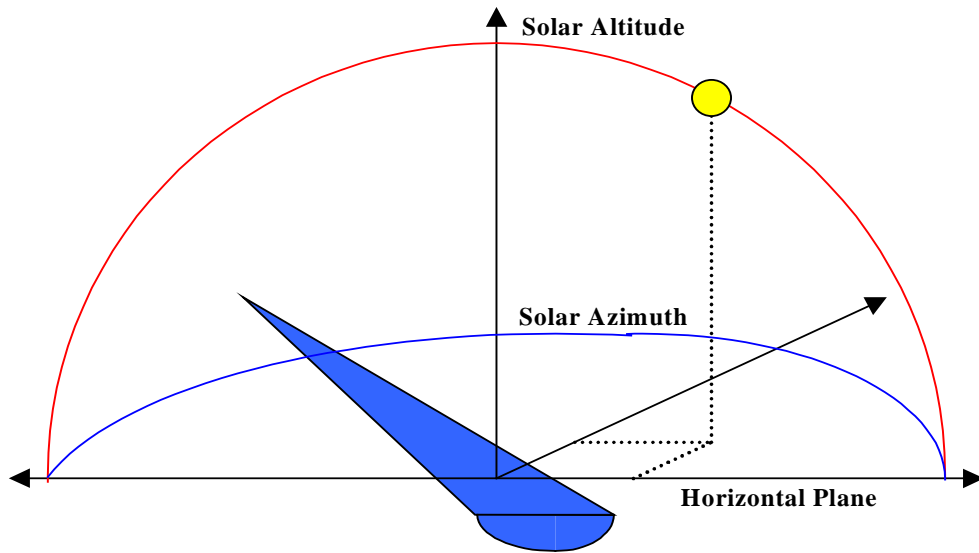
Percent effective shade is perhaps the most straightforward stream parameter to monitor/calculate and is easily translated into quantifiable water quality management and Geometric Relationships that Affect Stream Surface Shade recovery objectives. **Figure A-3** demonstrates how effective shade is monitored/calculated. Using solar tables or mathematical simulations, the *potential daily solar load* can be quantified. The *measured solar load* at the stream surface can easily be measured with a Solar Pathfinder[©] or estimated using mathematical shade simulation computer programs (Boyd, 1996 and Park, 1993).

Figure A-3. Effective Shade - Defined

Solar$_1$ – Potential Daily Solar Radiation Load
(Adjusted for Solar Altitude and Solar Azimuth)
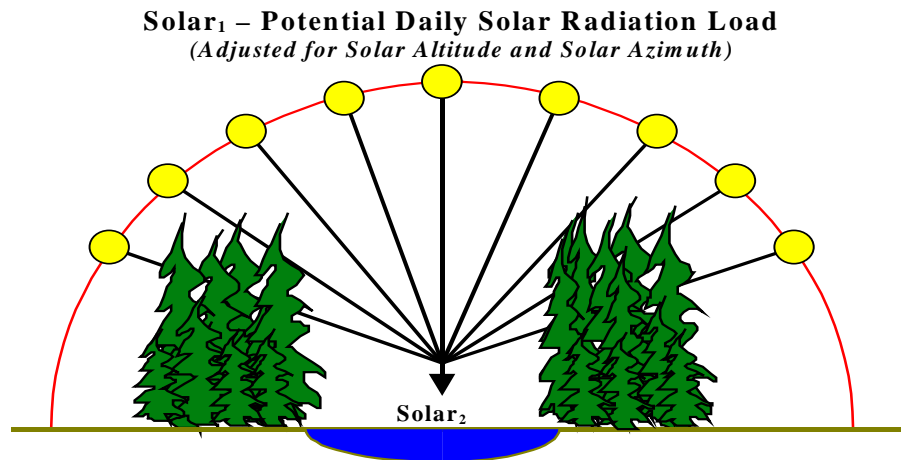
Solar$_2$

Effective Shade Defined:

$$\text{Effective} \quad \text{Shade} \quad = \frac{(\text{Solar}_1 - \text{Solar}_2)}{\text{Solar}_1}$$

Where,

Solar$_1$: Potential Daily Solar Radiation Load
Solar$_2$: Measured Daily Solar Radiation Load at Stream Surface

FLIR Thermal Imagery

FLIR thermal imagery facilitates visual observation of the effects that riparian vegetation has upon the stream and surrounding environment. FLIR thermal imagery measures the temperature of the outermost portions of the bodies/objects in the image (i.e., ground, riparian vegetation, stream). The bodies of interest are opaque to longer wavelengths and there is little, if any, penetration of the bodies.

Image A-1 displays FLIR thermal imagery collected along Fanno Creek. Contained in the thermal image are trees that are casting shadows. The ground temperatures are markedly cooler in the shadows cast by these three trees. There is greater than 20°F difference between the ground surface temperatures inside and outside of cast shadow. The ground temperature in "un-shaded" reaches is greater than the calibrated sensitivity of the FLIR instrumentation (i.e., greater than 86°F).

Image A-1. Surface Temperature in Shaded and "Un-Shaded" zones in the Fanno Creek[1]
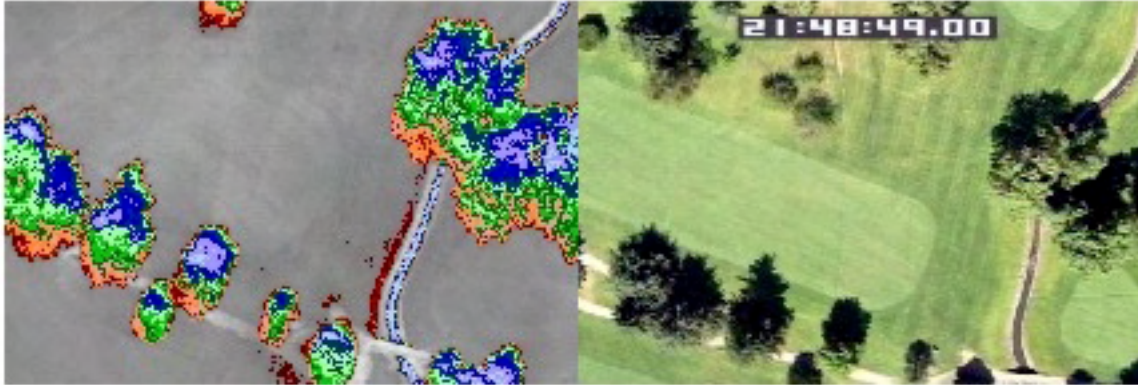
TUALATIN RIVER SUBBASIN VEGETATION CONDITIONS

Watershed Analysis have been completed for several watersheds within the Tualatin River subbasin, including Dairy-McKay (Hawksworth 1999a), Upper Tualatin-Scoggins (Hawksworth, 1999b, in print), Gales Creek (Breuner, 1998), Beaverton Creek (Brown and Caldwell, 1999), Fanno Creek (Kurahashi & Associates, 1997 and Brown & Caldwell 1998), and Upper Rock, Bronson and Willow Creeks (KCM Inc., 1996). Historical and current vegetative conditions, as well as stream channel morphology and hydrology, are discussed in detail within these reports. Together, these reports provide analysis for approximately two-thirds of the Tualatin River subbasin (**Figure A-4).**

Figure A-4. Tualatin River Subbasin areas currently covered by watershed assessments

---

[1] **FLIR Thermal Image Temperature Scale (^{o}C)**

Historical Riparian Vegetation

Historic vegetation data for the Tualatin River Subbasin is limited and often anecdotal in nature. The most rigorous analysis of historic vegetation was found in the Dairy-McKay and Upper Tualatin-Scoggins Watershed analyses (Hawksworth 1999a&b). Hawksworth noted that the anecdotal observations by early settlers in the region offer "valuable insight into the general distribution of landscape characteristics." Hawksworth then extrapolated the settler's observations based upon known geographic, geomorphic and biological principles to generally describe upland and riparian conditions within the entire watershed, noting that the result is "a reasonable description of assumed condition prior to extensive human impact."

The following excerpts from the Dairy-McKay Watershed Analysis and Upper Tualatin-Scoggins Watershed Analysis (Hawksworth 1999a&b) refer to historic vegetative conditions in the Tualatin River Subbasin:

"Prior to European settlement, the Northern Oregon Coast Range which forms the northern and western portions of the Dairy-McKay watershed was made up of larger blocks of later seral stage forests comprised of a wide range of tree sizes, large amounts of down wood, and abundant large snags… Old-growth habitat conditions extended down into moist riparian areas and shaded the streams which contained numerous pools as a result of many large logs and debris jams…"

"As was historically the case throughout the Tualatin subbasin, most stream channels throughout the Upper Tualatin-Scoggins watershed likely had abundant riparian vegetation. In all but the most poorly drained areas, the natural vegetation would have been riparian forest."

"Under undisturbed conditions, abundant stream canopy would have provided for stream temperature cooler than those currently experienced. It is unclear what the temperature regime would have been for wetland areas, nor for water contributed to streams from these wetlands. Although water stored in Wapato Lake and other wetlands would have received solar heating, most wetland contributions to streamflow would usually have proceed through subsurface pathways, where temperature would have moderated by the adjacent soil."

"In the mid 1800s, the Tualatin Plain was a forested region interspersed with wetlands and prairies. Letters by early pioneers describe the forests as consisting of fir and oak. Their descriptions of prairie size range from 1 square mile in area, to 2 to 10 in linear extent (Buan 1995). These prairies provided valuable grazing and farm land. One such prairie extended south of Banks. For the most part, the hills at the fringe of the plains were forested. The 1851 survey described one such hilly area in the East Fork Dairy Creek drainage as forested with fir and some cedar, with an understory of maple and fern (Fulton 1995)."

"The characteristics of Dairy Creek wetlands can be determined from early surveys of nearby wetlands just outside of the Dairy Creek drainage. 1852 surveys characterize Tualatin Valley bottomland as thickly forested with fir, ash, maple and Vine maple, with many swamps thickly wooded with 10- to 20- foot willow (Shively 1993). Cass and Miner (1993) state that western hemlock, western red cedar, hazel, dogwood, salal, and Oregon grape were also important components of wetland habitats. Based on these assessments, it would be reasonable to assume that many of the Dairy Creek wetlands were similarly wooded. However, settlers' accounts of lush meadow grasslands, together with the assumption that many of these grasslands were created by flooding, indicates the presence of marshy wetlands as well."

Breuner (1998) described the lower elevation valley foothills in the Gales Creek Watershed as having been "originally Oregon white oak and Douglas fir…."

These passages indicate that the Tualatin River subbasin historically contained a diverse collection of vegetation population; however, it can be concluded that large woody vegetation was historically a prominent feature within the Tualatin River subbasin.

Current Riparian Vegetation Conditions

It is important to note that many factors determine the types of vegetation that are found in a particular location, including elevation, slope, aspect, soil type and moisture, and the vegetative assemblage present in the region. In addition, landuse and natural disturbances also effect riparian vegetation community structure. A general assessment of current Tualatin River Subbasin-wide riparian conditions can be found in Hawksworth (1999a):

"Due to settlement, the pattern of vegetation has changed extensively from reference (historic) conditions. The reference landscape consisted of massive expanses of late-successional forest interspersed with occasional patches of early- and mid-successional vegetation where stand-replacement fires had occurred. In the valleys, there were also patch prairies where frequent flooding occurred. Following settlement, the scenario changed to the current highly fragmented landscape."

Basin-wide vegetative conditions can be observed using Western Oregon Digital Imaging Project (WODIP) satellite images.   WODIP is a vegetation mapping project using Thematic Mapper Satellite data collected in 1993, existing field inventory data, and advanced computer technology to produce a forest vegetation map of western Oregon. Its intended use is for watershed analysis, habitat analysis, and other environmental assessment projects. WODIP satellite data has a pixel size of 25 meters, meaning that the sensor on board the satellite records energy reflected from an area on the ground measuring 25 meters by 25 meters. The WODIP coverage for the Tualatin River subbasin (see **Figure A-5**) illustrates the fragmentation noted by Hawksworth on a basin-wide scale, with a large portion of the middle basin cultivated for agriculture, large urban areas in the lower basin, and timber harvests dotting the upper basin.

Figure A-5. WODIP Satellite coverage of the Tualatin River Subbasin
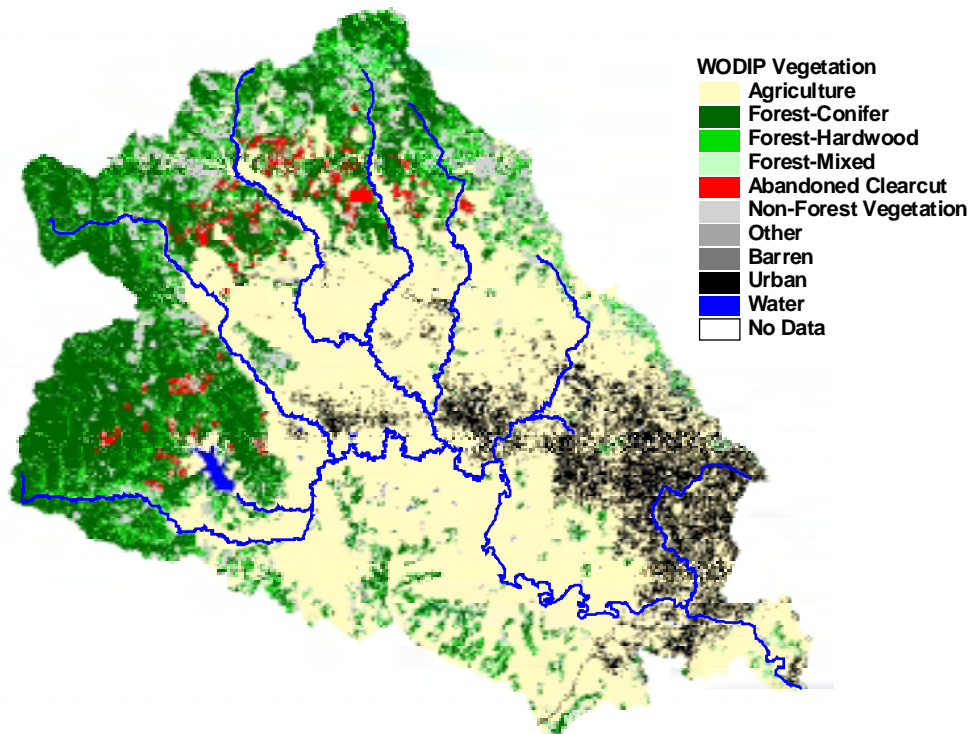
GALES CREEK WATERSHED

Breuner (1998) described the current conditions in the Gales Creek watershed as follows:

"Black cottonwood, bigleaf maple, Oregon ash, vine maple, and elderberry are the dominant plant species in the riparian zone of upper reaches of Gales Creek. The lower elevation valley foothills were originally Oregon white oak and Douglas fir but are now dominated by woodland, pastureland, vineyards, Christmas tree farms and orchards. The flat flood plain lands of the watershed are almost exclusively used for agricultural crops, including container nurseries. Some wetland species exist in a few small patches, mostly along the mainstem of Gales Creek and Little Beaver Creek. Riparian vegetation in the lower reach of Gales Creek includes a mix of native and introduced species: Douglas fir, western red cedar, willow, red alder, big-leaf maple, and black cottonwood. Understory species are red osier dogwood, Himalayan blackberry, snowberry, hawthorn, Douglas spirea, ninebark, oceanspray, cascara, horsetail, sedges, and reed canary grass."

Table A-2, summarized from Breuner (1998), lists plant species found in the Gales Creek watershed that have the potential to provide significant stream shading. This is by no means an exhaustive plant species list for the Gales Creek watershed. Rather, it provides a general accounting of the major shade-producing species present in the watershed.

Table A-2. Major shade-producing plant species found in the Gales Creek watershed	
Species Name	**Common Name**
Abies grandis	Grand fir
Acer circinatum	Vine maple
Acer macrophyllum	Big leaf maple
Alnus rubra	Red alder
Cornus stolonifera	Creek dogwood
Fraxius latifolia	Oregon ash
Pseudotsuga mensziesii	Douglas-fir
Salix spp.	Willow
Thuja plicata	Western red cedar

DAIRY-MCKAY WATERSHED

Hawksworth (1999a) (co-authored by a BLM watershed analysis committee) described the current riparian conditions in the Dairy-McKay watershed:

"Vegetation in the mountains is dominated by conifers, typically Douglas-fir (*Psuedotsuga menziesii*). Associated conifers include western red cedar (*Thujas plicata*) and western hemlock (*Tsuga heterophylla*). Hardwood stands dominated by red alder (*Alnus rubra*) are common in riparian areas. Red alder is also common on disturbed sites. Big leaf maple (*Acer macrophyllum*) is typically abundant on canyon walls, and often occurs as a minor stand component in upland Douglas-fir forests and drier portions of riparian forests. Similar species occur in the foothills, with Oregon white oak (*Quercus garryana*) becoming present in drier locations."

"Riparian zones in the lower reaches of the Dairy-McKay system are often dominated by Oregon ash (*Fraxinus latifolia*). Where riparian tree species do not provide an overstory, the streambanks are often dominated by shrubs such as the native red-osier dogwood (*Cornus stoloifera*) and the introduced invasive Himalayan blackberry (*Rubus procerus*)."

"Width of the riparian buffer in the valley plain is quite variable. Dairy Creek and McKay Creek (South of Highway 29) have wide riparian buffers over most of their extent. The West Fork of Dairy Creek, Council Creek, and McKay Creek north of Highway 26 generally have severely compromised buffers. Smaller tributaries commonly have minimal buffers and are often channelized."

UPPER TUALATIN – SCOGGINS WATERSHED

Hawksworth (1999b) (co-authored by a BLM watershed analysis committee) provides the following insights into riparian vegetation characteristics in the Upper Tualatin – Scoggins watershed:

"Although the composition of riparian forests was not quantified for this exercise, stand composition varies between the mountains and the valleys. The riparian forests in the mountains typically are composed of conifers and hardwoods in varying amounts. Red alder is typically the dominant hardwood in many mountainous riparian areas. Deciduous hardwoods such as Oregon ash typically dominate riparian forests in the valleys. Size of these hardwoods is quite variable; although large diameter trees are present and represent potential contributions of large wood to the stream systems, they represent a small proportion of the trees in the riparian zone."

"Brush-dominated riparian zones are most abundant in the Carpenter Creek and Mercer Creek sub-watersheds. These habitats are capable of providing bank stabilization and a limited amount of shade. Many native shrub species are capable of providing food and nesting habitats for wildlife. However, many of the brush-dominated riparian zones in the Upper Tualatin-Scoggins watershed are dominated by Himalayan blackberry, which provides a low habitat value and tends to out-compete native plant species. This reduces the diversity of both plant and, indirectly, wildlife species. Brush-dominated riparian zones usually border on agricultural, residential, and other intensive land uses."

"Portions of stream reaches in the Harris and Hill Creek sub-watersheds were analyzed to determine riparian characteristics. Land use in the sampled stream reaches was largely agricultural with some rural residential use. Most of the upper, forested portions of these sub-watersheds were not analyzed; therefore, these analyses should not be taken as representative of the complete subbasin. The results of the analysis are displayed in Appendix Table 6-5. These results show that riparian forest is lacking along most streams in agricultural portions of these sub-watersheds. This trait is representative of many small and medium sized streams in valley portions of the Upper Tualatin-Scoggins watershed. In most cases, this represents a diminished amount of riparian shading from reference conditions. Along some streams, however, these vegetation types may reflect a naturally herbaceous condition."

"The percent of total sub-watershed area in each forested riparian width class is given in Appendix Table 6-2. As might be expected, both the greatest proportion and width of forested riparian areas is found in the mountainous western sub-watersheds. The eastern sub-watersheds typically have narrower riparian buffers. This is largely a result of the more intensive agricultural and residential land uses in these areas, but in some cases, the lack of forest may reflect natural conditions."

With respect to grass-dominated riparian zones and riparian zones that apparently lack a vegetative buffer, Hawksworth (1999b) provides the following commentary:

"These two types are grouped together because consistent classification from aerial photography is difficult. Although an area may appear to lack a riparian buffer, field examination often shows that there is a narrow herbaceous layer. Unless they overhang very narrow streams, grass-dominated riparian zones provide very little shading value. However,

they do provide values for erosion control and nutrient filtration. In some areas, such as portions of the Upper Tualatin-Dilly, Upper Tualatin-Blackjack, and Lee Creek watersheds, wide areas of grass-dominated riparian zone indicate herbaceous wetlands. Nevertheless, sub-watersheds with large expanses of riparian zone in the GNN and BNN types are usually candidates for riparian improvement projects. The sub-watersheds in the Upper Tualatin-Scoggins watershed with the highest proportion of these riparian types include Wapato Creek, Goodin Creek, Mercer Creek, and Upper Wapato Creek. The Hill Creek and Harris Creek sub-watersheds also have substantial amounts of this riparian type, although the amounts were not quantitatively determined."

FANNO CREEK WATERSHED

Kurahashi & Associates (1997) described the remnant native plant communities present in the Fanno Creek Watershed:

"The healthy native plant communities that persist in the watershed are typically associated with relatively large habitat patches. The remnant native plant communities include:

- Wet meadow/Prairie wetlands (mixed native grasses, sedges, rushes, and herbs)
- Forested wetlands (Oregon ash, slough sedge, Pacific ninebark, snowberry)
- Riparian forest (red alder, willow, Indian plum, red-osier dogwood)
- Shrub/Scrub wetlands (willow, swamp rose, Douglas spirea, rushes, grasses, emergents)
- Headwater forests (Western red cedar, red alder, salmonberry, vine maple, sword fern)
- Upland forests (Douglas fir, big-leaf maple, vine maple, sword fern, Oregon grape)
- Oak savanna / Oak woodlands (Oregon white oak, native grasses and flowers)"

"In the remaining forested areas of the Fanno Creek watershed, the most common native conifer species are Western red cedar, Western hemlock, and Douglas fir. Red alder, Big leaf maple, and Oregon ash are the most common deciduous trees. Native shrubs include vine maple, Indian plum, and salmonberry. Sword fern and lady fern are common along each of the streams. In addition to these native species, numerous ornamental trees, shrubs, and ground covers have been introduced to the watershed. Some of these, such as Himalayan blackberry and English ivy, are invasive and have crowed out native plants in many areas."

BEAVERTON CREEK WATERSHED

Brown & Caldwell (1999) characterize current conditions in the upper Beaverton Creek watershed as "second-growth conifer and mixed headwater forest, with understories dominated by native shrubs and herbaceous plants. Slopes are relatively steep, riparian zones fairly narrow and there are few wetlands." Riparian conditions deteriorate downstream, where "impacts include fragmentation of the riparian corridor, encroachment of development into riparian and wetland buffers, and loss of structural and species diversity…." Structural and species diversity is low and shade cover is poor in the lower section of the Beaverton Creek watershed.

UPPER ROCK, BRONSON AND WILLOW CREEK WATERSHEDS

A stream assessment conducted in 1994 by Adolfson Associates Inc. identified several riparian areas within the Upper Rock, Bronson and Willow basins that have not been directly disturbed by development. The following is a summary of the findings (KCM 1996):

Upper Rock Creek

- From the confluence of Upper Rock Creek with Beaverton Creek to the southwest end of the Orenco Woods Golf Course, the area along the creek is predominantly a natural forest area of willow, alder, ash and cottonwood trees with shrubs including red osier dogwood and blackberry. Within the creek floodplain of this area, reed canary grass and slough sedge make up the natural floodplain vegetation.

- There are natural dense forest areas along the creek downstream and upstream of NW 216th avenue.
- Along the creek between NW 216th Avenue and NW Cornell road is a relatively wide corridor of natural upland forest and floodplain vegetation of reed canary grass.
- Along the creek between NW Evergreen Parkway and Highway 26 is a natural forest area, though it is possible that the creek channel in this area has been straightened. Trees in this area include alder and willow. A small tributary from the west enters the creek in this area surrounded by an upland forest of Douglas fir.
- There is a natural forest corridor of alder and a Douglas fir fringe along the creek downstream and upstream of old NW Cornell Road.
- At the headwaters of the Bethany Lake Tributary in the vicinity of NW Kaiser Road, the area along the creek is characterized by intermittent forest tracts and floodplain vegetated with reed canary grass. The stream banks are characterized by soft rush and reed canary grass with alder and willow above. The tributary headwater region outside the UGB also has areas of natural vegetation and forests.

Bronson Creek

- Between Walker Road and the Burlington Northern Railroad, the creek flows thorough a relatively forested area. Between Oregon Graduate Institute and the Primate Center is a natural alder swamp with surrounding dense upland forest.
- In the vicinity of Charlais Park between West Union Road and Highway 26, the creek flows through a wide floodplain of shrubs and forest. Vegetation in this area includes willow, alder, and Douglas fir, with blackberry, reed canary grass, and spirea.
- Upstream of NW Kaiser Road, the creek travels through an alder swamp to a wide floodplain of reed canary grass. Additional vegetation in the floodplain includes watercress, cattails, and Douglas spirea. As the creek approaches NW Kaiser Road, it enters a forest corridor.
- The headwaters region is made up of forested land with large alder and cedar trees. Downstream of NW Laidlaw Road before the creek reach Balkes Pond, there is a large area of Douglas fir and Pine forest providing wildlife habitat. In this vicinity near the creek there are wetland areas with rushes, sedges, and reed canary grass, as well as signs of recent beaver activity.

Willow Creek

- North of SW Baseline Road, the creek flows from the south end of the wildlife area near Heritage into an area with Douglas Fir and cedar as well as Pacific yew trees on the east side of the creek. The creek then travels through a less forested area with a broader floodplain.
- The confluence of the creek and its south fork is located south of NW Walker Road. This area is characterized by a pond and surrounding floodplain vegetated with reed canary grass with a cattail fringe.
- East of NW 173rd Avenue, upstream of Winthrop Park, the creek flows through a high quality, forested stream habitat. Vegetation in this forested area includes Douglas fir and upland forest community.
- Along the creek and within the Willow Creek Nature Park located south of NW Cornell Road, there is a broad, swampy floodplain. This area is characterized by a variety of vegetation including watercress, soft rush, reed canary grass, climbing nightshade, wild rose, evergreen blackberry, red osier dogwood, cottonwood, and alder.

Brown and Caldwell (1999) noted aerial photographs taken in 1936 showing the Willow Creek area to be "90 percent agriculture with less than 50 percent riparian vegetation."

Riparian Vegetation Height

Average mature riparian vegetation height for species commonly found within the Tualatin River Subbasin are presented in **Tables A-3** and **A-5**. Vegetation heights listed in

Tables A-3 and **A-5** are averages and represent trees from a wide geographic area and varied soil, slope and moisture regimes. Extensive agricultural development within the Tualatin River Subbasin indicates that a large percentage of the basin would be considered high quality habitat, especially within riparian zones. By all indications, average tree heights listed **Tables A-3** and **A-4** should represent a conservative estimate of average mature tree heights for species within the basin. A field survey conducted by DEQ field personnel in 1999 (**Table A-5**) provides data on current riparian vegetation heights at various locations throughout the Tualatin River Subbasin.

Figures A-6 through A-14 illustrate the distribution of vegetation in the riparian zone for the mainstem Tualatin River and tributaries, for both the right and the left stream banks. Sampled vegetation buffer width and vegetation height are presented in these figures. Vegetation information presented in these figures was sampled from a Graphical Information System (GIS) vegetation data layer. Note that the river miles (RM) presented in these figures were derived from a 1:5000 stream coverage used for DEQ modeling purposes and may differ slightly from other sources (such as OWRD or USGS river miles).

Table A-3. Riparian vegetation heights compiled by Pacific Habitat Services, 1998.		
Species Name	**Common Name**	**Average Mature Height (feet)**
Acer macrophyllum	Big leaf maple	90
Abies grandis	Grand Fir	120
Alnus rhombifolia	White alder	75
Alnus rubra	Red alder	100
Crataegus douglasii	Douglas hawthorn	20
Fraxinus latifolia	Oregon ash	75
Juniperus occidentalis	Western juniper	20
Picea sitchensis	Sitka spruce	120
Populus tremuloides	Quaking aspen	60
Populus trichocarpa	Cottonwood	120
Prunus emarginata	Bitter cherry	25
Psuedotsuga menziesii	Douglas fir	120-200+
Rhamnus purshiana	Cascara	35
Quercus garryana	Oregon white oak	60
Salix amygaloides	Peach leaf willow	35
Salix geyeriana	Geyer willow	20
Salix hookeriana	Hooker's willow	20
Salix lasiandra	Pacific willow	35
Salix lasiolepis	Arroyo willow	30
Salix scouleriana	Scouler's willow	30
Salix sessilifolia	Soft-leaved willow	20
Salix sitchensis	Sitka willow	20
Thuja plicata	Western red cedar	120
Tsuga heterophylla	Western hemlock	120

Table A-4. Riparian vegetation heights taken from Whitney, 1985.		
Species Name	**Common Name**	**Average Mature Height (feet)**
Cornus stolonifera	Red-osier (Creek) Dogwood	10-15
Acer circinatum	Vine Maple	25
Rubus spectabilis	Salmonberry	3-12
Spirea douglasii	Douglas Spirea	3-8
Physocarpus capitatus	Pacific Ninebark	8-15
Oemleria cerasiformis	Indian Plum	15-20
Sambucus spp.	Elderberry	20-25

Name	Date	Left Bank Buffer Height (ft)	Right Bank Buffer Height (ft)	Tree Comments
				Table A-5. DEQ Field Observations, Summer 1999.
Rock Cr. @ Baseline	7/29/99	30-50	30-50	alder- Red Osier dogwoods, huckleberry, Oregon ash
Rock Cr. @ Hwy 8	7/29/99	varies to 50	varies to 50	Red - Osier dogwood, Oregon ash
E. Beaver Cr @ Mouth	7/22/99	50	70	alder/Bigleaf maple
Beaverton Cr @ 185th	7/29/99	40-50	40-50	Oregon ash, alder
Gales Cr @ B St. Hwy 47	6/16/99	80	80	not specified
Gales Cr @ Stringtown Road	6/16/99	70	70	1-2 rows of trees next to agricultural land
Gales Cr @ Roderick Rd	6/16/99	100	100	cottonwood, Bigleaf maple & ash
Little Beaver Cr. @ Mouth	6/16/99	50	15	alder and Shrub
Gales cr @ Clapshaw u/s L. Beaver	6/16/99	70	25	not specified
Gales Cr @ Hwy 6 d/s Dorman	6/16/99	75	75	cottonwood, Bigleaf maple, ash, ash understory, and alder shrub
Gales Cr U/S Bateman Cr.	6/16/99	70-100	70	alder
Beaver Cr. @ Mouth	6/23/99	100	90	alder and Bigleaf maple
Gales Cr. @ Hwy 6 u/s Timber Jct.	6/16/99	120	130	conifers, Bigleaf maple, Vine maple, alder
Gales Cr. @ Hwy 6 u/s SF Gales	6/16/99	80	63	alder, maple
Gales Cr U/S Hwy 6	6/16/99	80	100	alder
Gales Cr @ Gales Cr. Campground	6/16/99	80	80	alder
Fanno Cr @ Durham Park	7/26/99	70	70	alder, ash, fir
Fanno Cr @ Durham Rd.	7/26/99	4	4	alder
Fanno Cr @ Bonita	7/26/99	2	2	not specified
Fanno U/S ash	7/26/99	20	20	shrubs
Fanno Cr @ Fanno Farmhouse	7/26/99	60	60	ash, alder
Fanno Cr @ Scholls Ferry Rd	7/26/99	103	60	alder, cedar, ash, cottonwood
Fanno Cr @ Nicoli (u/s of golf course)	7/26/99	60	65	ash, alder
Sylvan Cr @ Mouth	7/26/99	54	54	oak
Fanno Cr @ 56th	7/26/99	50	50	oak, alder, fir
Fanno @ SW 30th	7/26/99	53	43	willow, alder, ash,
Chicken Cr @ LaBeau	6/25/99	60	4	cedar, alder
Chicken Cr @ Kruger Rd	6/25/99	100	100	cedar, alder

Name	Date	Left Bank Buffer Height (ft)	Right Bank Buffer Height (ft)	Tree Comments
Chicken Creek @ Edy Rd	6/25/99	20	90	cedar, alder, maple
Tualatin R. @ Hwy 47	6/15/99	38	38	deciduous
Tualatin R. @ Gaston Gage	6/15/99	35	50	deciduous
W. Fork Dairy Cr @ Green Mt. Rd	7/23/99	20	25	not specified
W. Fork Dairy Cr @ Pihl Rd in Manning	7/23/99	60	60	alder, maple
W. Fork Dairy Cr @ Fisher Rd.	7/23/99	70	70	alder, maple, ash
W. Fork Dairy Cr @ Burgholzer	6/23/99	50	50	alder & Big Leaf maple
W. Fork Dairy Cr. @ Hwy 47, RM 18.2	6/23/99	130	70	conifers, alder
E. Fork Dairy Cr. @ End of Bridge 1366	6/23/99	75	75	not specified
E. Fork Dairy Cr. @ Fern Flat Rd	6/23/99	50	60	alder, Vine maple, conifers
Dairy Cr. @ Hwy 8	7/29/99	50	50	alder, willow, ash
Dairy Cr. @ Cornelius-Schefflin Rd	7/30/99	50	50	predominantly ash, some oak
WF Dairy Cr @ Roy Rd	7/30/99	40-50	40-50	ash, dogwood, oak, alder, maple
EF Dairy Cr @ Harrington Rd	7/30/99	50	50	Red-Osier dogwood, maple, Mountain ash, Oregon ash
EF Dairy Cr @ Mountaindale Rd	7/30/99	50	50	Red-Osier dogwood, ash, maple
EF Dairy Cr @ Ueble Rd	7/30/99	30-50	30-50	Red - Osier dogwood, Oregon ash, maple, alder
EF Dairy Cr @ Meacham Rd	7/30/99	30-45	30-45	maple, Red alder
WF Dairy Cr @ Marsh Rd	7/30/99	50-60	50-60	alder, ash, dogwood, sparse
WF Dairy Cr @ Evers Rd	7/30/99	50	50	Oregon ash, willow
WF Dairy Cr @ Greenville Rd.	7/30/99	50-60	50-60	ash, alder, Red-osier dogwoods
WF Dairy Cr @ Hwy 47	7/30/99	30-50	30-50	alder, ash, maple
WF Dairy Cr @ Hwy 6	7/30/99	50-60	50-60	alder, ash, dogwood, maple, willow
EF Dairy Cr @ Dairy Cr Rd	7/30/99	60-100	60-100	maple, cedar, alder, ash,
WF Dairy Cr (Williams Cr @ Hwy 47)	6/23/99	50	40	alder, Big leaf maple, very few conifer
Rock Cr @ NW Amberwood Rd.	6/30/99	100	100	not specified
Bronson Cr @ Mouth	6/30/99	25	25	not specified
Rock Cr @ 220th	6/28/99	40	40	cedar, alder
McKay Cr @ Glencoe Rd	6/30/99	80	80	not specified
McKay Cr @ Scotch Church Rd	6/30/99	90	90	cedar
McKay Cr @ West Union Rd	6/30/99	5	5	grasses

Table A-5 (continued). DEQ Field Observations, Summer 1999.

Table A-5 (continued). DEQ Field Observations, Summer 1999				
Name	**Date**	**Left Bank Buffer Height (ft)**	**Right Bank Buffer Height (ft)**	**Tree Comments**
Jackson Cr @ Jackson School Rd	6/29/99	0	0	none
Jackson Cr @ Jackson Quarry	6/29/99	40	40	alder
Jackson Cr @ Jackson Quarry	6/29/99	40	40	alder
McKay Cr @ Shadybrook	6/30/99	40	60	not specified
McKay CR @ Collins Rd, RM 16	6/30/99	60	80	alder
Brunswick Cr @ Mouth	6/30/99	100	100	Douglas fir, maple
McKay Cr @ Collins Rd, RM 17	6/30/99	70	100	fir, alder, maple
EF McKay Cr @ Dixie Mt. Rd	6/29/99	70	70	not specified
Waibel Cr @ Jackson School Rd	6/30/99	0	0	not specified
Tualatin River @ Sout Road	6/15/99	65	55	cedar

FIGURE A-6.   Gales Creek Vegetation Height Sampled from WODIP (BLM, 1999) and Enhanced with 1997 USGS Digital Orthophoto Quads
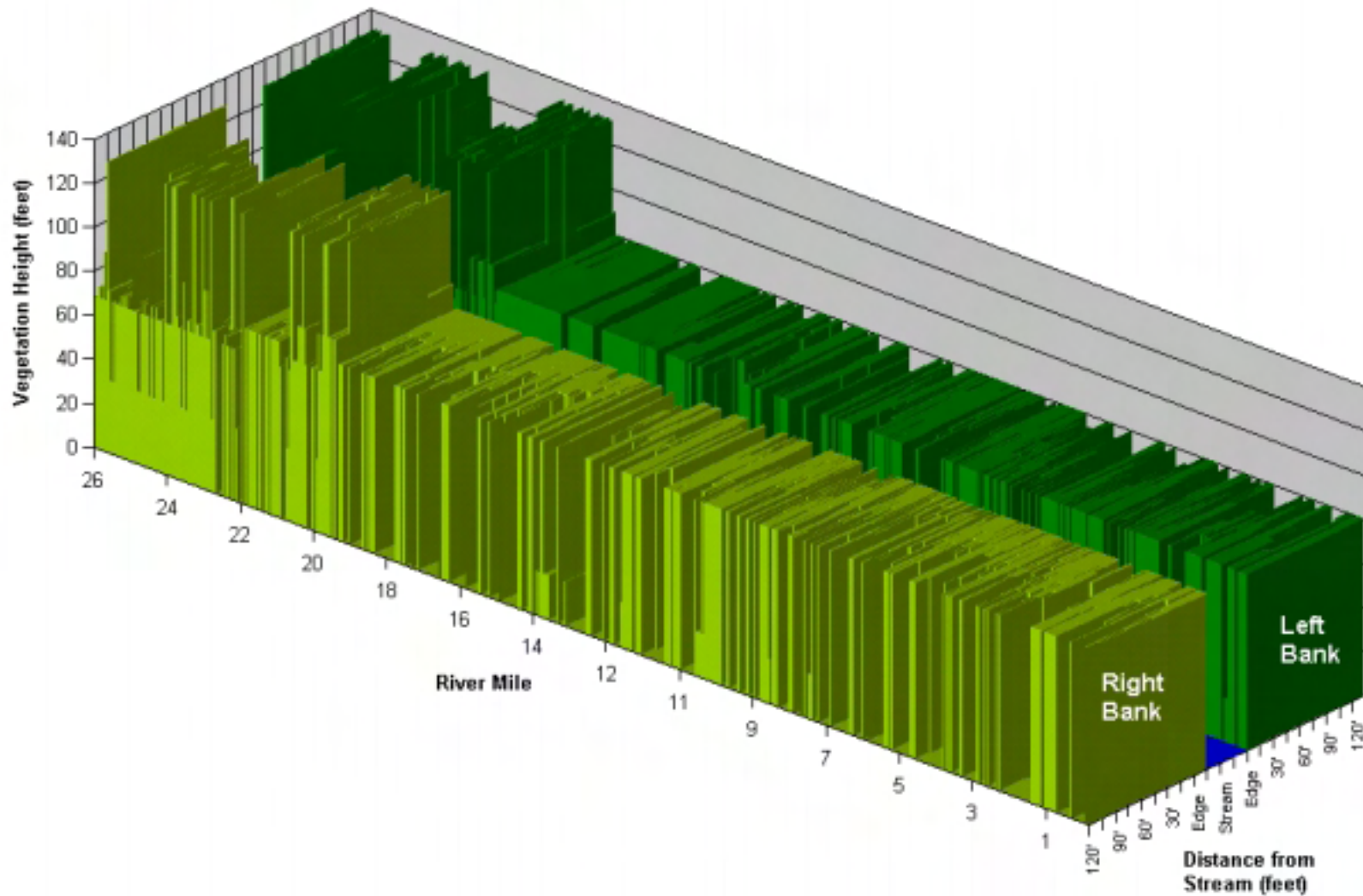
FIGURE A-7. (a) Tualatin River Vegetation Height Sampled from WODIP (BLM, 1999) and Enhanced with 1997 USGS DOQs
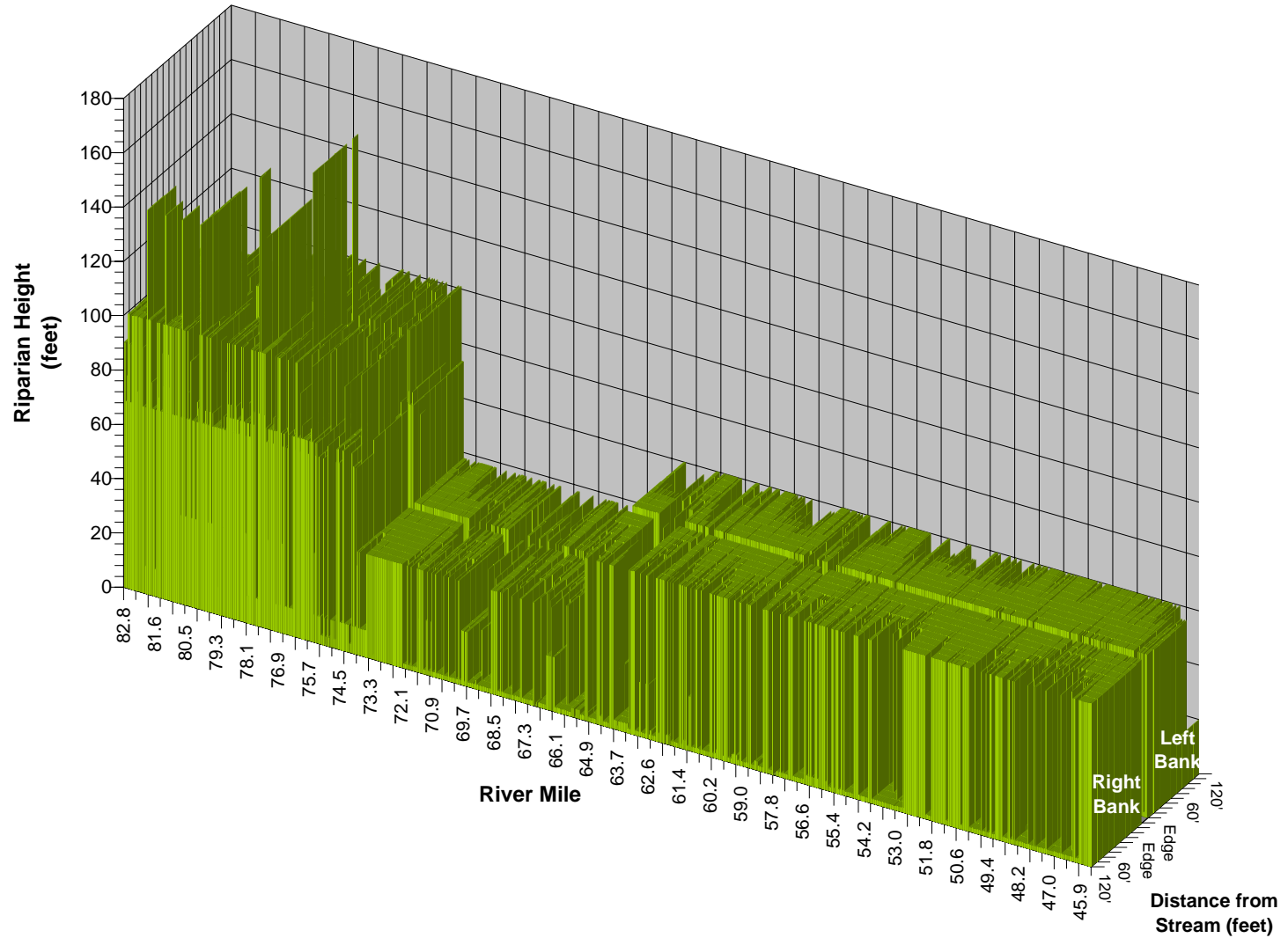
Figure 7. (b) Tualatin River Vegetation Height Sampled from WODIP (BLM, 1999) and Enhanced with 1997 USGS Digital Orthophoto Quads
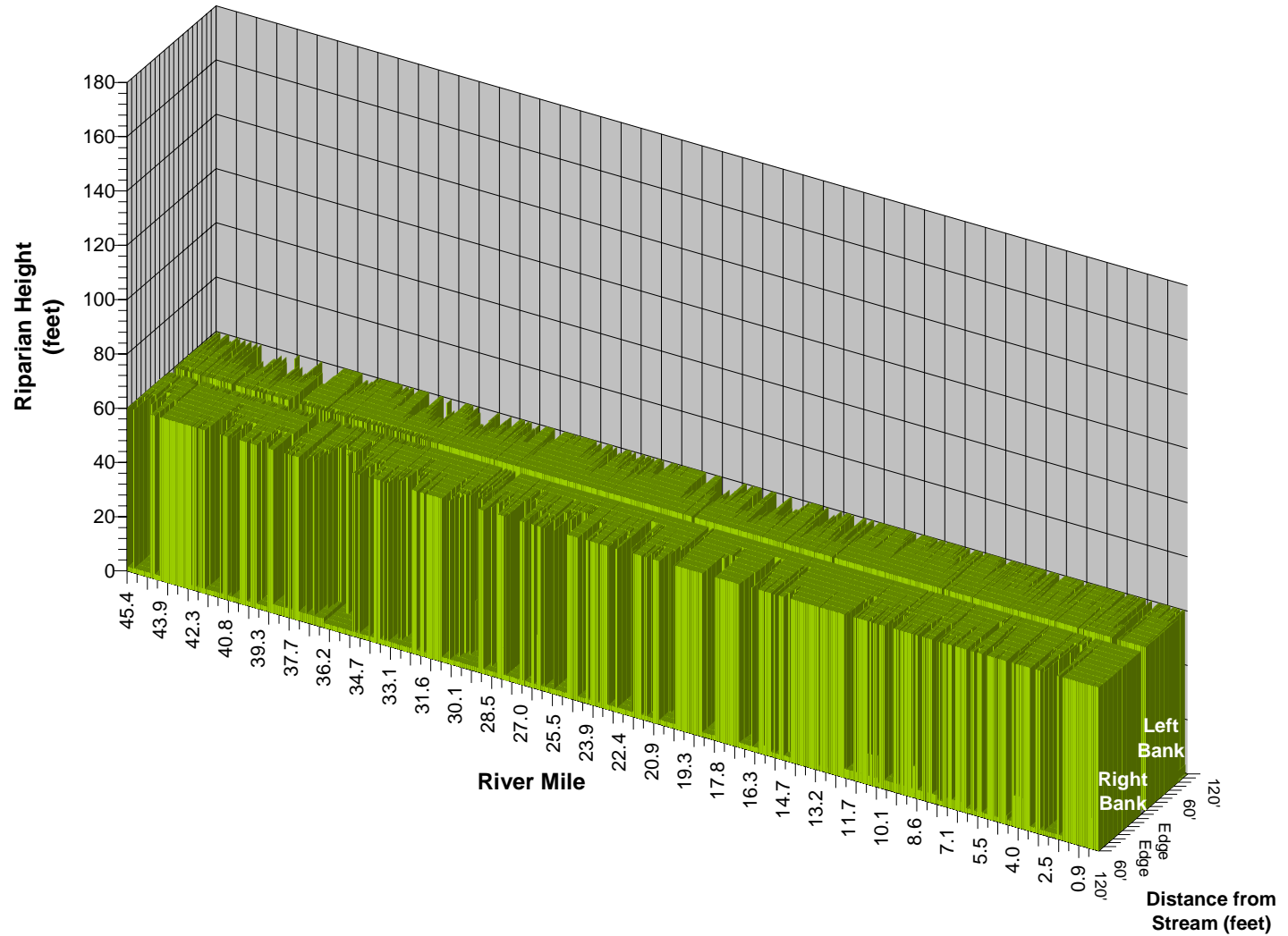
FIGURE A-8. Fanno Creek Vegetation Height Sampled from WODIP (BLM, 1999) and Enhanced with 1997 USGS Digital Orthophoto Quads
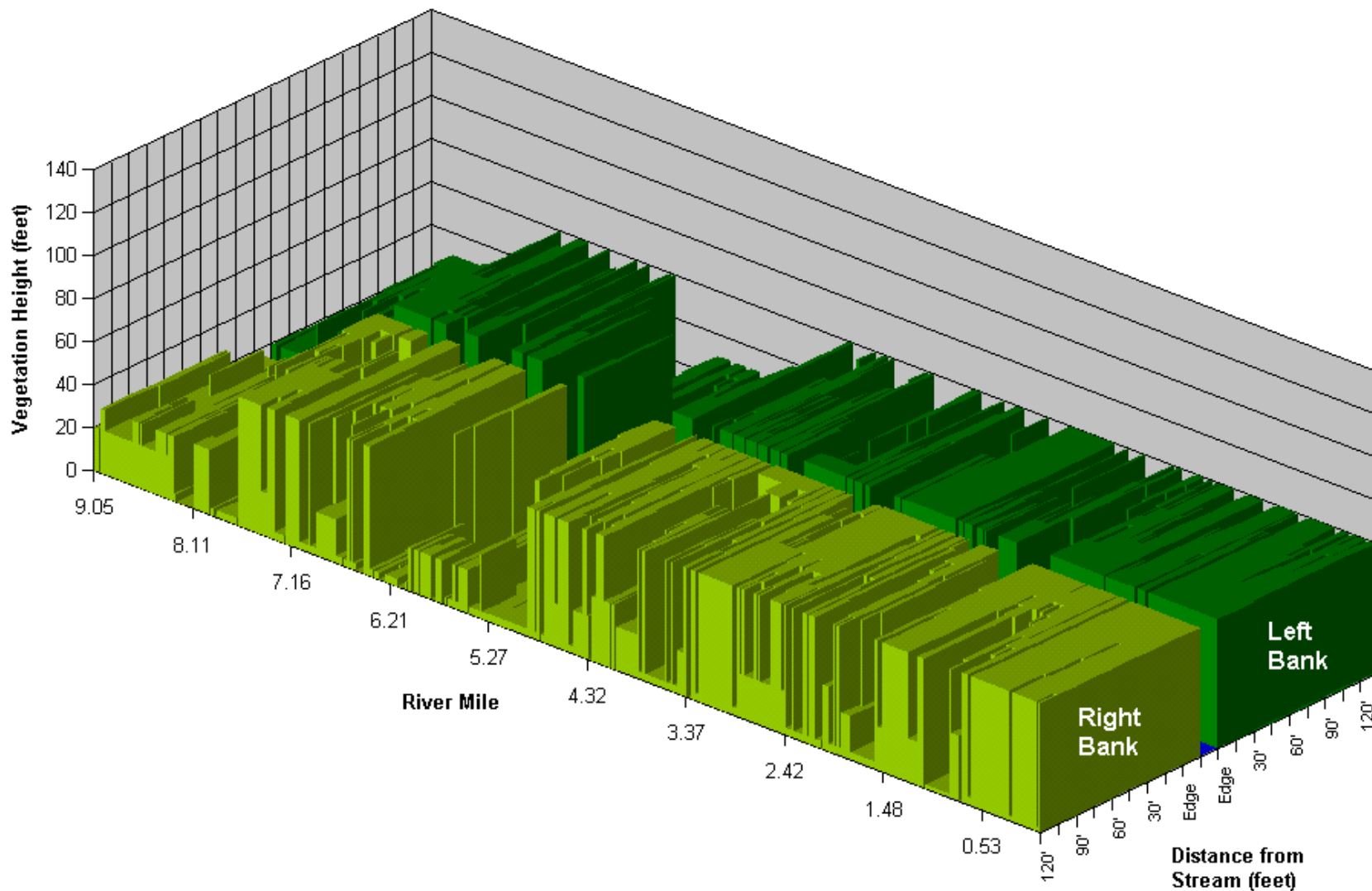
Figure A-9. Rock Creek Vegetation Height Sampled from WODIP (BLM, 1999) and Enhanced with 1997 USGS Digital Orthophoto Quads
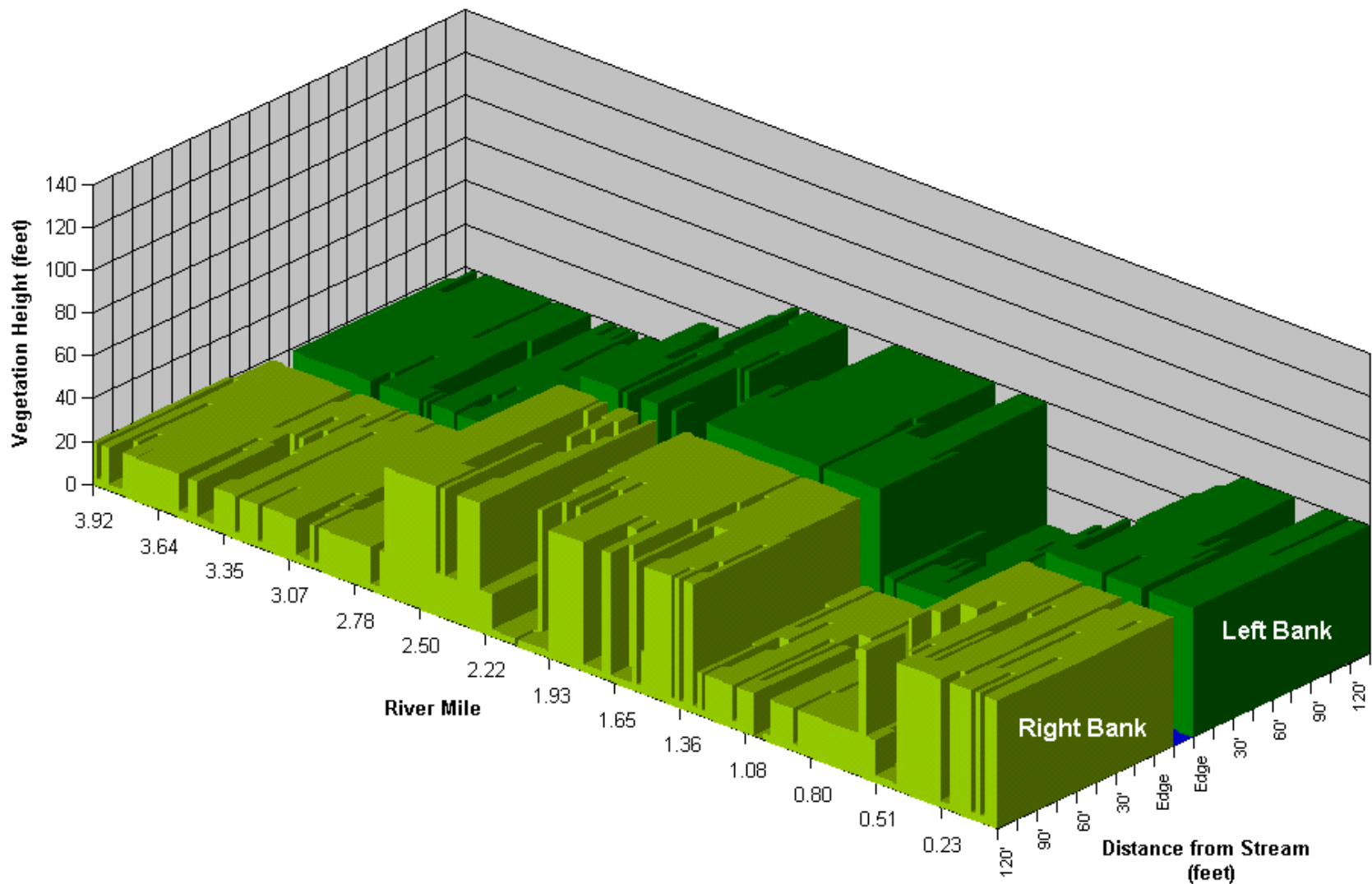
Figure A-10. Beaverton Creek Vegetation Height Sampled from WODIP (BLM, 1999) and 1997 USGS Digital Orthophoto Quads.
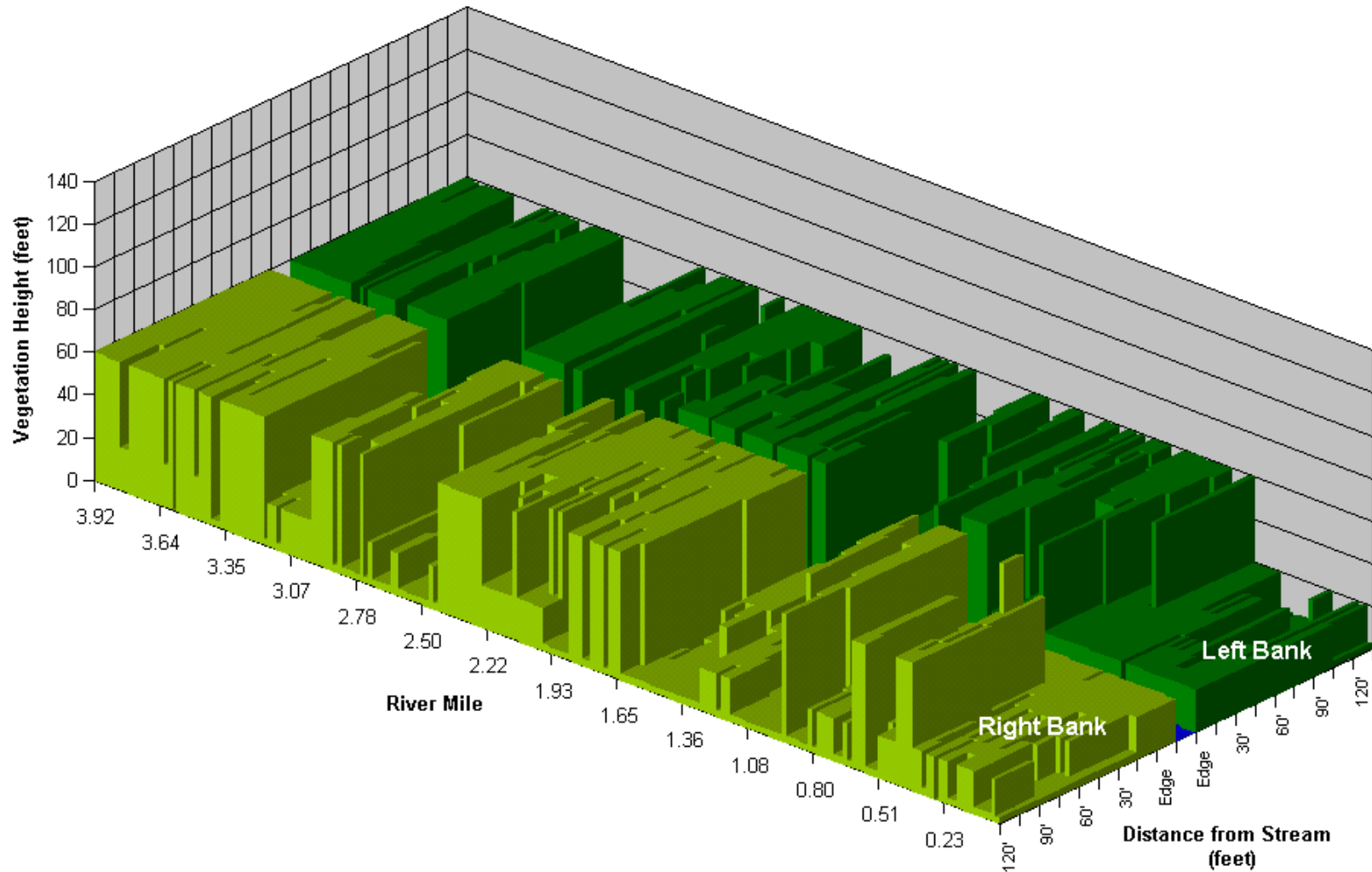
Figure A-11. East Fork Dairy Creek Vegetation Height Sampled from WODIP (BLM, 1999) and 1997 USGS Digital Orthophoto Quads.
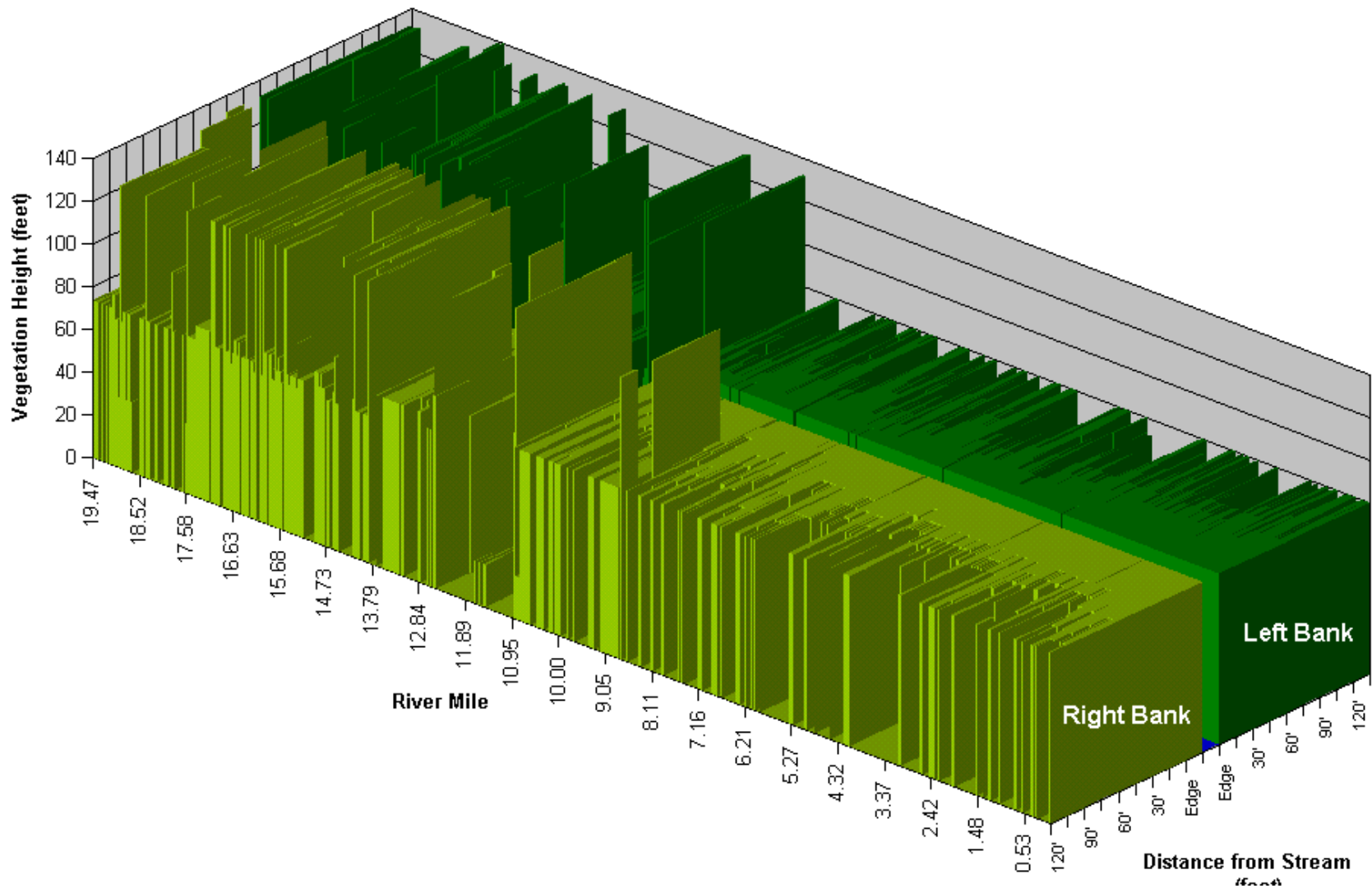
Figure A-12.   West Fork Dairy Creek Vegetation Height Sampled from WODIP (BLM, 1999) and 1997 USGS Digital Orthophoto Quads.
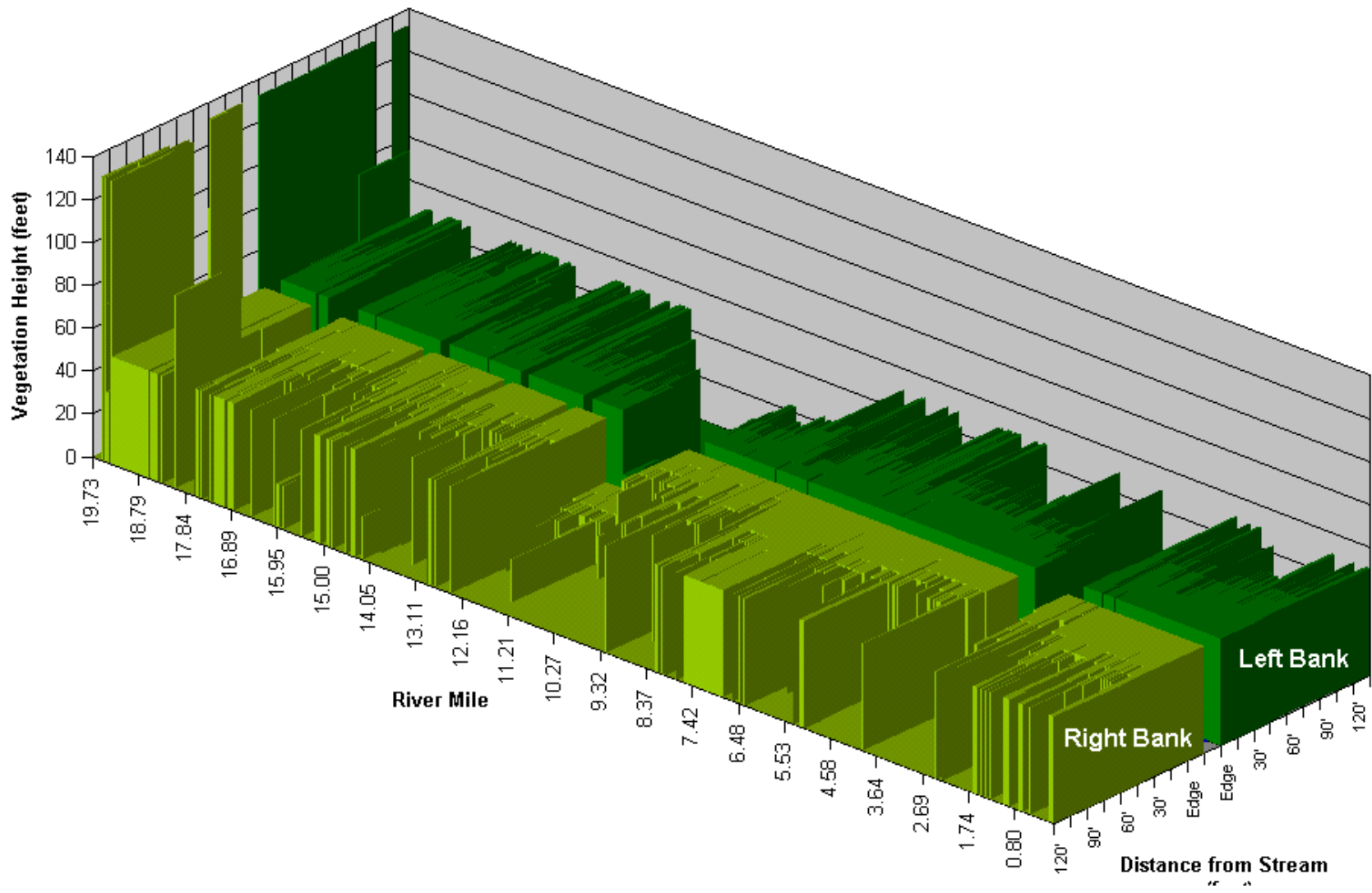
Figure A-13. Dairy Creek Vegetation Height Sampled from WODIP (BLM, 1999) and 1997 USGS Digital Orthophoto Quads.
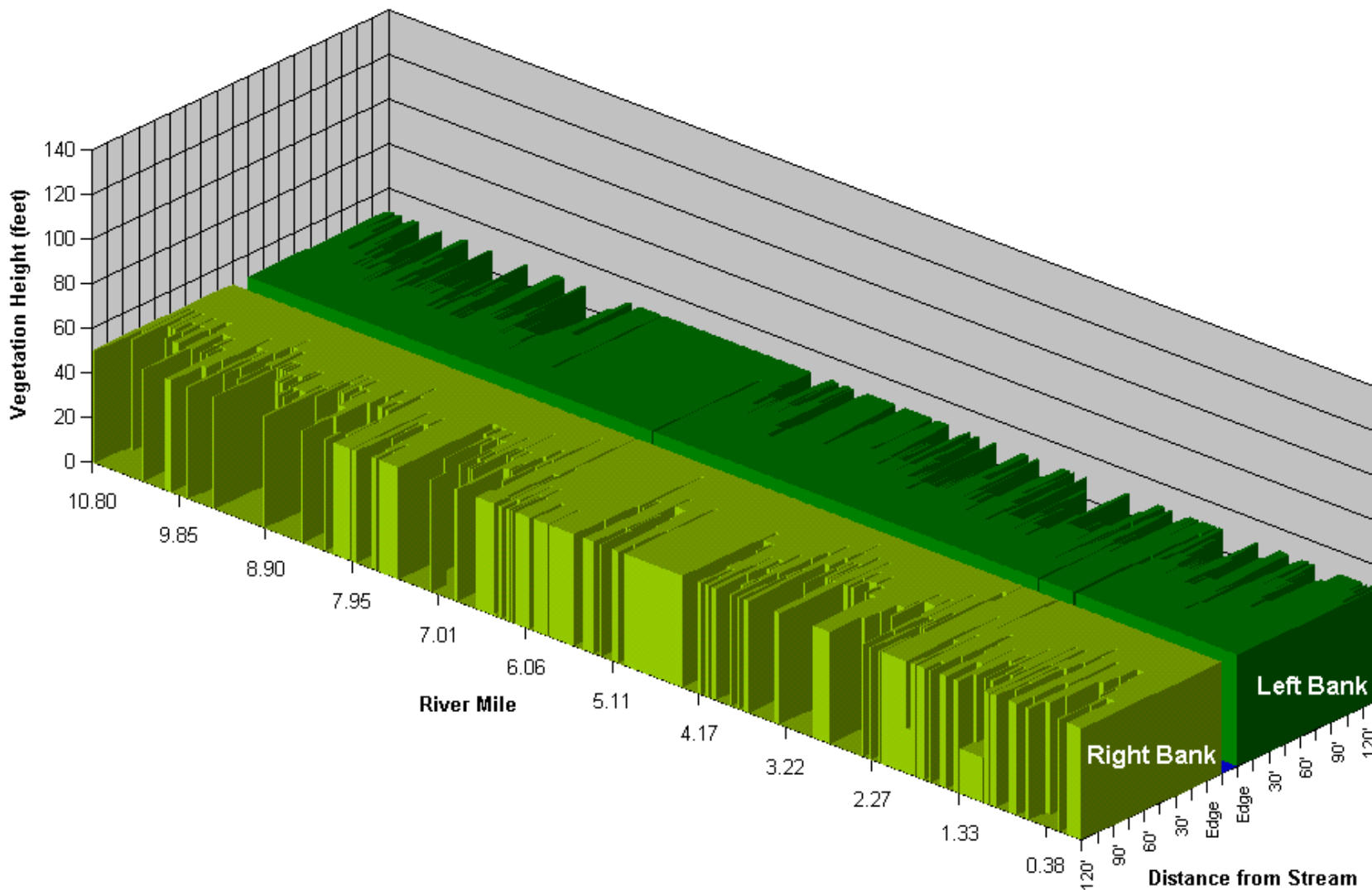
Figure A-14. McKay Creek Vegetation Height Sampled from WODIP (BLM, 1999) and 1997 USGS Digital Orthophoto Quads.
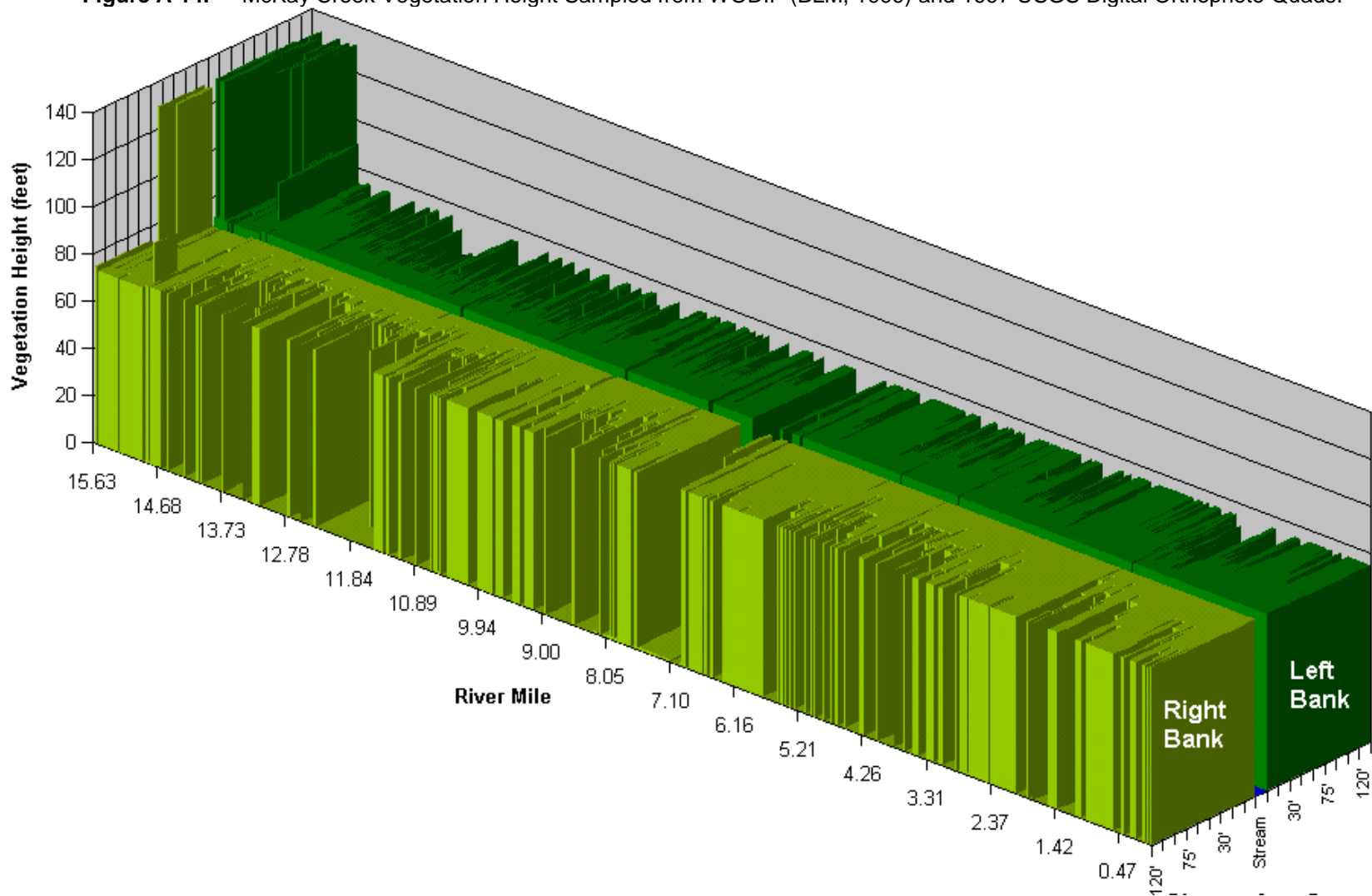
TUALATIN RIVER SUBBASIN ECOREGIONS

The term "ecoregion" is generally understood to describe regions of relative homogeneity in ecological systems or in relationships between organisms and their environments (Omernik and Gallant 1986). Ecoregions are delineated on the premise that ecological regions can be identified through the analysis of the patterns and composition of biotic and abiotic components, such as soil composition, vegetation, climate and topography. Simply, areas within a specific ecoregion are likely to share a common set of ecological characteristics with respect to vegetation, climate, topography, etc. The purpose of ecoregions is to provide a spatial map for research assessment, management, and monitoring of ecosystems and their components.

Currently, there are four levels of ecoregions in the United States, with level I being the coarsest and level IV being the most detailed. **Figure A-15** shows a map of the level IV ecoregions within the Tualatin River subbasin and **Table A-6** provides a short narrative describing the terrain and vegetation typical of the respective ecoregions.

Table A-6. Tualatin River Subbasin Ecoregions (Pater 1998 and Hawksworth 1999a)			
Level III ecoregion	**Level IV ecoregion**	**Terrain**	**Vegetation**
Coast Range	Willapa Hills	Low hills and mountains with moderate gradient streams and rivers. Elevation 500-2300 feet.	Historically Western hemlock, Western red cedar, and Douglas fir forest.
	Volcanics	Steeply sloping mountains with moderate to high gradient streams. Elevation 400-2200 feet.	Historically Western hemlock, Western red cedar, and Douglas fir forest. Forests are intensively managed.
Willamette Valley	Prairie Terraces	Undulating hills amid almost level terrain. Sluggish low gradient streams and rivers. mountains dissected by low-gradient, meandering streams and rivers Elevation 115-200 feet.	Oregon ash and Douglas fir occurred in wetter areas. Prairie and oak woodlands in dryer areas. Today extensively developed for agriculture and urban/rural residential development.
	Valley Foothills	Rolling hills mark the transitional zone between the Willamette Valley and the Coast Range. Elevation 200-1800 feet.	Oregon white oak in dryer areas and Douglas fir in wetter areas were originally dominant. Today rural residential development, tree farms, pastureland, and some urbanization are common.

Figure A-15. Tualatin River Subbasin Ecoregions

ECOREGIONS
- Willamette Valley - Prairie Terraces
- Willamette Valley - Foothills
- Coast Range - Willapa Hills
- Coast Range - Volcanics
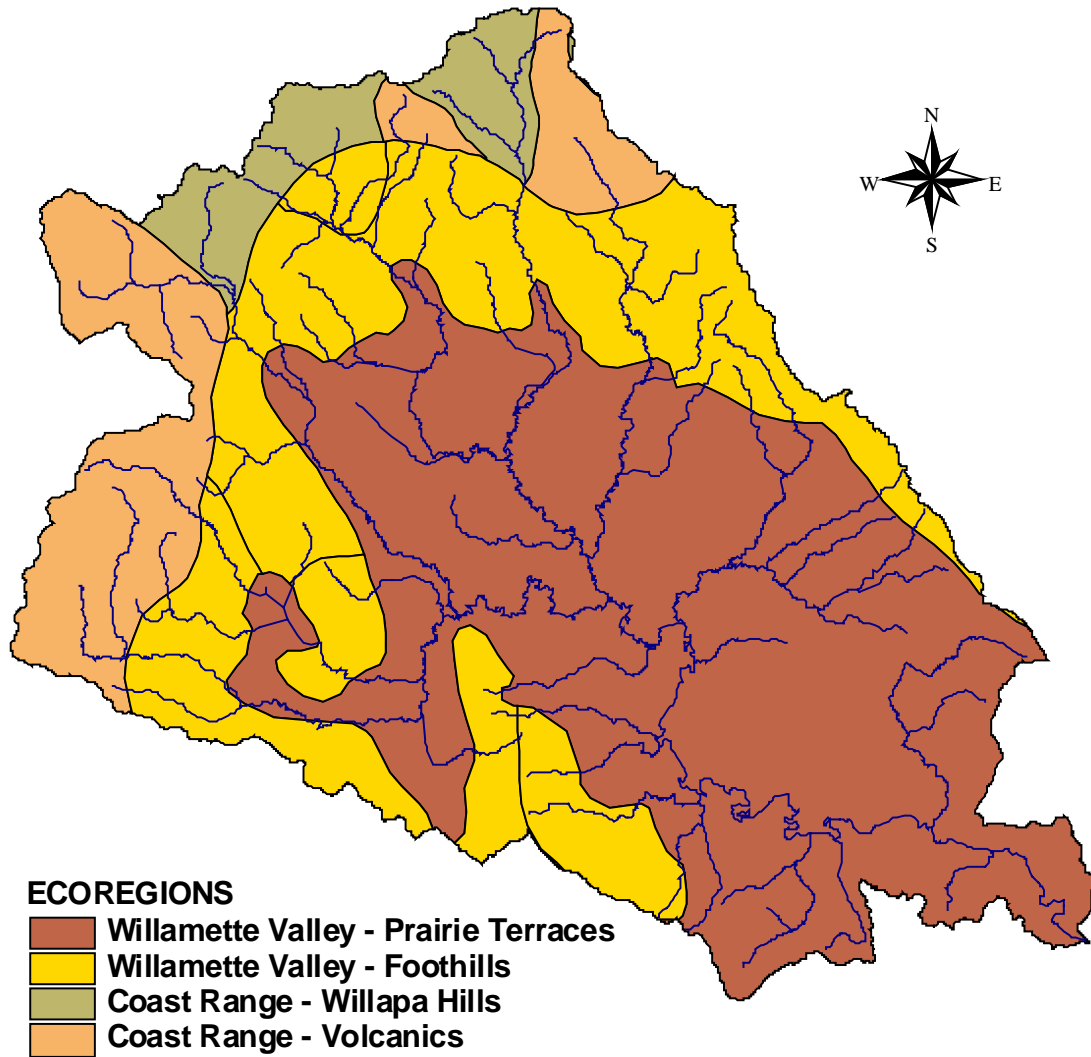
TUALATIN GAP ANALYSIS

Gap analysis is a scientific method for identifying the degree to which plant and animal communities are represented in our present-day mix of conservation lands. Those species and communities not adequately represented in the existing network of conservation lands constitute conservation "gaps." The purpose of the Gap Analysis Program (GAP) is to provide broad geographic information on the status of communities and their habitats in order to provide land managers, planners, scientists, and policy makers with the information they need to make better-informed decisions. The Gap Analysis Program is sponsored and coordinated by the Biological Resources Division of the U.S. Geological Survey. Vegetation is mapped from satellite imagery and other records using the National Vegetation Classification System.

A map of actual vegetation cover of Oregon was developed as part of the Oregon Gap Analysis Program, a project of the Idaho Cooperative Fish and Wildlife Research Unit, in cooperation with the Oregon Department of Fish and Wildlife and the Oregon Natural Heritage Program.

LANDSAT Multi-Spectral Scanner false-color infrared positive prints (taken in 1988) at a scale of 1:250,000 were visually photo-interpreted to identify boundaries of different vegetation cover types. A variety of ancillary maps were used to assist in labeling vegetation polygons, including U.S. Forest Service and Bureau of Land Management large-scale vegetation maps of various dates. Vegetative complexes are described by the dominant or co-dominant plant species in the uppermost vegetation layer. Neither the age nor condition of a vegetation polygon can be determined from the satellite imagery used in this mapping effort (Kagan and Caicco 1992).

Due to the relatively large minimum mapping unit (320 acres) and the fact that the GAP analysis classes urban and agricultural land together, GAP data are not useful for determining dominant tree types for much of the valley portion of the Tualatin River Subbasin (**Figure A-16**). However, the area "left out" in the GAP analysis closely corresponds to the Prairie Terraces ecoregion boundary, as shown in **Figure A-15.** Characteristics of the four dominant vegetation cover types found in the Tualatin River Subbasin (as noted by GAP) are shown in **Table A-7.**

Table A-7. Description of GAP Analysis Vegetation Cover Types (Kagan and Caicco 1992)		
Name	**Description**	**Dominant Tree Types**
Douglas fir - Western hemlock - Western red cedar forest	Closed-canopied lowland and lower montane forests in which Douglas fir is usually the dominant tree species, although numerous other evergreen conifers and deciduous trees may be abundant. These forests generally have a well-developed shrub layer, and a rich assemblage of ferns, forbs, herbs, mosses, and lichens. ELEVATION (ft): sea level-3500	Douglas fir, Western red cedar, Western Hemlock OTHER TREES: Grand fir, Big leaf maple, Red alder,
Douglas fir-Oregon white oak forests and woodlands	Mixed forests and woodlands in which Douglas fir and Oregon white oak are the usual dominants and vary in proportion. Under a natural fire regime, Douglas fir was of only minor importance, and oaks often occurred in groves or savannahs. Much of this original woodland has been cleared, and successful efforts at fire suppression have allowed the nearly ubiquitous invasion of Douglas fir. ELEVATION (ft): 75-1000	Big leaf maple, Douglas fir, Oregon white oak OTHER TREES: Grand fir
Oak-Douglas fir-Ponderosa pine/pasture-urban mosaic	Open woodland to closed-canopied forests in which Oregon white oak and/or California oaks dominate, although either Douglas fir or Ponderosa pine may be common locally. The abundance of conifers, as well as the degree of canopy closure, has increased due to fire suppression. Stands in the Willamette Valley may be comprised solely of Oregon oak. ELEVATION (ft): 75-1500	Douglas fir, Ponderosa pine, Oregon white oak OTHER TREES: Grand fir, Big leaf maple
Mixed evergreen and broadleaf deciduous forest	This is a closed-canopied lowland and lower montane forest in which Bigleaf maple and red alder are common overstory dominants. In general, maple is more prevalent in the Cascades foothills and alder is more common in the Coast Range. These are primarily second- growth forests resulting from prior timber harvest or, especially in the Coast Range, historic wildfires within the Douglas fir-western hemlock type. Douglas fir is nearly always present and may be accompanied by several other needleleaf conifers. The conifers may form a sub-canopy which is obscured by the deciduous overstory in aerial photographs and remote sensing imagery ELEVATION (ft): sea level-3500	Big leaf maple, Red alder, Douglas fir. OTHER TREES: Grand fir, Western red cedar, Western hemlock

Figure A-16. Tualatin River Subbasin GAP Analysis Vegetation Types
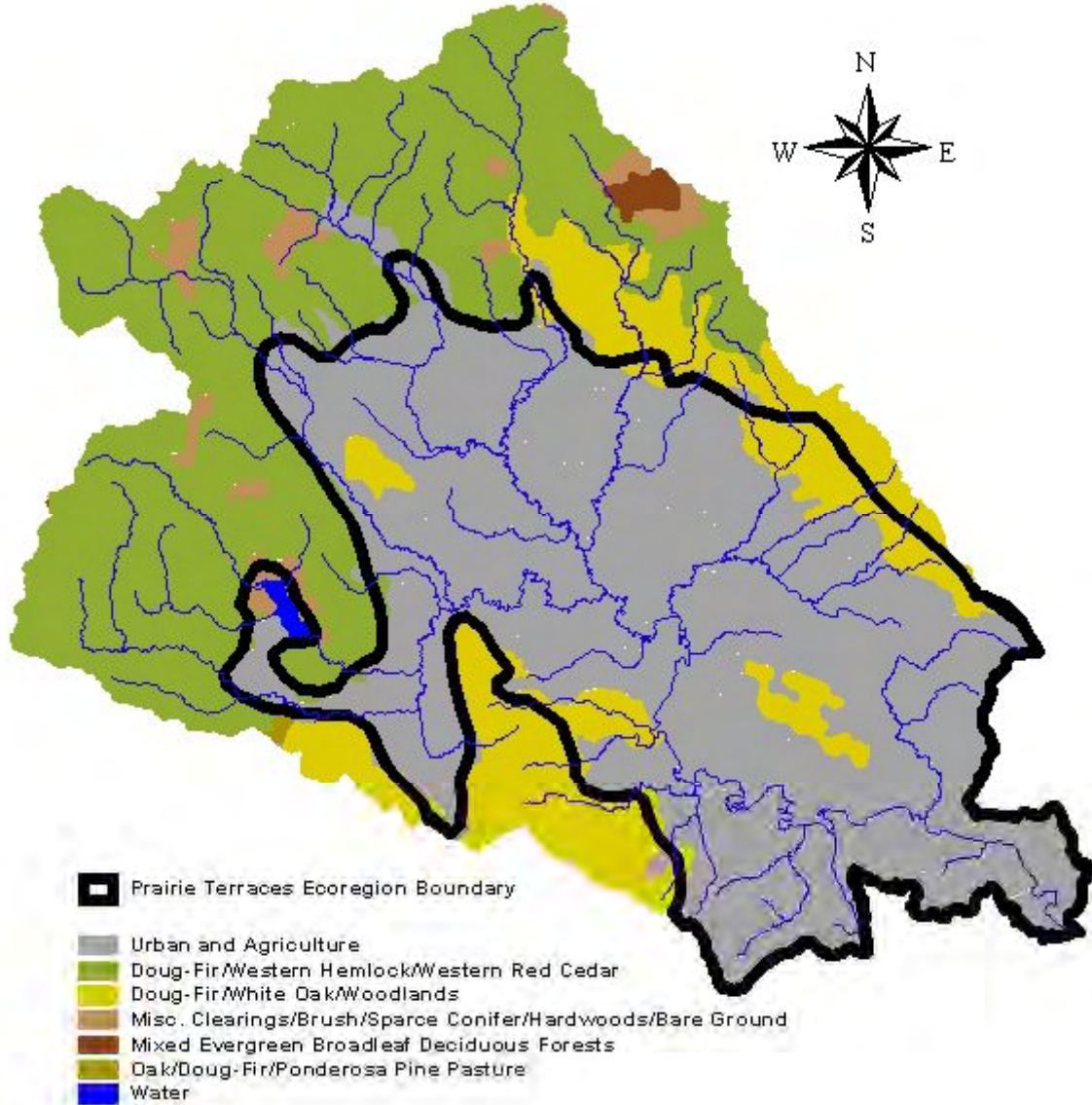
COMPOSITE VEGETATION DIMENSIONS BY ECOREGION

Data from the Gap Analysis Project, ecoregion characteristics and current and historical vegetation data from various watershed assessments were used in determining the dominant shade-producing tree species that are likely to occur along waterways within the Tualatin River subbasin. **Table A-8** summarizes the composite vegetation dimensions, by ecoregion, for the dominant native tree species within the Tualatin River subbasin. Red alder and Big leaf maple are included in the composite vegetation matrix because watershed analyses commonly noted them as being abundant in riparian areas throughout the basin. Potential mature vegetation densities have been assumed to be 90%.

		Near Stream Vegetation		
Ecoregion	Potential Overstory Vegetation	Height	Assumed Overhang	Assumed Canopy Density
Coast Range Willapa Hills	Western hemlock	120 feet		
	WESTERN RED CEDAR	120 feet		
	Douglas fir	160 feet		
	RED ALDER	100 feet	12% of Height	
	Big leaf maple	90 feet		
	Composite Dimension	**118 feet**	**14 feet**	**90%**
Coast Range Volcanics	Western hemlock	120 feet		
	Western red cedar	120 feet		
	Douglas fir	160 feet		
	Red alder	100 feet	12% of Height	
	Big leaf maple	90 feet		
	Composite Dimension	**118 feet**	**14 feet**	**90%**
Willamette Valley Prairie Terraces	Oregon ash	75 feet		
	Western red cedar	120 feet		
	Douglas fir	160 feet		
	Red alder	100 feet	12% of Height	
	Big leaf maple	90 feet		
	Composite Dimension	**109 feet**	**13 feet**	**90%**
Willamette Valley Valley Foothills	Oregon white oak	60 feet		
	Douglas fir	160 feet	12% of Height	
	Red alder	100 feet		
	Big leaf maple	90 feet		
	Composite Dimension	**102 feet**	**12 feet**	**90%**

Table A-8. System Potential Composite Near Stream Vegetation Dimensions by Ecoregion

CHANNEL MORPHOLOGY

Changes in channel morphology, namely channel widening, impact stream temperatures. As a stream widens, the surface area exposed to radiant sources and ambient air temperature increases, resulting in increased energy exchange between the stream and its environment (Boyd, 1996). Further, wide channels are likely to have decreased levels of shade due to simple geometric relationships between riparian height and channel width. Conversely, narrow channels are more likely to experience higher levels of shade. An additional benefit inherent to narrower/deeper channel morphology is a higher frequency of pools that contribute to aquatic habitat or cold water refugia.

Channel Width

The width to depth ratio is a fundamental measure of channel morphology. High width to depth ratios (greater than 10.0) imply wide shallow channels, while low width to depth ratios (less than 10.0) suggest that the channel is narrow and deep. In terms of reducing stream surface exposure to radiant energy sources, it is generally favorable for stream channels to be narrow and deep (low width to depth ratios).

FACTORS THAT AFFECT STREAM WIDTH

Channel widening is often related to degraded riparian conditions that allow increased stream bank erosion and sedimentation of the streambed. Both active stream bank erosion and sedimentation correlate strongly with riparian vegetation type and age. Riparian vegetation contributes to rooting strength and flood plain/stream bank roughness that dissipates erosive energies associated with flowing water. Established/Mature woody riparian vegetation adds the highest rooting strengths and flood plain/stream bank roughness. Annual (grassy) riparian vegetation communities offer less rooting strength and flood plain/stream bank roughness. It is expected that width to depth ratios would be lower (narrower and deeper channels) when established/mature woody vegetation is present. Annual (grassy) riparian communities may allow channels to widen and become shallower.

Further, channel morphology, namely wetted width:depth values, are not solely dependent on riparian conditions. Sedimentation can deposit material in the channel and agrade the streambed, reducing channel depth and increasing channel width. Flow events play a major role in shaping the stream channel. Channel modification usually occurs during high flow events. Naturally, land uses that affect the magnitude and timing of high flow events may negatively impact channel width and depth.

However, riparian vegetation conditions will affect the resilience of the stream banks/flood plain during periods of sediment introduction and high flow. Linking width to depth ratios to riparian vegetation is fundamental. Disturbance processes may have drastically differing results depending on the ability of riparian vegetation to shape and protect channels. Low width to depth ratios are thus related to riparian vegetation community composition and condition by:

- ✓ ***Building stream banks:*** *Trap suspended sediments, encourage deposition of sediment in the flood plain and reduce incoming sources of sediment.*
- ✓ ***Maintaining stable stream banks:*** *High rooting strength and high stream bank and flood plain roughness prevent stream bank erosion.*
- ✓ ***Reducing flow velocity (erosive kinetic energy):*** *Supplying large woody debris to the active channel, high pool:riffle ratios and adding channel complexity that reduces shear stress exposure to stream bank soil particles.*

Stream Bank Erosion

Stream bank erosion results from detachment, entrainment and removal of bank material as individual grains or aggregates via fluvial processes. *Stream bank failure* indicates a gravity-related collapse of the stream bank by mass movement. Both *stream bank erosion* and *stream bank failure* result in *stream bank retreat*, which is a net loss of stream bank material and a corresponding widening of the stream channel.

Stream bank stability reflects the condition of riparian vegetation contributing to rooting strength in stream bank soils and flood plain roughness. Riparian vegetation rooting structure serves to strengthen the stream bank and resist the erosive energy exerted on the stream bank during high flow conditions. Flood plain roughness reflects the ability of the flood plain to dissipate erosive flow energy during high flow events that over-top stream banks and inundate the flood plain. Riparian vegetation disturbance often has a compounding effect of increased stream bank erosion, increased kinetic energy exposure, decreased bank rooting strength, loss of soil cohesion and loss of flood plain roughness.

Stream Bank Protection and Riparian Vegetation

A stream bank erosion recovery process requires the concurrent occurrence of two elements that induce stream bank building: protect stream banks from kinetic energy (bank particle cohesion) and reduce kinetic energy (stream bank/flood plain roughness). High levels of stream bank cohesion tend to protect the stream bank from erosive kinetic energy associated with flowing water. Stream bank erosion reflects looseness of bank soil, rock and organic particles. The opposite condition is cohesion of stream bank soil, rock and organic particles. Vegetation strengthens particle cohesion by increasing rooting strength that helps bind soil and add structure to the stream bank. Different riparian vegetation communities (annual, perennial, deciduous, mixed and conifer dominated) offer a variety of rooting strengths to stream banks. It is a general observation that healthy/intact indigenous riparian vegetation communities will add preferable stream bank cohesion over bare soil/ground conditions.

REDUCE STREAM BANK EROSION

Protect Stream Banks from Kinetic Energy — *Reduce Kinetic Energy*

Increase Stream Bank Particle Cohesion

Increase Stream Bank and Flood Plain Roughness

Establish/Maintain Woody Riparian
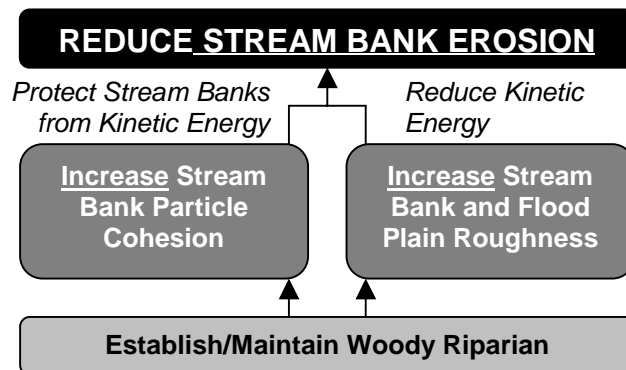
Physical relationships that relate to decreasing/preventing stream bank erosion can be summarized as:

- ✓ *Rough surfaces decrease local flow velocity,*

- ✓ *Reduced local velocity lowers shear stress acting on the stream bank,*

- ✓ *Lower shear stress acting on the stream bank will be less likely to detach and entrain stream bank particles.*

In an effort to control stream bank erosion processes, the focus then becomes to retain high stream bank and flood plain roughness via riparian vegetation. The species composition and condition of the riparian vegetation determines natural stream bank roughness. Values of roughness (Manning's n) correspond to various riparian conditions (**Figure A-17**).

Figure A-17. Manning's n (Roughness Coefficient) Related to Riparian Vegetation
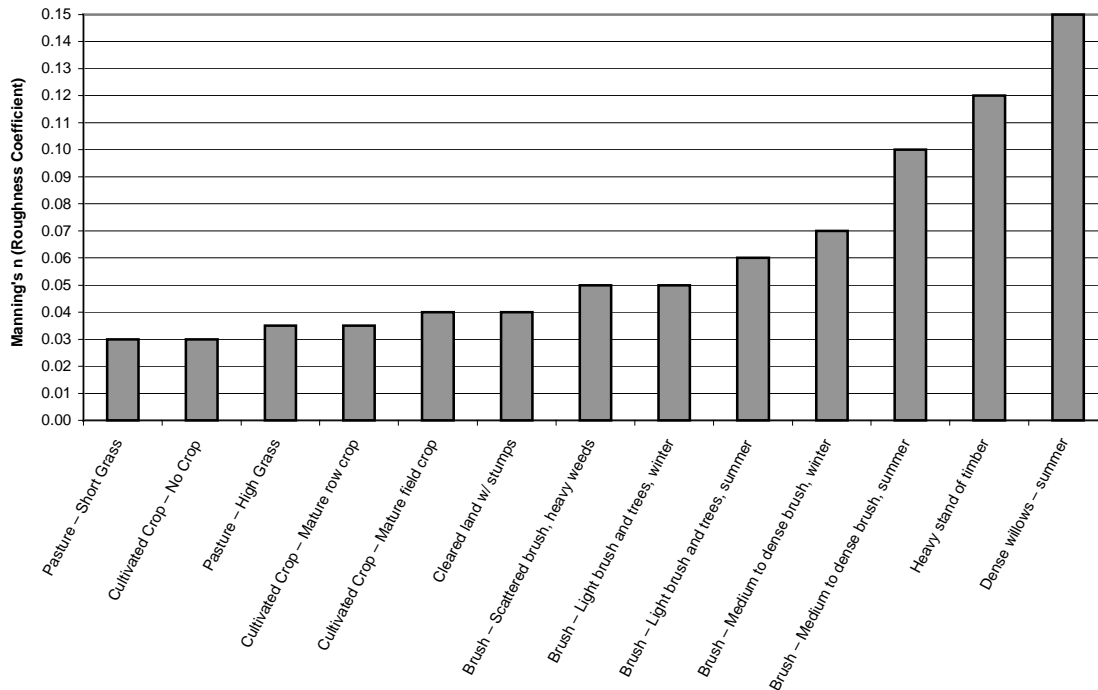
In essence, the roughness coefficients help explain the relationship between riparian vegetation types and active stream bank erosion:

✓ *Highest stream bank erosion rates correspond with annual/perennial riparian vegetation types that have a low Manning's n (roughness coefficient).*

✓ *Low stream bank erosion rates correspond with woody riparian vegetation types that have a high Manning's n (roughness coefficient).*

Higher values imply increasing roughness that reduces stream bank erosion, reduces local shear stress and slows local flow velocity (Chow, 1959).

Sedimentation

Streambed material classification defines *fines* as sand, silt and organic material that have a grain size of 6.4 mm or less. Sediments may affect the spawning success of salmonids. Sedimentation of spawning gravel has been shown to significantly impair the success of juvenile emergence from gravel *redds*. Sedimentation may affect survival through entombment of juvenile or through reduction of intergravel dissolved oxygen delivery.

Studies have shown that fry emergence is seriously compromised as fine sediments are introduced into spawning gravel (Tappel and Bjornn, 1993). When fine grain sized substrate cover spawning gravel (*redds*) anadromous *sac-fry* (larval fish) may emerge prematurely. *Sac-fry* are often forced out of gravel before they have absorbed their yolk sacs as a fine sediments fill the interstitial pore spaces of the *redd*, resulting in a lack of oxygen (Tappel and Bjornn, 1993). Low survival rates accompany *sac-fry* that have been forced to prematurely emerge from the *redd* (**Figure A-18**).

A-34

Figure A-18.   Percentage Sac Fry Emergence in Gravel/Sand Mixtures
[Fine sediment was granitic sand with particles less than 6.4 mm]
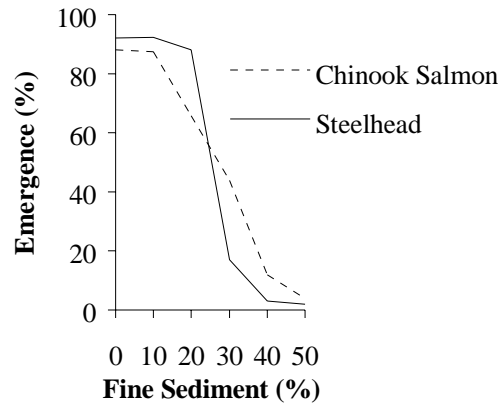
Everest et al. (1987) observed that stable channels containing stored sediments and large woody debris are more productive at every trophic level than either degraded channels devoid of sediment or channels that are agraded and unstable. Stowell et al. (1983) reported that increased fine sediment in spawning gravel has been shown to decrease survival of juvenile salmon emerging from the *redd.* Researchers have presented similar relationships (Waters, 1995; Irving and Bjornn, 1984; and Tappel, 1981). Deposition and embeddedness can influence embryo survival, emergence from the gravel and juvenile or adult use of the habitat. Harvey (1993) found no functional predictors that would quantify the effects of sedimentation on the survival or rearing of salmonids, but recommended that any incremental increase in embeddedness should be avoided.

Increases in bed sediments, affected by landscape and bank mass failures, are often accompanied by channel widening and braiding resulting in increased bank erosion and decreased pool riffle amplitude. Reduced channel complexity may be associated with reduced habitat complexity for aquatic species (salmonids and food sources such as macroinvertebrate communities).

Beschta et al. (1981) concluded that bedload processes are extremely important in shaping the character of quality of stream habitats. Sedimentation of the stream substrate, particularly the gravel used for spawning, produces significant detrimental effects on salmonid resources (Iwamoto et al., 1978). Everest et al (1987) observed that watershed characteristics, as well as the erosion and bedload processes, will affect the level of risk to salmonids by accelerated sedimentation. Fine sediments can act directly on the fish by (Newcombe and McDonald 1991):

- ✓ *Killing salmonids or reducing growth or reducing disease resistance,*
- ✓ *Interfering with the development of eggs and larvae,*
- ✓ *Modifying natural movements and migration of salmonids, or*
- ✓ *Reducing the abundance of food organisms.*

Sediment sources, both upslope and instream, are elevated in some portions of the Tualatin River Subbasin. Before lasting improvements in channel substrate can take place, these sources must be reduced, in some cases, dramatically. Further, if the stream channel, riparian zone and/or upslope landscape is in a degraded state, the same high flow events that transport sediments out of the stream channel can introduce large quantities of fine sediment.

Sediment, once introduced into the stream channel, either becomes deposited in the bed substrate, deposits along banks or remains suspended in the water column (i.e., transported

downstream). Fine sediment deposited in the stream bed material must be re-suspended during high flow events and transported downstream or deposited in the flood plain/stream bank areas bordering the stream channel. These processes occur during hydrologic events that are relatively infrequent. Major sediment moving events have return periods measured in decades.

In conclusion, the condition of the stream channel and upslope landscape will create drastically different consequences in terms of sedimentation during high flow events:

> ***Resilient/Healthy System:*** *Prevent large introductions of fine sediment from upslope or riparian areas, maintain stream bank stability, encourage deposition in the flood plain and bank building processes, introduce disturbed riparian vegetation (large woody debris into the active channel) and allow the resuspension and transportation of existing stream bed fine substrate in the downstream direction.*

> ***Degrading/Impaired System:*** *Allow large introductions of fine sediment from upslope or riparian areas, experience moderate to high rates of active stream bank erosion, allow erosion in the flood plain and bank retreating processes, is unable to introduce disturbed riparian vegetation (large woody debris into the active channel) and resuspended/transported stream bed fine substrate is replaced by incoming fine sediment sources.*

HYDROLOGY

Groundwater Mixing

Groundwater inflow has a cooling effect on summertime stream temperatures. Subsurface water is insulated from surface heating processes and most often groundwater temperatures fluctuate little and are cool (45°F to 55°F). Many land use activities that disturb riparian vegetation and associated flood plain areas may affect the connectivity of the Tualatin River and its tributaries to groundwater sources. Groundwater inflow not only cools summertime stream temperatures, but also augments summertime flows. Reductions or elimination of groundwater inflow will have a compounding warming effect on the Tualatin River and its tributaries.

The ability of riparian soils to capture, store and slowly release groundwater is largely a function of the level of riparian disturbance. Human land use can reduce the storage capacity of riparian soils. Riparian disturbance can also separate the connectivity of the flood plain and the stream.

Surrounding Thermal Environment

Ground temperatures can be a source of heat energy to the stream. When the ground is warmer than the stream, heat will transfer from the stream bank to the water column. In fact, ground surfaces can conduct heat to the stream hundreds of times faster than that of the air column surrounding the stream. Solids (ground surfaces) have higher conductivity than gases (air). Conductivities of soils are on the order of 500 to 3,500 times greater than that of air (Halliday and Resnick, 1988).

Degraded riparian areas that allow excessive stream bank warming will introduce heat into the stream faster than cooler, highly vegetated stream banks. Once again, riparian condition is implicated as a controlling factor in stream temperature dynamics because ground/soil temperatures are a function of the shading.

Air affects stream temperatures at a slower *rate.* Nevertheless, this should not be interpretted to mean that air temperatures do not affect stream temperature. Air can deliver heat to a stream via the convection/conduction pathway, which is the slowest of the water energy transfer processes (Bowen, 1926; Beschta and Weatherred, 1984; Boyd, 1996; Chen, 1996). However, prolonged exposure to air temperatures warmer than the stream can induce gradual stream heating. Because the rate of energy transfer is slow, air temperature related stream column heating cannot explain the rapid daily heating and cooling cycles that streams experience.

Flow Volume

Stream temperature change is generally inversely related to flow volume. As flows decrease, stream temperature tends to increase, if energy processes remain unchanged (Boyd, 1996). Runoff in the Tualatin River subbasin is primarily derived from precipitation, with peaks typically occurring in the winter. Late summer low flows are common for many streams in the Tualatin River subbasin due to low summer precipitation combined with extensive irrigation withdrawals. Stream discharge within urbanized reaches may be reduced during the summer flow period due to a prevalence of impervious surface area impeding ground water recharge throughout the year.

Mainstem flows during the summer period are augmented by released from Barney Reservoir and Hagg Lake, with water being stored during the high flow winter period and release during low flow periods.

POINT SOURCES

Warm point source discharges are often sources of stream heating. The locations of the NPDES cooling water and general NPDES permitted discharge points are mapped in **Figure A-19**. Facilities that discharge during the critical summertime temperature period are listed in **Table A-9**. Discharge temperatures range from 66°F to 88°F. Discharge rates are generally very low; however, two major wastewater treatment facilities discharge a combined 61 cfs into the Tualatin River (Rock Creek Waste Water Treatment Plant – RM 38.0 and Durham Waste Water Treatment Plant – RM 9.5).

Figure A-19.   Map of Tualatin Basin showing Urban Areas Including Point Sources of Pollution with Facility NPDES Permits.
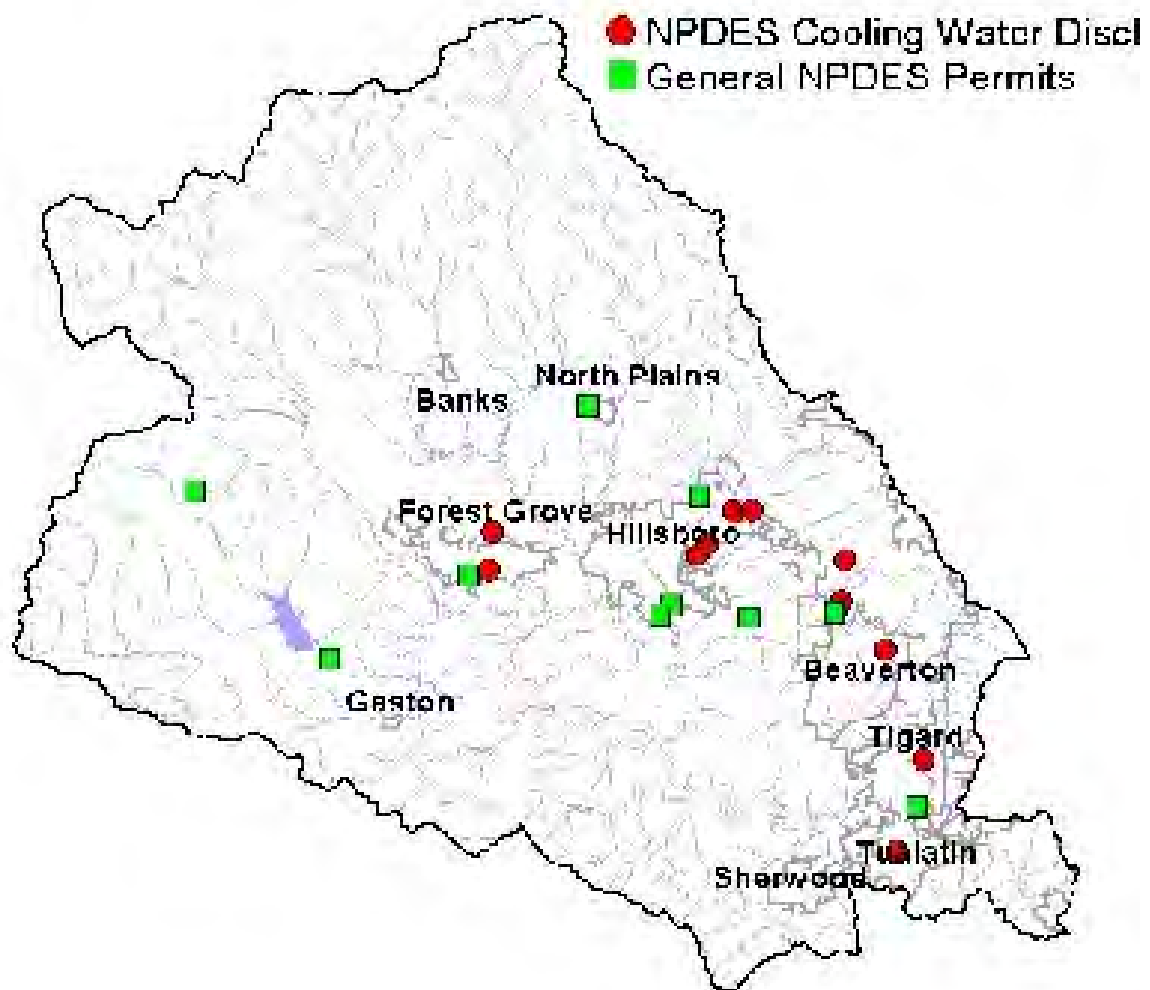
Table A-9. NPDES Permitted Facilities for Cooling Water and General Discharge						
Facility Name	**City**	**Receiving Water**	**River Mile**	**Permit Type**	**Flow Rate (cfs)**	**Critical Temp.**
PACIFIC FOODS OF OR., INC.	TUALATIN	Tualatin R.	8.5	GEN01	0.0032	76 °F
USA DURHAM STP	TIGARD	Tualatin R.	9.5	NPDES	27.0	71 °F
USA ROCK CREEK STP	HILLSBORO	Tualatin R.	38.0	NPDES	33.9	71 °F
MATSUSHITA ELEC. MAT., INC.	FOREST GROVE	Tualatin R.	50.0	GEN01	0.0021	82 °F
WILLIAMS CONTROLS INC	PORTLAND	Fanno Cr.	1.5	GEN01	0.0267	81 °F
WILLAMETTE INDUSTRIES	BEAVERTON	Fanno Cr.	9.0	GEN01	0.0170	72 °F
PERMAPOST	HILLSBORO	Rock Cr.	1.0	NPDES	0.0572	70 °F
FUJITSU COMP. PROD. OF AMER., INC.	HILLSBORO	Rock Cr.	3.2	GEN01	0.0002	76 °F
KOEI AMERICA INCORP.	HILLSBORO	Rock Cr.	3.6	GEN01	0.0095	88 °F
EPSON PORTLAND INC.	HILLSBORO	Rock Cr.	7.0	GEN01	0.0004	90 °F
TEKTRONIX BEAV. CAMP. (INDUST. WWTP)	BEAVERTON	Beaverton Cr.	6.7	GEN01	0.0024	78 °F
MAXIM WAFER FAB OPER.	BEAVERTON	Beaverton Cr.	7.0	GEN01	0.0023	71 °F
OREGON-CANADIAN FOR. PROD.	NORTH PLAINS	McKay Cr.	8.5	NPDES	0.0010	82 °F
HENNINGSEN COLD STOR. CO.	FOREST GROVE	Council Cr.	10.0	GEN01	0.0081	69 °F
FORESTEX CO. (ABN)	GASTON	Scoggins Cr.	4.0	NPDES	0.0021	No data

ANALYTICAL FRAMEWORK

Conceptual Model

At any particular instant of time, a defined stream reach is capable of sustaining a particular water column temperature. Stream temperature change that results within a defined reach is explained rather simply. The temperature of a parcel of water traversing a stream/river reach enters the reach with a given temperature. If that temperature is greater than the energy balance is capable of supporting, the temperature will decrease. If that temperature is less than energy balance is capable of supporting, the temperature will increase. Stream temperature change within a defined reach, is induced by the energy balance between the parcel of water and the surrounding environment and transport of the parcel through the reach. The general progression of the model is outlined in the model flow chart, **Figure A-20**.

Figure A-20.   Temperature Model Flow Chart
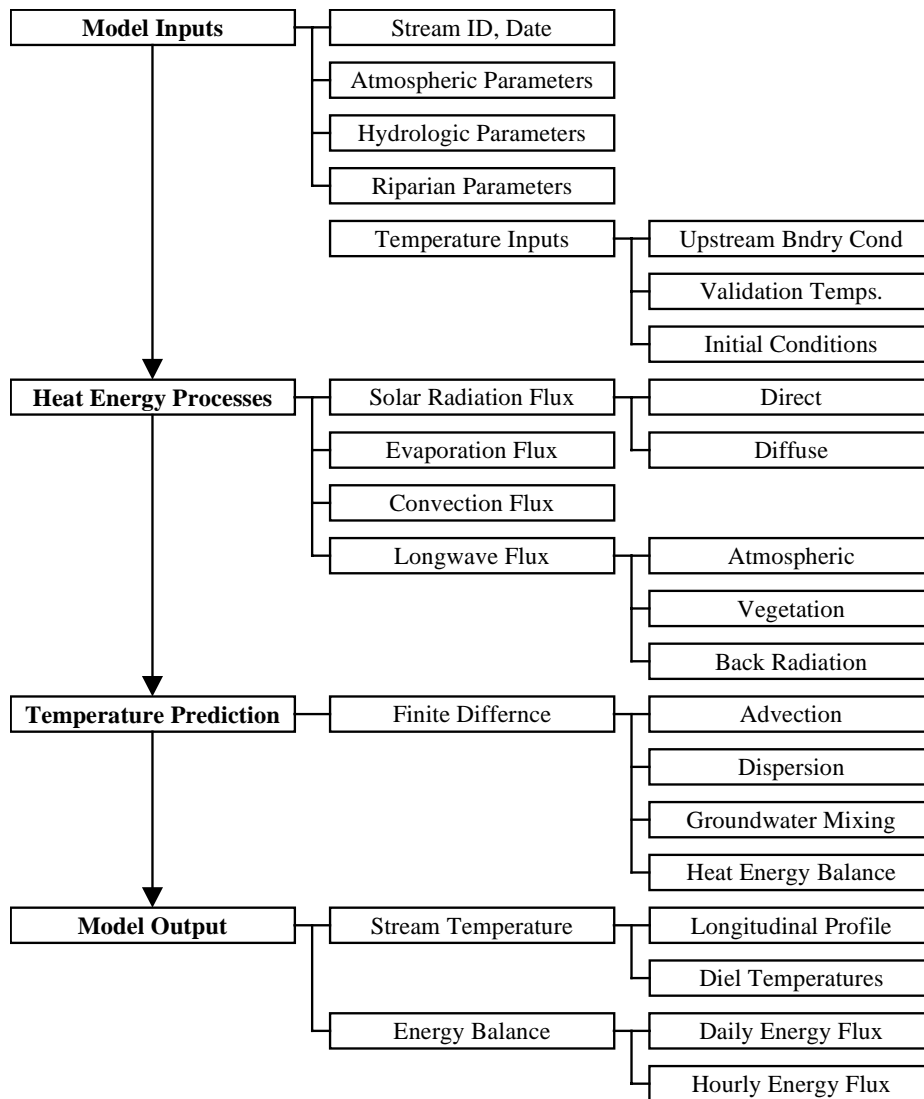
It takes time for the water parcel to traverse the longitudinal distance of the defined reach, during which the energy processes drive stream temperature change. At any particular instant of time, water that enters the upstream portion of the reach is never exactly the temperature that is supported by the defined reach. And, as the water is transferred downstream, heat energy and hydraulic process that are variable with time and space interact with the water parcel and induce water temperature change. The described modeling scenario is a simplification; however, understanding the basic processes in which stream temperatures change occurs over the course of a defined reach and period of time is essential.

Governing Equations

HEAT ENERGY PROCESSES

Water temperature change is a function of the total heat energy transfer in a discrete volume and may be described in terms of energy per unit volume. It follows that large volume streams are less responsive to temperature change, and conversely, low flow streams will exhibit greater temperature sensitivity.

Equation A-1. Heat Energy per Unit Volume,

$$\Delta T_w \propto \frac{\Delta Heat\ \ Energy}{Volume}$$

Water has a relatively high heat capacity ($c_w = 10^3$ cal kg^{-1} K^{-1}) (Satterlund and Adams 1992). Conceptually, water is a heat sink. Heat energy that is gained by the stream is retained and only slowly released back to the surrounding environment, represented by the cooling flux ($\Phi_{cooling}$). Heating periods occur when the net energy flux (Φ_{total}) is positive: ($\Phi_{heating} > \Phi_{cooling}$).

Equation A-2. Heat Energy Continuity,

$$\Phi_{total} = \Phi_{heating} - \Phi_{cooling}$$

In general, the net energy flux experienced by all stream/river systems follows two cycles: a seasonal cycle and a diurnal cycle. In the Pacific Northwest, the seasonal net energy cycle experiences a maximum positive flux during summer months (July and August), while the minimum seasonal flux occurs in winter months (December and January). The diurnal net energy cycle experiences a daily maximum flux that occurs at or near the sun's zenith angle, while the daily minimum flux often occurs during the late night or the early morning. It should be noted, however, that meteorological conditions are variable. Cloud cover and precipitation seriously alter the energy relationship between the stream and its environment.

The net heat energy flux (Φ_{total}) consists of several individual thermodynamic energy flux components, namely: solar radiation (Φ_{solar}), long-wave radiation ($\Phi_{longwave}$), conduction ($\Phi_{conduction}$), groundwater exchange ($\Phi_{groundwater}$) and evaporation ($\Phi_{evaporation}$).

Equation A-3. Net Heat Energy Continuity,

$$\Phi_{total} = \Phi_{solar} + \Phi_{longwave} + \Phi_{convection} + \Phi_{evaporation} + \Phi_{streambed} + \Phi_{groundwater}$$

Stream temperature is an expression of heat energy per unit volume, which in turn is an indication of the rate of heat exchange between a stream and its environment. The heat transfer processes that control stream temperature include solar radiation, longwave radiation,

convection, evaporation and bed conduction (Wunderlich, 1972; Jobson and Keefer, 1979; Beschta and Weatherred, 1984; Sinokrot and Stefan, 1993; Boyd, 1996). With the exception of solar radiation, which only delivers heat energy, these processes are capable of both introducing and removing heat from a stream. **Figure A-21** displays heat energy processes that solely control heat energy transfer to/from a stream.

Figure A-21. Heat Energy Processes
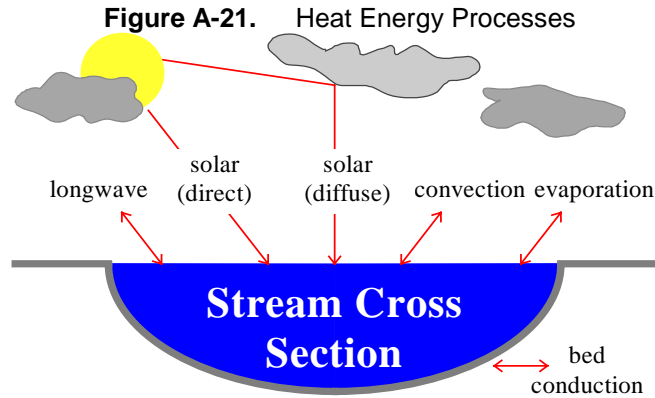
When a stream surface is exposed to midday solar radiation, large quantities of heat will be delivered to the stream system (Brown 1969, Beschta et al. 1987). Some of the incoming solar radiation will reflect off the stream surface, depending on the elevation of the sun. All solar radiation outside the visible spectrum (0.36μ to 0.76μ) is absorbed in the first meter below the stream surface and only visible light penetrates to greater depths (Wunderlich, 1972). Sellers (1965) reported that 50% of solar energy passing through the stream surface is absorbed in the first 10 cm of the water column. Removal of riparian vegetation, and the shade it provides, contributes to elevated stream temperatures (Rishel et al., 1982; Brown, 1983; Beschta et al., 1987). The principal source of heat energy delivered to the water column is solar energy striking the stream surface directly (Brown 1970). Exposure to direct solar radiation will often cause a dramatic increase in stream temperatures. The ability of riparian vegetation to shade the stream throughout the day depends on vegetation height, width, density and position relative to the stream, as well as stream aspect.
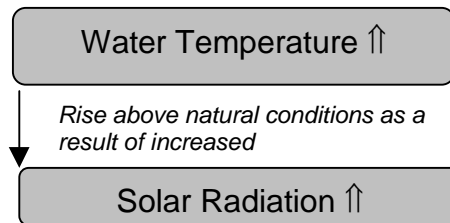
Both the atmosphere and vegetation along stream banks emit longwave radiation that can heat the stream surface. Water is nearly opaque to longwave radiation and complete absorption of all wavelengths greater than 1.2μ occurs in the first 5 cm below the surface (Wunderlich, 1972). Longwave radiation has a cooling influence when emitted from the stream surface. The net transfer of heat via longwave radiation usually balances so that the amount of heat entering is similar to the rate of heat leaving the stream (Beschta and Weatherred, 1984; Boyd, 1996).

Evaporation occurs in response to internal energy of the stream (molecular motion) that randomly expels water molecules into the overlying air mass. Evaporation is the most effective method of dissipating heat from water (Parker and Krenkel, 1969). As stream temperatures increase, so does the rate of evaporation. Air movement (wind) and low vapor pressures increase the rate of evaporation and accelerate stream cooling (Harbeck and Meyers, 1970).

Convection transfers heat between the stream and the air via molecular and turbulent conduction (Beschta and Weatherred, 1984). Heat is transferred in the direction of warmer to cooler. Air can have a warming influence on the stream when the stream is cooler. The opposite is also true.

The amount of convective heat transfer between the stream and air is low (Parker and Krenkel, 1969; Brown, 1983). Nevertheless, this should not be interpreted to mean that air temperatures do not affect stream temperature.

Depending on streambed composition, shallow streams (less than 20 cm) may allow solar radiation to warm the streambed (Brown, 1969). Large cobble (> 25 cm diameter) dominated streambeds in shallow streams may store and conduct heat as long as the bed is warmer than the stream. Bed conduction may cause maximum stream temperatures to occur later in the day, possibly into the evening hours.

The instantaneous heat transfer rate experienced by the stream is the summation of the individual processes:

$$\Phi_{Total} = \Phi_{Solar} + \Phi_{Longwave} + \Phi_{Evaporation} + \Phi_{Convection} + \Phi_{Conduction}.$$

Solar Radiation (Φ_{Solar}) is a function of the solar angle, solar azimuth, atmosphere, topography, location and riparian vegetation. Simulation is based on methodologies developed by Ibqal (1983) and Beschta and Weatherred (1984). *Longwave Radiation* ($\Phi_{Longwave}$) is derived by the Stefan-Boltzmann Law and is a function of the emissivity of the body, the Stefan-Boltzmann constant and the temperature of the body (Wunderlich, 1972). *Evaporation* ($\Phi_{Evaporation}$) relies on a Dalton-type equation that utilizes an exchange coefficient, the latent heat of vaporization, wind speed, saturation vapor pressure and vapor pressure (Wunderlich, 1972). *Convection* ($\Phi_{Convection}$) is a function of the Bowen Ratio and terms include atmospheric pressure, and water and air temperatures. *Bed Conduction* ($\Phi_{Conduction}$) simulates the theoretical relationship ($\Phi_{Conduction} = K \cdot dT_b / dz$), where calculations are a function of thermal conductivity of the bed (K) and the temperature gradient of the bed (dT_b/dz) (Sinokrot and Stefan, 1993). Bed conduction is solved with empirical equations developed by Beschta and Weatherred (1984).

The ultimate source of heat energy is solar radiation both diffuse and direct. Secondary sources of heat energy include long-wave radiation, from the atmosphere and streamside vegetation, streambed conduction and in some cases, groundwater exchange at the water-stream bed interface. Several processes dissipate heat energy at the air-water interface, namely: evaporation, convection and back radiation. Heat energy is acquired by the stream system when the flux of heat energy entering the stream is greater than the flux of heat energy leaving. The net energy flux provides the rate at which energy is gained or lost per unit area and is represented as the instantaneous summation of all heat energy components.

NON-UNIFORM HEAT ENERGY TRANSFER EQUATION

The rate change in stream temperature is driven by the heat energy flux (Φ_i). It is easily shown that a defined volume of water will attain a predictable rate change in temperature, provided an accurate prediction of the heat energy flux. The rate change in stream temperature (T) is calculated as shown in **Equation A-4**.

Equation A-4. Rate Change in Temperature Caused by Heat Energy Thermodynamics,

$$\frac{\partial T}{\partial t} = \left(\frac{Ax_i \cdot \Phi_i}{\rho \cdot c_p \cdot V_i} \right),$$

Which reduces to,

$$\frac{\partial T}{\partial t} = \left(\frac{\Phi_i}{\rho \cdot c_p \cdot D_i} \right).$$

A-43

Where,

Ax_i:		cross-sectional area (m^2)
C_p:		specific heat of water (cal kg$^{-1} \cdot {}^{\circ}C^{-1}$)
D_i:		average stream depth (m)
t:		time (s)
T:		Temperature (${}^{\circ}C$)
V_i:		volume (m^3)
Φ_i:		total heat energy flux (cal m-$^2 \cdot$ s^{-1})
ρ:		density of water (kg/m^3)

Advection (U_x) redistributes heat energy in the positive longitudinal direction. No heat energy is lost or gained by the system during advection, and instead, heat energy is transferred downstream as a function of flow velocity. In the case where flow is uniform, the rate change in temperature due to advection is expressed in the first order partial differential equation below.

Equation A-5. Rate Change in Temperature Caused by Advection,

$$\frac{\partial T}{\partial t} = -U_x \cdot \frac{\partial T}{\partial x}$$

Dispersion processes occur in both the upstream and downstream direction along the longitudinal axis. Heat energy contained in the system is conserved throughout dispersion, and similar to advection, heat energy is simply moved throughout the system. The rate change in temperature due to dispersion is expressed in the second order partial differential equation below.

Equation A-6. Rate Change in Temperature Caused by Dispersion,

$$\frac{\partial T}{\partial t} = D_L \cdot \frac{\partial^2 T}{\partial x^2}$$

The dispersion coefficient (D_L) may be calculated by stream dimensions, roughness and flow. In streams that exhibit high flow velocities and low longitudinal temperature gradients, it may be assumed that the system is advection dominated and the dispersion coefficient may be set to zero (Sinokrot and Stefan 1993). In the event that dispersion effects are considered significant, the appropriate value for the dispersion coefficient can be estimated with a practical approach developed and employed in the QUAL 2e model (Brown and Barnwell 1987). An advantage to this approach is that each parameter is easily measured, or in the case of Manning's coefficient (n) and the dispersion constant (K_d), estimated.

Equation A-7. Physical Dispersion Coefficient,

$$D_L = C \cdot K_d \cdot n \cdot U_x \cdot D^{\frac{5}{6}}$$

Where,

C:		Unit conversion
		C = 3.82 for English units
		C = 1.00 for Metric units
D:		Average stream depth (m)
D_L:		Dispersion coefficient (m^2/s)
K_d:		Dispersion constant
n:		Manning's coefficient
U_x:		Average flow velocity (m/s)

The simultaneous non-uniform one-dimensional transfer of heat energy is the summation of the rate change in temperature due to heat energy thermodynamics, advection and dispersion. Given that the stream is subject to steady flow conditions and is well mixed, transverse temperature gradients are negligible (Sinokrot and Stefan 1993). An assumption of non-uniform flow implies that cross-sectional area and flow velocity vary with respect to longitudinal position. The following second ordered parabolic partial differential equation describes the rate change in temperature for non-uniform flow.

Equation A-8. Non-Uniform One-dimensional Heat Energy Transfer,

$$\frac{\partial T}{\partial t} = -U_x \cdot \frac{\partial T}{\partial x} + D_L \cdot \frac{\partial^2 T}{\partial x^2} + \frac{\Phi}{c_p \cdot \rho \cdot D_i}$$

$$\text{Steady Flow: } \frac{\partial U_x}{\partial t} = 0$$

$$\text{Non-Uniform Flow: } \frac{\partial U_x}{\partial x} \neq 0$$

The solution to the *one-dimensional heat energy transfer equation* is essentially the summation of thermodynamic heat energy exchange between the stream system and the surrounding environment and physical processes that redistribute heat energy within the stream system. It is important to note that all heat energy introduced into the stream is conserved, with the net heat energy value reflected as stream temperature magnitude. Further, heat energy is transient within the stream system, due to longitudinal transfer of heat energy (i.e., advection and dispersion). The net heat energy flux (Φ) is calculated at every distance step and time step based on physical and empirical formulations developed for each significant energy component. The dispersion coefficient (D_L) is assumed to equal zero.

BOUNDARY CONDITIONS AND INITIAL VALUES

The temperatures at the upstream boundary (i_o) for all time steps (t_o, t_1,..., t_{M-1}, t_M) are supplied by the upstream temperature inputs. At the downstream boundary temperature at longitudinal position i_{n+1} is assumed to equals that of i_n with respect to time t. Initial values of the temperatures at each distance node (i_o, i_1,..., i_{N-1}, i_N) occurring at the starting time (t_o) can be input by the model user or assumed to equal the boundary condition at time t_o.

SPATIAL AND TEMPORAL SCALE

The lengths of the defined reaches are 100 feet. The temperature model is designed to analyze and predict stream temperature for one day and is primarily concerned with daily prediction of the diurnal energy flux and resulting temperatures on July 27 through 30, 1999. Prediction time steps are limited by stability considerations for the finite difference solution method.

INPUT PARAMETERS

Data collected during this TMDL effort has allowed the development of temperature simulation methodology that is both spatially continuous and spans full day lengths (diurnal). Detailed spatial data sets have been developed for the following parameters:

- ✓ River and Tributary Digital Mapping at 1:5,000 scale (**Figure A-22**),
- ✓ Riparian Vegetation Species, Size and Density Digital Mapping at 1:3,000 scale (**Figure A-23**),
- ✓ West, East and South Topographic Shade Angles calculations at 1:5,000 scale (**Figure A-24**),
- ✓ Stream Elevation and Gradient at 1:5,000 scale,
- ✓ Hydrology Developed from Field Data - Spatially Continuos Flow, Wetted Width, Velocity and Depth Profiles.

All input data is longitudinally referenced in the model allowing spatial and/or continuous inputs to apply to certain zones or specific river segments.

Spatial Input Parameters

Longitudinal Distance (meters): Defines the modeled reaches for which spatial input parameters reference. Model reaches are 100 feet each, are derived from DOQ 1:5000 river layer digitized from Digital Orthophoto Quarter Quads (DOQQs), and are measured in the downstream direction (**Figure A-22**).

Elevation (meters): Sampled for each model reach either from Digital Raster Graphic (DRG) or Digital Elevation Model (DEM).

Gradient (%): Is the difference between the upstream and downstream elevations divided by the reach length.

Bedrock (%): The percent of streambed material that has a diameter of 25 cm or greater. Values are derived from stream survey data or assumed where data is limited.

Aspect (decimal degrees from North): Calculated for each reach break (**see Figure A-22**) and represents the direction of stream flow.

Flow Volume (cubic meters per second): Measured by DEQ with standard USGS protocols with interpolation between flow measurement sites, while taking into account known water withdrawals and inputs.

Flow Velocity (meters per second): Derived from Manning's equation and Leopold power functions calibrated to measured flow velocity data.

Wetted Width (meters): Derived from Manning's equation and Leopold power functions calibrated to measured wetted width data.

Average Depth (meters): Derived from Manning's equation and Leopold power functions calibrated to measured average depth data. Calculated based on assuming rectangular channel.

Near-Stream Disturbance Zone Width (meters): Based upon ODEQ field measurements and USGS reported values.

Channel Incision (meters): Depth of the active channel below riparian terrace or floodplain. Measured by ODEQ and reported by USGS.

Riparian Height (meters): Obtained from WODIP satellite vegetation coverage and ODEQ field observations.

Canopy Density (%): Obtained from WODIP vegetation coverage and aerial photograph (DOQ) interpretation.

Riparian Overhang (meters): Distance of riparian vegetation intrusion over Near-Stream Disturbance Zone. Based on ODEQ field observations.

Topographic Shade Angle (decimal degrees): The angle made between the stream surface and the highest topographic features to the west, east and south as calculated from DEM at each stream reach (**Figure A-24**).

Continuous Input Parameters

Wind Speed (meters per second): Hourly values measured at Forest Grove and at Hillsboro Airport.

Relative Humidity (%): Hourly values measured at Forest Grove and at Hillsboro Airport.

Air Temperature (^{o}C): Hourly values measured at Forest Grove and at Hillsboro Airport.

Stream Temperature (^{o}C): Hourly values measured by ODEQ.

Tributary Temperature (^{o}C): Hourly values measured by ODEQ.

Tributary/Flow Volume (cubic meters per second): Measured flow volumes for all major tributaries.

DATA SOURCE DESCRIPTIONS

Existing Vegetation:

1. WODIP satellite vegetation coverage that has been delineated into polygons according to vegetation species, size, and canopy density (BLM, 1999). The pixel size of this data is 25 meters. Tree sizes were presented as diameter at breast height (DBH) ranges. The mid-range DBH was used to calculate approximate heights for each species. All coverage was verified using Digital Orthophoto Quarter Quads (DOQQs) or Digital Orthophoto Quads (DOQs). (**Figure A-25**)
2. In agricultural areas, WODIP overlooked narrow riparian buffers. In these areas, ODEQ digitized the vegetation from DOQQs at a 1:3000 scale (**Figure A-22**). Canopy densities were assigned according to aerial photograph (DOQQ) interpretation, while heights were assigned based upon field measurements. Additionally, roads were digitized from the DOQQs for all areas.

Digital Elevation Models (DEM): 30-meter DEMs are available for the entire state of Oregon. These DEMs have a 30-meter pixels, each of which have an elevation associated with it.

Digital Orthophoto Quarter Quads (DOQQs): DOQQs for the Tualatin River subbasin are available from the United States Geologic Survey (the aerial photos were taken in 1997). USGS DOQQs correspond to the topographic map quarter quadrants.

Figure A-22.   Model Methodology - Stream Digitization and 100-Foot Reach Breaks on a Digital Orthophoto Quarter Quad (DOQQ) (1:3000 Scale)

Figure A-23.   Model Methodology - Vegetation Data (300 feet on both sides of the stream) Overlaying DOQQs for Visual Inspection (1:3000 Scale)

Figure A-24. Model Methodology - Calculation of Topographic Shade from the DEM
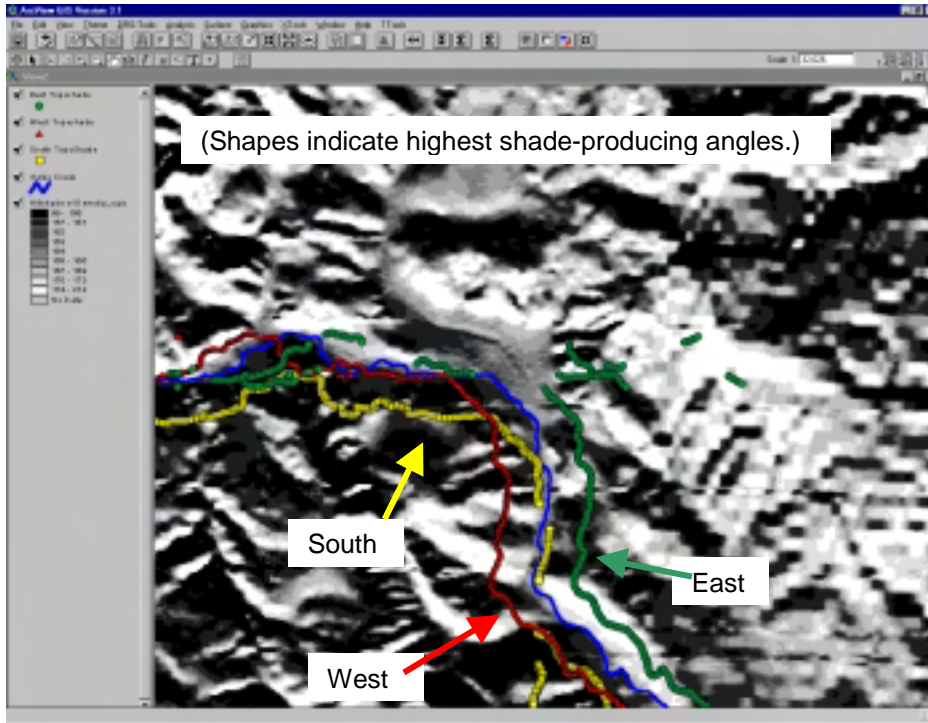
Figure A-25. Model Methodology – WODIP Vegetation Layer.
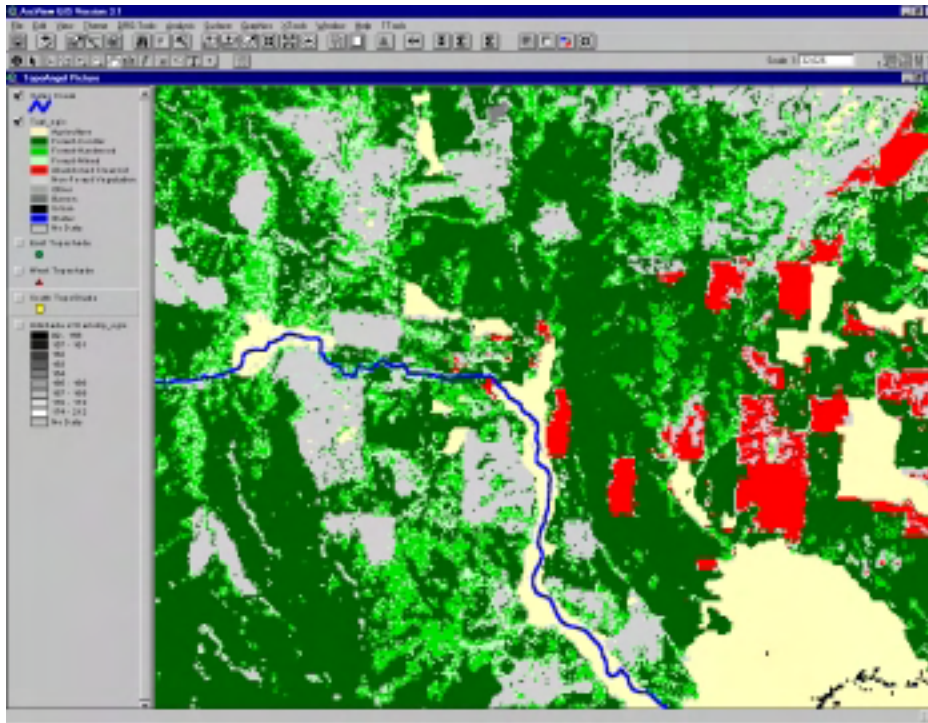
CURRENT CONDITIONS, MODEL INPUTS, AND MODEL RESULTS

TUALATIN RIVER SUBBASIN OVERVIEW

303(d) Stream Temperature Impairments

Extensive water temperature monitoring has occurred in the Tualatin River Subbasin during the past several decades. Two types of temperature data exist for the Tualatin River and tributaries: continuous measurements (Temporal) and forward-looking infrared radiometer (FLIR) thermal imagery (Spatial). A seven-day moving average of daily maximums (7-day statistic) was adopted as the statistical measure of the stream temperature standard. Absolute numeric criteria are deemed action levels and water quality standard compliance (**Table A-10**). Based on this past data collection, numerous streams within the Tualatin River subbasin are listed as violating the temperature standard **(OAR 340-41-0445)** (**Figure A-26**)

Willamette Basin Temperature Standard

OAR 340-41-445(2)(b)(A) No measurable surface water temperature increase resulting from anthropogenic activities is allowed:
(i)   In a basin for which salmonid fish rearing is a designated beneficial use, and in which surface water temperatures exceed 64°F (17.8^{o}C);
(iv)   In waters and periods of the year determined by the Department to support native salmonid spawning, egg incubation and fry emergence from the egg and from the gravels in a basin which exceeds 55°F (12.8^{o}C);
(vi)   In waters determined by the Department to be ecologically significant cold-water refugia[*];
(vii)   In stream segments containing federally listed Threatened and Endangered species if the increase will impair the biological integrity of the Threatened and Endangered population.
(viii) In Oregon waters when the dissolved oxygen (DO) levels are within 0.5 mg/l or 10% saturation of the water column or intergravel DO criterion for a given stream reach or subbasin;
(ix)   In natural lakes.

Table A-10. Applicable Water Temperature Standards	
OAR 340-41-445(2)(b)(A) WATER TEMPERATURE STANDARD	**7-Day Statistic**
Basic Absolute Criterion – Applies year long in all streams in the basin, with the exception of those that qualify for the *salmonid spawning, egg incubation and fry emergence criterion* -or- *bull trout criterion.*	$\leq 64^{o}$F (17.8^{o}C)
Salmonid Spawning, Egg Incubation and Fry Emergence Criterion – Applies to stream segments designated as supporting native salmonid spawning, egg incubation and fry emergence for the specific times of the year when these uses occur.	$\leq 55^{o}$F (12.8^{o}C)
Bull Trout Criterion – Applies to waters determined by the Department to support or to be necessary to maintain the viability of Bull Trout in the basin.	$\leq 50^{o}$F (10.0^{o}C)

---

[*] Ecologically Significant Cold-Water Refugia exists when all or a portion of a waterbody supports stenotype cold-water species (flora or fauna) not otherwise supported in the sub-basin, and either: (a) maintains cold water temperatures (below numeric criterion) throughout the year relative to other stream segments throughout the sub-basin, or (b) supplies cold water to a receiving stream or downstream reach that supports cold water biota.

Figure A-26. Tualatin River Subbasin Stream Segments on the 1998 303(d) List for Temperature Violations (Bolded Lines).

Continuous Stream Temperature Data Availability

In an attempt to quantify the temporal thermal patterns of the Tualatin River and its tributaries, several academic institutions and government agencies have collected continuously recording stream temperature data. Digital thermistors have excellent temperature resolution ($\pm0.2^{o}$C) and are capable of collecting thousands of measurements at user defined time intervals. Continuos temperature data is necessary to calculate the 7-day temperature statistic. A summary of calculated seven-day temperature statistics for waters the Tualatin River Subbasin during 1996 through 1998 are listed in **Table A-11** and site locations are illustrated in **Figure A-27**.

Figure A-27.   Tualatin River Subbasin Continuous Temperature Monitoring Sites (1996-1998)
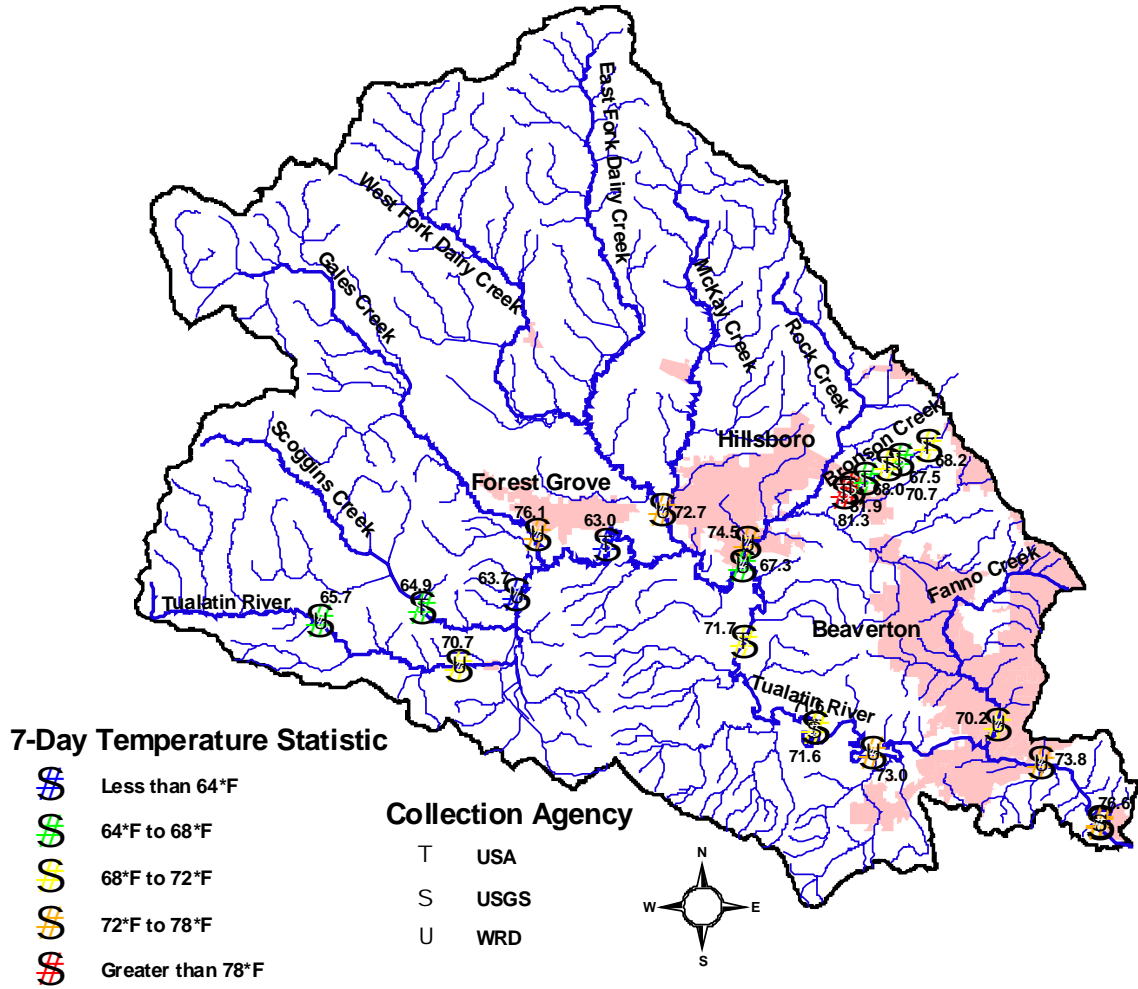
Table A-11. Temperature Monitoring Sites and calculated 7-day Statistics ("-" indicates that no temperature data was Available)		Maximum 7-day Statistic		
Site	River Mile	1996	1997	1998
Bronson Creek				
Bronson Creek at Saltzman	5.1	68.7	65.7	68.1
Bronson Creek at 143rd	4.0	-	67.4	-
Bronson Creek at West Union	3.1	68.0	68.5	70.7
Bronson Creek at Bronson Blvd.	2.2	68.4	65.4	70.2
Bronson Creek at Bronson Creek Park	2.0	68.1	-	-
Bronson Creek at Tanasbourne Pond (Upper end)	2.0	72.5	-	78.3
Bronson Creek at Tanasbourne Pond (Lower end)	2.0	85.9	-	83.8
Bronson Creek at 185th	1.4	80.7	81.8	-
Bronson Creek at Walker Road	1.1	81.4	-	-
Bronson Creek at Banister	1.0	-	62.9	63.8
Tualatin River				
Tualatin River at Lee Falls	71.07	-	67.2	65.7
Tualatin River at Gaston	63.87	-	72.1	70.6
Tualatin River at Scoggins Creek	60.0	-	62.9	65.0
Tualatin River at Dilley	57.84	-	61.9	63.7
Tualatin River at Golf Course Road	51.54	-	63.1	62.9
Tualatin River at Rood	38.44	-	66.0	67.2
Tualatin River at Farmington	33.3	-	68.3	-
Tualatin River at RM 24.5	24.5	-	70.4	71.7
Tualatin River at Elsner	16.22	-	72.1	73.0
Tualatin River at Lake Oswego Canal	6.7	-	72.4	73.8
Tualatin River at Lake Oswego Dam	3.4	-	74.0	75.7
Tualatin River at West Linn	1.75	-	76.0	76.7
Dairy Creek				
Dairy Creek at Highway 8	2.06	-	70.4	72.8
Dawson Creek				
Dawson Creek at Shute	2.3	-	67.8	72.5
Dawson Creek at Airport	1.7	-	74.7	-
Dawson Creek at Brookwood	0.6	-	73.7	72.5
Fanno Creek				
Fanno Creek at Durham Road	1.2	-	71.0	70.2
Gales Creek				
Gales Creek at Highway 47	1.7	-	73.4	76.0
Rock Creek				
Rock Creek at Highway 8	1.25	-	71.4	74.5

Supplemental Data Availability

During the summer of 1999, the Oregon Department of Environmental Quality collected continuous water temperature, flow, and habitat data at over seventy sites along several tributaries streams of the Tualatin River subbasin. Efforts focussed on **1)** Gales Creek, **2)** West Fork Dairy Creek, **3)** East Fork Dairy Creek, **4)** Dairy Creek, **5)** McKay Creek, **6)** Rock Creek, **7)** Fanno Creek, as well as **8)** the upper Tualatin River. Site locations are illustrated in **Figure A-28**. Discussion pertaining towards collected ODEQ temperature data is presented below.

Figure A-28.   DEQ 1999 Data Collection Sites.
[Circles indicate site locations]
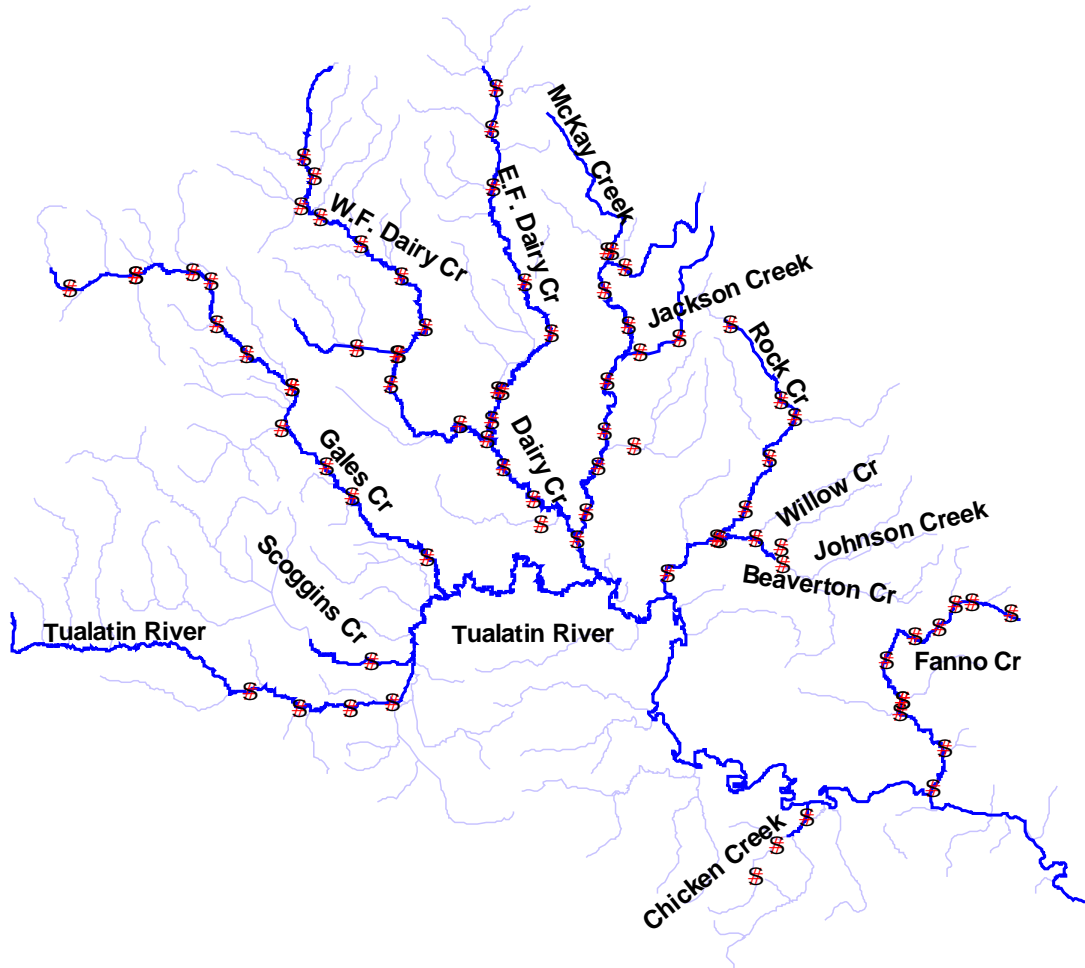
FLIR Stream Temperature Data Availability

Forward -Looking Infrared Radiometer (FLIR) thermal imagery was collected for the Tualatin River and many tributary reaches (**Table A-12**). Specifically, a total of 245.1 stream miles were "flown" with FLIR in the Tualatin River subbasin during the summer of 1999. FLIR imagery coupled with color video and geographic positioning systems (GPS) produces spatially continuous temperature imagery. Data collection occurred between July 26th and 30th, 1999. Late days near maximum temperatures were sampled. FLIR images are collected with instruments mounted to a helicopter, which measured surface temperatures.

The overriding strength of FLIR temperature analysis is spatial continuity and perhaps the greatest contribution of FLIR technology is its ability to display thermal habitat fragmentation of warmed reaches separated by isolated cool-water refugia. Before the advent of FLIR stream temperature analysis, the variability of stream temperature was vastly understated. This variability has been cited for the continued existence of cold water fish in relatively warm water rivers/streams. McIntosh et al. (1995) and Torgersen et al. (1995) demonstrated that cold water fish commonly utilize cooler reaches and habitats during times that vast portions of rivers/streams maintain stressful and/or lethal warm water temperatures. The presence of cool-water refugia can help salmonids avoid areas with adverse stream temperatures. When ambient stream temperatures are too warm, sensitive aquatic species can inhabit these patches of cool-water habitat. Deep pools, cool springs, hyporheic flow, and the junction of cooler tributary streams are all examples of cool-water refugia.

Table A-12. FLIR Temperature Sampled Locations in the Tualatin River Subbasin.			
Stream	**Date**	**Local Time (PM)**	**Miles**

Tualatin River
 	
    Lower (Mouth to Wapato Creek)
    Upper (Wapato Crk to Head waters)
	27 July 99	2:58 – 4:04
		5:19 – 5:35
			80.7

Scoggins Creek	28 July 99	2:15 – 2:30	14.8
Gales Creek	28 July 99	2:42 – 3:16	27.4
Dairy Creek	28 July 99	4:49 – 5:02	10.1
West Fork Dairy Creek	28 July 99	5:02 – 5:27	20.0
East Fork Dairy Creek	29 July 99	5:00 – 5:23	21.5
McKay Creek	29 July 99	4:16 – 4:48	22.4
Fanno Creek	29 July 99	2:28 – 2:54	12.5
Rock Creek	30 July 99	2:18 – 2:29	12.6
Beaverton Creek	30 July 99	2:38 – 2:47	7.8
Chicken Creek	30 July 99	4:18 – 4:23	6.6
McFee Creek	30 July 99	4:29 – 4:32	2.9
Clear Creek	30 July 99	4:52 – 4:56	4.0
Wapato Creek	27 July 99	4:00 – 4:12	1.8
Total Miles Surveyed			**245.1**

FLIR DATA COLLECTION METHODS

Data are collected using a FLIR and a Day TV video camera. The two sensors are co-located in a gyro-stabilized mount that is attached to the underside of a helicopter. The helicopter is flown longitudinally over the center of the stream channel with the sensors in a vertical (or near vertical) position. Data collection is timed to capture daily maximum stream temperatures, which typically occur between 14:00 and 18:00 hours. The flight altitude depends upon several factors including stream width, sinuosity, and flight safety. Typical altitudes are between 1000 ft and 2500 ft above ground level. At these altitudes, the ground sample size per image pixel is less then 0.5 meters.

The FLIR sensor detects emitted radiation at wavelengths from 8-12 microns (also known at the thermal infrared long wave). This band is used for two reasons. First, solar reflections are insignificant in this band. And second, natural objects such as water have their peak emitted thermal infrared energy in this band. The sensor used for the 1999 FLIR surveys is calibrated

and has an instrumental accuracy of within 0.1^oC (when tested against an extended area blackbody).

FLIR images are recorded directly from the sensor to an on-board computer. Each image pixel contains a measured value that can be directly converted to a temperature. The pixel values represent the full dynamic range of the sensor. Images are collected at a rate that provides 40 to 60% overlap between images. All images are tagged with time and position data provided by a Global Positioning System (GPS).

Day TV images are recorded to an on-board a videocassette recorder at a rate of 30 frames/second. GPS time and position are encoded on the recorded video. The Day TV camera is aligned to present the same ground area as the thermal infrared. The day TV video supplements the interpretation and analysis of the FLIR images. In addition, day TV video provides a record of the conditions in the basin at the time of the survey.

In-stream data loggers are distributed in the basin prior to the survey. These sensors are used to ground truth (i.e., verify the accuracy of) the FLIR imagery. The number and location of the sensors depends on the survey characteristics such as survey length. A long survey may use four or more points. As a minimum, at least two sensors are "flown over" per flight and at least one per stream. Meteorological conditions including air temperature, wind speed, relative humidity, and sky conditions are recorded for the time(s) of the survey.

FLIR DATA PROCESSING

Pre-processing

A computer program is used to scan the FLIR imagery and create a GIS (geographic information system) point coverage. This coverage shows the spatial extent of the survey and allows for the integration of the FLIR with other spatially explicit data layers. In addition, the coverage is used to identify the FLIR images associated with the ground truth locations.

The data collection software is used to extract radiant temperature values from the associated images at the location of the in-stream data loggers. The temperature calculation is based on the radiant energy emitted from the water and corrected for atmospheric effects. The radiant temperatures are compared to the kinetic temperatures from the in-stream data loggers to assess the accuracy of the FLIR data. In most cases, the FLIR data is consistent to with the in-stream data loggers. If a consistent offset is observed (i.e., all in-stream measurements are 1^oC warmer then the radiant values), this information is used to adjust the atmospheric transmission value, which is estimated in the calculation.

The ground truth method provides a way to fine tune of the imagery and also provides a measure of overall accuracy. The advertised accuracy of in-stream data loggers (such as Vemcos or Onset Stowaways) is typically very good ($\pm 0.2^o$C). If an inconsistency is observed (typically > 1^oC) between the radiant and measured in-stream temperature, then the reason for this inconsistency is investigated.

The image points are associated with a river kilometer using the dynamic segmentation features of Arc/Info GIS software. The river kilometers are derived from 1:100K "routed" stream covers from the Environmental Protection Agency (EPA). The route measures provide a spatial context for developing longitudinal temperature profiles of stream temperature.

FLIR Temperature Data Processing

In the laboratory, a computer algorithm was used to convert the raw thermal images (radiance values) to a generic "raw" image format. During the conversion, the program records the minimum and maximum temperature value found in each image. The images can then be displayed in the GIS environment for a selected image point. The images are color-coded in one-degree increments over temperature range normally associated with natural water.

Once in the raw format, the images are analyzed to derive the minimum, maximum, and median stream temperatures. To derive these measures, an analyst uses a GIS program to sample the image pixel (temperature) values in the stream channel. Ten sample points are taken longitudinally in the center of the stream channel. Samples are taken to provide complete coverage without sampling the same water twice (there is approximately 40-60% overlap between images). Where there are multiple channels, only the main channel (as determined by width and continuity) is sampled. In cases where the channel is obscured by vegetation the next image where the stream channel was clearly visible is sampled. For each sampled image, the sample minimum, maximum, median, and standard deviation are recorded directly to the point coverage attribute file.

The temperature of tributaries and other detectable surface inflows are also sampled from images. These inflows are sampled at their mouth using the same techniques described for sampling the mainstem channel. If possible, the surface inflows are identified on the USGS 24K base maps. The inflow name and median temperature are then entered into the point coverage attribute file.

FLIR Quality Checks

Thermal accuracy is checked against in-stream data loggers. Observed accuracy is on average within $\pm 0.4^{\circ}$C of the in-stream sensors. This is characteristic of the "noise" observed during sampling.

FLIR sensors measure the temperature at the water surface. On free flowing streams, water columns are usually well mixed and surface temperatures represent the temperature of the water column. The exception is in thermally stratified areas that may occur in slow, deep channels; upstream of impoundments; in deep pools and pools with large gravel bars at the upstream end; and in certain shallow pools with subsurface seepage. Some of these areas are identified in the analysis based on a number of different methods including image interpretation, flow conditions, stream gradient, in-stream sensors, and local knowledge.

The longitudinal profile is reviewed to look for outliers in the profile. These image points are checked for sampling errors.

TUALATIN RIVER MAINSTEM[*]

CURRENT CONDITION

Continuous temperature data measured by digital thermistors can provide a spatial component when longitudinal sampling is performed (i.e., multiple monitoring sites along a particular stream reach). Utilizing such a technique illustrates that observed water temperature in the Tualatin River increase dramatically as the river travels downstream from the headwaters to the mouth (**Figure A-29**). It is important to note that observed water temperatures are already above the 64°F temperature criteria less than 10 miles from the headwaters and continue to increase downstream.

The cooling effect from Henry Hagg Lake dam releases, via Scoggins Creek, is a prominent feature in the stream heating trend illustrated in **Figure A-29**. It is important to point out that water temperatures progressively increase as the river travels further downstream from this location, with the 7-day statistics approaching 78°F near the mouth of the Tualatin River. Very little annual variability was observed between the 1997 and 1998 sampling seasons indicating that similar stream heating conditions occurred between years.

Figure A-29.   Maximum 7-day Statistics in the Tualatin River During 1997 and 1998
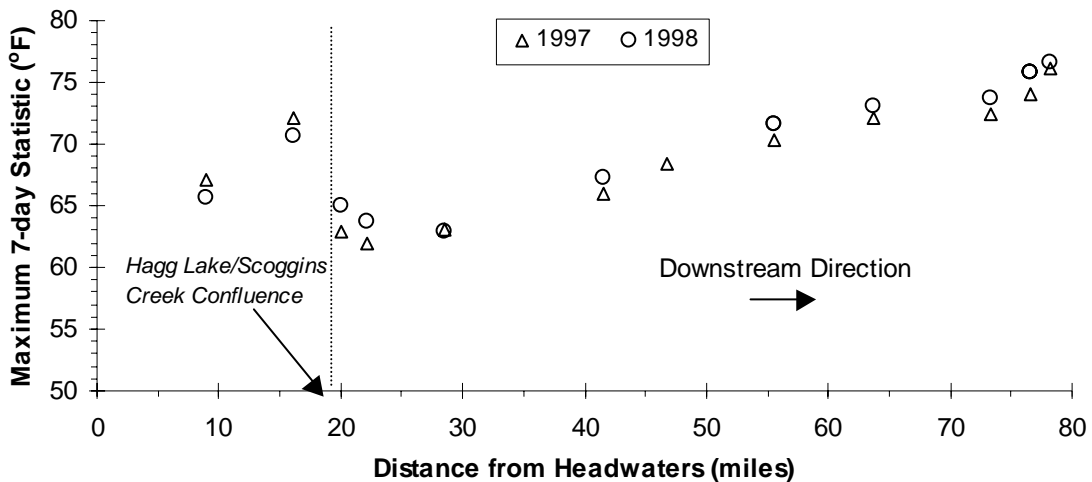
TEMPERATURE PATTERNS

Both stream temperature and flow in the Tualatin River subbasin vary seasonally from year to year. Water temperatures are coolest in winter and early spring months. Stream temperatures exceed State water quality standards in summer and early fall months (June, July, August and September). **Figure A-30** illustrates seasonal temperature patterns observed in the mainstem Tualatin River during the summer of 1998. Warmest stream temperatures correspond to prolonged solar radiation exposure, warm air temperature, low flow conditions and decreased groundwater contribution. These conditions occur during summer and early fall. During the summer of 1998, it appears that the Hagg Lake withdrawal water was significantly cooler than the

---

[*] Note that the river miles (RM) presented in this report were derived from a 1:5000 stream coverage used for ODEQ modeling purposes and may differ slightly from other sources (such as OWRD or USGS river miles).

Tualatin River mainstem. In contrast, during the fall months the Hagg Lake withdrawal water was **warmer** than the Tualatin River mainstem (**see Figure A-30**).

Figure A-30.   Tualatin River Mainstem Seasonal Variability (*1998*)
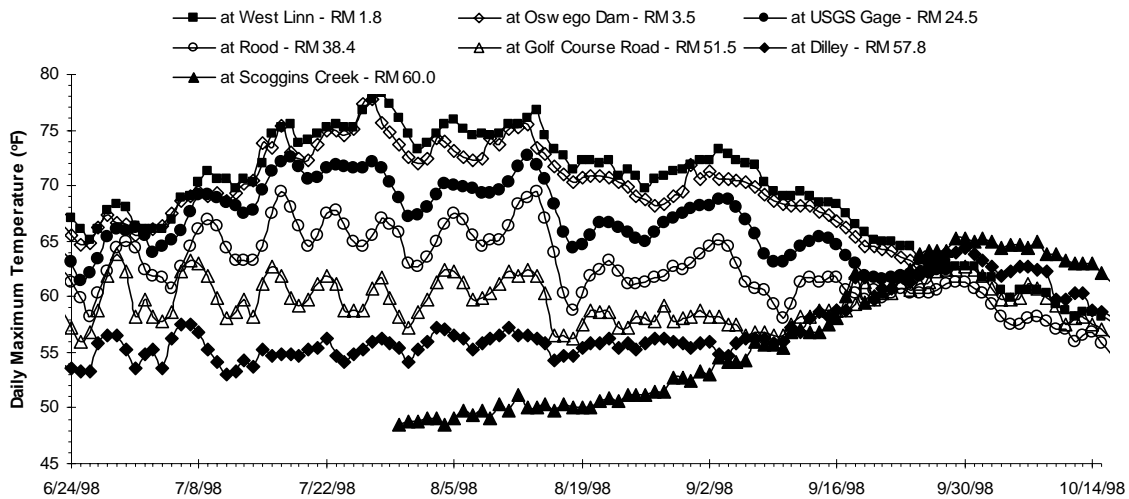
The diurnal water temperature trend observed in the mainstem Tualatin River shows that water temperature are at a daily maximum during the late afternoon, and at a daily minimum during the early morning period (**Figure A-31**). It is important to point out that the diurnal temperature variability decreases at downstream locations, with very little variability observed on the Tualatin River at Oswego Dam (RM 6.7). This may be expected because deep water bodies generally lose and gain heat energy at a much slower rate than shallow rivers with large exposed surface areas. Finally, a longitudinal water temperature increase is clearly illustrated in **Figure A-31**. That is, water temperature increases in a downstream direction.

Figure A-31.   Tualatin River Diurnal Temperature Profiles
Downstream of the Scoggins Creek Confluence

A-59
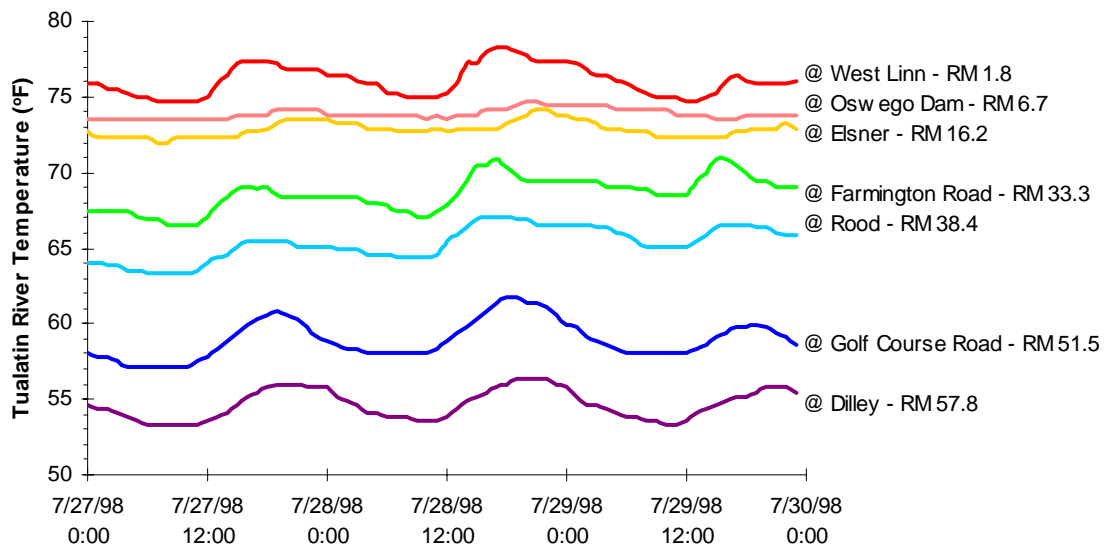
The Oregon Department of Environmental Quality collected water quality data in the Tualatin River mainstem during the summer of 1999. This effort included the collection of continuous temperature data, FLIR temperature data, flow measurement and site descriptions. Sampling locations are illustrated in **Figure A-32**. Digital photographs taken at several Tualatin River sampling locations are presented in **Image A-2** through **Image A-5**.

Tualatin River temperatures increase during the summer period, with maximum temperatures occurring in late July (**Figure A-30**). Accordingly, FLIR thermal imagery was collected on July 27, 1999. Flow measurements were also collected during this period. The longitudinal 7-Day temperature statistic profile for the Tualatin River and several tributaries are presented in **Figure A-34**. Observed tributary temperatures were often well above the temperature criteria. Calculated 7-day temperature statistics for the Tualatin River in 1999 are presented in **Table A-13**. It is important to note that additional water temperature data was collected for the mainstem Tualatin River by several agencies. However, 7-Day Temperature Statistics were only calculated from ODEQ data. Recall that **Table A-11** presents calculated 7-Day Statistic for the Tualatin River mainstem from 1996 through 1998.

Figure A-32.   Water Quality Sampling locations for Tualatin River during the Summer of 1999.
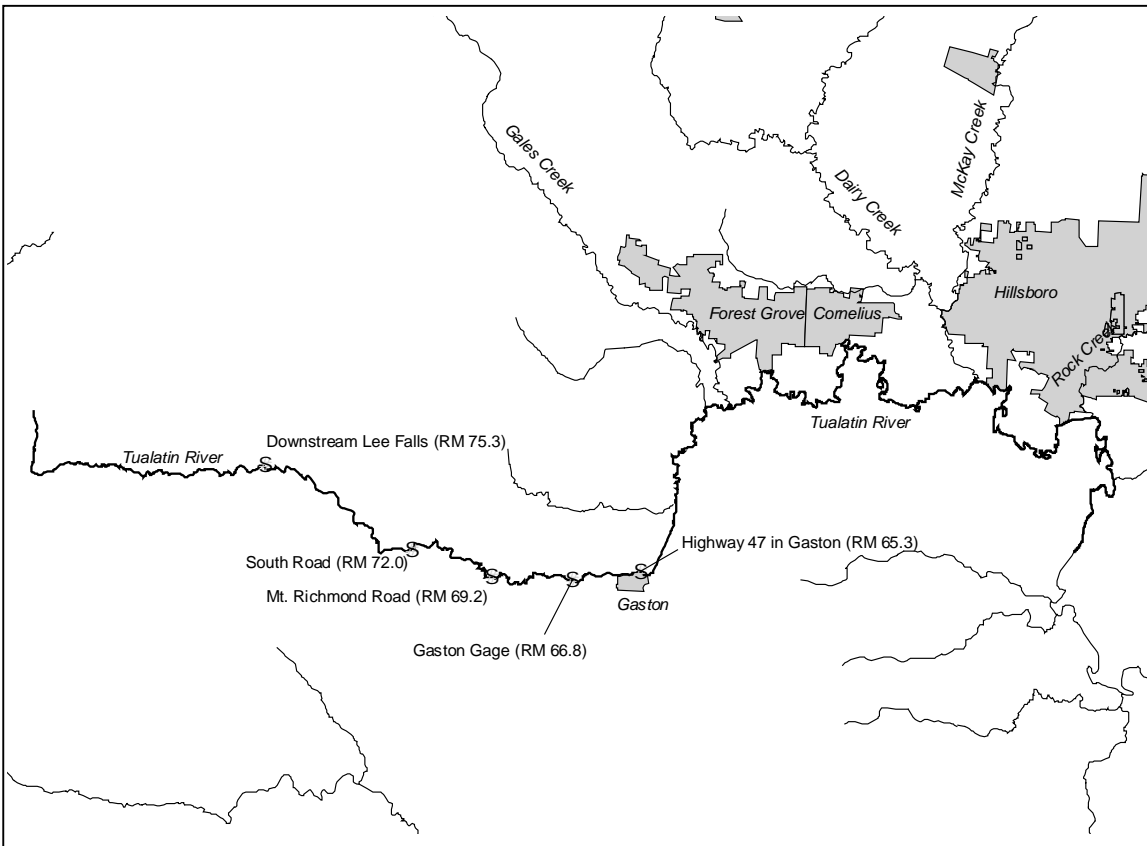
Image A-2. Upper Tualatin River at Hwy 47 (Gaston) (River Mile 65.3).
[Temp. Statistic – 69.4*F, Flow – 30.5 cfs, Potential Effective Shade (ES) – 88%, Measured ES – 78%]

Image A-3. Upper Tualatin River at Gaston Gage (River Mile 66.8).
[Temp. Statistic – 70.2*F, Flow – 29.7 cfs, Potential Effective Shade (ES) – 93.1%, Measured ES – 82%]
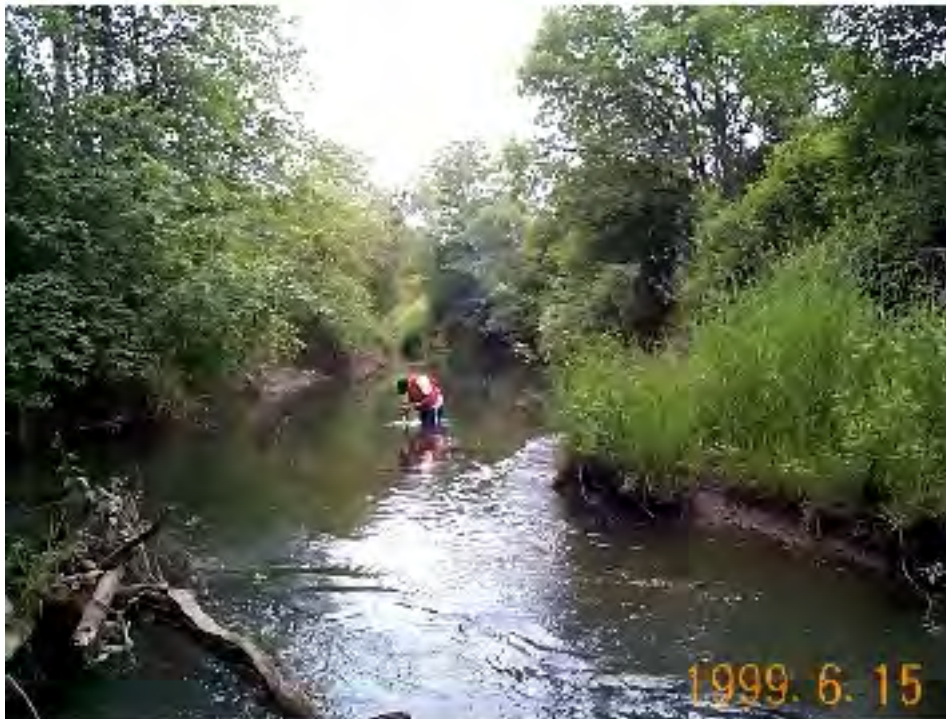
Image A-4. Upper Tualatin River @ Mount Richmond Road (River Mile 69.2).
[Temp. Statistic – 70.3*F, Flow – 32.0 cfs, Potential Effective Shade (ES) – 79%, Measured ES – 56%]

Image A-5. Upper Tualatin River @ South Road (River Mile 72.0).
[Temp. Statistic – N/A, Flow – 33.3 cfs, Potential Effective Shade (ES) – 87%, Measured ES – 94%]

Figure A-33.   Observed daily maximum temperatures for the Tualatin River in 1999.
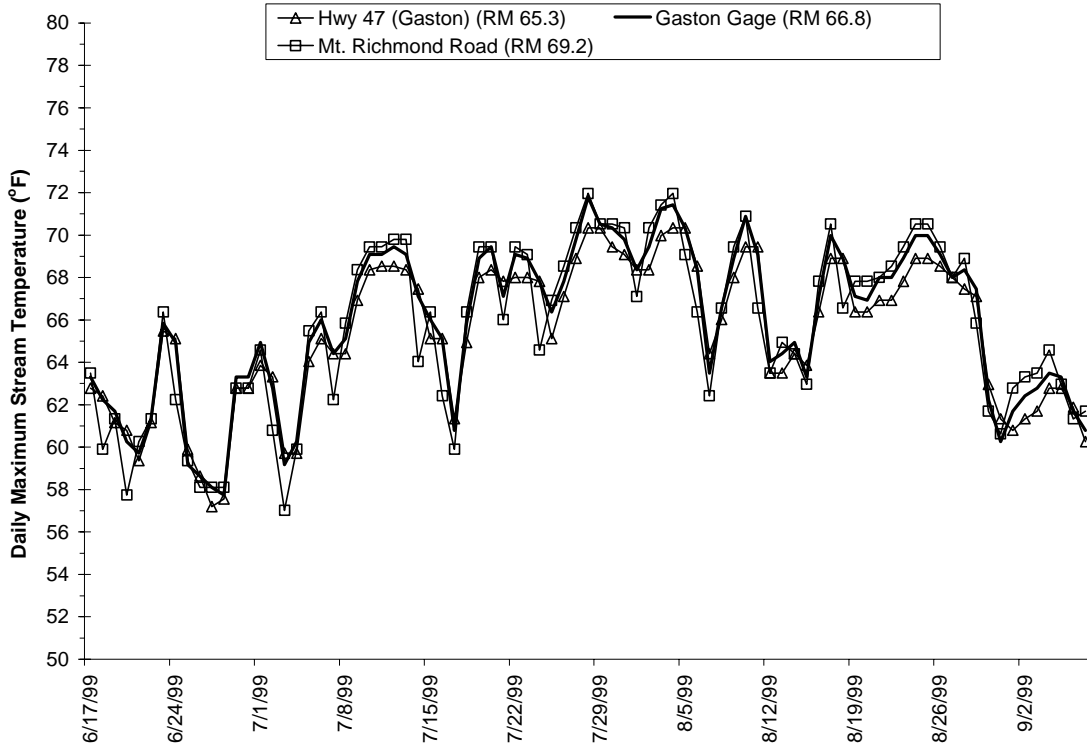
Table A-13. Calculated 7-Day Temperature Statistics for the Tualatin River in 1999.						
Temperature Site *(RM = River Mile from mouth)*	*Start* *Date*	*End* *Date*	*Max Temp.* *(Date)*	*(°F)*	*7-Day Statistic* *(Date)*	*(°F)*
Upper Tualatin River						
RM 62.25 (@ Hwy 47 (Gaston))	6/17/99	9/13/99	8/05	70.3	8/01	**69.4**
RM 63.8 (@ Gaston Gage)	6/17/99	9/13/99	7/28	71.8	7/31	**70.2**
RM 66.2 (@ Mount Richmond Road)	6/17/99	9/13/99	8/04	72.0	7/31	**70.3**

Figure A-34.   Observed daily maximum temperatures for the Tualatin River in 1999.
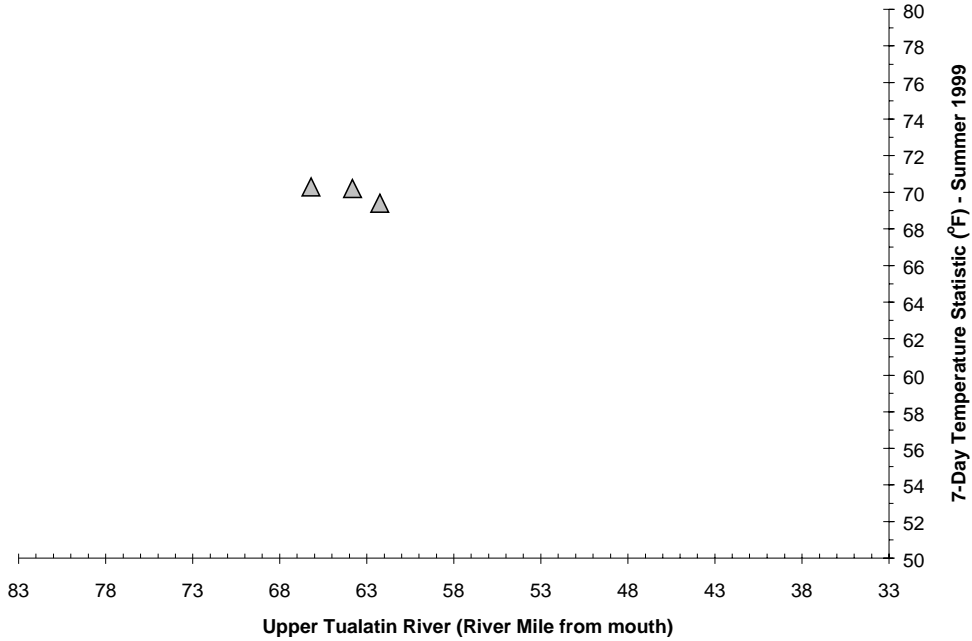
Water temperatures in the Tualatin River varied through out the course of the day, with maximum temperatures occurring in the late afternoon and minimums temperature occurring during the early morning hours. Diurnal temperature profiles for the Tualatin River on July 27, 1999 are presented in **Figure A-35**.

Figure A-35.   Diurnal temperature trends observed in the Tualatin River on July 27, 1999.
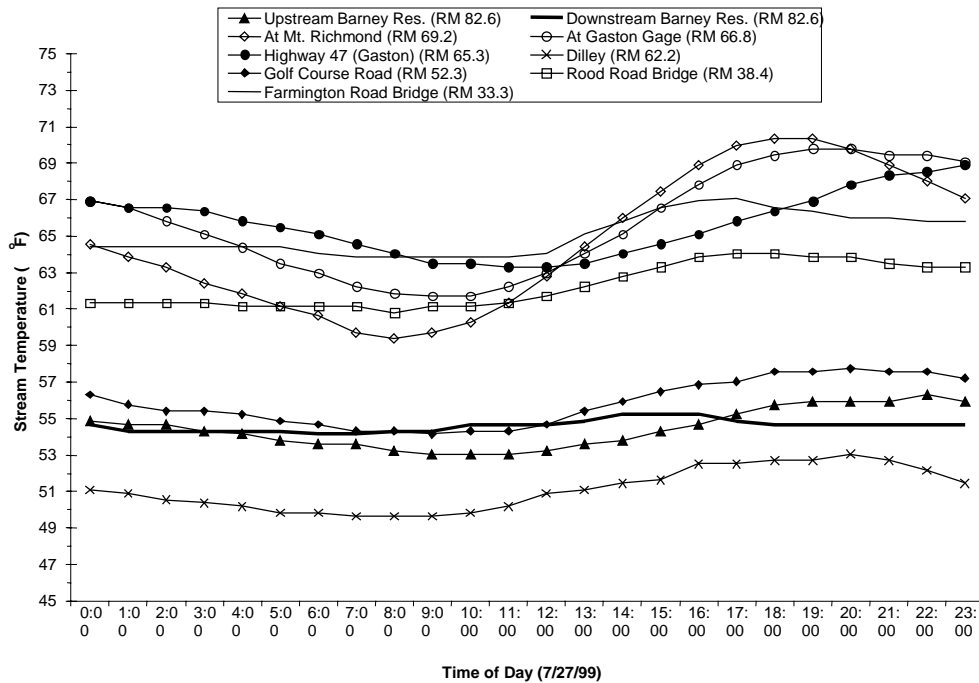
Flows were measured throughout the Tualatin River during the period of FLIR sampling, which corresponds to the period of summer maximum water temperatures. Flow rates generally increase in a downstream direction. Releases from Hagg Lake enter the Tualatin River via Scoggins Creek, increasing the mainstem flow by approximately 170 cubic feet per second. Nearly five miles downstream from Scoggins Creek, the Springhill Pumping Plant was withdrawing 105 cubic feet per second for municipal and irrigation uses on July 27, 1999.

Figure A-36. Water discharge observed in the Tualatin River on July 27, 1999.
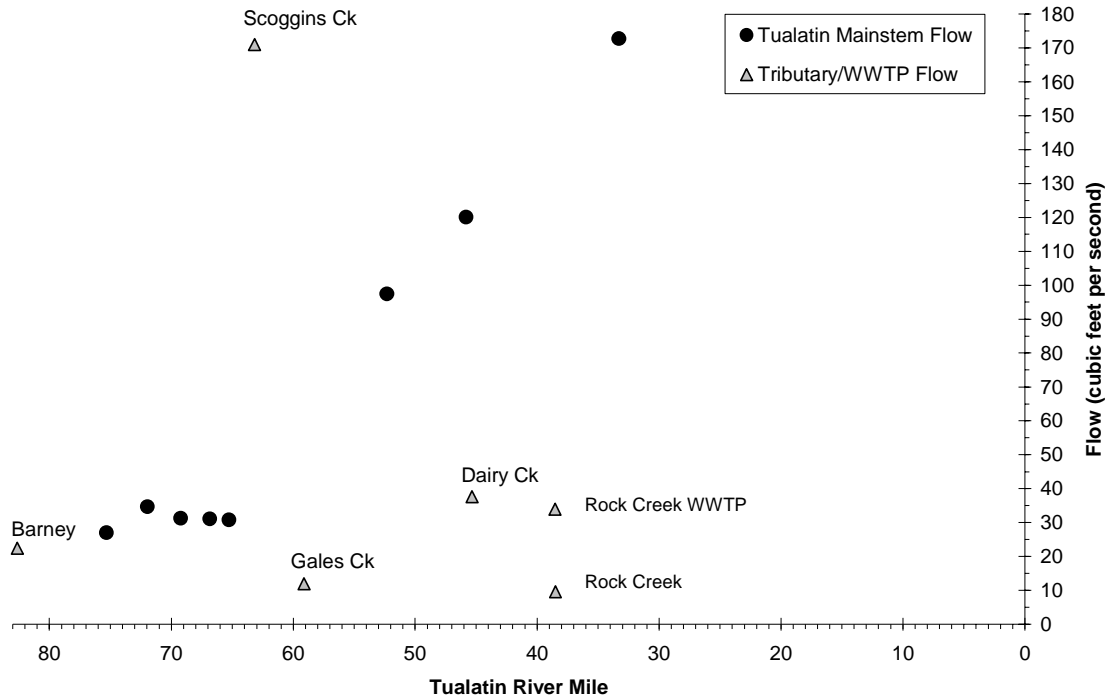
Figure A-37 presents the measured FLIR temperature profile for the Tualatin River, which was sampled in two parts on July 27, 1999. As can be seen in this image, portions of the Upper Tualatin River are below 64°F. **Table A-14** shows that only 40.5 percent of the Upper Tualatin River within this reach was below the 64°F temperature criteria on July 27, 1999. These areas were located in the upper reaches of the river. A similar trend was observed from continuous temperature monitoring during 1997 and 1998 (see **Figure A-30**).

Figure A-37.   Measured FLIR temperature profile for the Tualatin River on July 27,1999.
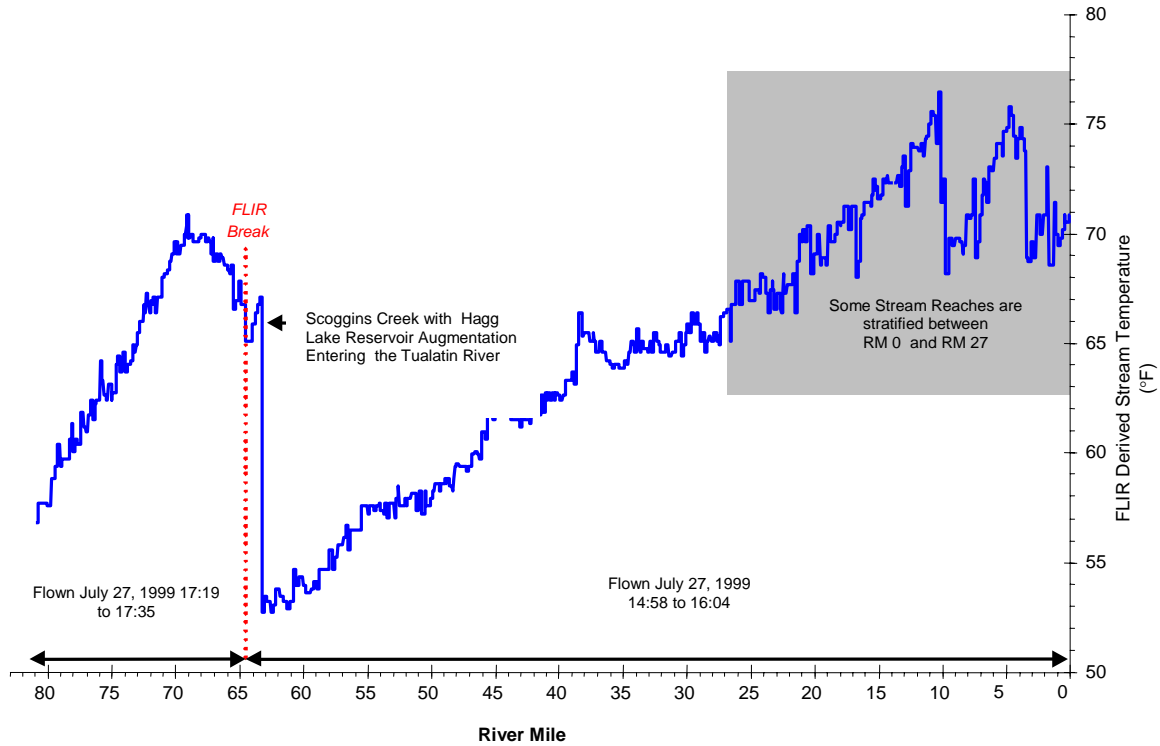
Table A-14. FLIR Derived Water temperatures in the Tualatin River (7/27/99) between river miles 0 and 80.9. Note that river mile 30 to the mouth has some stratified reaches and FLIR derived temperatures would not accurately represent water column temperatures in these areas.

Temperature (°F)	Distance (Miles)	Percent of Total	Mode of Thermal Mortality
Less than 55.0	5.3	6.6%	
55.0 to 59.5	12.6	15.5%	
59.5 to 64.0	13.7	17.0%	
64.0 to 68.5	24.0	29.6%	Sub-Lethal Limit
68.5 to 73.0	19.8	24.4%	
73.0 to 77.5	5.6	6.9%	
Greater than 77.5	0.0	0.0%	Incipient Lethal Limit
Totals	80.9	100.0%	

The following selected FLIR images were observed in the Tualatin River on July 27, 1999. FLIR thermal imagery codes temperatures utilizing a Celsius temperature scale. The conversion of temperature into the Fahrenheit scale is presented in the Glossary of this document.

Image A-6 presents at typical image of the upper Tualatin River through agricultural reaches. **Image A-7** illustrates a nearby location which cut banks are a predominate feature. *Note that the day image is shifted slightly forward from the thermal image.* **Image A-8 and A-9** illustrate temperature condition immediately downstream of the Rock Creek confluence in the Tualatin River.

Image A-6. Upper Tualatin River between the Mount Richmond and South Road bridges.[2]
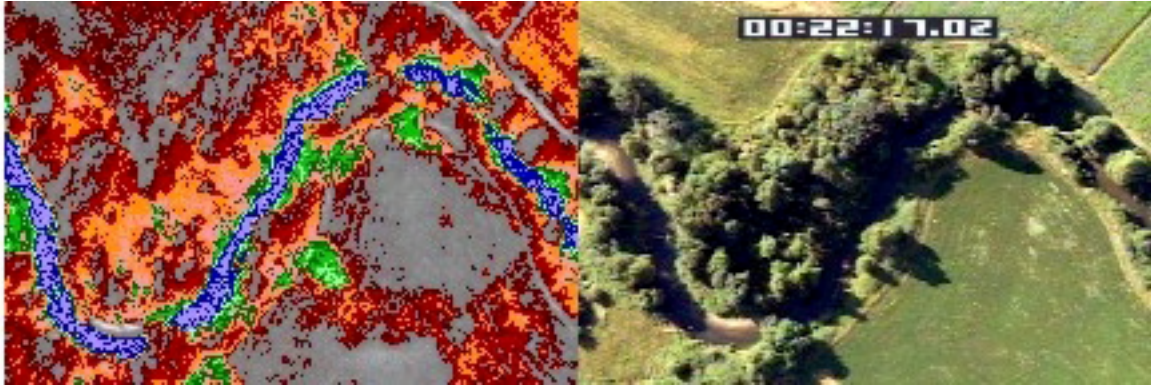
Image A-7. Upper Tualatin River between the Mount Richmond and South Road bridges.

FLIR Image Temperature Scale (°C)

Image A-8. Image mosaic of the Tualatin River at the confluence of Rock Creek. Tualatin River surface water temperature is 17.5^{o}C upstream of the confluence and 18.9^{o}C downstream. [3]
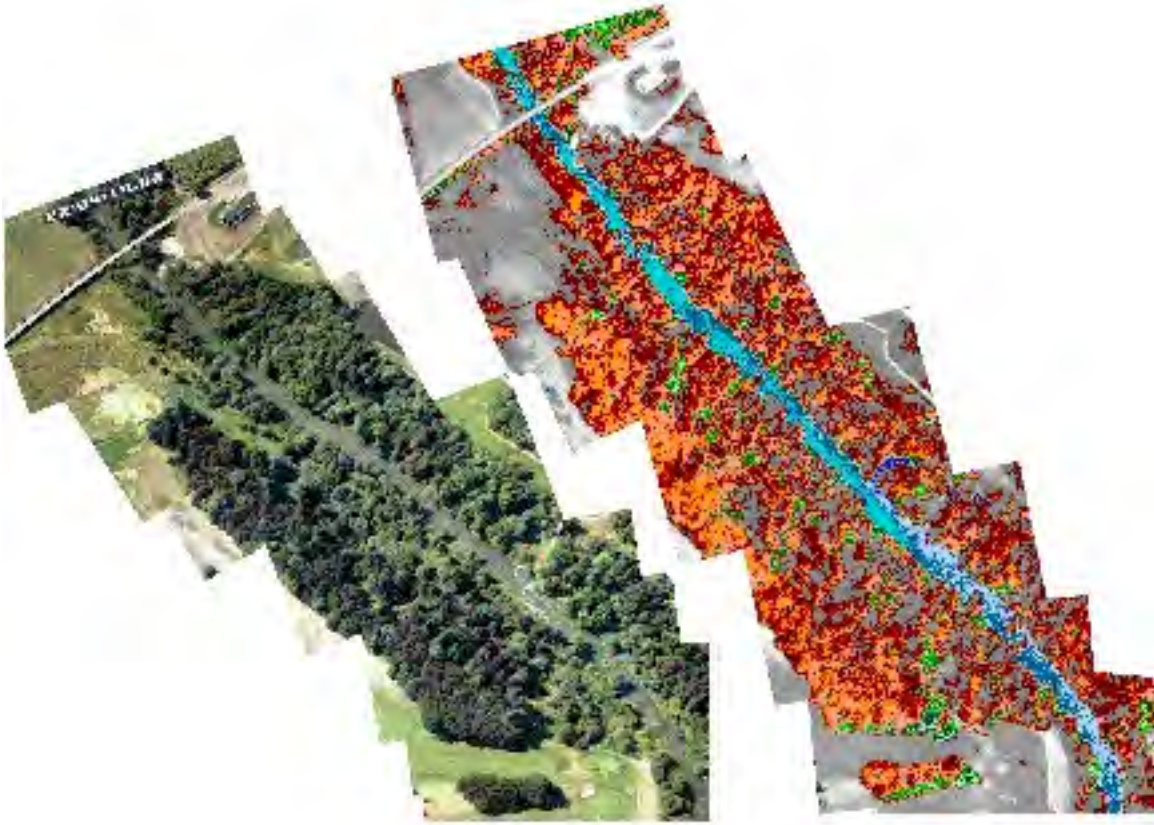
Image A-9. Thermal mixing in the Tualatin River just downstream of its confluence with Rock Creek.
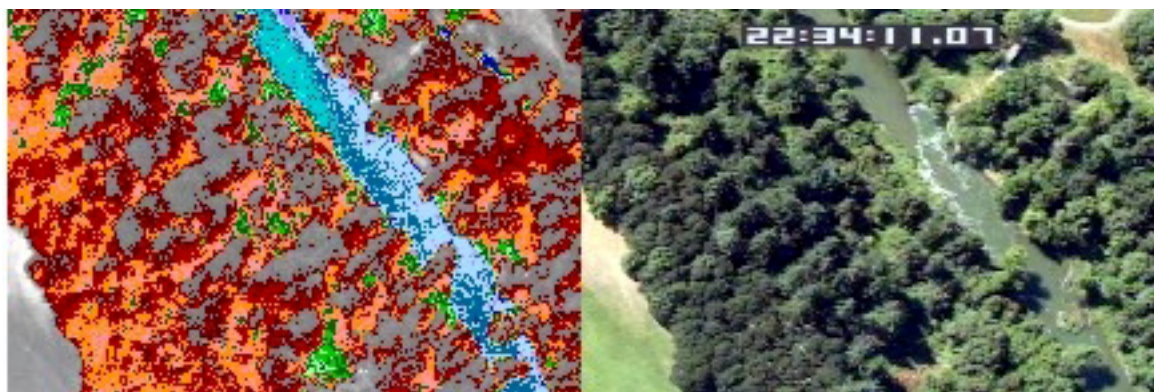
FLIR Image Temperature Scale (^{o}C)

Image A-10. Confluence of the Tualatin River (16.8^{o}C downstream) and Dairy Creek (19.5^{o}C). Dairy Creek flows in from the right side of the image and the Tualatin River flows from the top to the bottom of the image. [4]
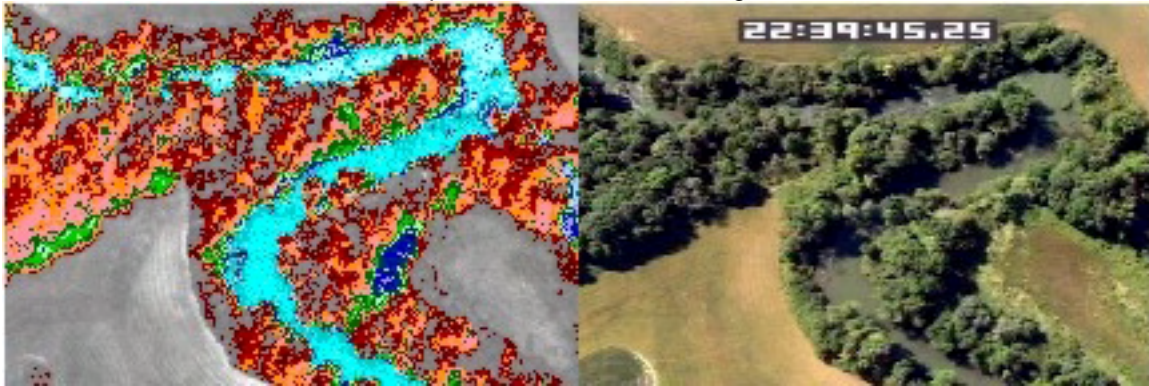
Image A-11. Confluence of the Tualatin River (12.4^{o}C) and Gales Creek (22.3^{o}C). Gales Creek flows in from the top right of the image.
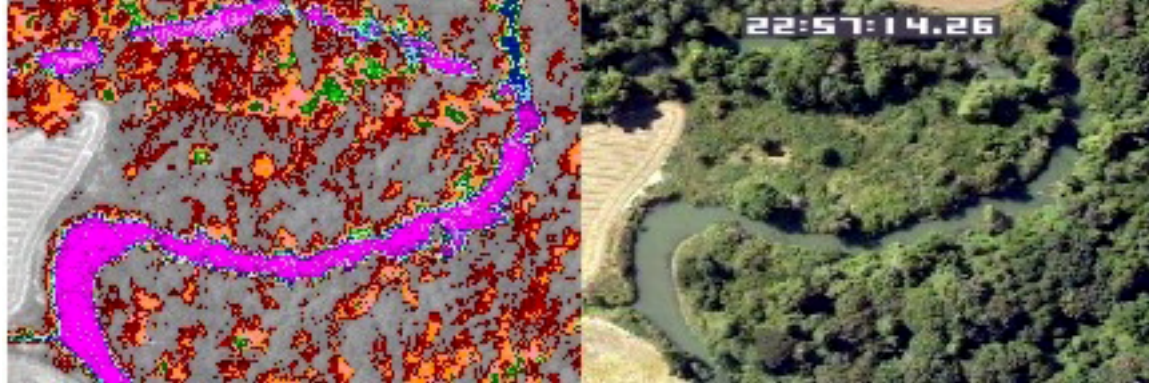
Image A-12. Confluence of the Tualatin River and Scoggins Creek (11.0^{o}C). The Tualatin River flows from the top to the bottom of the image and is 19.9^{o}C upstream of the confluence and 11.8^{o}C downstream.
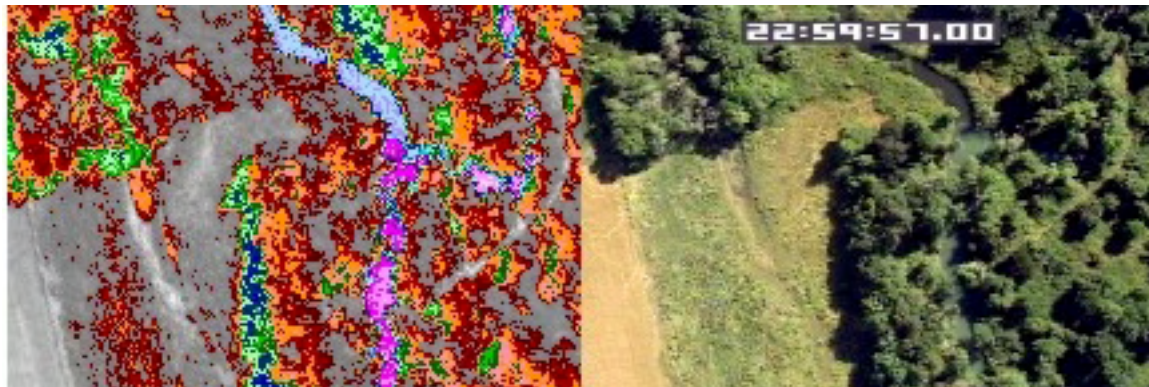
FLIR Image Temperature Scale (^{o}C)

Past research has determined that the Tualatin River downstream of the Farmington Recording Stream Gage (River Mile 33.3) is thermally stratified during the summer period. That is, river water is not mixed and warmer water temperatures are observed at the surface and cooler water is observed at lower depths. It is important to remind the reader that FLIR measures only surface temperatures and therefore extreme caution should be used when interpreting observed FLIR temperatures within these thermally stratified prone regions of the Tualatin River.

Image A-13 illustrates a thermal image that shows evidence of thermal stratification in the Tualatin River. The same image is presented using two different color schemes. The image on the left is presented in gray scale and on the right is the same image presented in color where temperatures normally associated with natural water are assigned a color to emphasize in-stream differences. The Tualatin River (Location 1) runs in the direction of the arrow and cool water streaks (Location 2) are noticeable behind in-stream objects. These streaks indicate areas of mixing downstream of the object and are 1.5 to 2°C cooler then the measured surface temperature. **Image A-14** illustrates an area where the surface temperature of the Tualatin River (Location 1) changes fairly drastically. The 2.6^{o}C drop in surface temperature seems to be due to a change from a stratified condition to a well-mixed condition, although the reason for this change is not apparent from the image. However, several shallow areas are present in the lower Tualatin River that may cause such a disruption of thermal stratification.

Image A-13.   Tualatin River area of probable stratification as evidenced by the cool water streaks behind in-stream objects. (*River Mile 10.7*).
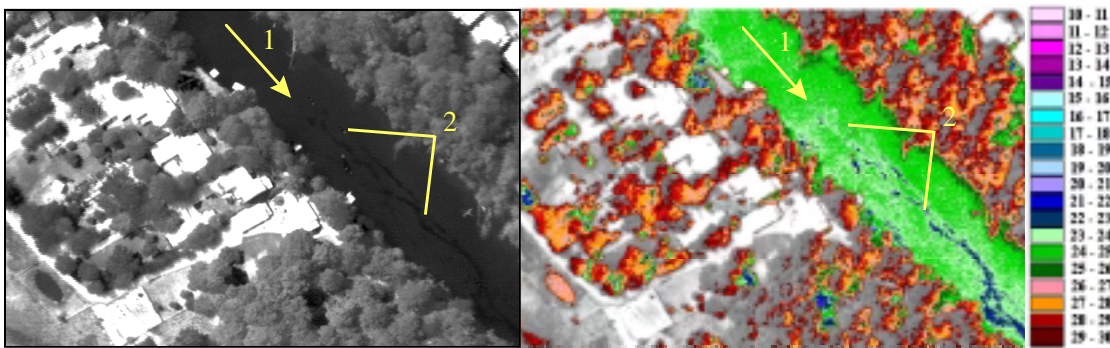
Image A-14.   Tualatin River Location showing a 2.6^{o}C drop in median surface temperature in the downstream direction (Location 1) (*River Mile 9.9*).
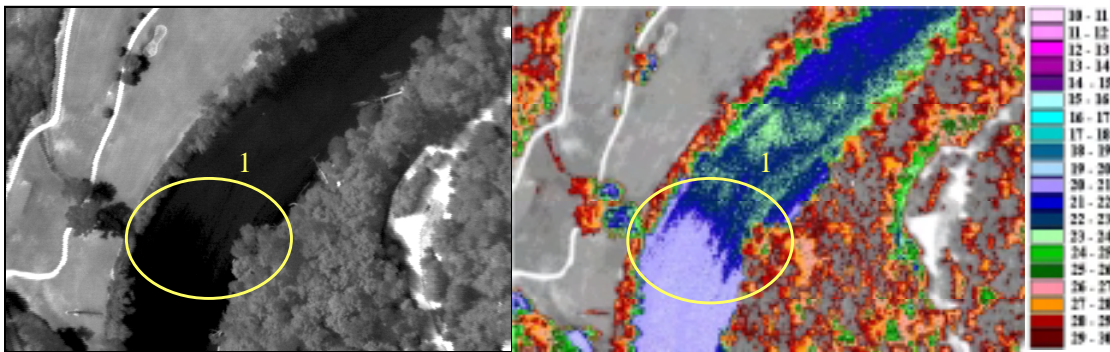
TUALATIN RIVER MODEL INPUT DATA

The Tualatin River was modeled from Barney Reservoir (river mile 83) to Farmington Road (river mile 33). Model segment lengths are each 100 feet. This section graphically displays the model input data for each of the 100-foot model segments. The various data sources and methodology used to assemble model input data are presented earlier in this Appendix.

- ➢ Elevation and Gradient (**Figure A-38**)
- ➢ Vegetation Geometry (**Figure A-39**)
- ➢ Aspect (**Figure A-40**)
- ➢ Near Stream Disturbance Zone Widths and Wetted Widths (**Figure A-41**)
- ➢ Topographic Shade (**Figure A-42**)
- ➢ Flow Volume (**Figure A-43**)
- ➢ Flow Velocity (**Figure A-44**)
- ➢ Water Column Depth (**Figure A-45**)

Figure A-38.   Tualatin River Elevation and Gradient
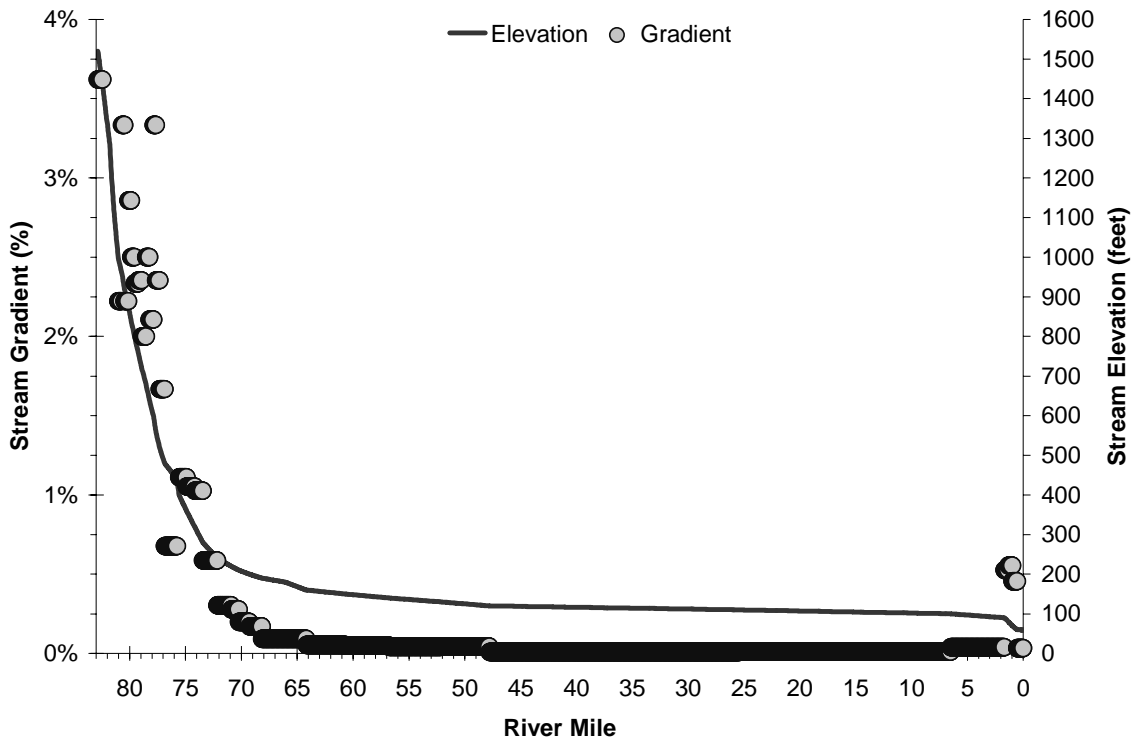
Figure A-39. Tualatin River Current Vegetation Heights (Headwaters to Dairy Creek)
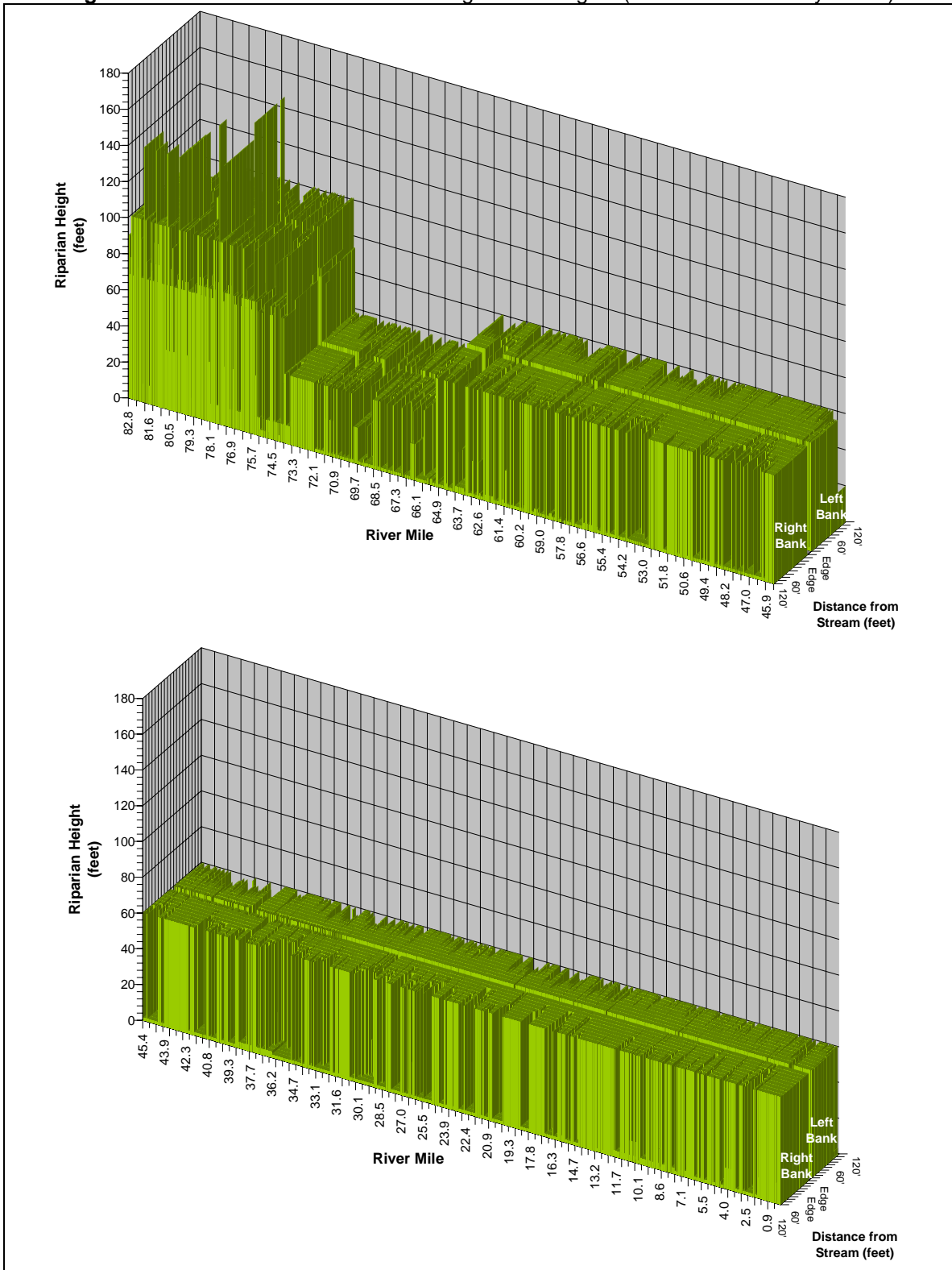
Figure A-40. Tualatin River Aspect
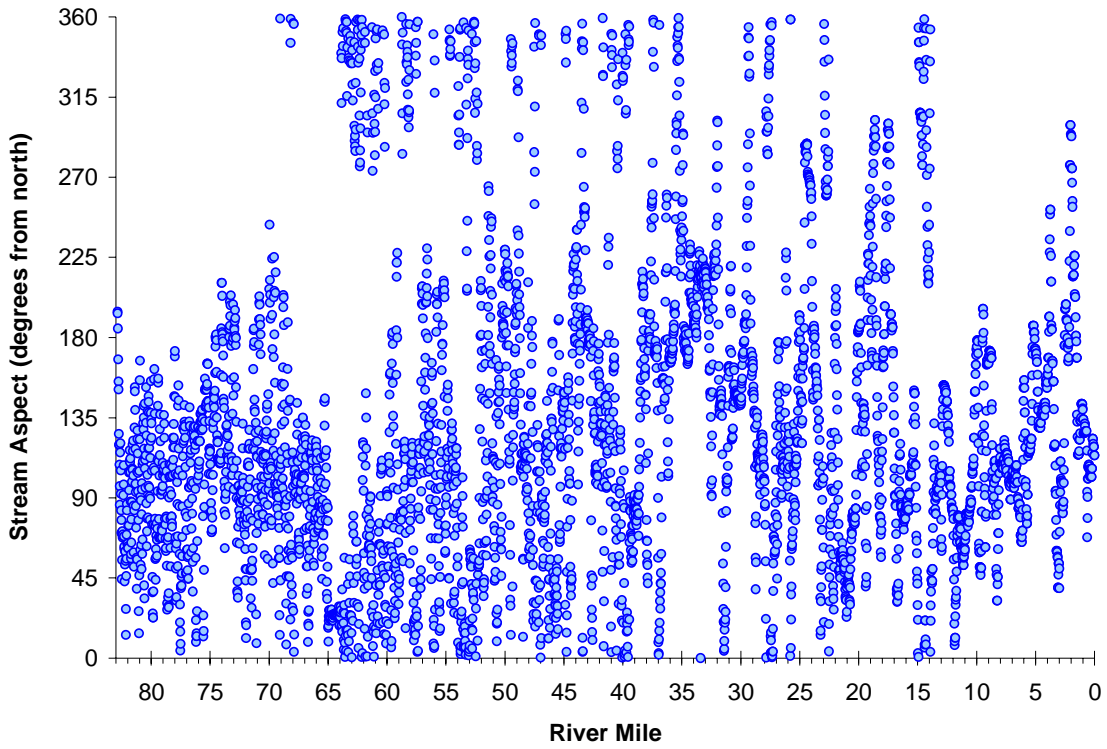
Figure A-41. Tualatin River Wetted Width and NSDZ Width
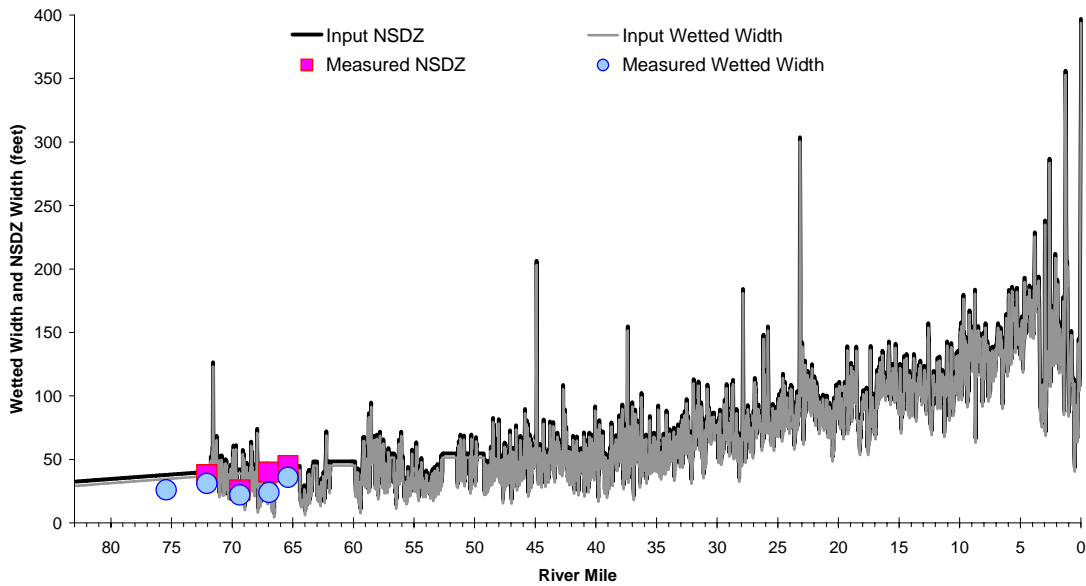
Figure A-42.   Tualatin River Topographic Shade
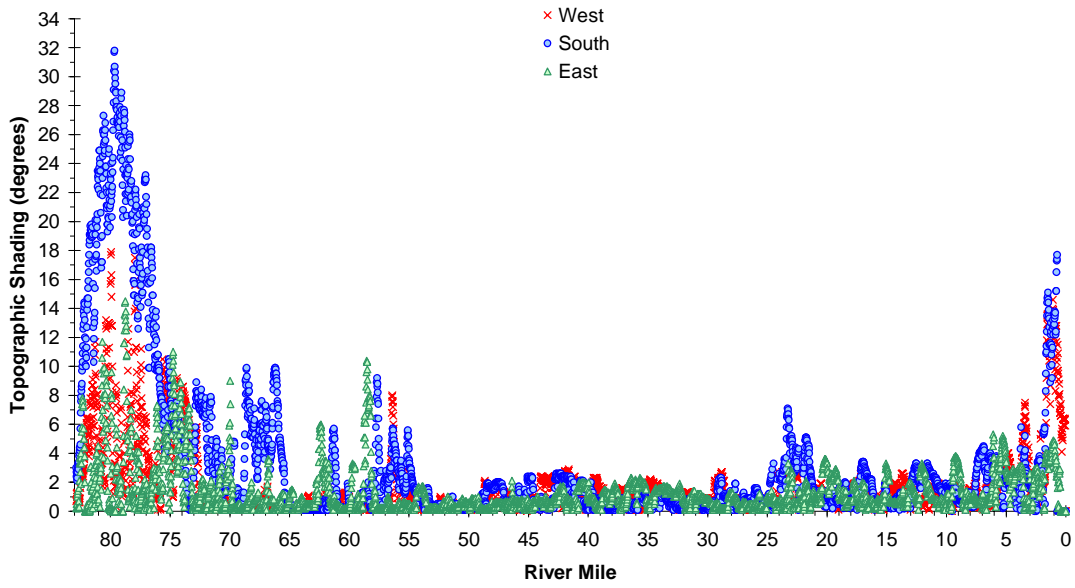
Figure A-43.   Tualatin River Measured and Interprolated Flow Volume.
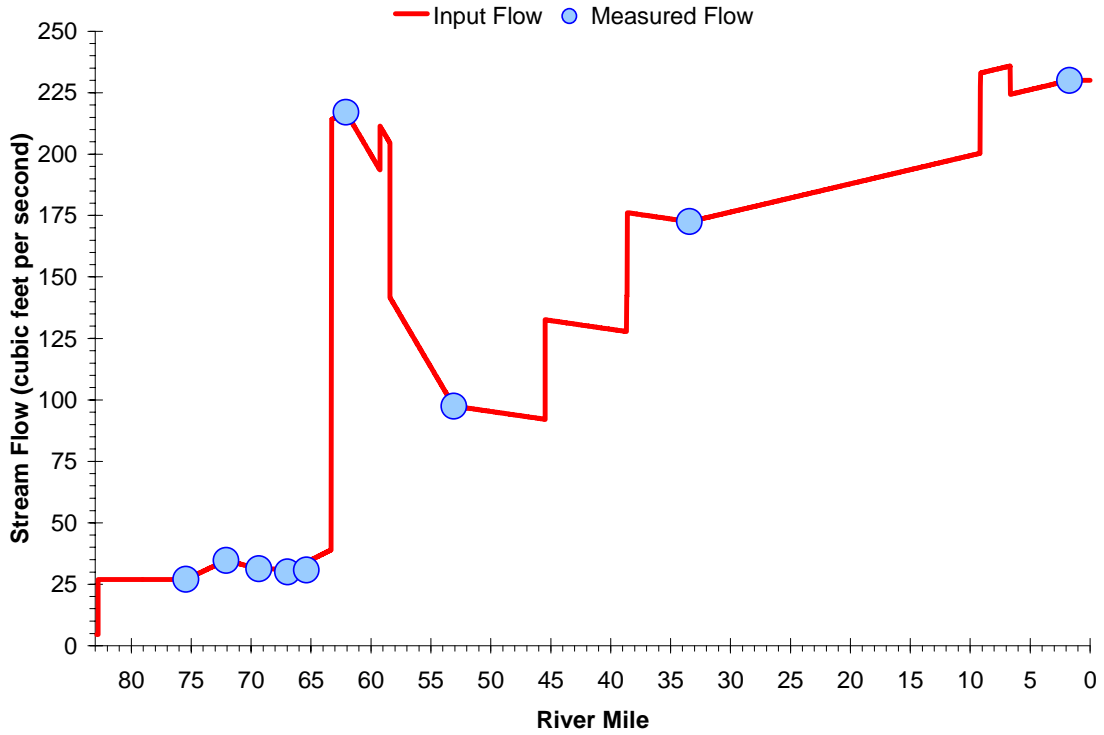
Figure A-44. Tualatin River Measured and Manning's Derived Longitudinal Flow Velocities
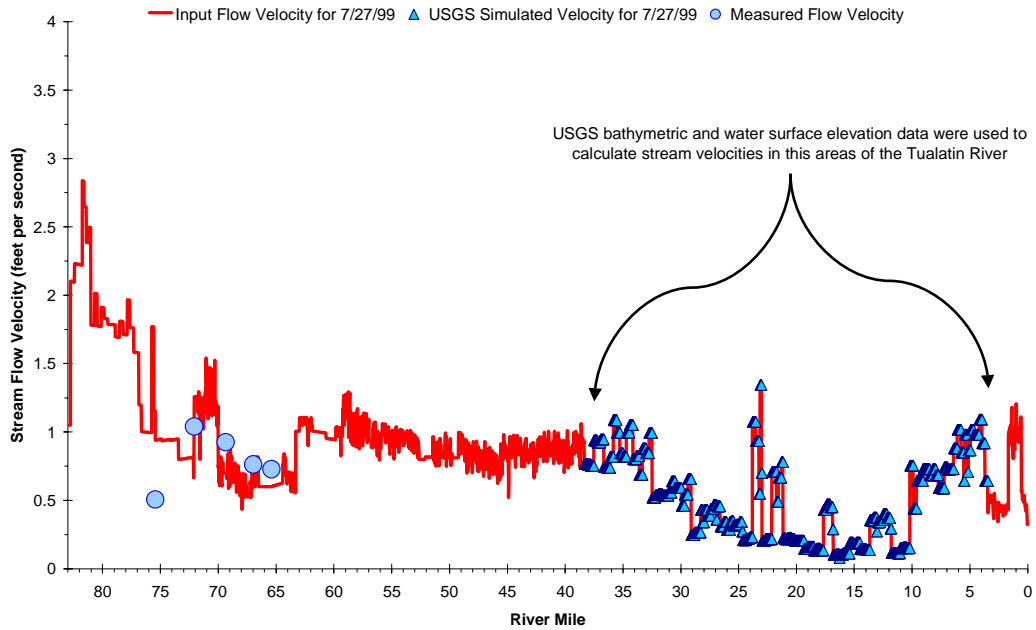
Figure A-45. Tualatin River Measured and Manning's Derived Longitudinal Water Column Depths
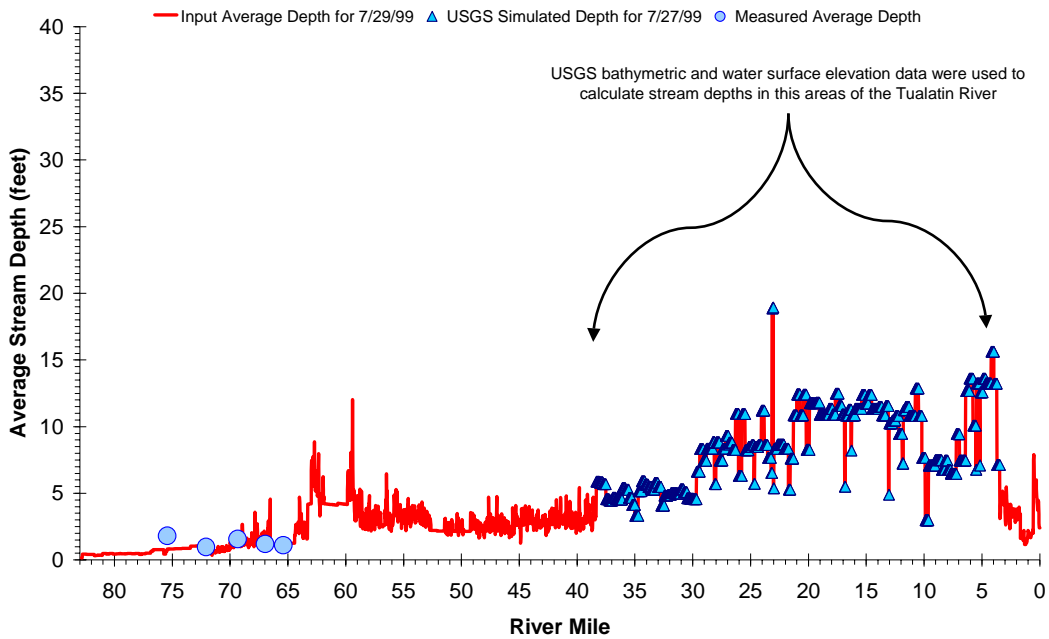
TUALATIN RIVER MODEL RESULTS

This section presents temperature modeling results for the Tualatin River. Graphical and statistical validation of the Tualatin River calibrated model are shown, in addition to temperature predictions for potential vegetation and flow conditions. Recall that the model was calibrated with data collected on July 27, 1999 and thus is representative of critical stream temperature, stream flow, and climatic conditions. In other words, this modeling effort has captured the period when stream temperatures were near their peak. Spatial validation of the calibrated model is presented in **Figure A-46**. As previously mentioned, the Tualatin River was flown in two separate flights due to its length. Thus, river miles 33.3 through 62.9 were calibrated to 4:00 PM FLIR temperatures, while the upper portion was calibrated to 6:00 PM FLIR temperatures.

The standard error and average deviation for the spatial data calibration are:

$$Standard\ Error = 1.00^oC\ (1.81^oF)$$

$$Average\ Deviation = 1.07^oC\ (1.93^oF)$$

$$Correlation\ Coefficient\ (R^2) = 0.89$$

Figure A-46. Tualatin River Observed and Predicted Spatial Temperature Data on 7/27/99.
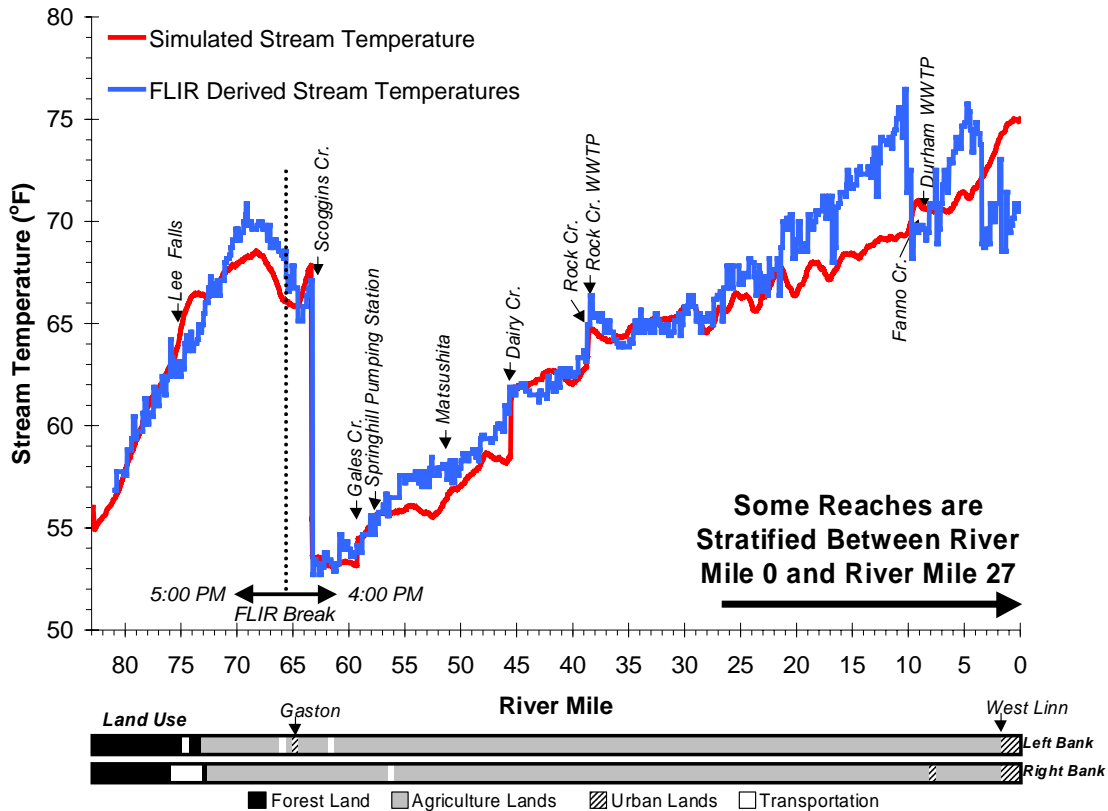
Observed and predicted hourly temperatures at nine continuous temperature monitoring locations on the Tualatin River are presented in **Figure A-47**. Node 1 is the upper boundary condition and remains constant, therefore it is not graphed. Standard errors and average deviations are presented for each node. The mean standard error and mean average deviation for the continuous data are:

$$Mean\ Standard\ Error = 0.35^oC\ (0.63^oF)$$

$$Mean\ Average\ Deviation = 0.73^oC\ (1.32^oF)$$

Figure A-47. Tualatin River Model Continuous Data Validation
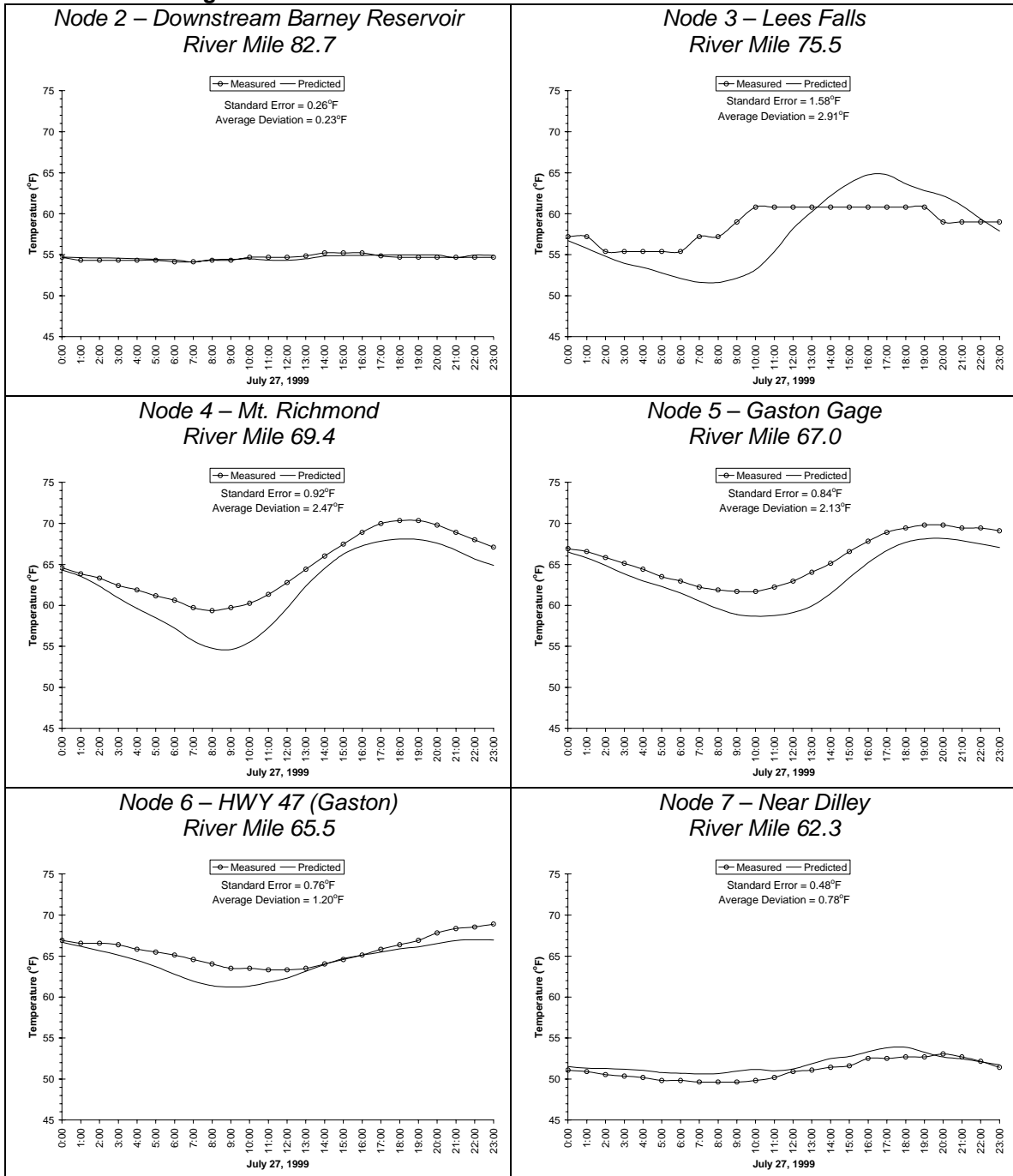
Figure A-47 (continued). Tualatin River Model Continuous Data Validation
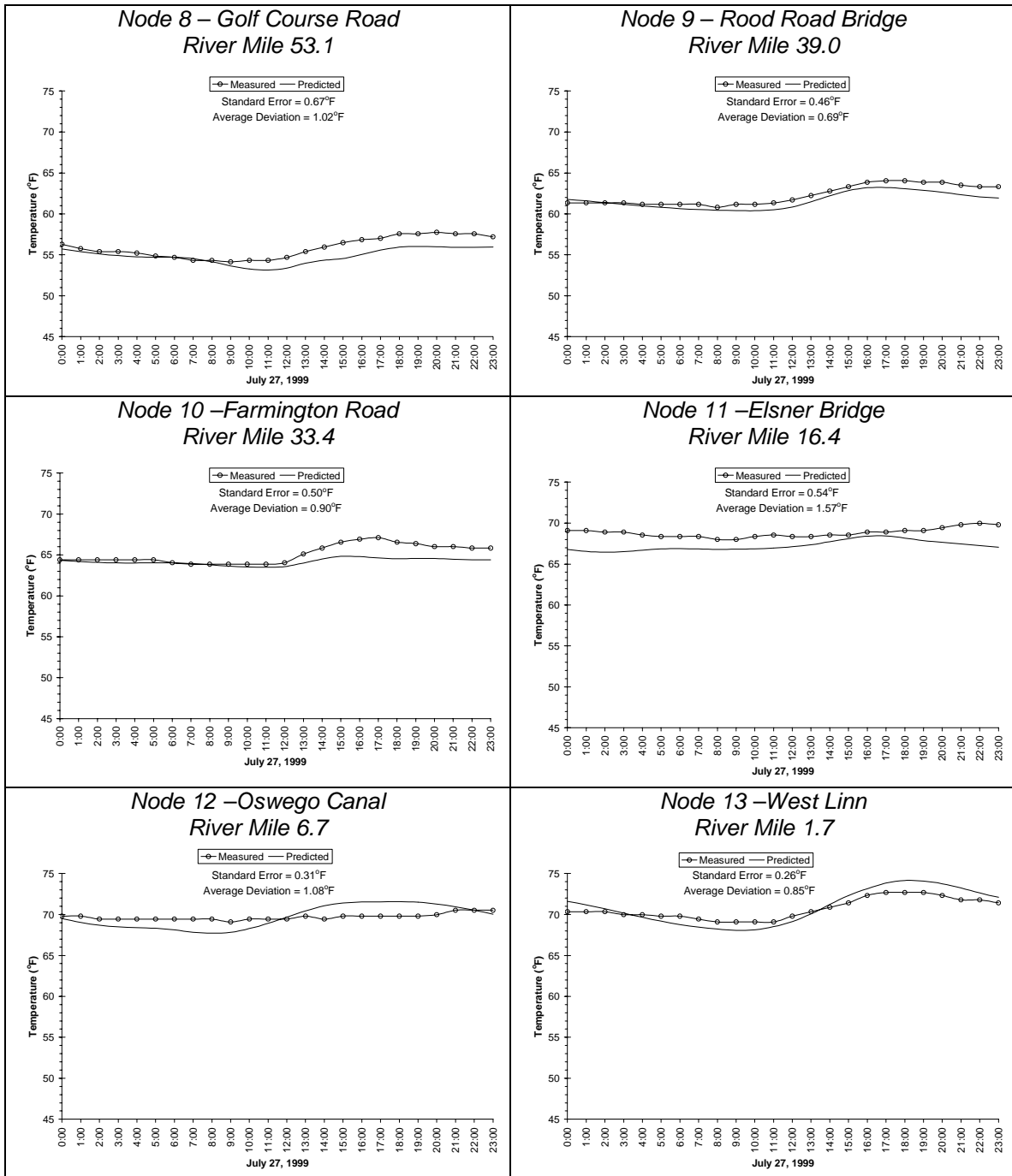
The calibrated Tualatin River model was used to predict stream temperatures under various scenarios. **Figure A-50** displays predicted Tualatin River temperatures at 6:00 PM on July 27, 1999 with the following scenarios: 1) Non-Point Sources are at Current Conditions and Point Source Discharge is removed; and 2) Non-Point Source are at Current Conditions and Point Sources are at Waste Load Allocation.

Loading Capacity - 40 CFR 130.2(f)

Loading Capacity is based on the condition that meets the ***no measurable surface water temperature increase resulting from anthropogenic activities***. This condition is termed ***System Potential*** and is achieved when (1) non-point source solar radiation loading reflects a riparian vegetation condition without human disturbance and (2) point source discharges cause no measurable increases in surface water temperatures.

Solar radiation loading was calculated using system potential riparian vegetation, at current channel and stream aspect conditions. A detailed description of potential vegetation conditions is presented in **Table A-8**. Current and System Potential solar loading for the Tualatin River are presented in **Figure A-48**. Solar radiation loading for Current Condition and System Potential condition is presented for every 100 meters of modeled stream length. As can be seen in **Figure A-48**, solar radiation loading at System Potential is much less than levels currently observed on the Tualatin River (i.e., Current Condition).

Figure A-48.   Tualatin River Solar Radiation Load at System Potential and Current Conditions
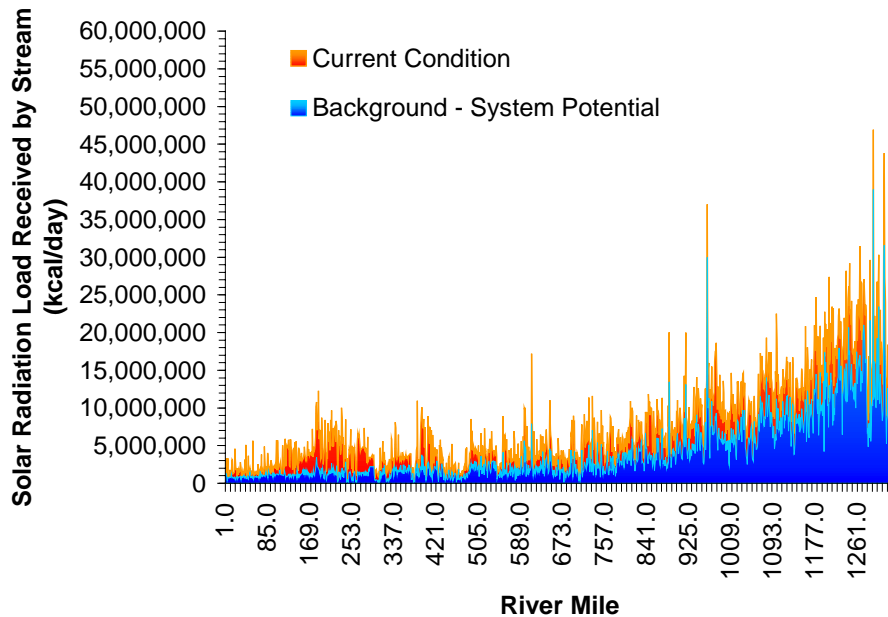
Allocations – 40 CFR 130.2(g) and 40 CFR 130.2(h)

*Load Allocations (Non-Point Sources) - The **temperature standard** targets system potential (i.e. no measurable temperature increases from anthropogenic sources). To meet this requirement the system potential solar radiation heat load ($5.6 \cdot 10^9$ Kcal/day) is allocated to background nonpoint sources. Anthropogenic nonpoint sources are not given a heat load.*

Wasteload Allocations (Point Sources) - Surface water discharges into Tualatin River Subbasin receiving waters have been given a heat load based on the 0.25^oF allowable increase in the mixing zone as specified in the temperature standard. Heat loads have been converted to allowable effluent temperatures as well. It should be noted that the wasteload allocation is the point source heat load and not the calculated maximum effluent temperatures. There are several options for meeting the allocated heat loads (i.e. passive effluent temperature reductions, changes in facility discharge operation, purchasing instream flows, pollutant trading, etc.).

Temperature Allocation Summary **Non-Point Sources**	
Source	*Loading Allocation* Allowable Nonpoint Source Solar Radiation Heat Load (kcal/day)
Natural	$5.6 \cdot 10^9$ Kcal/day
Agriculture	$\varnothing$
Forestry	$\varnothing$
Urban	$\varnothing$
Future Sources	$\varnothing$

Point Sources - Allowable Point Source Effluent Source Heat Loading

		Q_R	Q_{PS}	T_{PS}	Max T_P	H_{PS}	H_{WLA}
Facility Name	**Rec. Water**	Receiving Water 7Q10 Low Flow (cfs)	Facility Design Flow (cfs)	Point Source Effluent Temp. (^{o}F)	Max Daily Site Potential River Temp. (^{o}F)	Current Point Source Heat Loading on River (kcal/day)	Allowable Point Source Heat Loading in Zone of Dilution (kcal/day)
Pacific Foods	Tualatin R. RM - 8.5	76.0 cfs	0.06 cfs	76 ^{o}F	62 ^{o}F	$1.1 \cdot 10^6$	$1.1 \cdot 10^6$
Durham WWTP	Tualatin R. RM - 9.5	76.0 cfs	34.00 cfs	71 ^{o}F	61 ^{o}F	$2.5 \cdot 10^8$	$6.5 \cdot 10^6$
Rock Cr. WWTP	Tualatin R. RM - 38.0	102.6 cfs	50.00 cfs	71 ^{o}F	57 ^{o}F	$6.5 \cdot 10^8$	$8.7 \cdot 10^6$
Matsushita	Tualatin R. RM - 50.0	40.2 cfs	0.08 cfs	82 ^{o}F	55 ^{o}F	$3.4 \cdot 10^6$	$3.4 \cdot 10^6$

Surrogate Measures – 40 CFR 130.2(I)

The solar radiation load (Kcal/day) at system potential condition was calculated by multiplying the stream surface area by the solar radiation flux (ly/day). Percent effective shade was used as a surrogate measure of the solar radiation flux calculated at system potential conditions (**Figure A-49**). The individual points in the figure represent the current and allocated conditions for every 100 meters. Accordingly, System Potential heat load condition along the Tualatin River translates into approximately 70% or greater effective shade throughout much of the system.

Figure A-49.   Tualatin River Surrogate Measure for Non Point Sources – *Effective Shade*
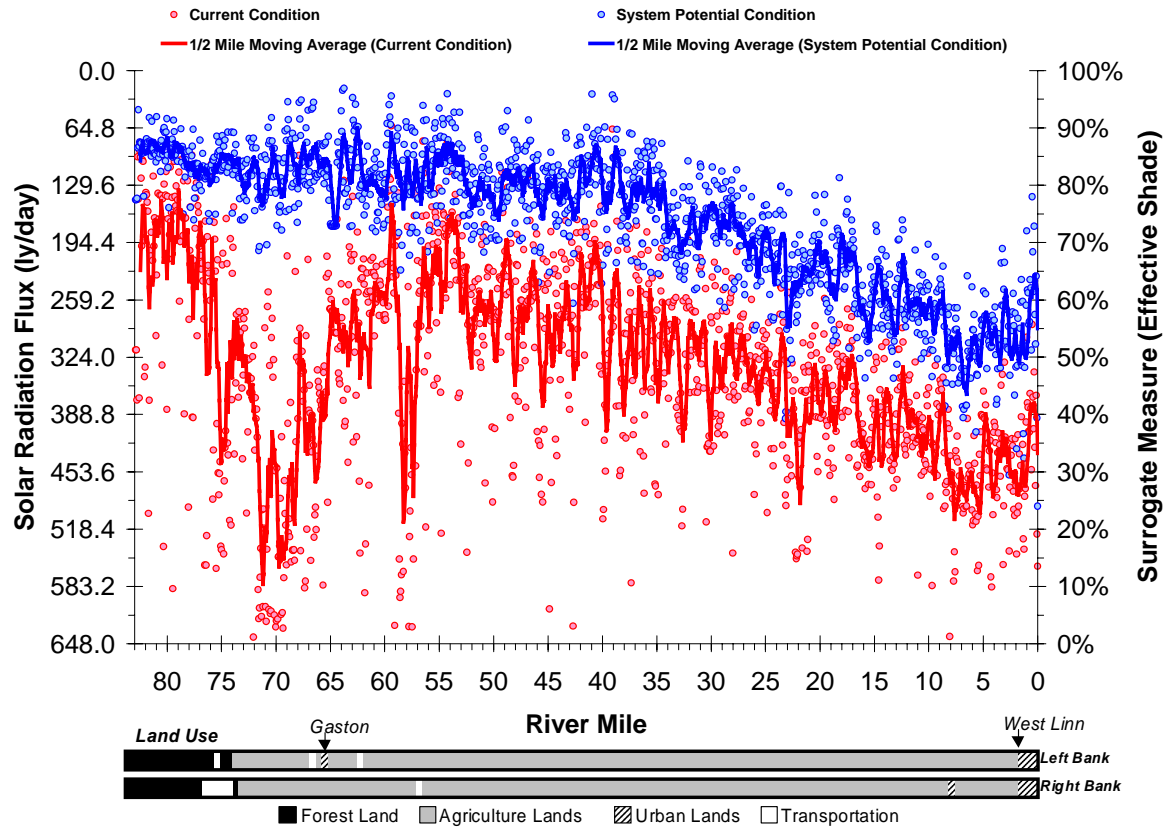
Water Quality Standard Attainment Analysis – CWA §303(d)(1)

Figure A-50 illustrates predicted Tualatin River temperatures at 6:00 PM on July 27, 1999 with the following scenarios: 1) non-point sources at Load Allocations and point source discharges at current levels, and 2) non-point source at Load Allocation and point source discharges removed. Predicted temperatures in the Tualatin River decrease dramatically at both Load Allocation scenarios. Point source discharge at current levels can dramatically raise stream temperatures under the Loading Allocation. **Figure A-50** also illustrates the effect of the 30 cfs flow augmentation from Hagg Reservoir on mainstem Tualatin River temperatures.

Two scenarios were run in which non-point sources were maintained at current conditions and point source discharge conditions were modified. **Figure A-51** displays predicted Tualatin River temperatures at 5:00 PM on July 27, 1999 with the following scenarios: 1) non-point sources at Current Conditions and point source discharges removed; and 2) non-point sources at Current Conditions and point sources at Waste Load Allocations. As can be seen in **Figure A-51**, the general temperature profiles were similar between these scenarios and Current Conditions; however, a localized effect downstream of the point source can be observed.

Figure A-50. Tualatin River Longitudinal Temperature Profile – Model Output Showing Range of Daily Temperatures – (a) Current Conditions without a 30 cfs flow augmentation from Hagg Reservoir (b) Non-Point Source Load Allocation and Current Point Source Discharge, and Non-Point Source Load Allocation and Remove Point Source Discharge –July 27, 1999.
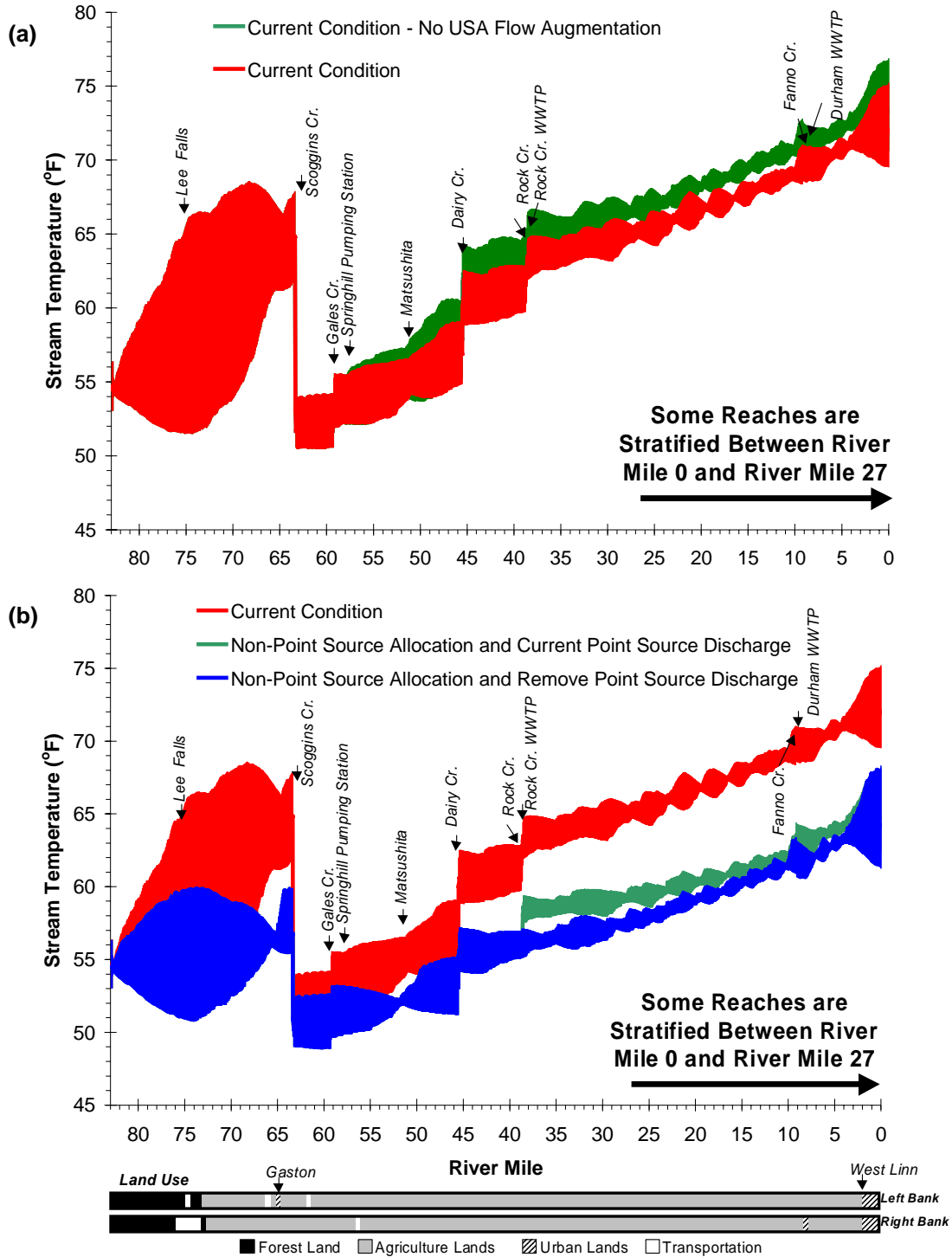
Figure A-51. Tualatin R. Longitudinal Temperature Profile - Model Output Showing Range of Daily Temperatures – 1) Non-Point Source Current Condition and Remove Point Source Discharge, and 2) Non-Point Source Current Condition and Point Source Waste Load Allocation – July 27, 1999.
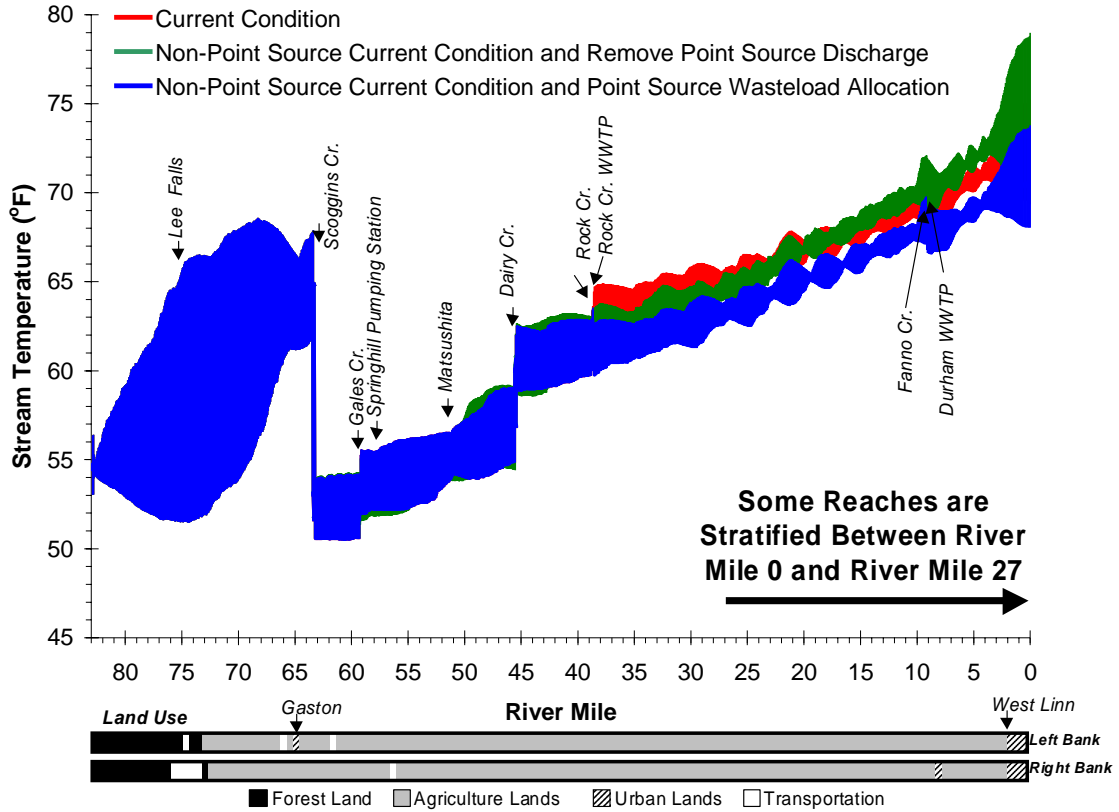
As mentioned above, *System Potential* is achieved when (1) non-point source solar radiation loading reflects a riparian vegetation condition without human disturbance and (2) point source discharges cause no measurable increase in surface water temperature. Accordingly, **Figure A-52** presents predicted Tualatin River temperatures at a Waste Load Allocation and Load Allocation scenario. **Table A-10** in the Temperature TMDL document presents Waste Load Allocation. **Figure A-53** illustrates that implementing Waste Load Allocations and Load Allocations will drastically reduce temperatures in the Tualatin River.

Figure A-52. Tualatin River Daily Temperature Range for Current Conditions Compared with Allocated Measures - July 27, 1999.
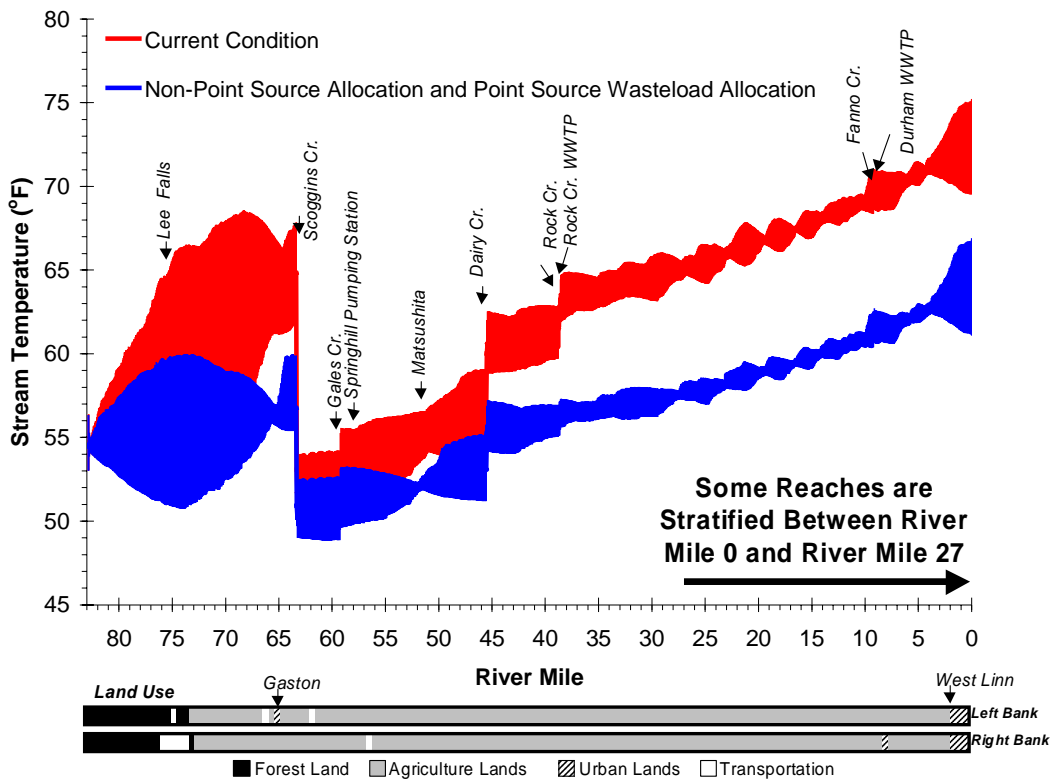
Figure A-53. Tualatin River Current and System Potential (Allocated) Temperature Distributions
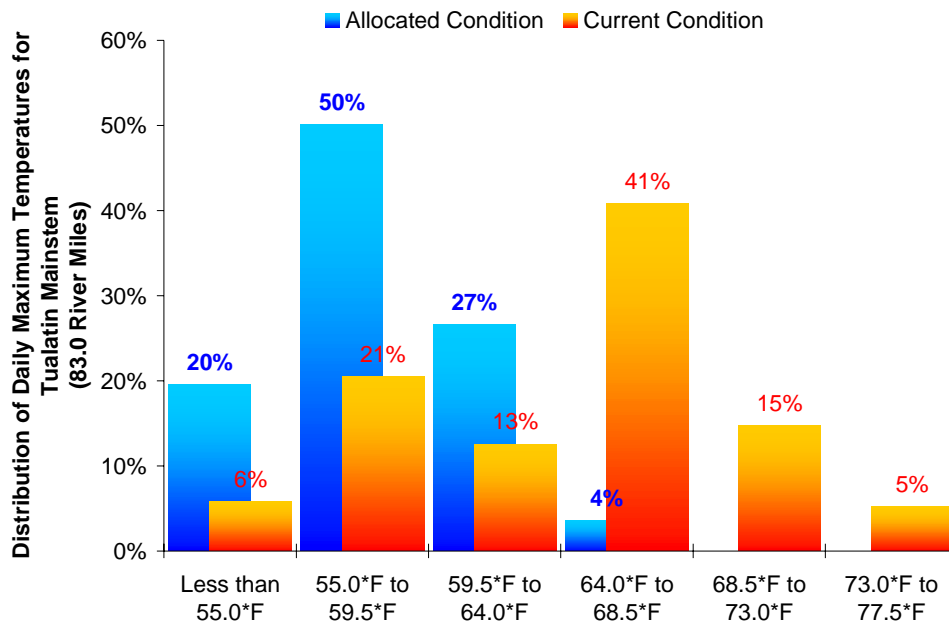
GALES CREEK[*]

GALES CREEK CURRENT CONDITION

The Oregon Department of Environmental Quality collected water quality data in Gales Creek during the summer of 1999. This effort included the collection of continuous hourly temperature data, FLIR temperature data, flow measurement, and site descriptions. Sampling locations are illustrated in **Figure A-54**. Digital photographs taken at several Gales Creek sampling locations are presented in **Image A-15** through **Image A-18**.

Figure A-54.   Water Quality Sampling locations for Gales Creek during the Summer of 1999.
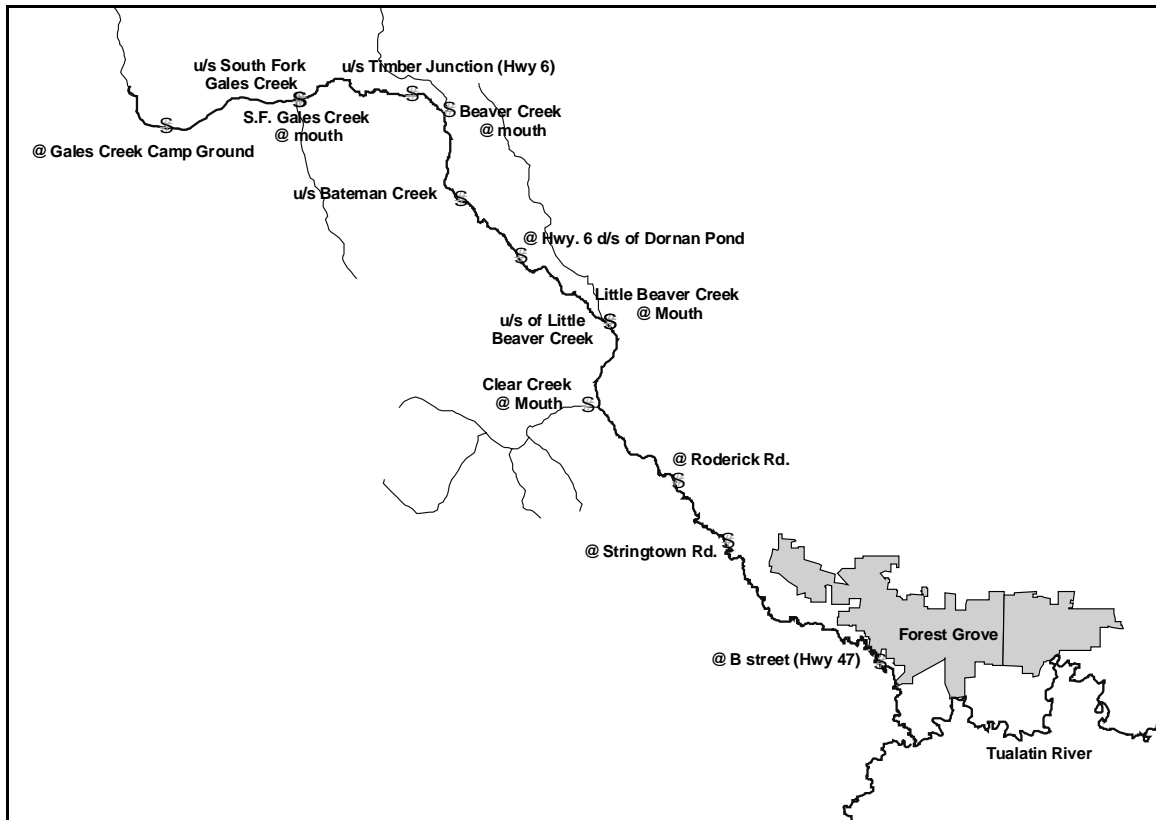
Water temperatures in Gales Creek increase during the summer period, with maximum temperatures occurring in late July (**Figure A-55**). Accordingly, FLIR thermal imagery was collected for Gales Creek on July 28, 1999. Flow measurements were also collected during this period of summer maximum temperatures. The longitudinal profile of the calculated 7-Day temperature statistics for Gales Creek, and several of its tributaries, are presented in **Figure A-57**. Only the upper reaches of Gales Creek had 7-day temperature statistics recorded below the 64°F standard in 1999. Calculated 7-day temperature statistics for Gales Creek and tributaries in 1999 are also presented in **Table A-15**.

---

[*] Note that the river miles (RM) presented in this report were derived from a 1:5000 stream coverage used for ODEQ modeling purposes and may differ slightly from other sources (such as OWRD or USGS river miles).

Image A-15. Gales Creek at Stringtown Road Bridge (RM 7.9).

[Temp. Statistic – 73.8*F, Flow – 15.5 cfs, Potential Effective Shade (ES) – 92%, Measured ES – 40%]

Image A-16. Gales Creek upstream of Dorman Ponds (RM 15.6).

[Temp. Statistic – 68.0*F, Flow – 11.9 cfs, Potential Effective Shade (ES) – 93%, Measured ES – 74%]
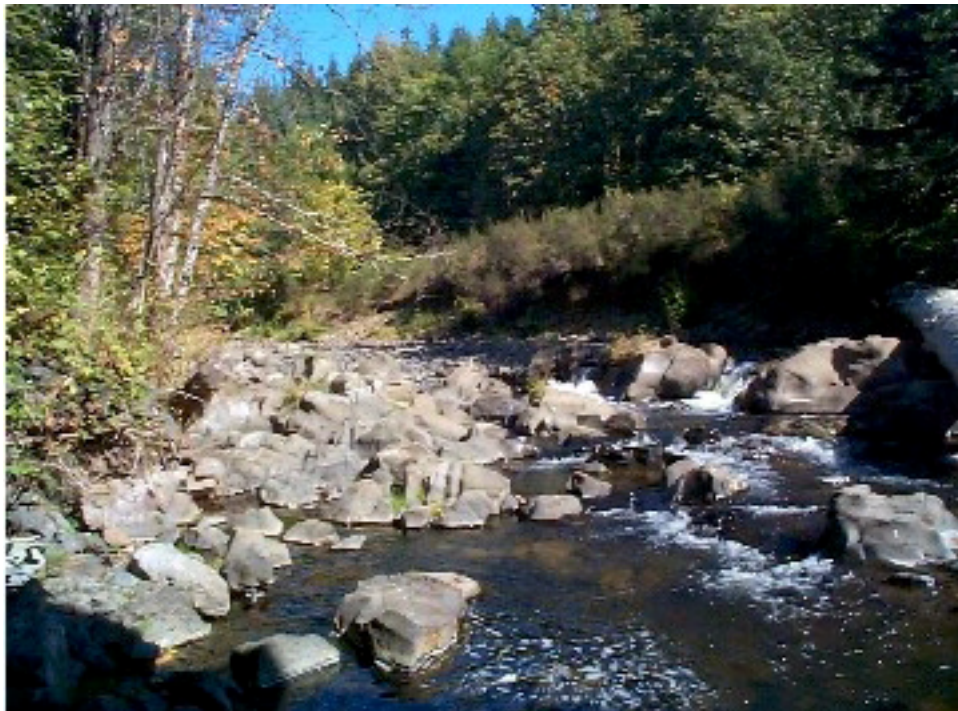
Image A-17.   Gales Creek upstream of the City of Timber (RM 19.6).
[Temp. Statistic – N/A, Flow – N/A, Potential Effective Shade (ES) – 97%, Measured ES – 93%]

Image A-18.   Gales Creek upstream of the Gales Creek Campground (RM 24.5).
[Temp. Statistic – 56.7*F, Flow – 4.1 cfs, Potential Effective Shade (ES) – 98%, Measured ES – 100%]
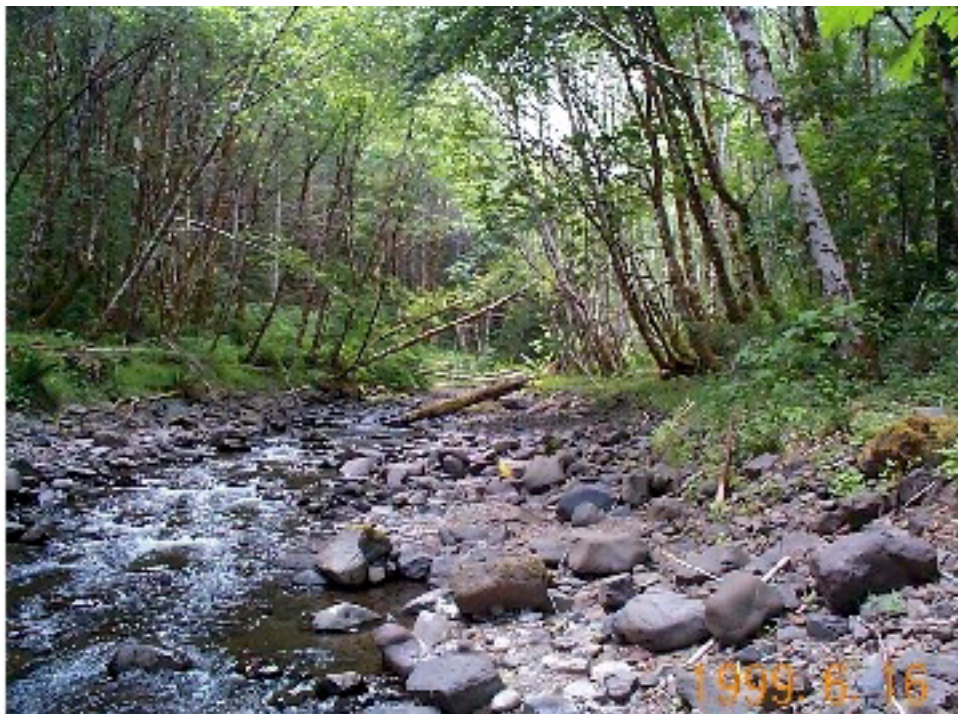
Figure A-55.   Observed daily maximum temperatures for Gales Creek in 1999.
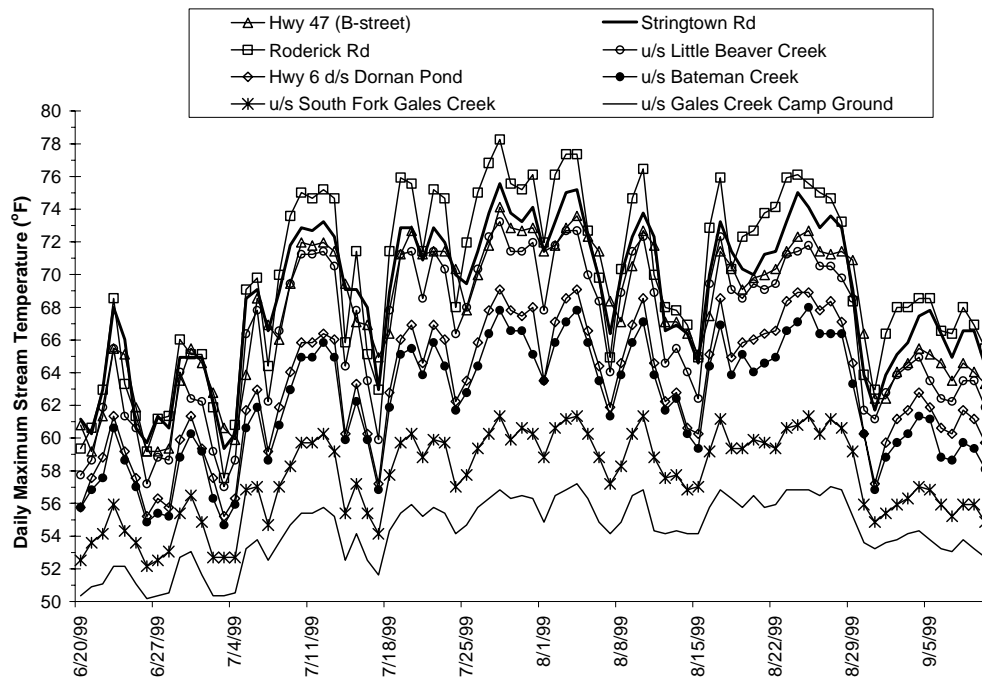
Figure A-56.   Observed 7-Day temperature Statistics for Gales Creek during the summer of 1999.
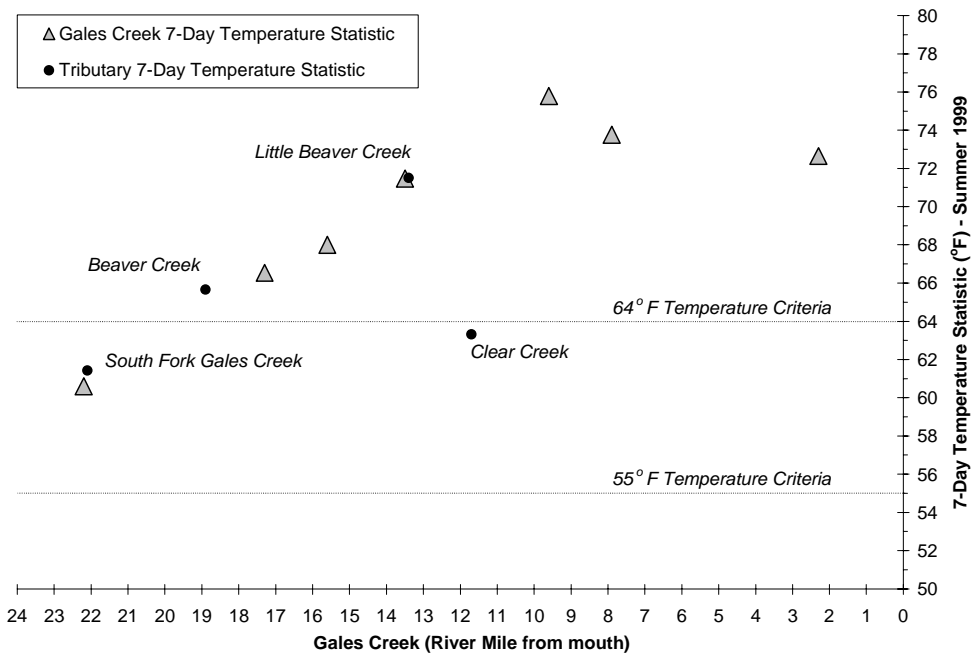
Temperature Site (RM = River Mile from mouth)	Start Date	End Date	Max Temp. (Date)	(°F)	7-Day Statistic (Date)	(°F)
Table A-15. Calculated 7-Day Temperature Statistics for Gales Creek and Tributaries in 1999.						
Gales Creek						
RM 2.3 (@ Hwy 47 (B Street))	6/17/99	9/13/99	7/28	74.1	7/31	**72.7**
RM 7.9 (@ Stringtown Road)	6/17/99	9/14/99	7/28	75.6	7/31	**73.8**
RM 9.6 (@ Roderick Road)	6/17/99	9/14/99	7/28	78.3	7/31	**75.8**
RM 13.4 (u/s Little Beaver Creek)	6/17/99	9/14/99	7/28	73.2	7/31	**71.5**
RM 15.6 (@ Hwy 6 d/s Dorman Pond)	6/17/99	9/14/99	8/04	69.1	8/25	**68.0**
RM 17.3 (u/s Bateman Creek)	6/17/99	9/14/99	8/25	68.0	8/25	**66.5**
RM 22.1 (u/s South Fork Gales Creek)	6/17/99	9/14/99	8/25	61.3	8/25	**60.6**
RM 24.5 (u/s Gales Creek Camp Ground)	6/17/99	9/13/99	8/04	57.2	8/25	**56.7**
Gales Creek Tributaries						
(RM 11.7) Clear Creek @ Mouth	6/17/99	9/14/99	7/28	64.9	8/25	**63.3**
(RM 13.4) Little Beaver Creek @ Mouth	6/17/99	9/14/99	8/04	72.9	8/25	**71.5**
(RM 18.9) Beaver Creek @ Mouth	6/24/99	9/14/99	7/28	67.1	7/31	**65.7**
(RM 22.1) South Fork Gales Creek @ Mouth	6/17/99	9/14/99	8/25	62.2	8/26	**61.4**

Water temperatures in Gales Creek varied through out the course of the day, with maximum temperatures occurring in the late afternoon and minimum temperatures occurring during the early morning hours. Diurnal temperature profiles for Gales Creek on July 28, 1999 are presented in **Figure A-57**. Diurnal temperature variability generally increased in a downstream direction with the largest variability observed at Roderick Road (River Mile 9.6). However, diurnal temperature variability decreases dramatically downstream of this location and temperature remain elevated above the standard throughout the course the day.

Flows were measured throughout the Gales Creek system during the period of FLIR sampling, corresponding to the period of summer maximum water temperatures (**Figure A-58**). Flows generally increase in the downstream direction, reaching a maximum value of 15.5 cfs at Stringtown Road. Observed tributary flows on this day were much lower than mainstem levels.

Figure A-57. Diurnal temperature trends observed in Gales Creek on July 28, 1999.
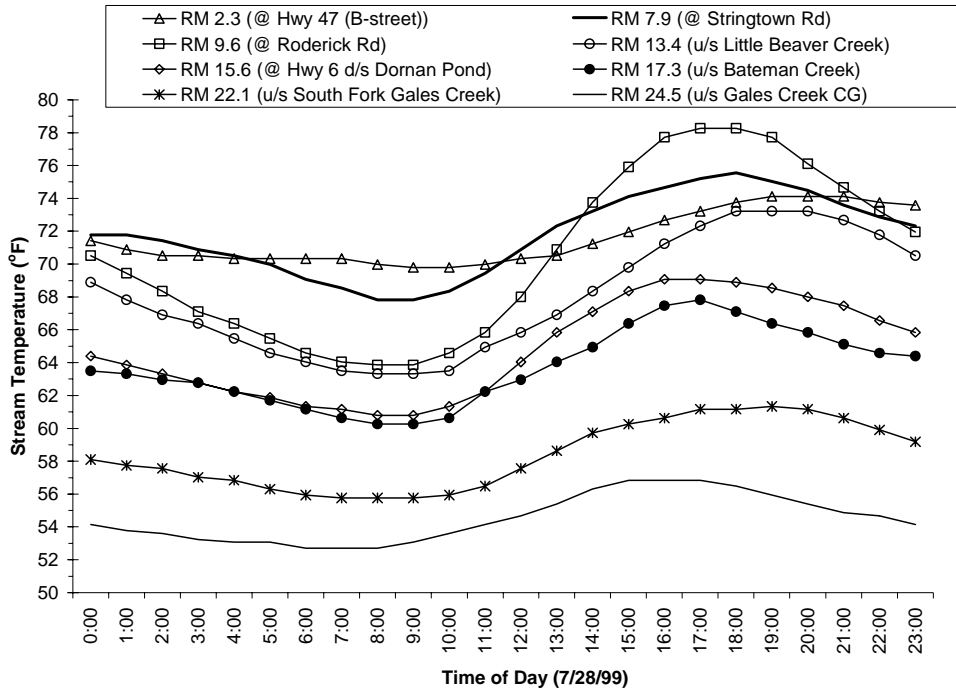
Figure A-58. Water discharge observed in Gales Creek on July 28, 1999.
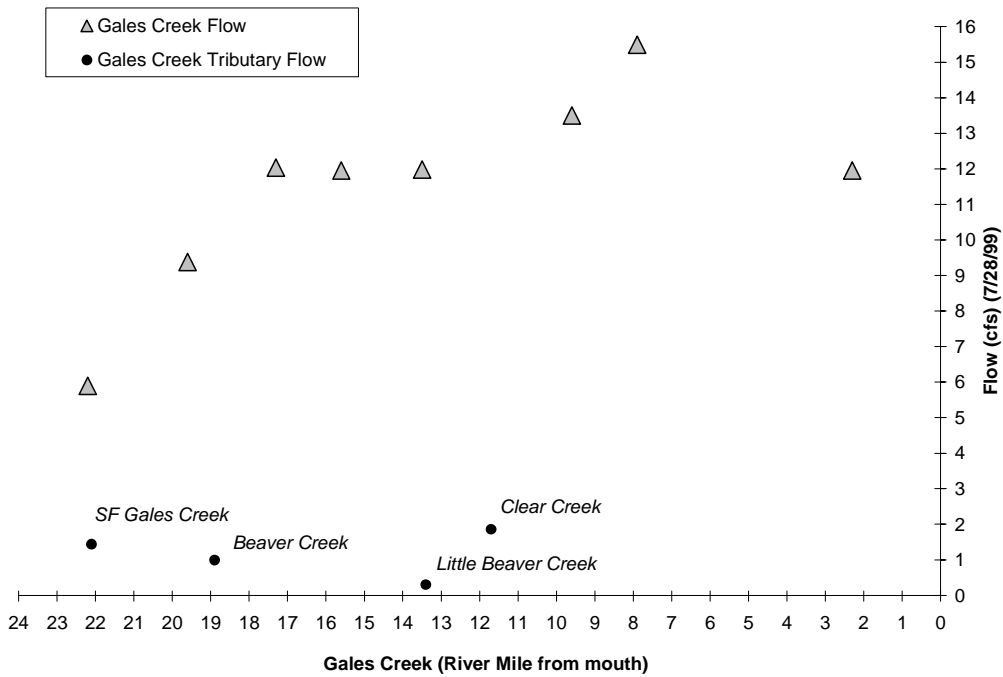
Figure A-59 presents the measured FLIR temperature profile for Gales Creek, which was sampled on July 28, 1999 between 2:42 to 3:16 PM. Specifically, **Table A-16** shows that only 24.7% of Gales Creek was below 64°F on this date and were located in the upper reaches of the river. In addition, river temperatures remained relatively constant downstream of River Mile 10. Similar trends were observed from continuous temperature monitoring data.

Figure A-59. Measured FLIR temperature profile for Gales Creek on July 28,1999.
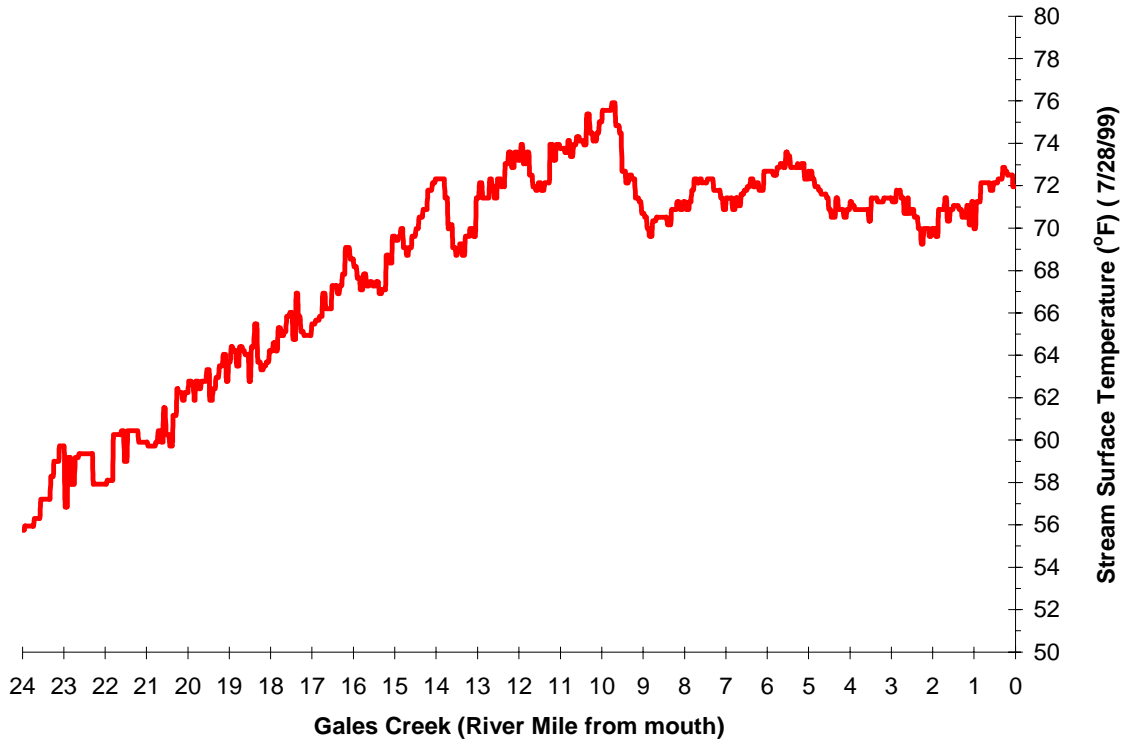
Table A-16.	FLIR Derived Water temperatures in the Gales Creek (7/28/99)		
Temperature (°F)	Distance (Miles)	Percent of Total	Mode of Thermal Mortality
Less than 55.0	-	-	
55.0 to 59.5	2.4	10.1%	
59.5 to 64.0	3.6	14.6%	
64.0 to 68.5	4.2	17.2%	Sub-Lethal Limit
68.5 to 73.0	10.5	42.7%	
73.0 to 77.5	3.8	15.4%	
Greater than 77.5	-	-	Incipient Lethal Limit
Totals	24.5	100%	

The following FLIR images were taken in Gales Creek on July 28, 1999. FLIR thermal imagery interprets temperatures utilizing a Celsius temperature scale. The conversion of temperature into the Fahrenheit scale is presented in the Glossary of this document. Note that 64°F is equal to 17.8^{o}C.

Image A-19 presents Gales Creek at the confluence with the Tualatin River. Median water temperature of the Tualatin River at the time of FLIR sampling was 11.3^{o}C and Gales Creek was 22.4^{o}C. Large riparian vegetation stands are observed in the video image.

Image A-20 was taken upstream of the confluence at the Highway 47 bridge. This image provides a characteristic view of the lower portion of Gales Creek, with abundant riparian vegetation along the stream bank flanked by agricultural fields. The median water temperature in this image is 21.4^{o}C.

Further upstream, **Image A-21** presents conditions in Gales Creek near the Roderick Creek confluence. As can be seen in this image, the stream channel is wide, and there are locations that riparian vegetation is absent. Observed water temperature at this location is 21.4^{o}C.

Image A-22 presents conditions in Gales Creek at a dam upstream of the Little Beaver Creek confluence. Gales Creek flows from the top to the bottom of the image and there is evidence of thermal stratification upstream of the dam. The median water temperature is 22.7^{o}C upstream of the dam and 20.8^{o}C below the dam.

Gales Creek in **Image A-23** (immediately upstream of Dorman Ponds) is partially hidden by canopy and is very difficult to see in the day video image, but detectable in the thermal image. Highway Route 6 is visible on the left side of the image. The median water temperature is 19.4^{o}C.

Image A-24 illustrates a headwaters reach of Gales Creek (River Mile 24.6) with boulder/cobble substrate. Gales Creek flows from the top to the bottom of the image and the water temperature is 11.7^{o}C. Large riparian vegetation can be observed in the video image.

Image A-19.   Surface temperature at the Confluence of Gales Creek and the Tualatin River.[5]
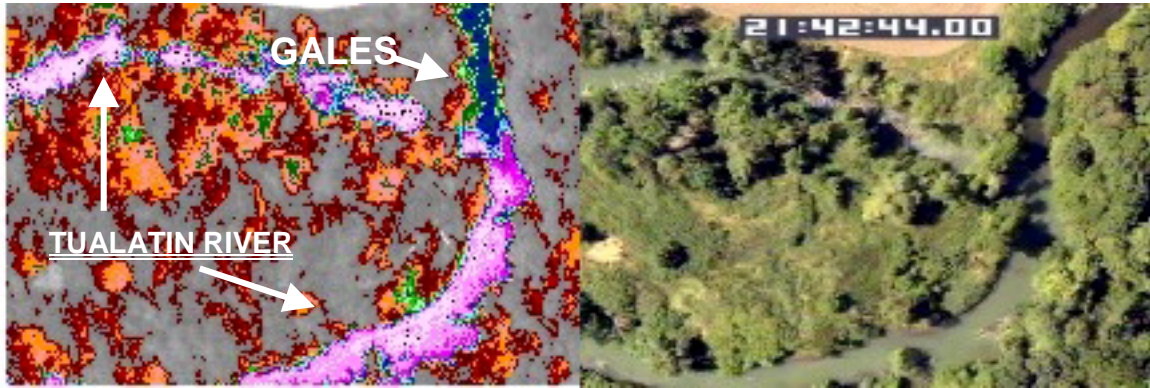
Image A-20.   Gales Creek at the Hwy 47 Bridge.
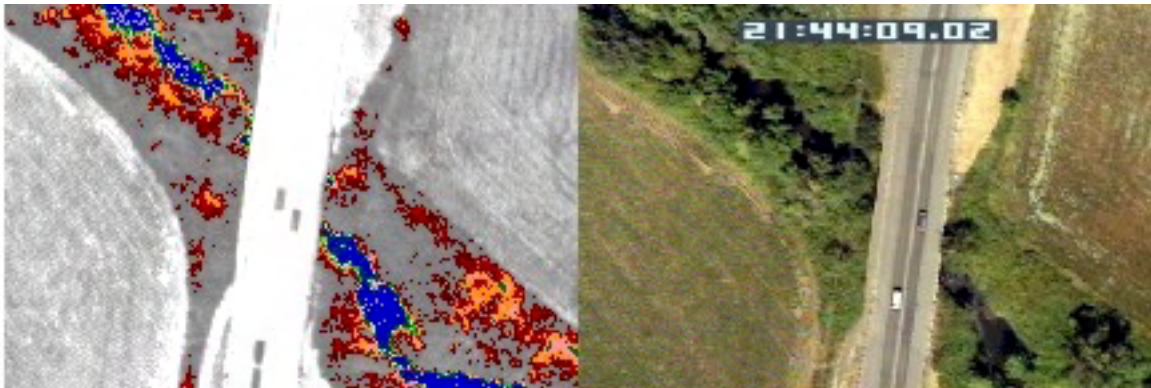
Image A-21.   Gales Creek upstream of the Roderick Creek confluence.

FLIR Image Temperature Scale (°C)

Image A-22. Gales Creek at a dam located upstream of Little Beaver Creek. [6]

Image A-23. Gales Creek immediately upstream of Dorman Ponds.

Image A-24. An upper Gales Creek reach with bedrock channel.
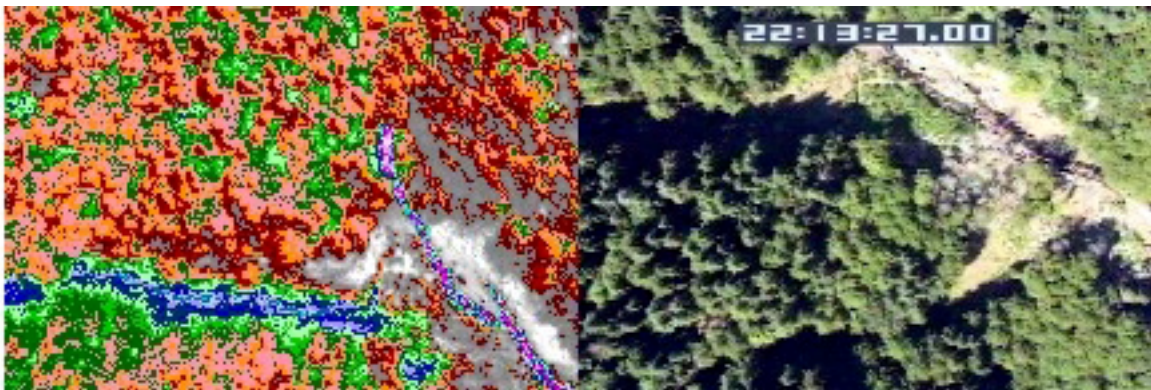
FLIR Image Temperature Scale (°C)

GALES CREEK MODEL INPUT DATA

Gales Creek was modeled from upstream of the Gales Creek Camp Ground (river mile 24.5) to the mouth (river mile 0.0). Model segment lengths were 100 feet. This section graphically displays model input data for each of the 100-foot model segments. Data sources and methodology used to assemble the model input were presented earlier in this Appendix.

- Elevation and Gradient (**Figures A-60**)

- Aspect (**Figures A-61**)

- Near Stream Disturbance Zone Widths and Wetted Widths (**Figures A-62**)

- Topographic Shade (**Figures A-63**)

- Vegetation Geometry (**Figures A-64**)

- Flow Volume (**Figures A-65**)

- Flow Velocity (**Figures A-66**)

- Water Column Depth (**Figures A-67**)

Figure A-60.   Gales Creek Elevation and Gradient at Each 100-foot Model Reach.
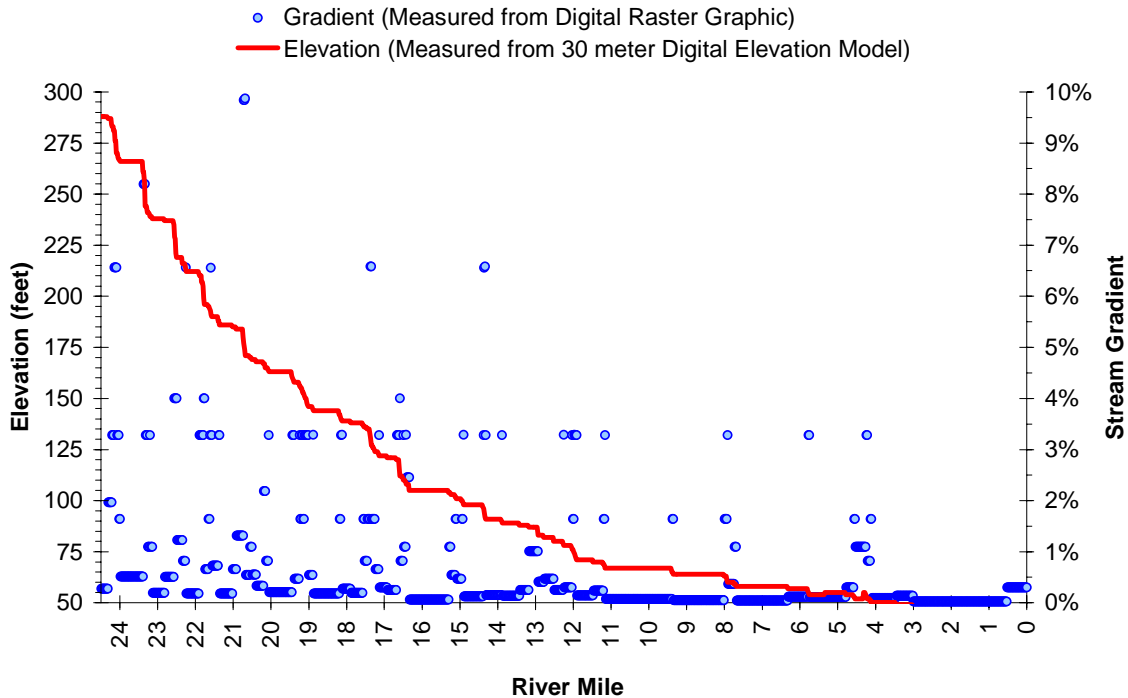
Figure A-61. Gales Creek Aspect at Each 100-foot Model Reach.
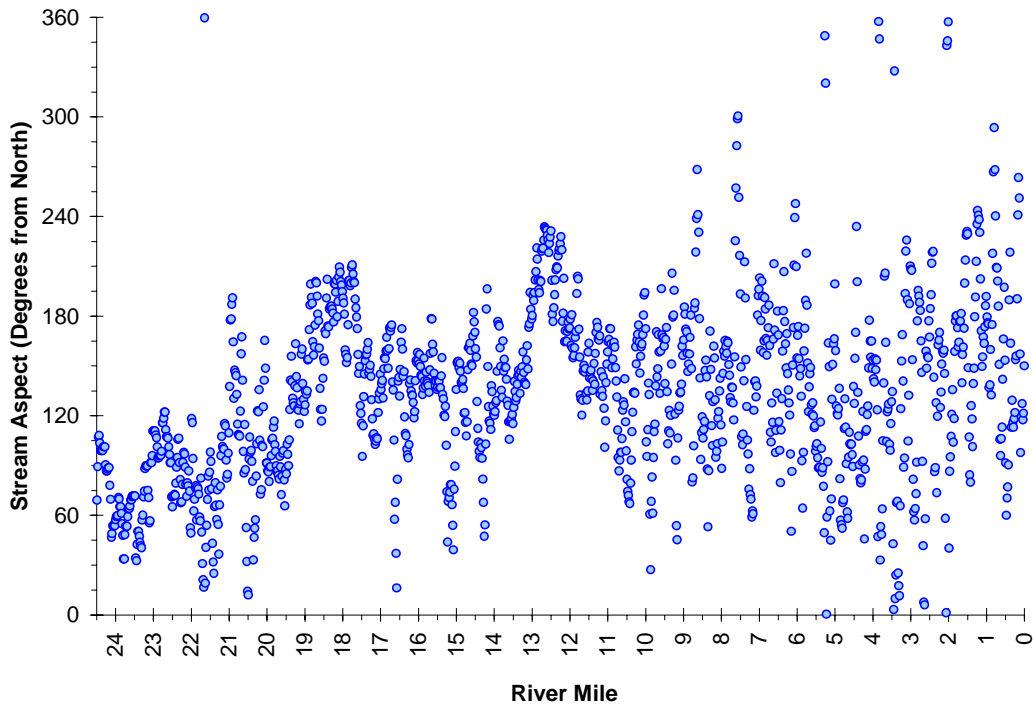
Figure A-62. Gales Creek NSDZ and Wetted Widths.
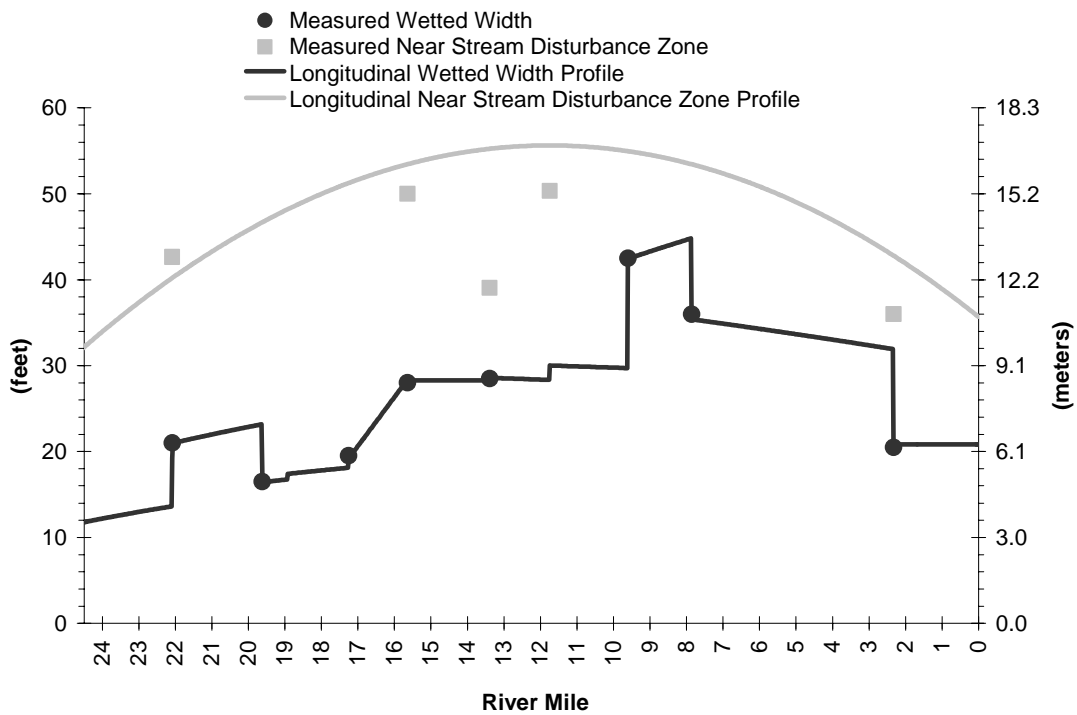
Figure A-63.   Gales Creek Topographic Shade at Each 100-foot Model Reach.
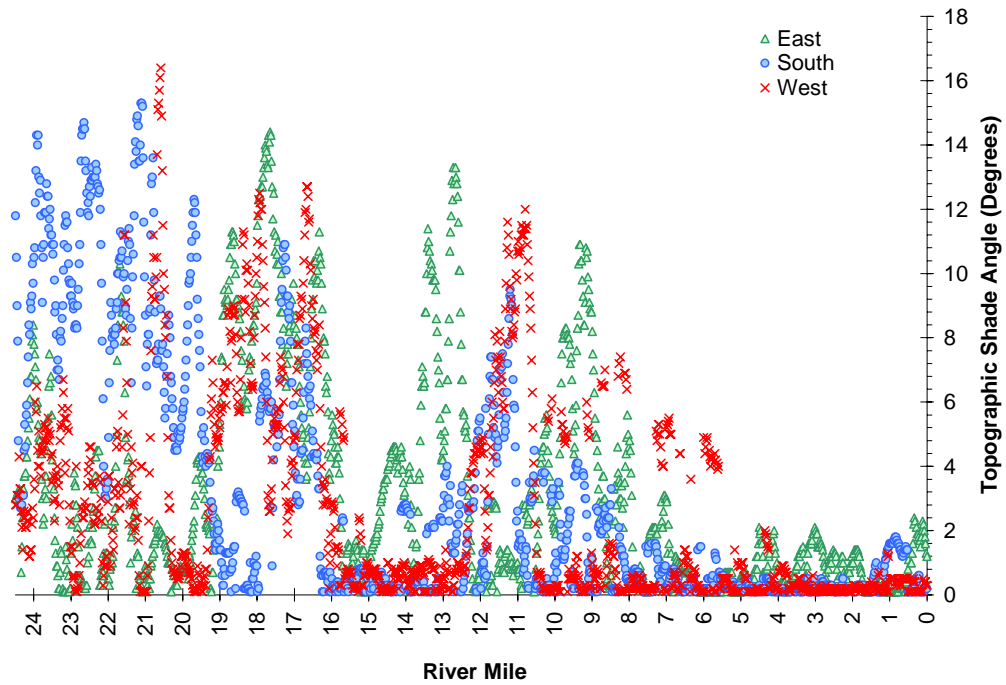
Figure A-64.   Gales Creek Existing Vegetation Heights and Riparian Widths at Each 100-foot Model Reach.
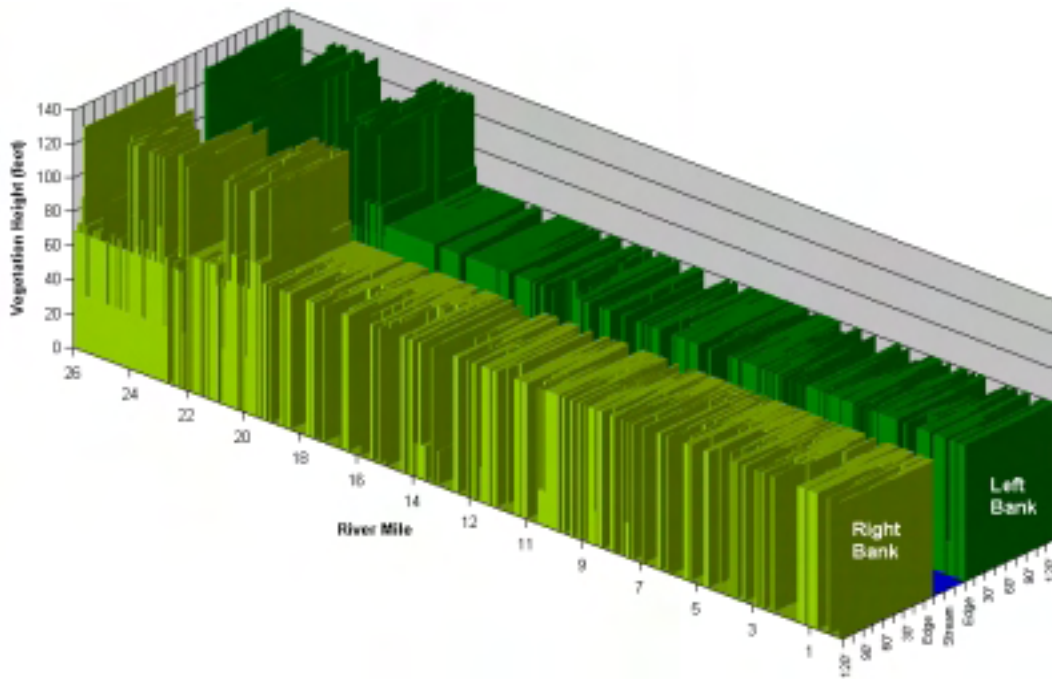
Figure A-65.   Gales Creek Measured and Interpolated Longitudinal Flow Volume
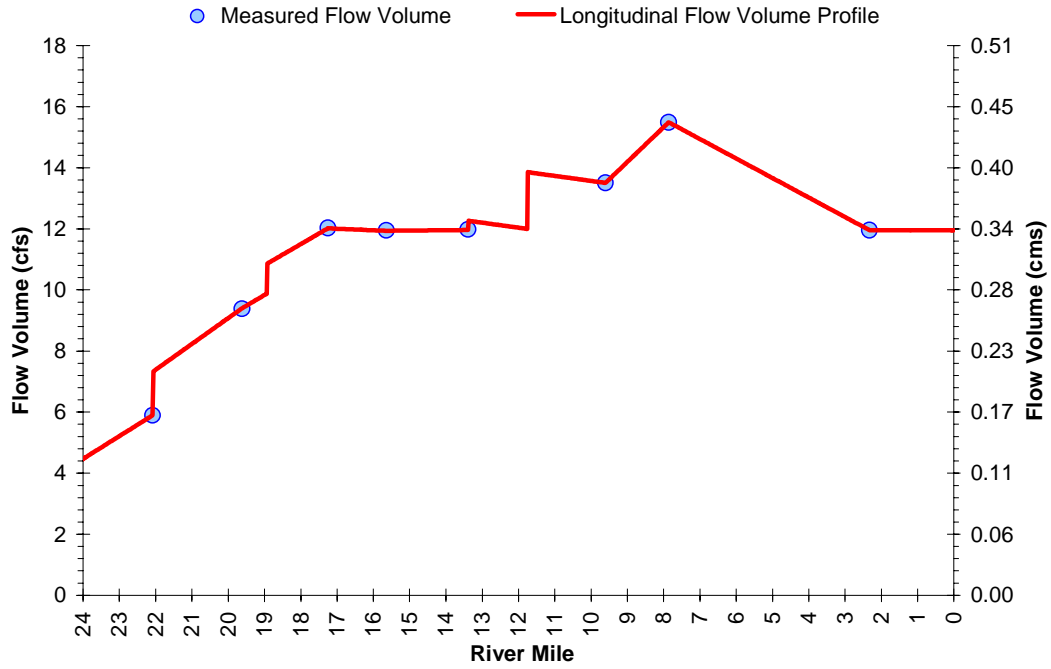
Figure A-66.   Gales Creek Measured and Mannings Derived Longitudinal Flow Velocities.
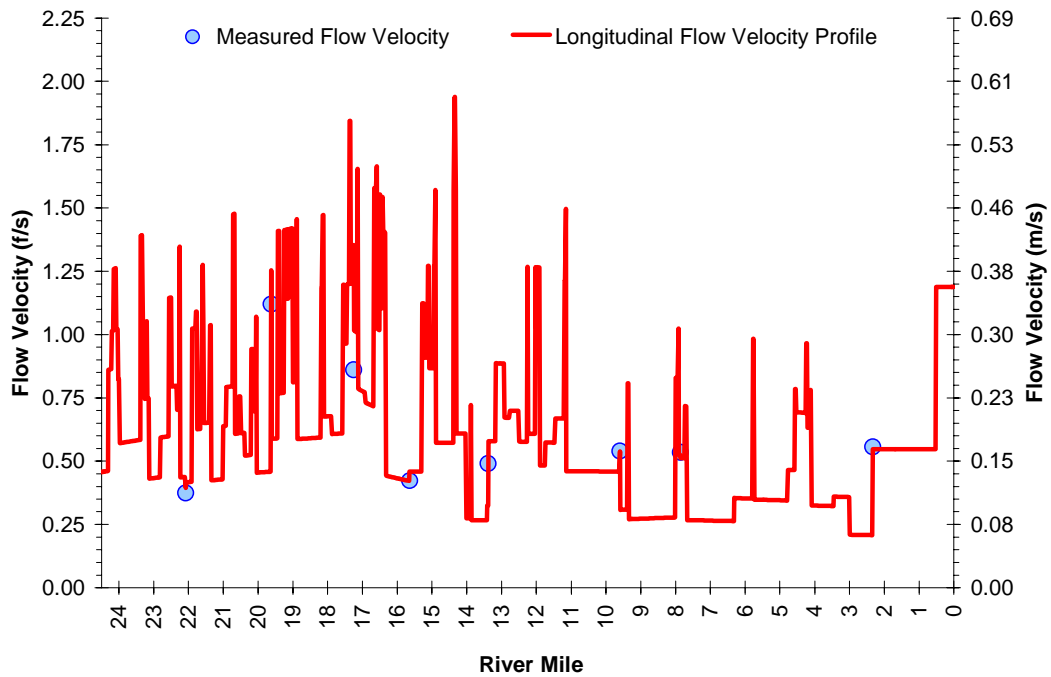
Figure A-67. Gales Creek Measured and Mannings Derived Longitudinal Water Column Depths.
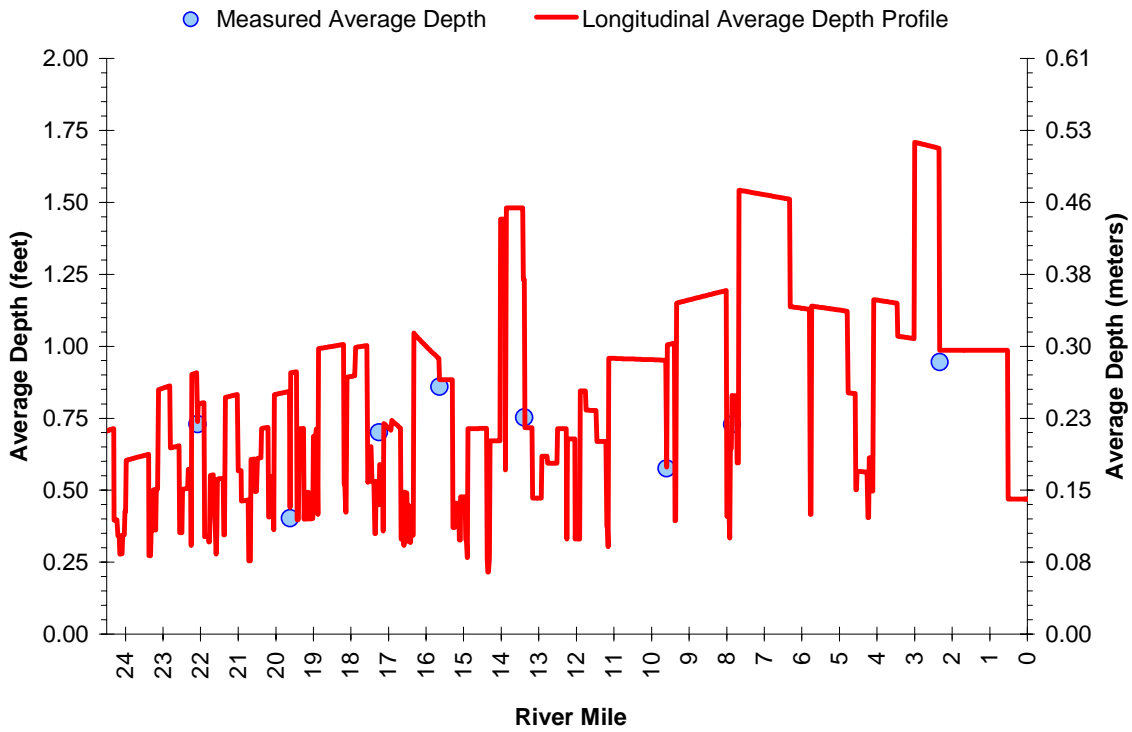
GALES CREEK MODEL RESULTS

This section presents temperature modeling results for Gales Creek. Graphical and statistical validation of the Gales Creek calibrated model are shown, in addition to temperature predictions for potential vegetation and flow conditions. Recall that the modeled was calibrated with data collected on July 28, 1999 and thus is representative of critical stream temperature, stream flow, and climatic conditions. In other words, this modeling effort has captured the period when stream temperatures were near their peak. Spatial validation of the calibrated model is presented in **Figure A-68**. The solid line is the calibrated model temperature prediction at 3:00 PM on July 28, 1999, while the dots represent the FLIR-measured temperatures at that same time. Notice how the Gales Creek temperatures exceeded 64°F below river mile 18.

The standard error and average deviation for the spatial data calibration are:

$$Standard\ Error = 0.85^oC\ (1.53^oF)$$

$$Average\ Deviation = 0.20^oC\ (0.35^oF)$$

Figure A-68. Gales Creek Observed and Predicted Spatial Temperature Data on 7/28/99.
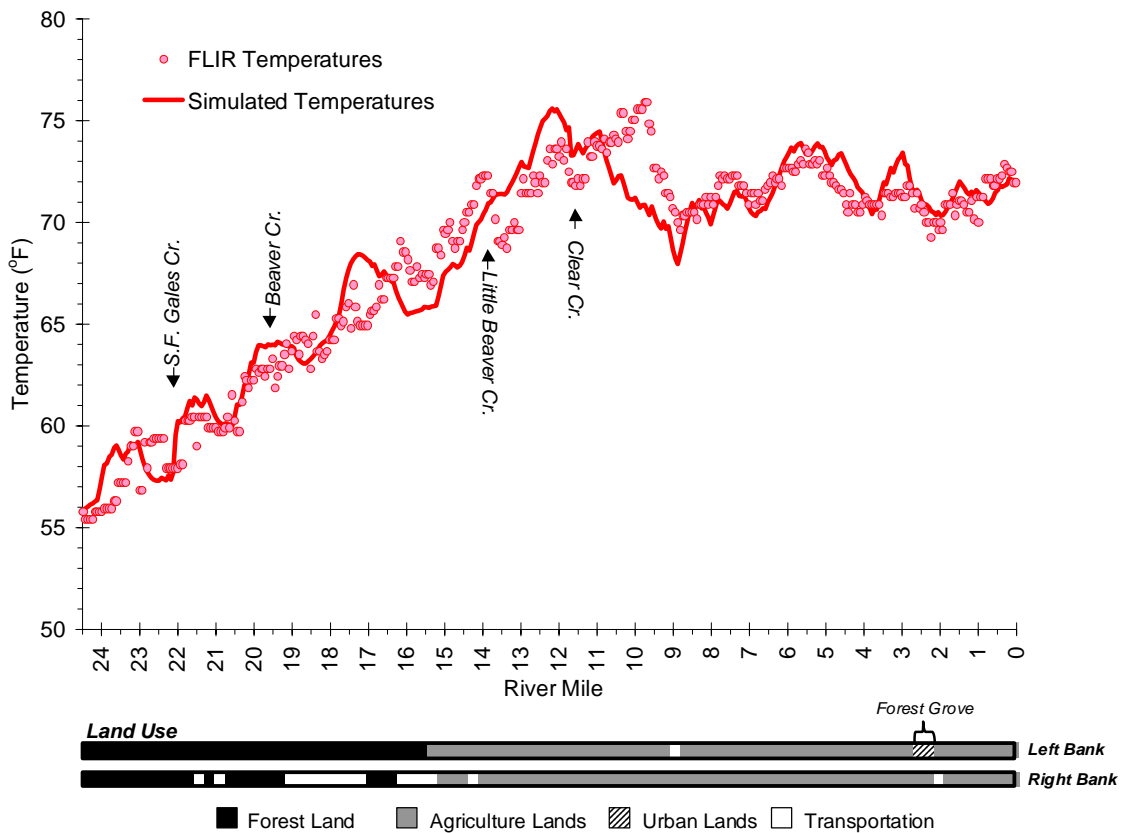
Observed and predicted hourly temperatures at seven continuous temperature monitoring locations on Gales Creek are presented in **Figure A-69**. Node 1 is the upper boundary condition and remains constant, therefore it is not graphed. Standard errors and average deviations are presented for each node. The mean standard error and mean average deviation for the continuous data are:

$$Mean\ Standard\ Error = 0.47^{o}C\ (0.84^{o}F)$$

$$Mean\ Average\ Deviation = 0.97^{o}C\ (1.75^{o}F)$$

Figure A-69.   Gales Creek Model Continuous Data Validation
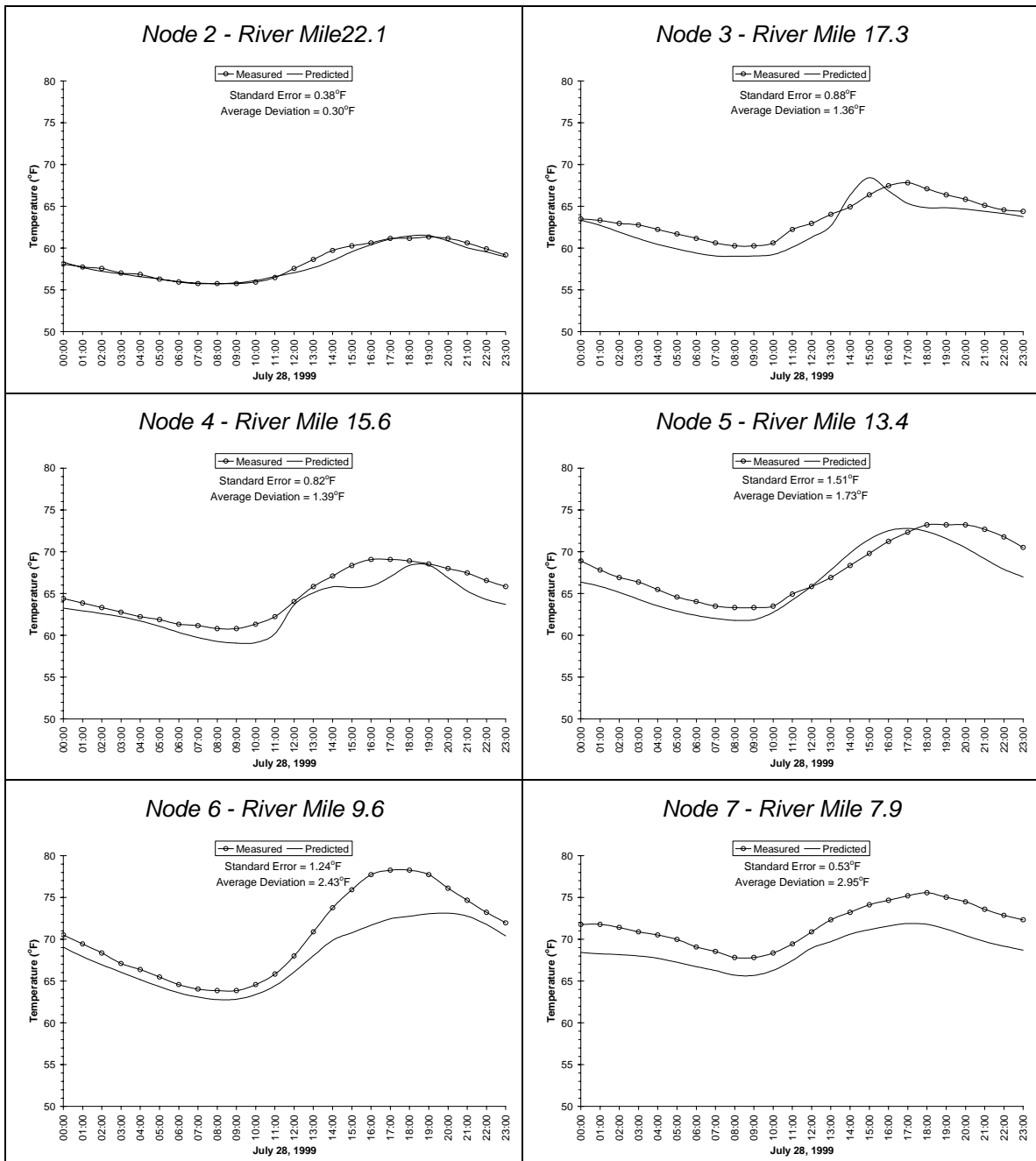
Figure A-69 (continued). Gales Creek Model Continuous Data Validation
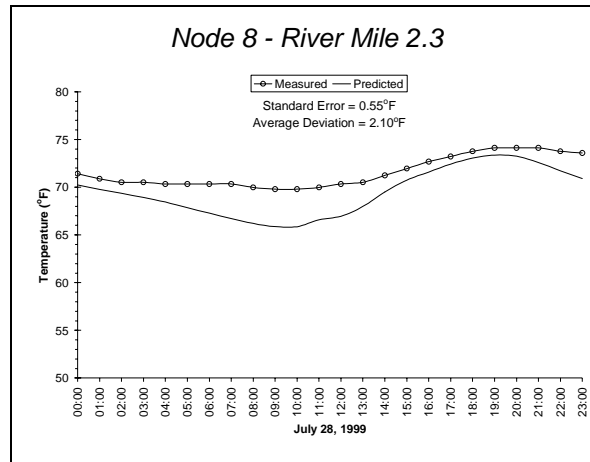
Loading Capacity - 40 CFR 130.2(f)

Loading Capacity is based on the condition that meets the ***no measurable surface water temperature increase resulting from anthropogenic activities***, as described in Section 2.2.2 in the Temperature TMDL document. This condition is termed ***System Potential*** and is achieved when (1) non-point source solar radiation loading reflects a riparian vegetation condition without human disturbance and (2) point source discharges cause no measurable increases in surface water temperatures.

Solar radiation loading was calculated using system potential riparian vegetation, at current channel and stream aspect conditions. A detailed description of potential vegetation conditions is presented in **Table A-8**. Current and System Potential solar loading for the Gales Creek are presented in **Figure A-70**. Solar radiation loading for Current Condition and System Potential condition is presented for every 100 meters of modeled stream length. As can be seen in **Figure A-70**, solar radiation loading at System Potential is much less than levels currently observed on Gales Creek (i.e., Current Condition).

Figure A-70. Gales Creek Solar Radiation Load at System Potential and Current Conditions
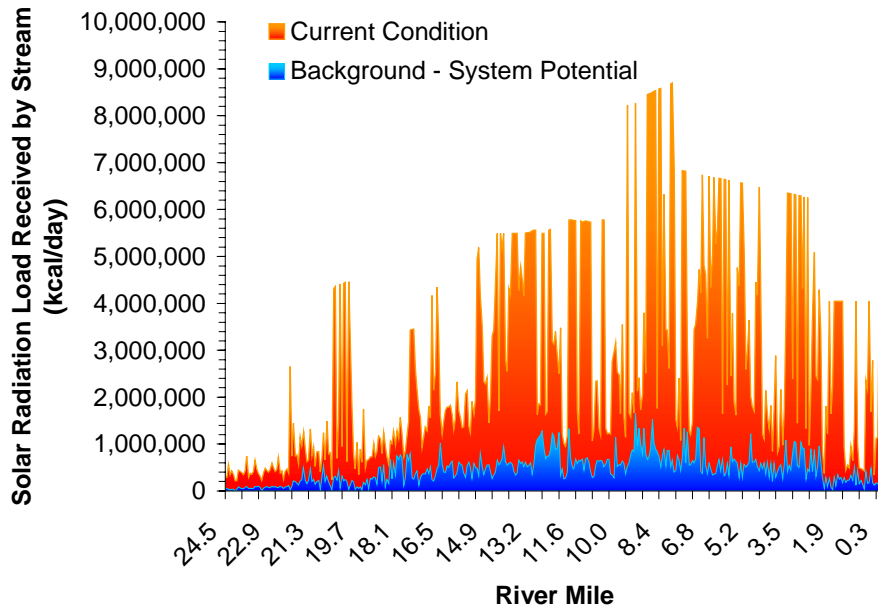
Allocations – 40 CFR 130.2(g) and 40 CFR 130.2(h)

*Load Allocations (Non-Point Sources) - The **temperature standard** targets system potential (i.e. no measurable temperature increases from anthropogenic sources). To meet this requirement the system potential solar radiation heat load ($6.6 \cdot 10^7$ Kcal/day) is allocated to background nonpoint sources. Anthropogenic nonpoint sources are not given a heat load.*

***Wasteload Allocations (Point Sources)** - Surface water discharges into receiving waters have been given a heat load based on the 0.25^oF allowable increase in the mixing zone as specified in the temperature standard. Heat loads have been converted to allowable effluent temperatures as well. It should be noted that the wasteload allocation is the point source heat load and not the calculated maximum effluent temperatures. There are several options for meeting the allocated heat loads (i.e. passive effluent temperature reductions, changes in facility discharge operation, purchasing instream flows, pollutant trading, etc.).*

Temperature Allocation Summary **Non-Point Sources**	
Source	*Loading Allocation* *Allowable Nonpoint Source Solar Radiation Heat Load* *(kcal/day)*
Natural	$1.8 \cdot 10^8$ Kcal/day
Agriculture	$\varnothing$
Forestry	$\varnothing$
Urban	$\varnothing$
Future Sources	$\varnothing$

No permitted point sources currently discharge into Gales Creek. Therefore, no specific waste load analysis was conducted for Gales Creek.

Surrogate Measures – 40 CFR 130.2(I)

The solar radiation load (Kcal/day) at system potential condition was calculated by multiplying the stream surface area by the solar radiation flux (Iy/day). Percent effective shade was used as a surrogate measure of the solar radiation flux calculated at system potential conditions (**Figure A-71**). The individual points in the figure represent the current and allocated conditions for every 100 meters. Accordingly, System Potential heat load condition along Gales Creek translates into approximately 85% or greater effective shade throughout much of the system.

Figure A-71.   Gales Creek Surrogate Measure for Non Point Sources – *Effective Shade*
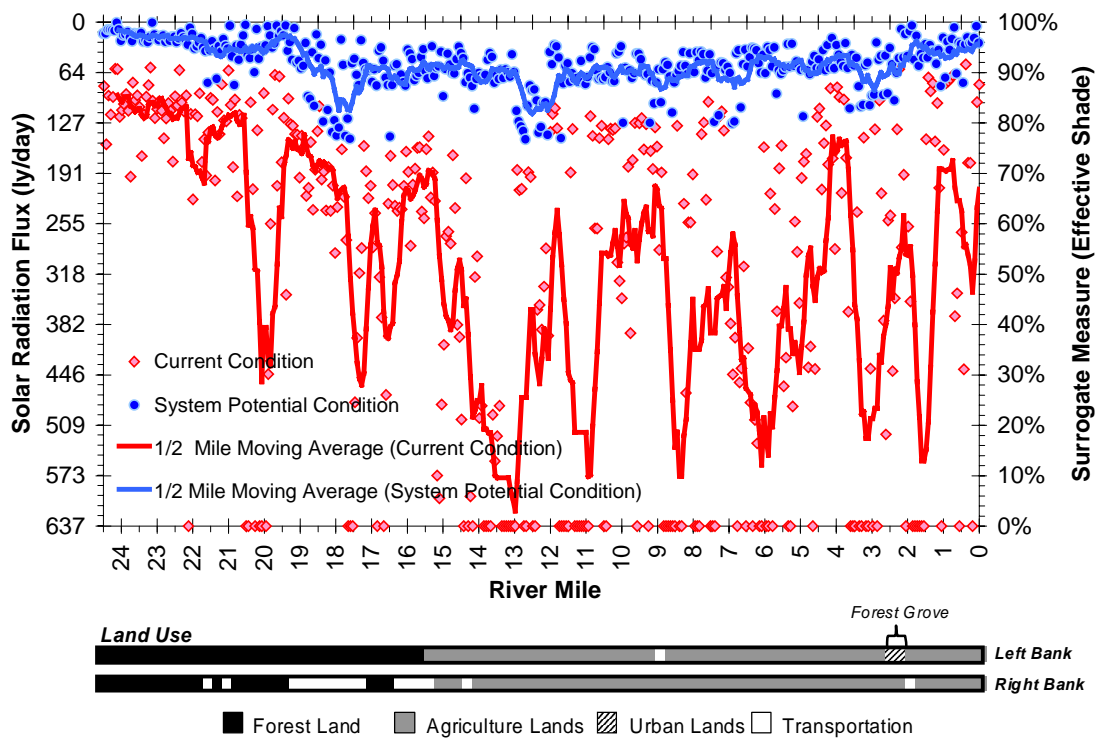
Water Quality Standard Attainment Analysis – CWA §303(d)(1)

System Potential is achieved when (1) non-point source solar radiation loading reflects a riparian vegetation condition without human disturbance and (2) point source discharges cause no measurable increase in surface water temperature. Accordingly, **Figure A-72** presents predicted Gales Creek temperatures at a Waste Load Allocation and Load Allocation scenario. **Figure A-73** illustrates that implementing Waste Load Allocations and Load Allocations will drastically reduce temperatures in Gales Creek.

Figure A-72. Gales Creek Daily Temperature Range for Current Conditions Compared with Allocated Measures - July 28, 1999.
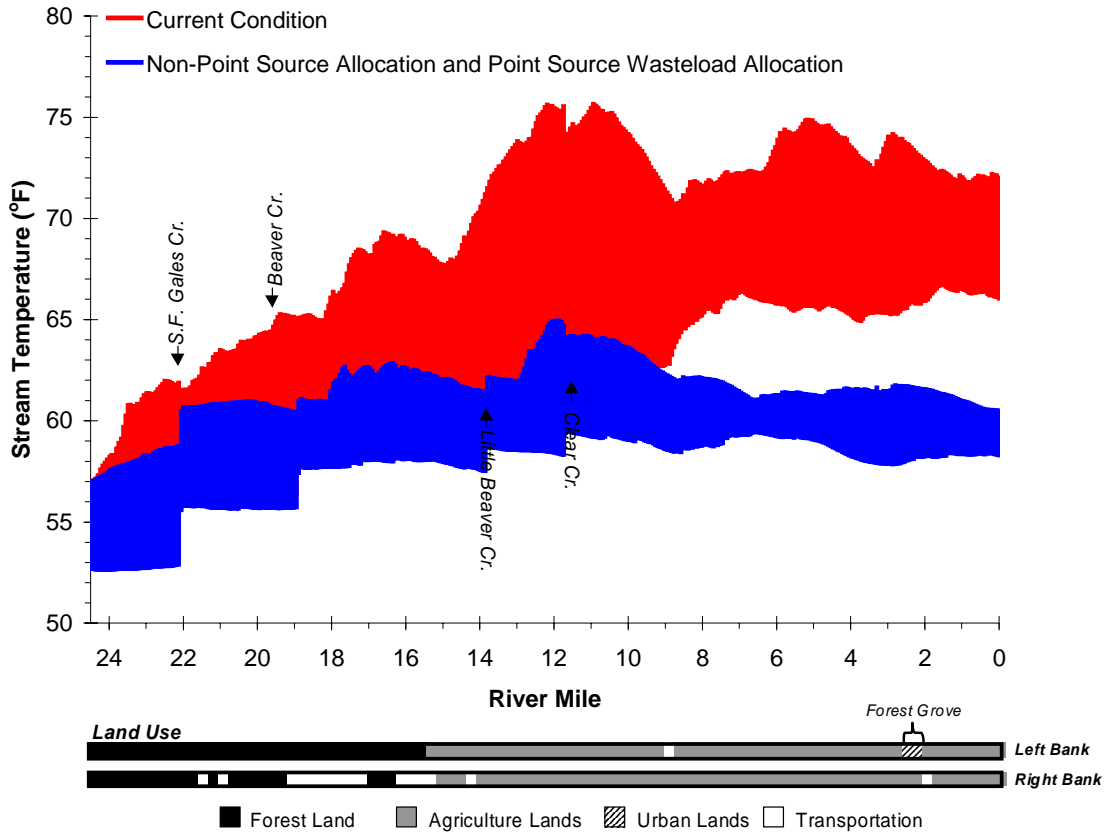
Figure A-73. Gales Creek Current and System Potential (Allocated) Temperature Distributions
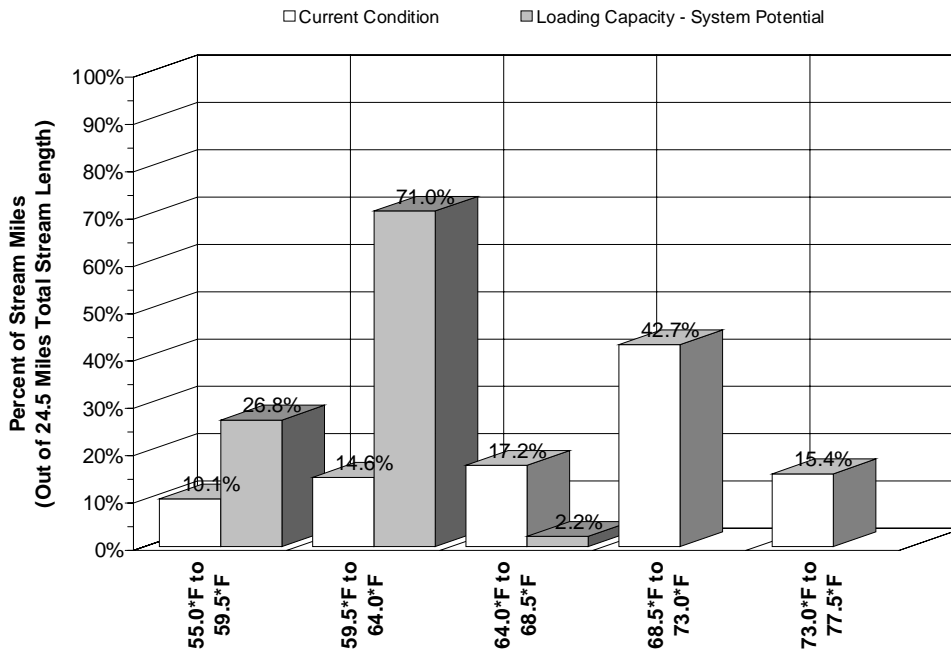
EAST FORK DAIRY CREEK

EAST FORK DAIRY CREEK* CURRENT CONDITION

The Oregon Department of Environmental Quality collected stream temperature, flow, and site descriptions along East Fork Dairy Creek during the summer of 1999. **Figure A-74** illustrates the locations of data collection sites. Digital photographs taken at some of the sampling sites are presented in **Images A-25** through **A-28**.

Figure A-74. Water Quality Summer Sampling Locations for East Fork Dairy Creek during 1999.
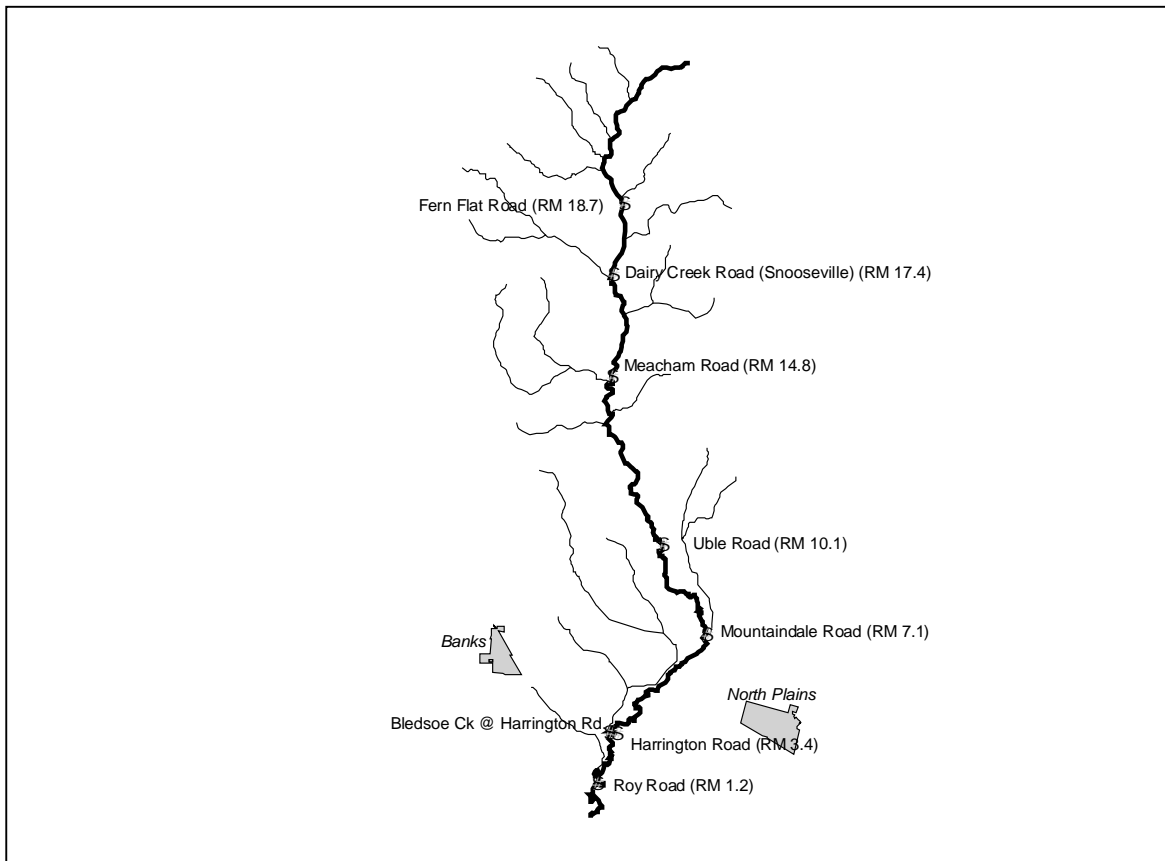
East Fork Dairy Creek temperatures increase during the summer period, with daily maximums occurring in late July and August (**Figure A-75**). The longitudinal profile of the calculated 7-day temperature statistics are presented in **Figure A-76**. The upper portion of East Fork Dairy Creek was below the 64°F temperature criteria in 1999, while the lower half exceeded the criteria. As can be seen in these figures, observed daily maximum temperatures and calculated 7-Day maximum remain relatively constant downstream of East Fork Dairy Creek at Meacham Road Bridge (RM 14.8). **Table A-17** summarizes the calculated stream temperature statistics for East Fork Dairy Creek.

---

* Note that the river miles (RM) presented in this report were derived from a 1:5000 stream coverage used for ODEQ modeling purposes and may differ slightly from other sources (such as OWRD or USGS river miles).

Image A-25. East Fork Dairy Creek at Fern Flat Road (River Mile 18.7).
[Temp. Statistic – 59.7*F, Flow – 6.1 cfs, Potential Effective Shade (ES) – 97%, Measured ES – 81%]

Image A-26. East Fork Dairy Creek at Meacham Road (River Mile 14.8).
[Temp. Statistic – 63.3*F, Flow – 16.5 cfs, Potential Effective Shade (ES) – 91%, Measured ES – 65%]
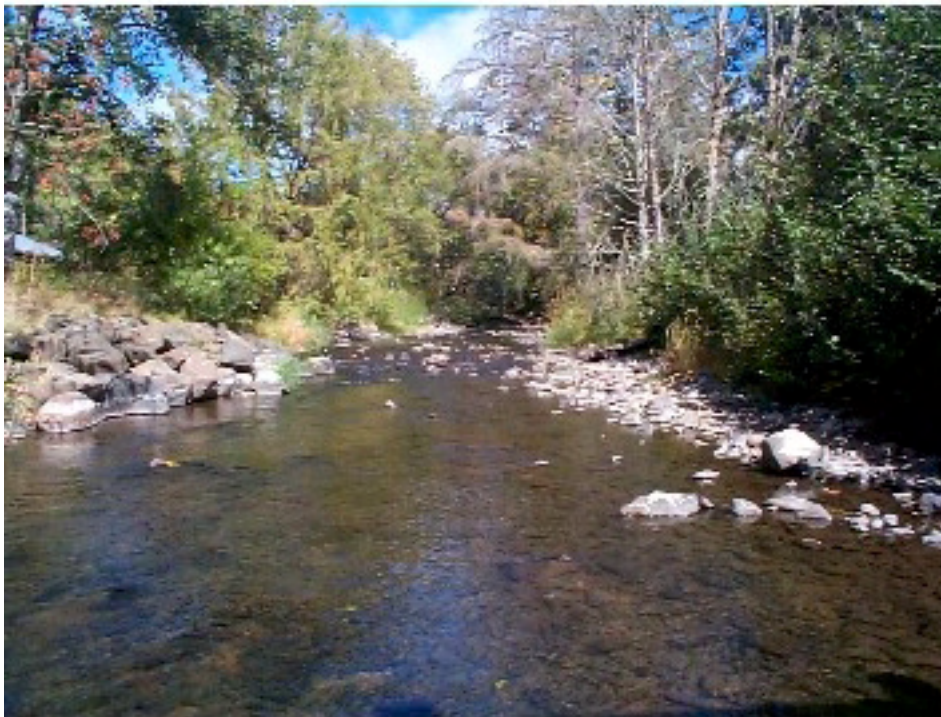
Image A-27.   East Fork Dairy Creek at Mountaindale Road (River Mile 7.1).
[Temp. Statistic – 67.3*F, Flow – 16.9 cfs, Potential Effective Shade (ES) – 85%, Measured ES – 62%]

Image A-28.   East Fork Dairy Creek at Harrington Road (River Mile 3.4).
[Temp. Statistic – 66.7*F, Flow – 16.9 cfs, Potential Effective Shade (ES) – 93%, Measured ES – 84%]
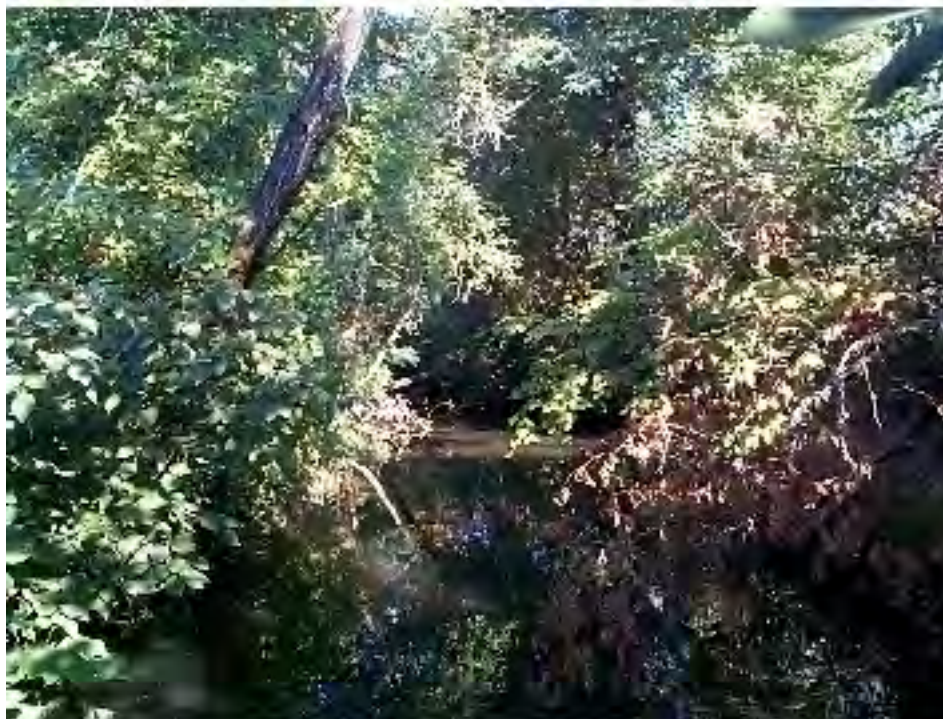
Figure A-75. Observed Daily Maximum Stream Temperatures for East Fork Dairy Creek.
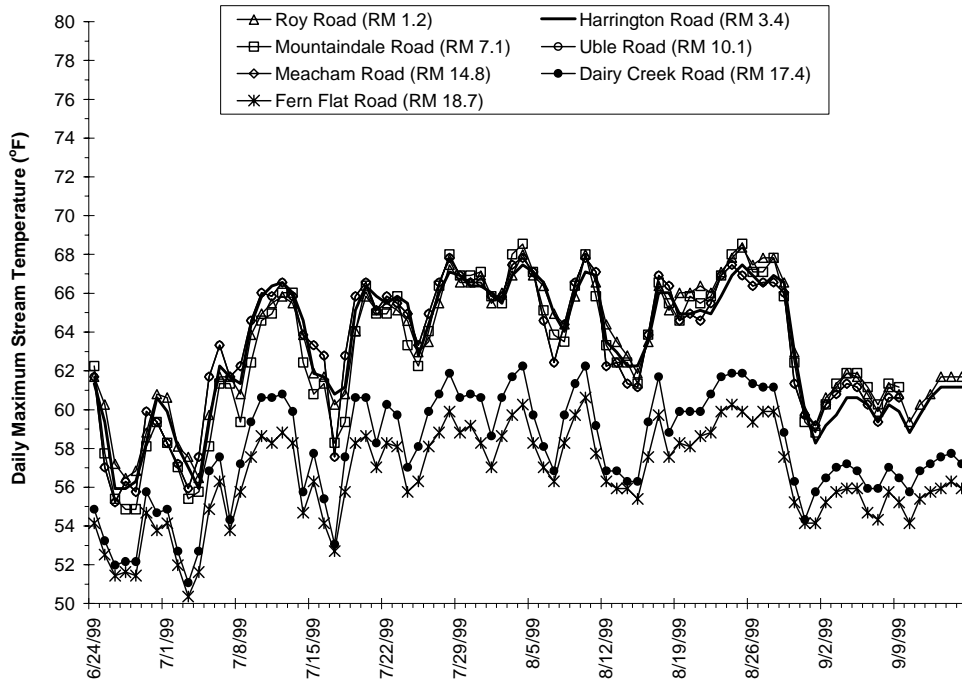
Figure A-76. Observed Maximum 7-Day Temperature Statistics for East Fork Dairy Creek.
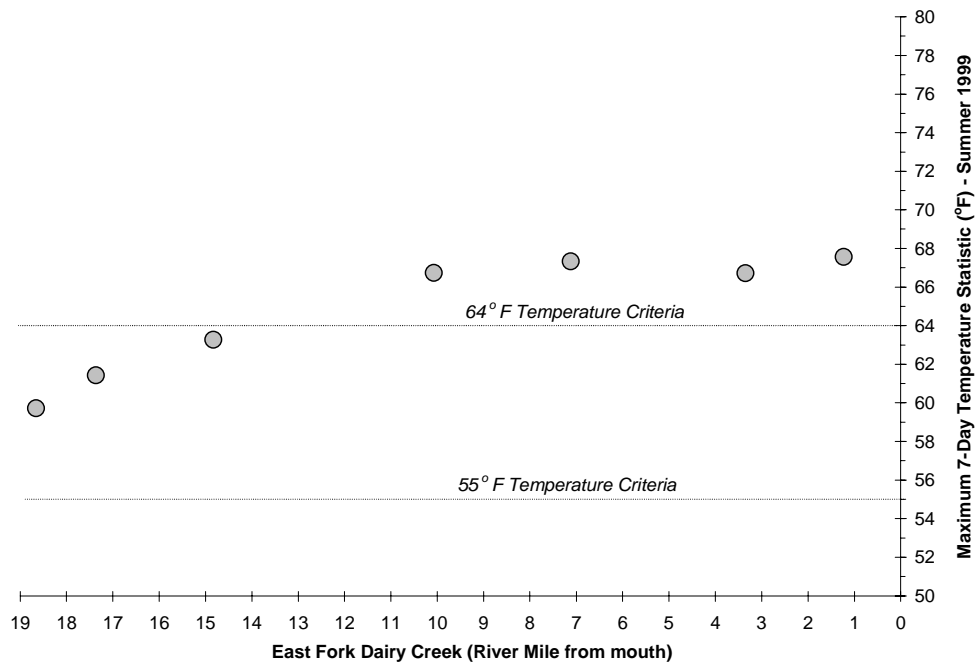
Table A-17. Calculated Stream Temperature Statistics for East Fork Dairy Creek						
Temperature Site	Start	End	Max. Daily Temp		Max. 7-Day Statistic	
(RM = River Mile from mouth)	*Date*	*Date*	*Date*	*(^{o}F)*	*Date*	*(^{o}F)*
RM 1.2 Roy Road	6/24/99	9/21/99	8/25/99	68.4	8/26/99	67.6
RM 3.4 Harrington Road	6/24/99	9/21/99	8/25/99	67.5	8/26/99	66.7
RM 7.1 Mountaindale Road	6/18/99	9/15/99	8/25/99	68.5	8/26/99	67.3
RM 10.1 Uble Road	6/18/99	9/15/99	8/10/99	67.8	8/02/99	66.7
RM 14.8 Meacham Road	6/18/99	9/15/99	8/10/99	64.4	8/25/99	63.3
RM 17.4 Dairy Creek Rd. (Snooseville)	6/18/99	9/15/99	8/10/99	62.2	8/25/99	61.4
RM 18.7 Fern Flat Road	6/18/99	9/15/99	8/10/99	60.6	8/25/99	59.7

Water temperatures in East Fork Dairy Creek varied through out the course of the day, with maximum temperatures occurring in the late afternoon and minimums temperature occurring during the early morning hours. The diurnal temperature profile for East Fork Dairy Creek on July 29, 1999 is presented in **Figure A-77**. Very little diurnal temperature variability was observed within East Fork Dairy Creek. Diurnal temperature variability decreased at lower sections of the river. This indicates that the hydrological conditions within these lower reaches are different than upstream conditions.

River discharge was measured throughout the East Fork Dairy Creek River system during the period of FLIR sampling, which corresponds to the period of summer maximum water temperatures (**Figure A-78**). Water discharge rates generally increase in a downstream direction, reaching a maximum value of 17 cfs.

Figure A-77. Diurnal Temperature Trends Observed in East Fork Dairy Creek on July 29, 1999.
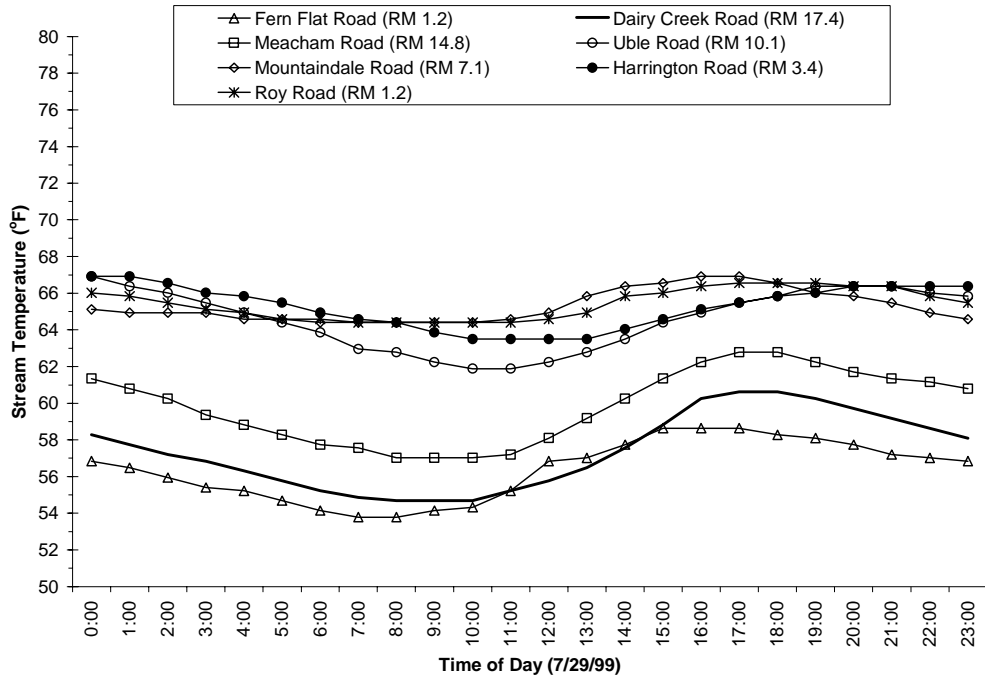
Figure A-78. Stream Flow Observed in East Fork Dairy Creek on July 29, 1999.
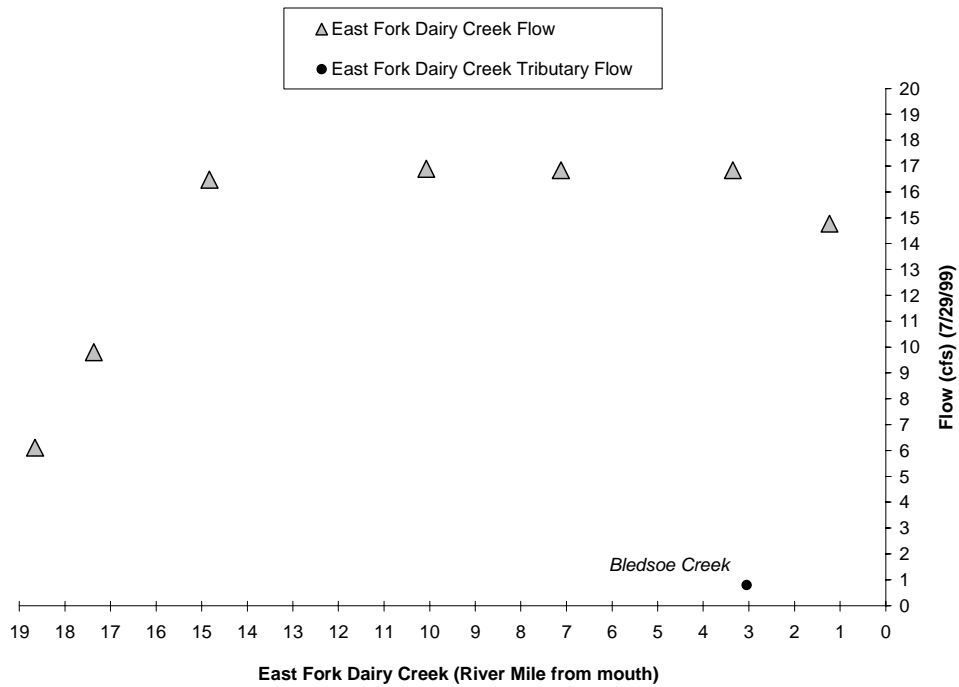
Figure A-79 presents the measured FLIR temperature profile for East Fork Dairy Creek, which was sampled on July 29, 1999 between 5:00 to 5:23 PM. As can be seen in this image, there was a gradual temperature increase from 60°F to 68°F over the 19 stream miles that were flown. Of the stream length flown, over about 75% of the recorded temperatures fell within the sub-lethal limit for salmonids (**Table A-18**).

Figure A-79.   East Fork Dairy Creek FLIR Temperature Profile (17:00 to 17:23 on 7/29/99)

East Fork Dairy Creek (River Mile from mouth)
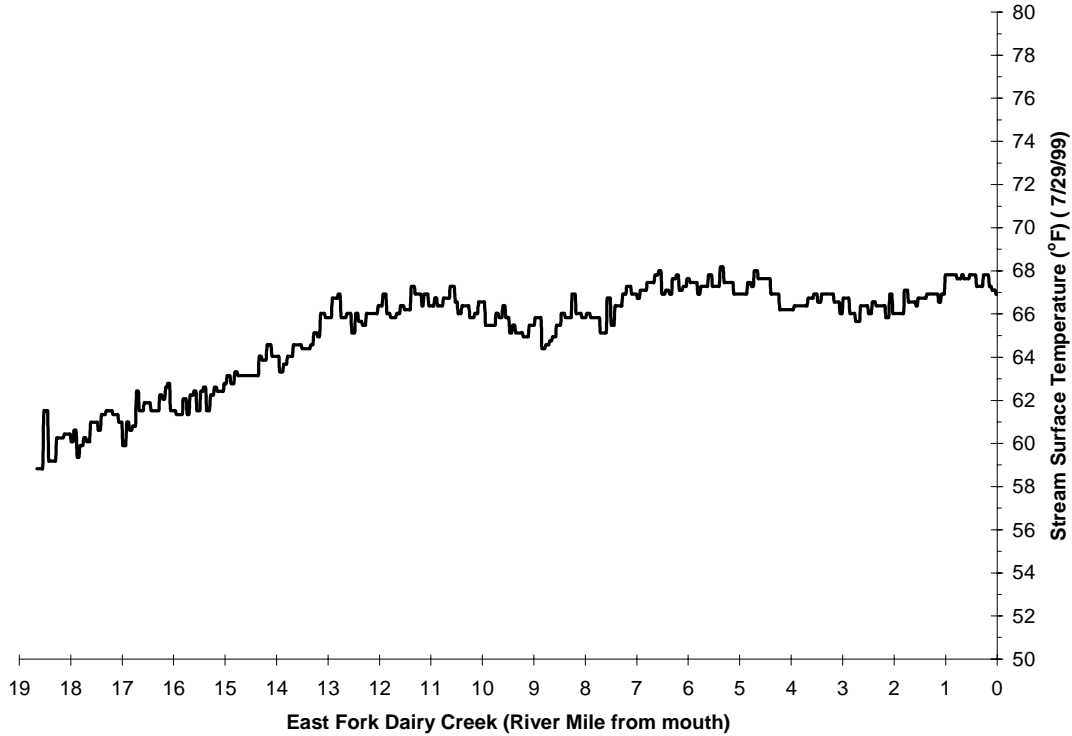
Table A-18. FLIR-derived Water Temperatures in East Fork Dairy Creek (7/29/99)			
Temperature (°F)	Distance (miles)	Percent of Total	Mode of Thermal Mortality
Less than 55.0	-	-	
55.0 to 59.5	0.2	1.0%	
59.5 to 64.0	4.4	23.7%	
64.0 to 68.5	14.0	75.3%	
68.5 to 73.0	-	-	Sub-Lethal Range
73.0 to 77.5	-	-	
Greater than 77.5	-	-	Incipient Lethal Range
Totals	18.6	100.0%	

The following FLIR images were taken in East Fork Dairy Creek on July 29, 1999. FLIR thermal imagery interprets temperatures utilizing a Celsius temperature scale. Note that the 64°F is equal to 17.8^{o}C. **Image A-29** illustrates a characteristic view of East Fork Creek within this section of the river (RM 0.2). The stream is sinuous and hidden by dense stands of riparian vegetation. **Image A-30** shows a thermal microclimate associated with riparian vegetation (RM 5.1).

Image A-29.   East Fork Dairy Creek (RM 0.2) 7.
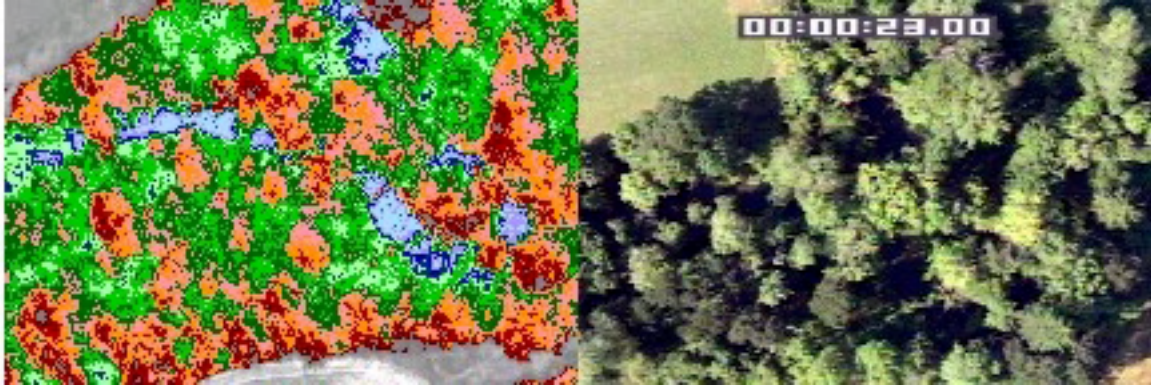
Image A-30.   East Fork Dairy Creek (RM 5.1).

FLIR Image Temperature Scale (^{o}C)

A-113

EAST FORK DAIRY CREEK MODEL INPUTS

The East Fork Dairy Creek was modeled from river mile 18.6 to its mouth. Model segment lengths were each 100 feet. This section graphically displays the model input data for each of the 100-foot model segments. The various data sources and methodology used to assemble model input data are presented earlier in this Appendix.

- Elevation and Gradient (**Figure A-80**)

- Aspect (**Figure A-81**)

- Near Stream Disturbance Zone Widths and Wetted Widths (**Figure A-82**)

- Topographic Shade (**Figure A-83**)

- Vegetation Geometry (**Figure A-84**)

- Flow Volume (**Figure A-85**)

- Flow Velocity (**Figure A-86**)

- Water Column Depth (**Figure A-87**)

Figure A-80.   East Fork Dairy Creek Elevation and Gradient at each 100-foot Model Reach.
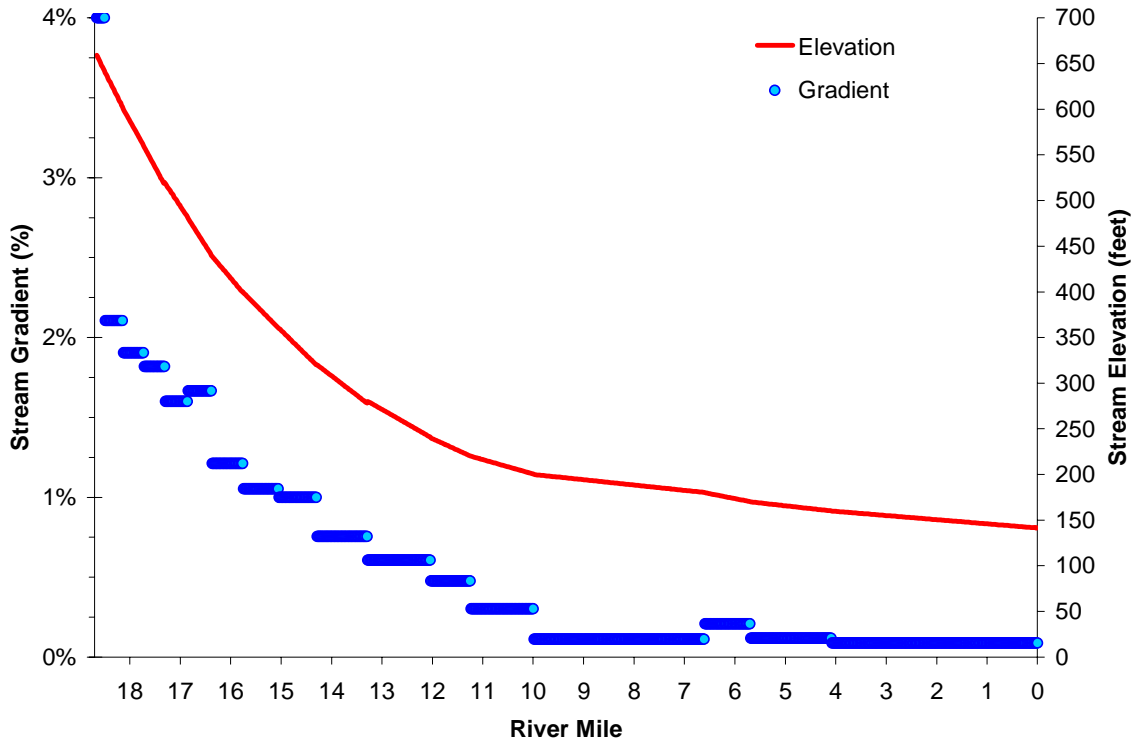
Figure A-81. East Fork Dairy Creek Aspect at Each 100-foot Model Reach.
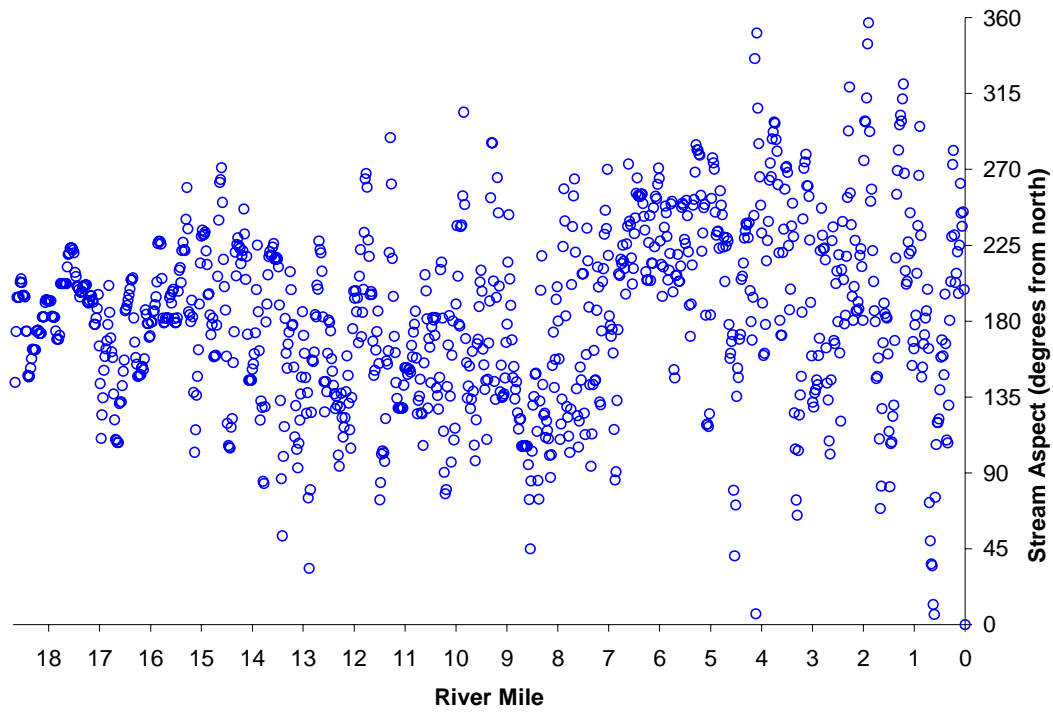
Figure A-82. East Fork Dairy Creek Wetted Widths and NSDZ Widths
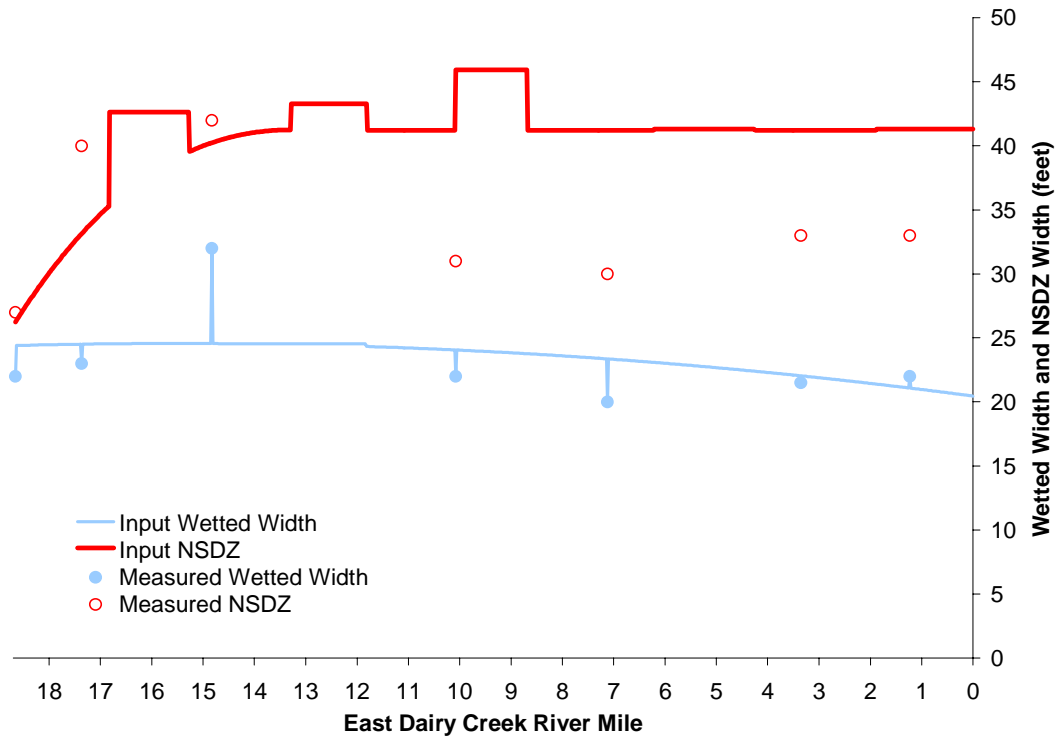
Figure A-83. East Fork Dairy Creek Topographic Shade at Each 100-foot Model Reach
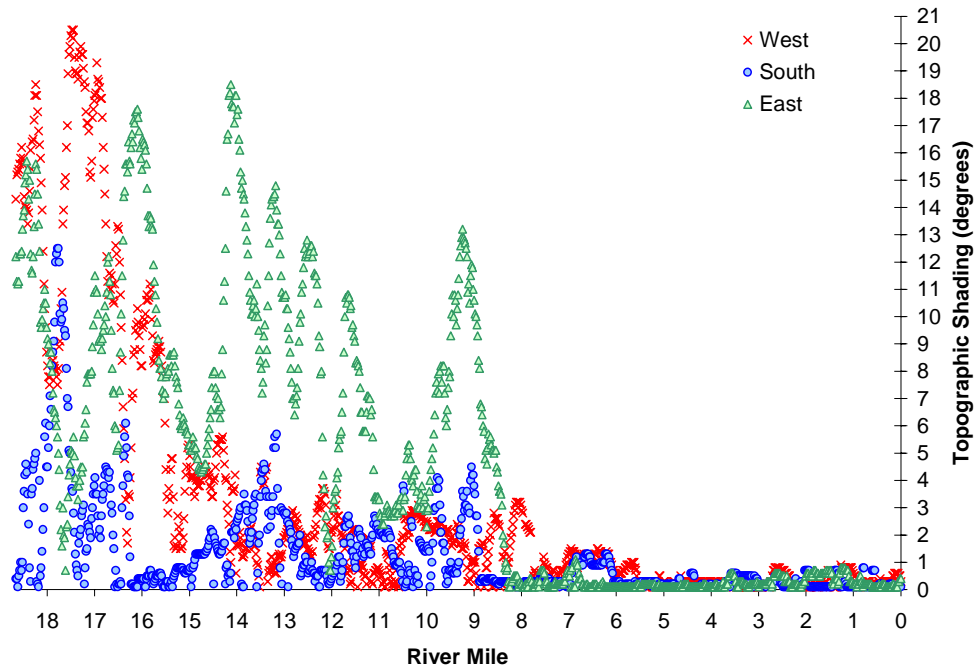
Figure A-84. East Fork Dairy Creek Current Vegetation Heights for each 100-foot Model Reach.
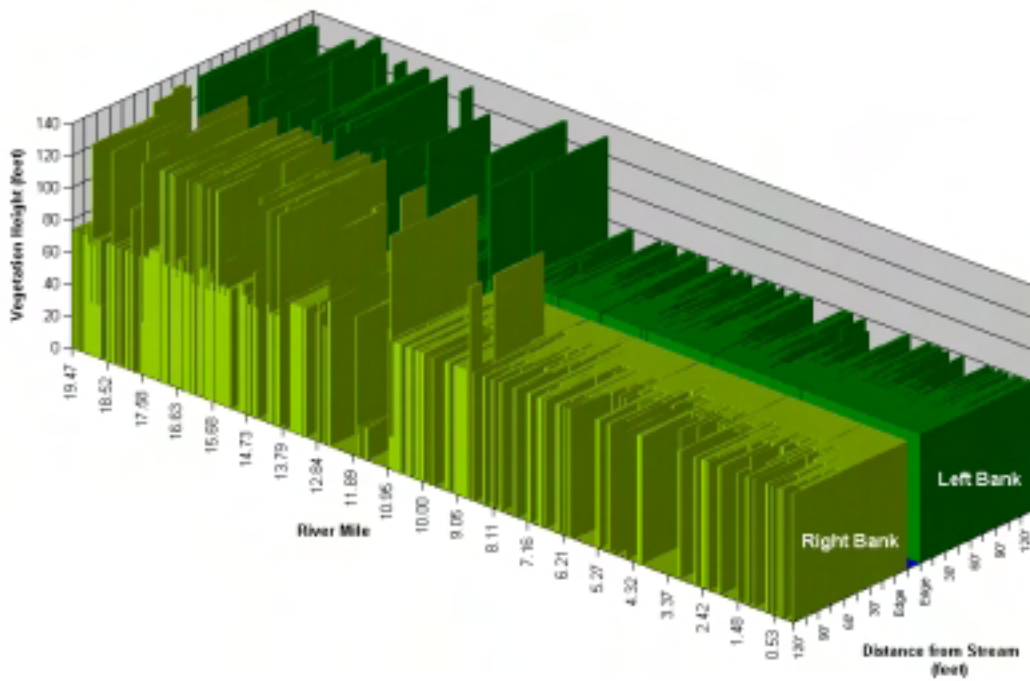
Figure A-85. East Fork Dairy Creek Measured and Interpolated Flow Volume
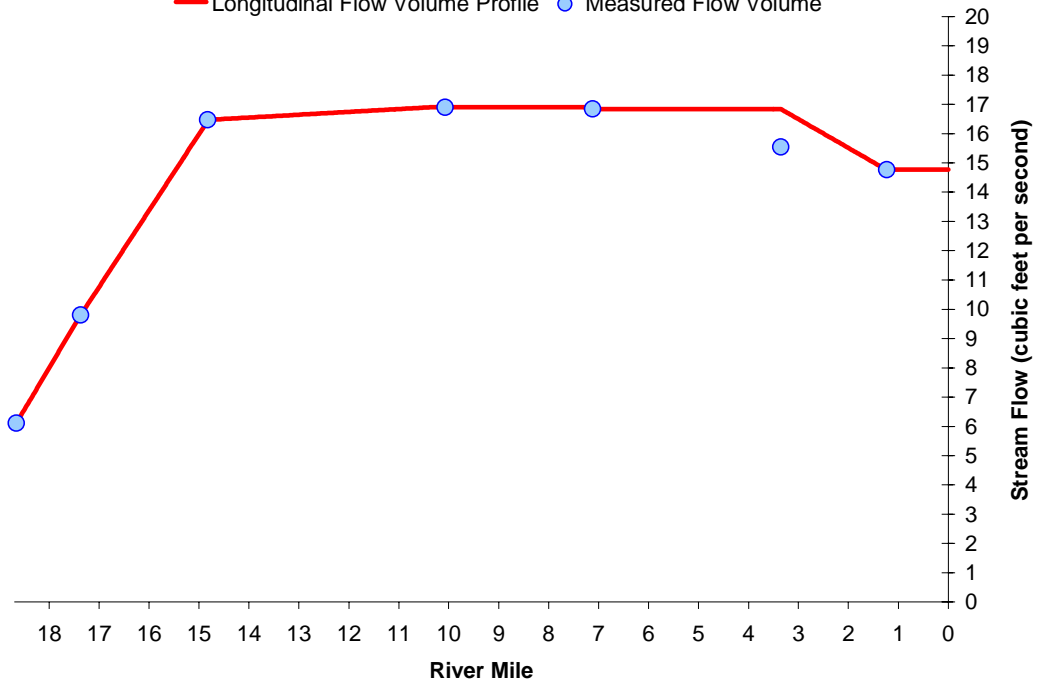
Figure A-86. East Fork Dairy Creek Measured and Mannings Derived Longitudinal Flow Velocities[8]

---
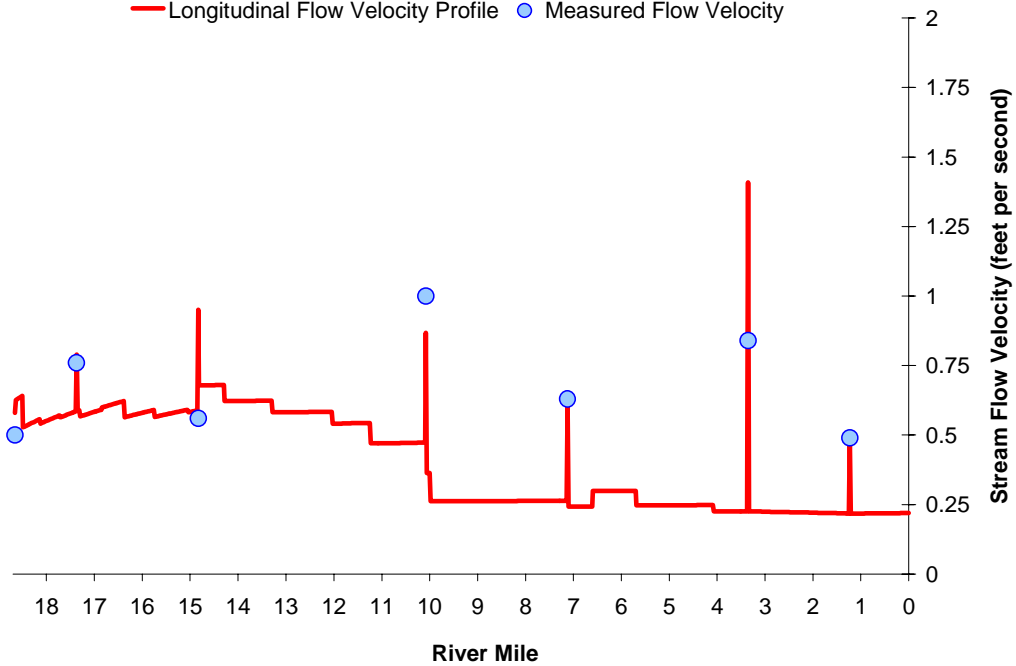
[8] Note that due to the low gradient nature of East Fork Dairy Creek, DEQ data collection targeted riffles to provide more accurate flow measurements (faster velocities).

Figure A-87. East Fork Dairy Creek Measured and Mannings Derived Longitudinal Water Column Depths[9]

---
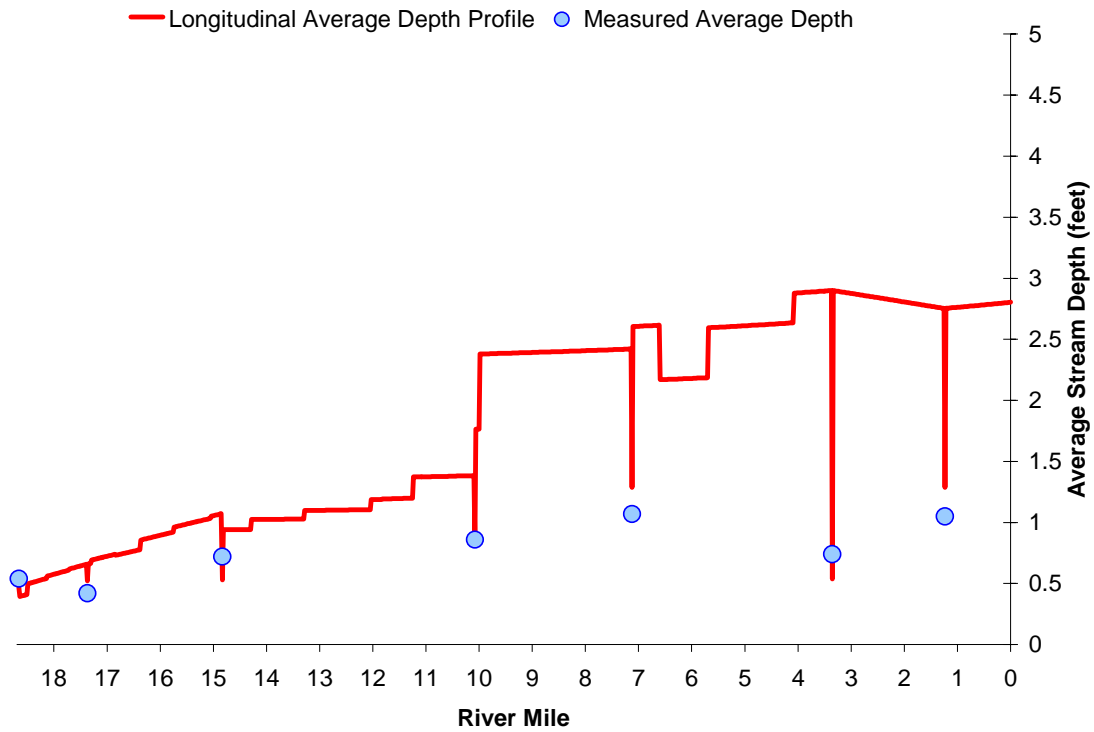
[9] Note that due to the low gradient nature of East Fork Dairy Creek, DEQ data collection targeted riffles to provide more accurate flow measurements (faster velocities).

Eᴀsᴛ Fᴏʀᴋ Dᴀɪʀʏ Cʀᴇᴇᴋ Mᴏᴅᴇʟ Rᴇsᴜʟᴛs

The East Fork Dairy Creek model was calibrated to the FLIR temperatures measured on July 29, 1999 from 17:00 to 17:23. In addition, the model was calibrated to hourly instream temperature data recorded at various locations on July 29, 1999.

Figure A-88 displays the calibrated East Fork Dairy Creek model predictions. Land uses for the right and left banks (looking in the downstream direction) are also displayed. The standard error and averaged deviation for the spatial data are:

$$Standard\ Error = 0.54^{o}C\ (0.98^{o}F)$$

$$Average\ Deviation = 0.10^{o}C\ (0.19^{o}F)$$

Figure A-88.   East Fork Dairy Creek Observed and Predicted Spatial Temperature Data
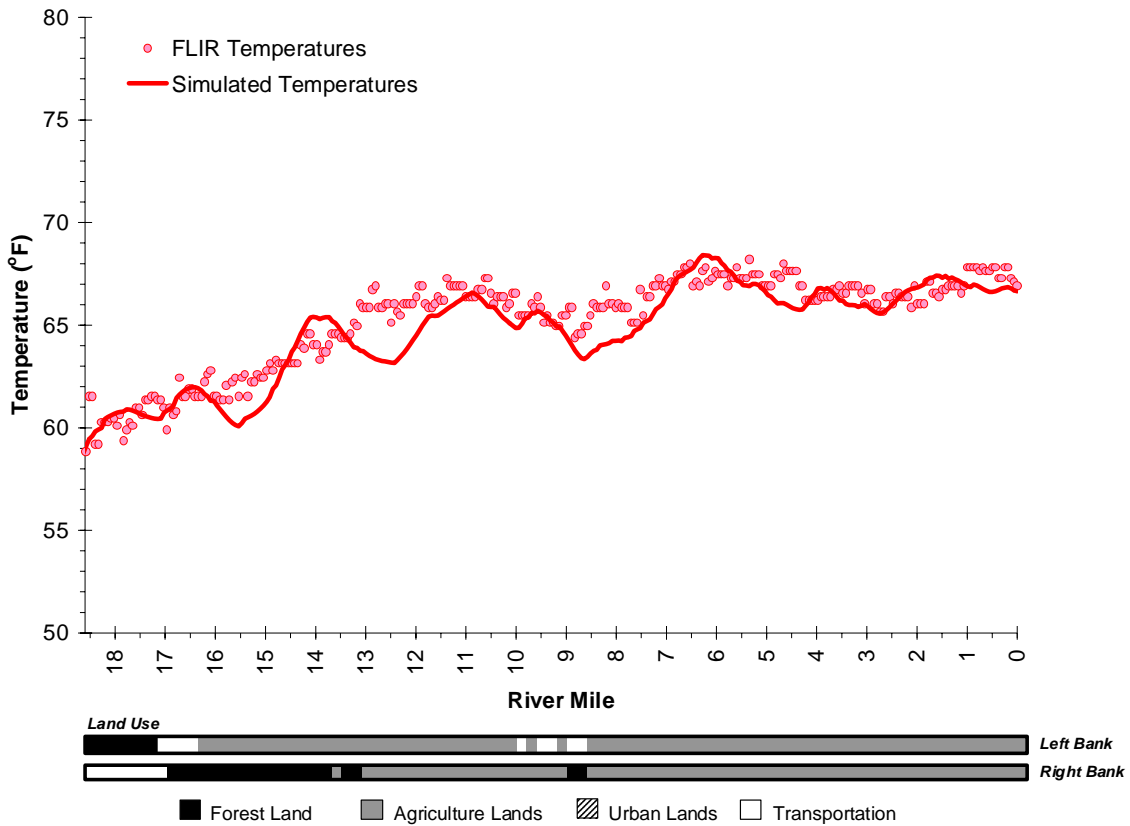
Figure A-89 displays the measured and predicted hourly temperatures for the continuous monitoring locations. The mean standard error and mean average deviation are:

$$Mean\ Standard\ Error = 0.32^{o}C\ (0.58^{o}F)$$

$$Mean\ Average\ Deviation = 0.59^{o}C\ (1.06^{o}F)$$

Figure A-89. East Fork Dairy Creek Model Continuous Data Validation.

Loading Capacity - 40 CFR 130.2(f)

Loading Capacity is based on the condition that meets the *no measurable surface water temperature increase resulting from anthropogenic activities*. This condition is termed *System Potential* and is achieved when (1) non-point source solar radiation loading reflects a riparian vegetation condition without human disturbance and (2) point source discharges cause no measurable increases in surface water temperatures.

Solar radiation loading was calculated using system potential riparian vegetation, at current channel and stream aspect conditions. A detailed description of potential vegetation conditions is presented in **Table A-8**. Current and System Potential solar loading for the East Fork Dairy Creek are presented in **Figure A-90**. Solar radiation loading for Current Condition and System Potential condition is presented for every 100 meters of modeled stream length. As can be seen in **Figure A-90**, solar radiation loading at System Potential is much less than levels currently observed on East Fork Dairy Creek (i.e., Current Condition).

Figure A-90. East Fork Dairy Creek Solar Radiation Load at System Potential and Current Conditions
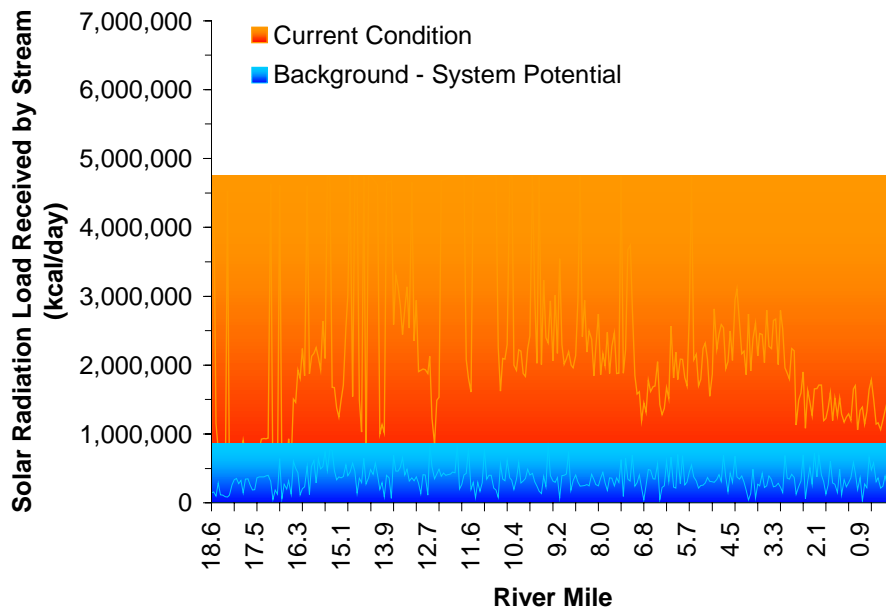
Allocations – 40 CFR 130.2(g) and 40 CFR 130.2(h)

Load Allocations (Non-Point Sources) - *The **temperature standard** targets system potential (i.e. no measurable temperature increases from anthropogenic sources). To meet this requirement the system potential solar radiation heat load ($3.4 \cdot 10^7$ Kcal/day) is allocated to background nonpoint sources. Anthropogenic nonpoint sources are not given a heat load.*

***Wasteload Allocations (Point Sources)** - Surface water discharges into receiving waters have been given a heat load based on the 0.25^oF allowable increase in the mixing zone as specified in the temperature standard. Heat loads have been converted to allowable effluent temperatures as well. It should be noted that the wasteload allocation is the point source heat load and not the calculated maximum effluent temperatures. There are several options for meeting the allocated heat loads (i.e. passive effluent temperature reductions, changes in facility discharge operation, purchasing instream flows, pollutant trading, etc.).*

Temperature Allocation Summary **Non-Point Sources**	
Source	*Loading Allocation* *Allowable Nonpoint Source Solar Radiation Heat Load* *(kcal/day)*
Natural	$1.1 \cdot 10^8$ Kcal/day
Agriculture	$\varnothing$
Forestry	$\varnothing$
Urban	$\varnothing$
Future Sources	$\varnothing$

No permitted point sources currently discharge into East Fork Dairy Creek. Therefore, no specific waste load analysis was conducted for East Fork Dairy Creek.

Surrogate Measures – 40 CFR 130.2(I)

The solar radiation load (Kcal/day) at system potential condition was calculated by multiplying the stream surface area by the solar radiation flux (ly/day). Percent effective shade was used as a surrogate measure of the solar radiation flux calculated at system potential conditions (**Figure A-91**). The individual points in the figure represent the current and allocated conditions for every 100 meters. Accordingly, System Potential heat load condition along East Fork Dairy Creek translates into approximately 90% or greater effective shade throughout much of the system.

Figure A-91.   East Fork Dairy Creek Surrogate Measure for Non Point Sources – *Effective Shade*
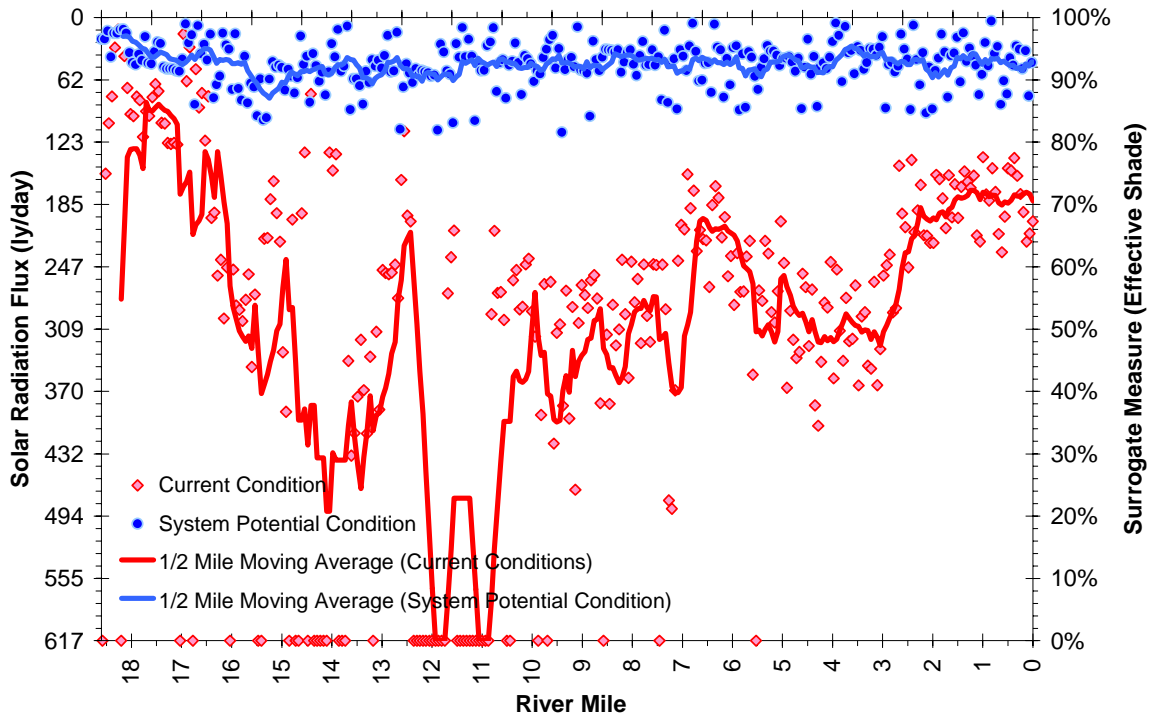
Water Quality Standard Attainment Analysis – CWA §303(d)(1)

System Potential is achieved when (1) non-point source solar radiation loading reflects a riparian vegetation condition without human disturbance and (2) point source discharges cause no measurable increase in surface water temperature. Accordingly, **Figure A-92** presents predicted East Fork Dairy Creek temperatures at a Waste Load Allocation and Load Allocation scenario. **Figure A-93** illustrates that implementing Waste Load Allocations and Load Allocations will drastically reduce temperatures in East Fork Dairy Creek.

Figure A-92. East Fork Dairy Creek Daily Temperature Range for Current Conditions Compared with Allocated Measures - July 29, 1999.
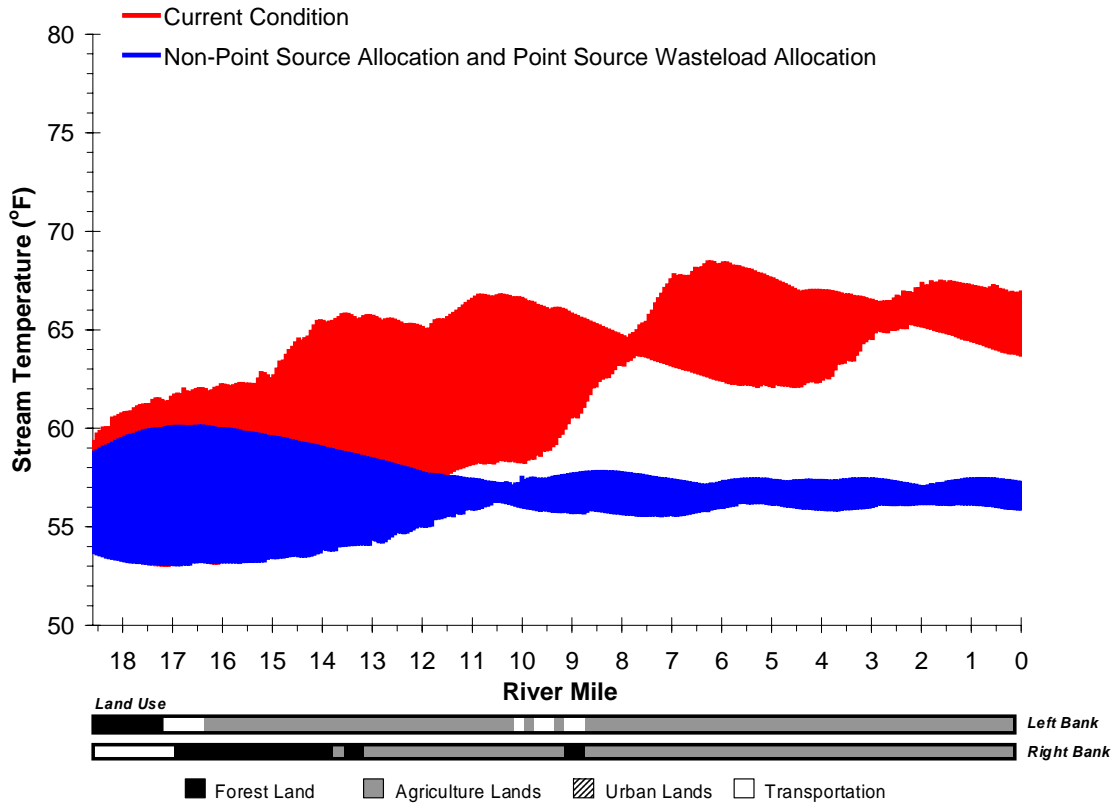
Figure A-93. East Fork Dairy Creek Current and System Potential (Allocated) Temperature Distributions
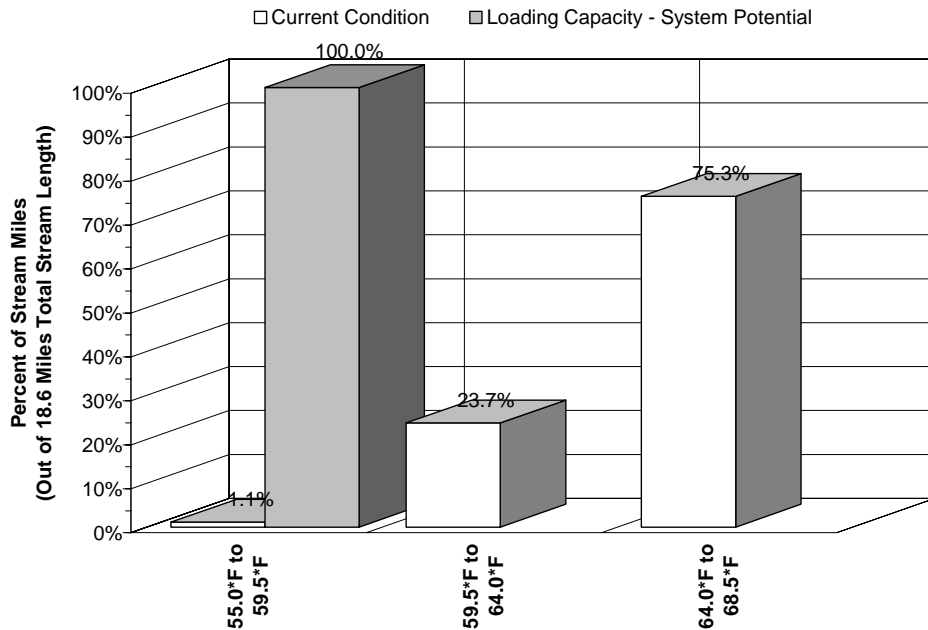
WEST FORK DAIRY CREEK AND DAIRY CREEK

WEST FORK DAIRY CREEK* CURRENT CONDITIONS

The Oregon Department of Environmental Quality collected stream temperature, flow, and site descriptions along West Dairy Creek during the summer of 1999. **Figure A-94** depicts the data collection sites. Digital photographs taken at several sampling locations are presented in **Images A-31** through **A-34.**

Figure A-94. Water Quality Summer Sampling Sites for West Fork Dairy Creek during 1999.
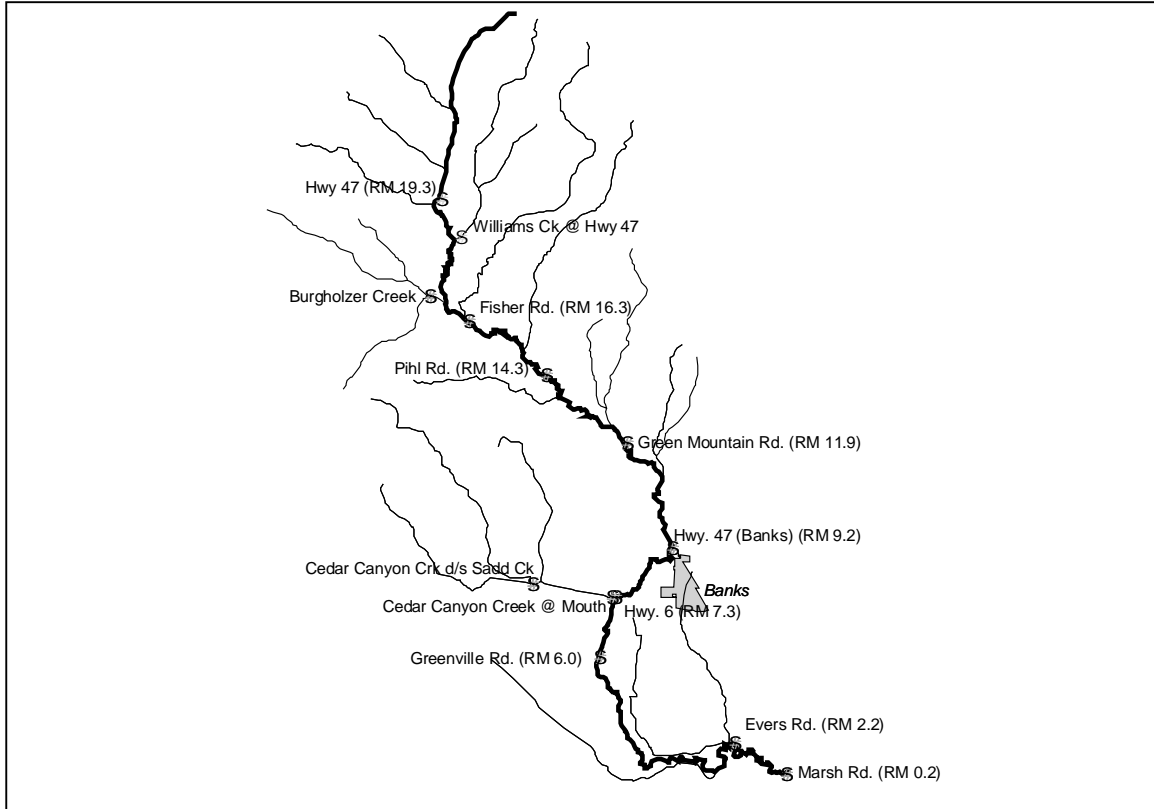
It was determined that water temperatures in West Fork Dairy Creek increases during the summer period, with maximum temperatures occurring in late July (**Figure A-95**). Accordingly, FLIR thermal imagery was collected for West Fork Dairy Creek on July 28, 1999. It is important to note that flow measurements were also collected during this period. The longitudinal profile of the calculated 7-Day temperature Statistics for West Fork Dairy Creek, and several of its tributaries, are presented in **Figure A-96**. The 64°F temperature criteria in West Fork Dairy Creek was exceeded at all sampling locations in 1999. As can be seen in these Figures, observed water temperature remain within a relatively narrow range throughout West Fork Dairy Creek. **Table A-19** summarizes calculated temperature statistics for West Fork Dairy Creek in 1999.

---

* Note that the river miles (RM) presented in this report were derived from a 1:5000 stream coverage used for ODEQ modeling purposes and may differ slightly from other sources (such as the OWRD or USGS river miles).

Image A-31. West Fork Dairy Creek near Upper Highway 47 Bridge (River Mile 19.3).
[Temp. Statistic – 65.8*F, Flow – 0.6 cfs, Potential Effective Shade (ES) – 98%, Measured ES – 95%]

Image A-32. West Fork Dairy Creek at Fisher Road (River Mile 16.3).
[Temp. Statistic – 67.5*F, Flow – 4.2 cfs, Potential Effective Shade (ES) – 98.5%, Measured ES – 68%]
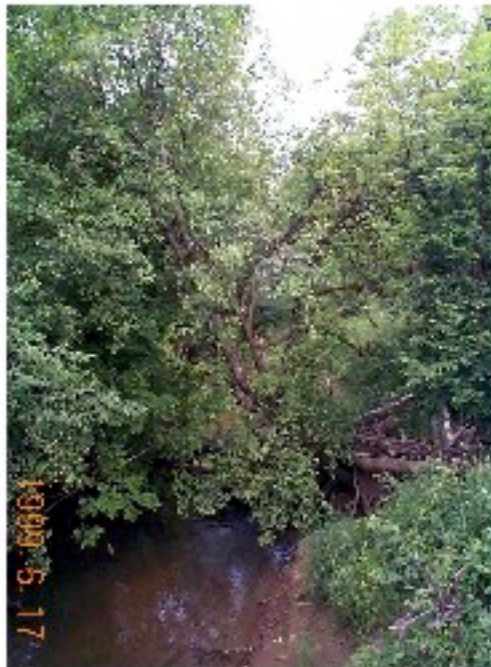
Image A-33. West Fork Dairy Creek at Highway 47 in Banks (River Mile 9.2).
[Temp. Statistic – 68.5*F, Flow – 7.1 cfs, Potential Effective Shade (ES) – 99%, Measured ES – 49%]

Image A-34. West Fork Dairy Creek at Marsh Road (River Mile 0.2).
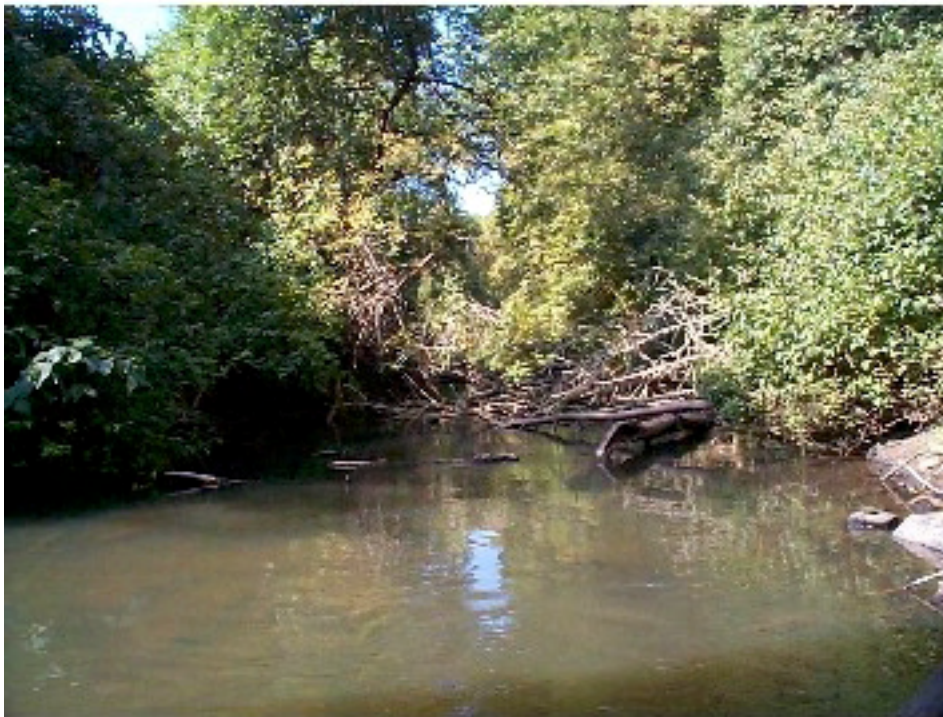[Temp. Statistic – 67.1*F, Flow – 10.6 cfs, Potential Effective Shade (ES) – 96.5%, Measured ES – 88%]

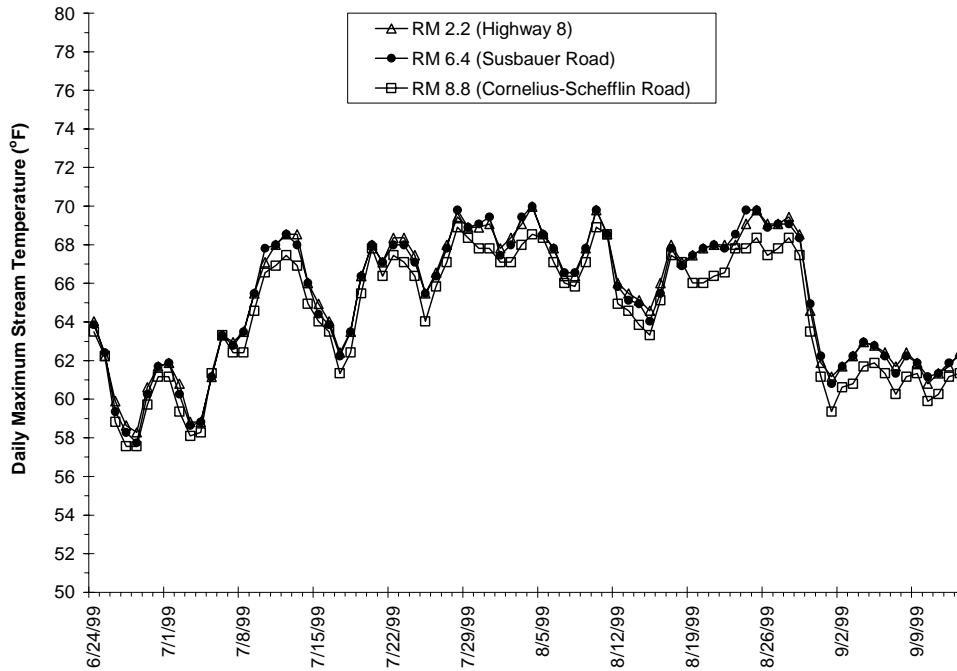**Figure A-95.** Observed Daily Maximum Stream Temperatures for West Fork Dairy Creek.
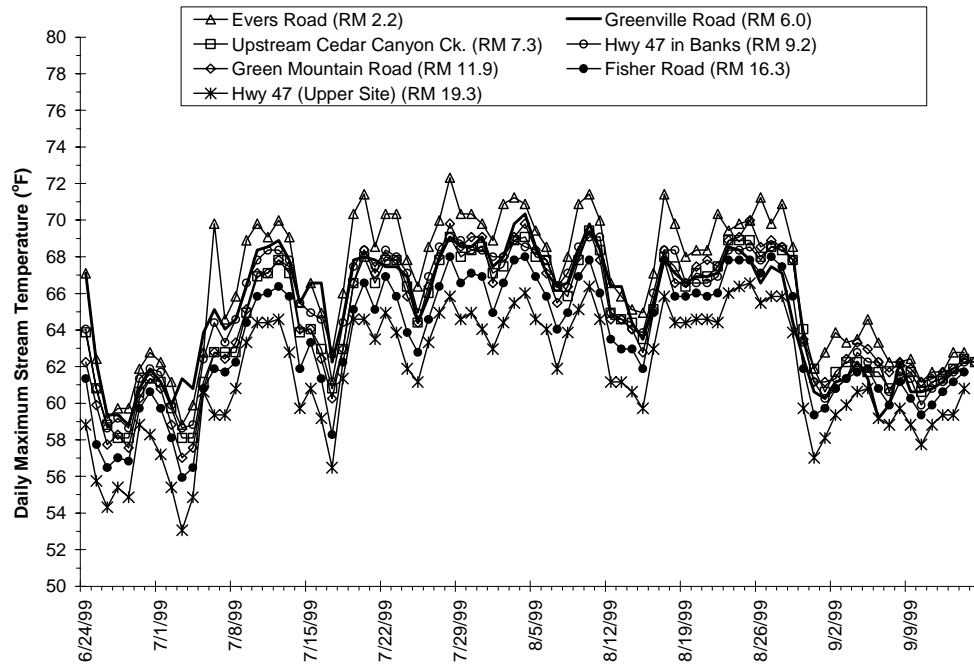
**Figure A-96.** Observed Maximum 7-Day Temperature Statistics for West Fork Dairy Creek.
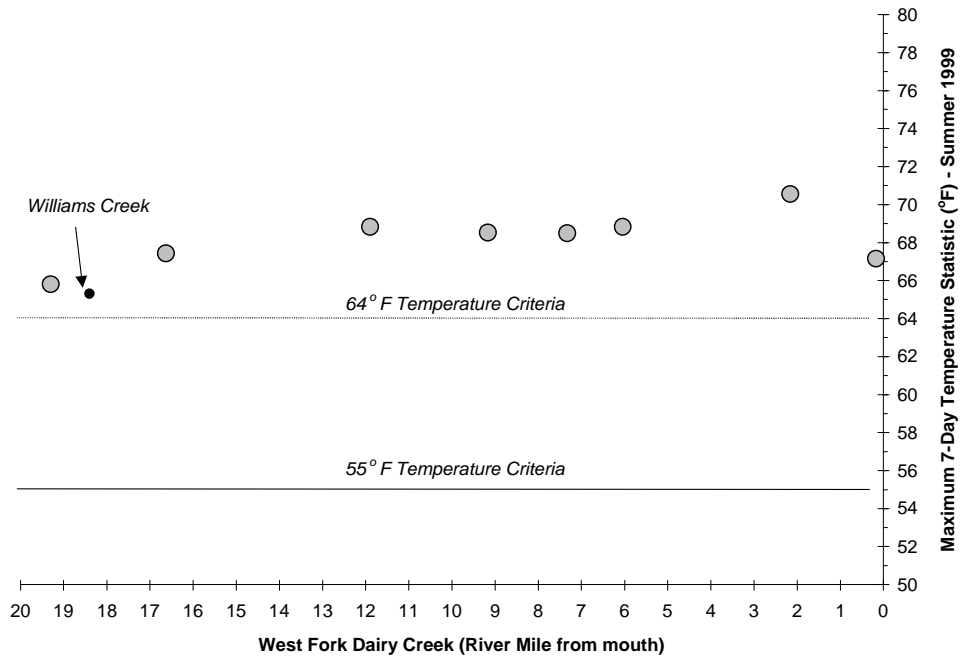
Table A-19. Calculated Stream Temperature Statistics for West Fork Dairy Creek						
Temperature Site	Start	End	Max. Daily Temp		Max. 7-Day Statistic	
(RM = River Mile from mouth)	Date	Date	Date	(^{o}F)	Date	(^{o}F)
RM 19.3 Upper Highway 47 Bridge	6/18/99	9/14/99	8/25/99	66.6	8/25/99	65.8
RM 16.3 Fisher Road	6/18/99	9/14/99	8/27/99	68.0	8/25/99	67.5
RM 11.9 Green Mountain Road	6/18/99	9/14/99	8/25/99	70.0	8/26/99	68.9
RM 9.2 Highway 47 in Banks	6/18/99	9/15/99	8/11/99	69.1	7/31/99	68.5
RM 7.3 Upstream Cedar Canyon Ck	6/18/99	9/15/99	8/10/99	69.4	8/26/99	68.5
RM 6.0 Greenville Road	6/24/99	9/14/99	8/4/99	70.3	8/2/99	68.9
RM 2.2 Evers Road	6/24/99	9/14/99	7/28/99	72.3	7/31/99	70.5
RM 0.2 Marsh Road	6/24/99	7/26/99	7/12/99	68.5	7/22/99	67.1
West Fork Dairy Creek Tributary						
Williams Creek	6/18/99	9/14/99	8/10/99	66.6	8/26/99	65.3

Water temperatures in West Fork Dairy Creek varied through out the course of the day, with maximum temperatures occurring in the late afternoon and minimums temperature occurring during the early morning hours (**Figure A-97**). Relatively small diurnal variability was observed West Fork Dairy Creek, which is typical of a deep, low gradient stream. Observed flow volumes for the West Fork Dairy Creek and Council Creek are shown in **Figure A-98**.

Figure A-97. Diurnal Temperature Trends Observed in West Fork Dairy Creek on July 28, 1999.
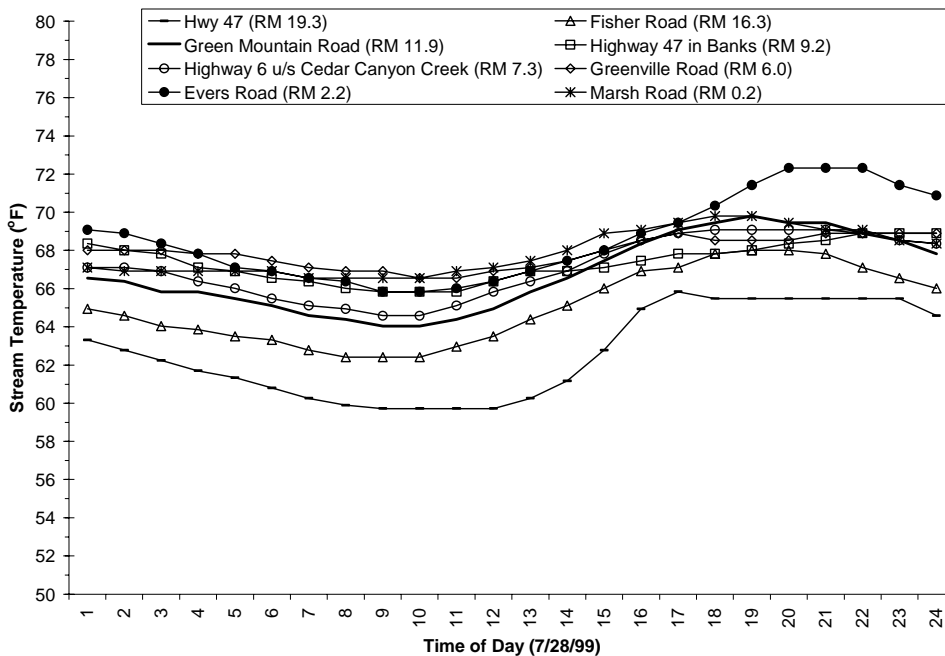
Figure A-98. Stream Flow Observed in West Fork Dairy Creek on July 28, 1999.
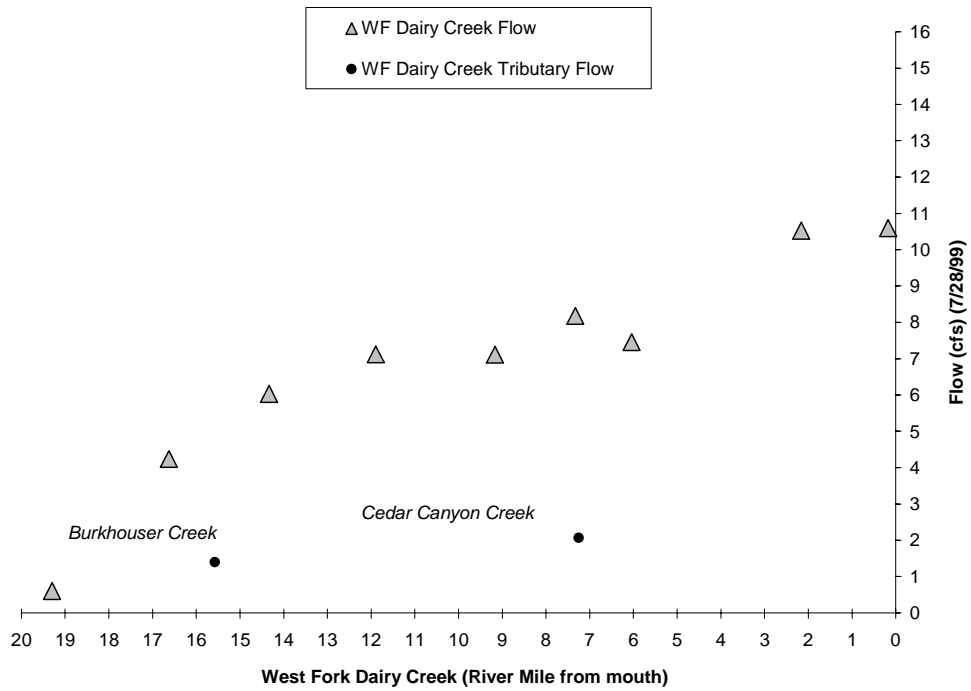
The West Fork Dairy Creek was flown for FLIR on July 28, 1999 from 17:02 to 17:27. The longitudinal stream temperature profile is presented in **Figure A-99**. Note that there is a slight longitudinal heating trend. All of the stream temperatures recorded during the FLIR flight fall within the sub-lethal temperature range for salmonids (**Table A-20**).
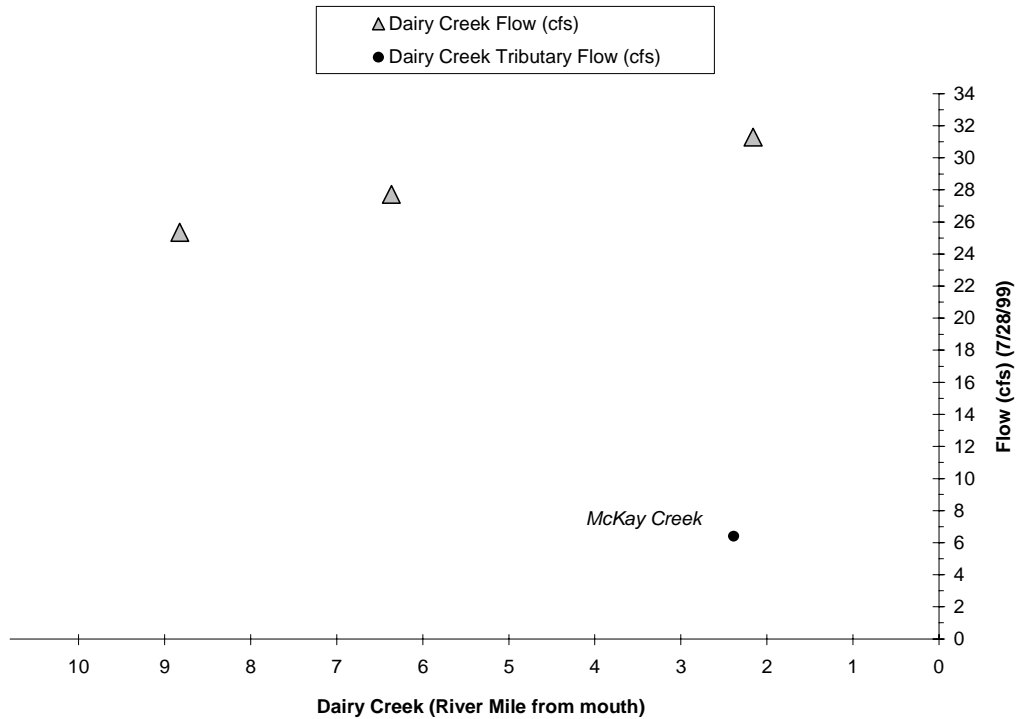
Figure A-99. West Fork Dairy Creek FLIR Temperature Profile (17:02 to 17:27 on 7/28/99)
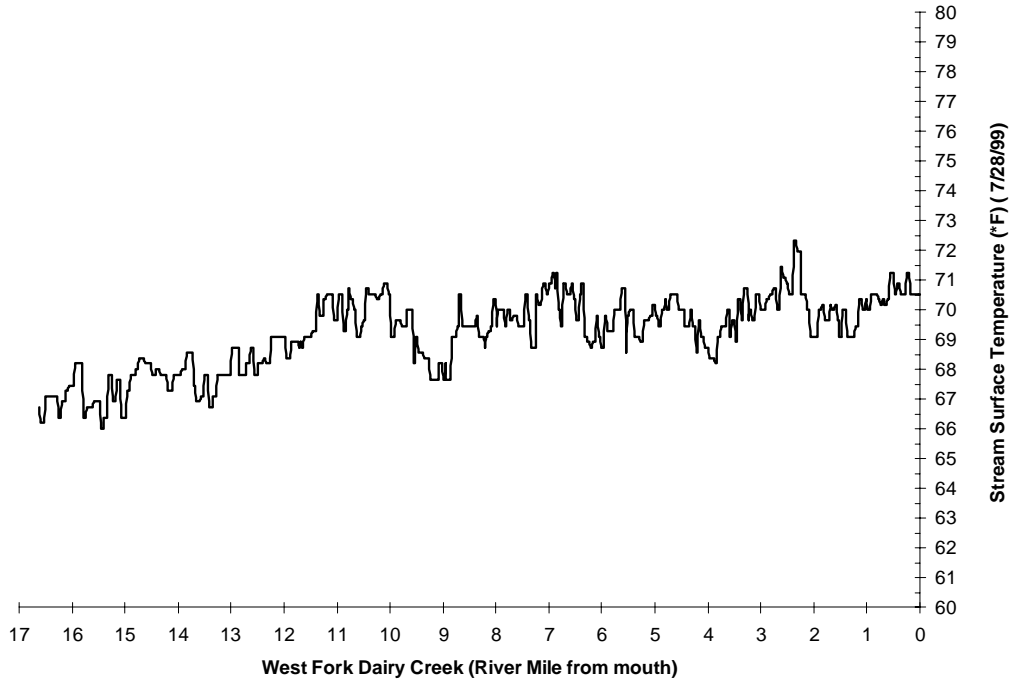
Table A-20. FLIR-derived Water Temperatures in West Fork Dairy Creek (7/28/99)			
Temperature (°F)	Distance (miles)	Percent of Total	Mode of Thermal Mortality
Less than 55.0	-	-	
55.0 to 59.5	-	-	
59.5 to 64.0	-	-	
64.0 to 68.5	4.8	28.9%	
68.5 to 73.0	11.8	71.1%	Sub-Lethal Range
73.0 to 77.5	-	-	
Greater than 77.5	-	-	Incipient Lethal Range
Totals	16.6	100%	

Below are selected FLIR and video images from the West Fork Dairy Creek FLIR flight. The lower portion of the stream is diverted through a canal system (**Image A-36**).

Image A-35. West Fork Dairy Creek at river mile 3.4..
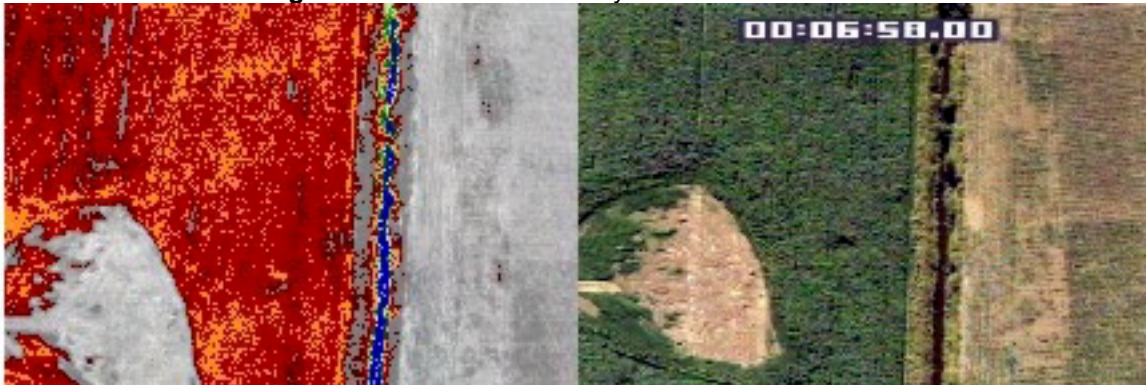
Image A-36. West Fork Dairy Creek (river mile 4.2) as part of the canal.
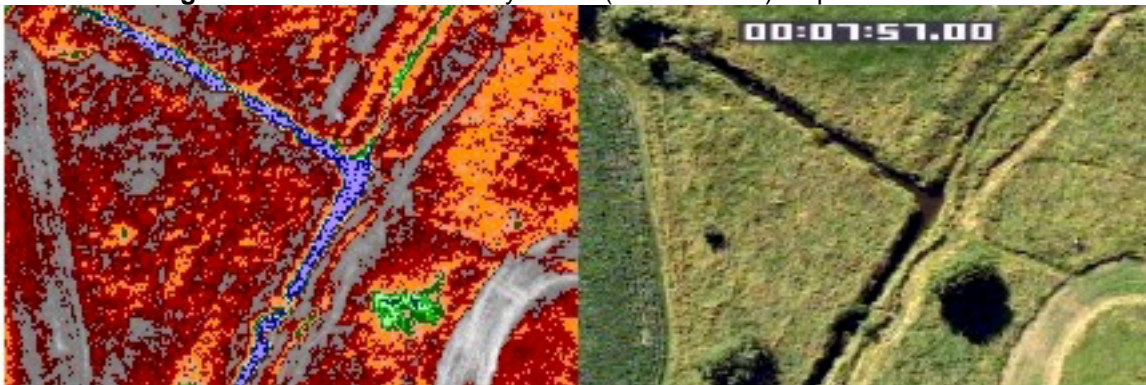
FLIR Image Temperature Scale (°C)

Image A-37.   West Fork Dairy Creek (river mile 13.6) showing warm surface inflow from the left side of the image. West Fork Dairy Creek flows from the top right of the image and makes a sharp left bend in the center of the image.

Image A-38.   West Fork Dairy Creek (river mile 18.0) flowing from the top to bottom of the image. The frame shows characteristic thermal environment for this reach. ..

FLIR Image Temperature Scale (^{o}C)

DAIRY CREEK* CURRENT CONDITION

The Oregon Department of Environmental Quality collected stream temperature, flow, and site descriptions along Dairy Creek during the summer of 1999. **Figure A-100** depicts the data collection sites. Digital photographs taken at some of the sampling sites are presented in **Images A-39** through **A-41**.

Figure A-100. Water Quality Sampling Locations for Dairy Creek During the Summer of 1999.
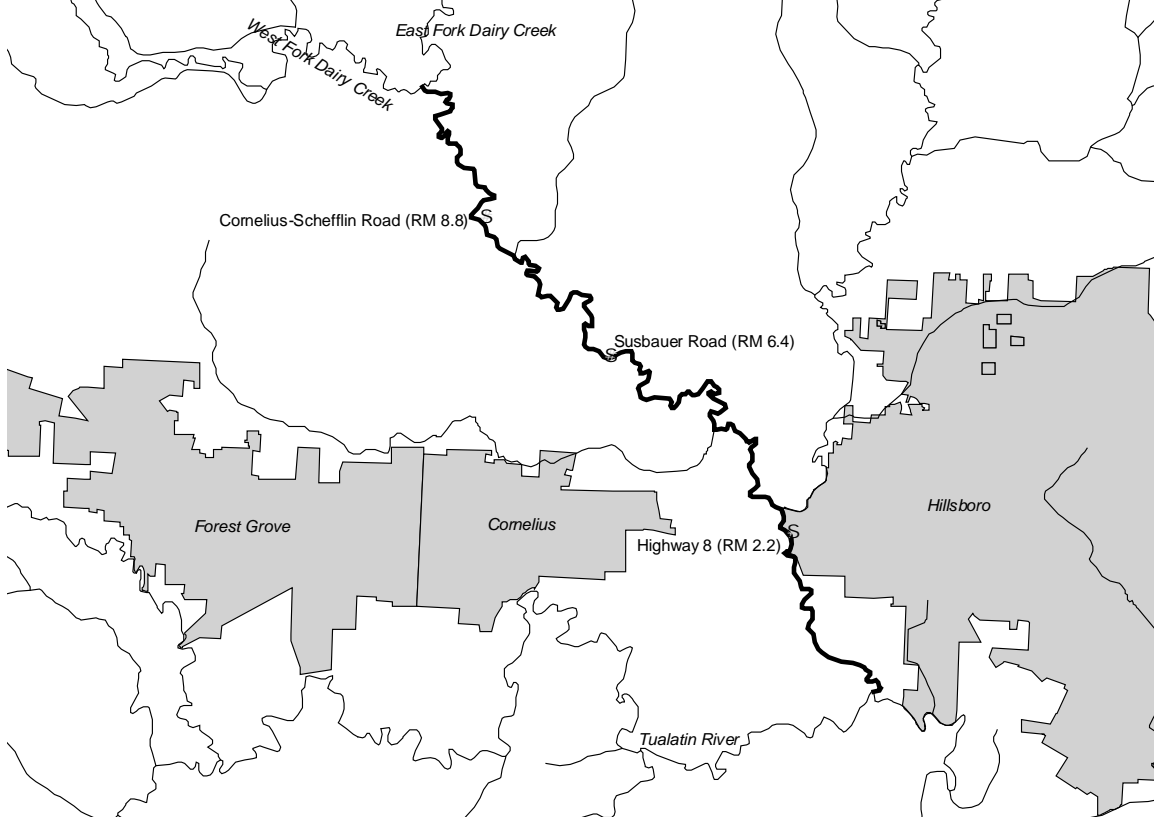
Dairy Creek temperatures increase during the summer period, with daily maximums occurring in late July and August (**Figure A-101**). The entire Dairy Creek mainstem is low-gradient and not much longitudinal heating is observed. The 1999 maximum 7-day temperature statistics indicates that Dairy Creek exceeds the 64°F temperature criteria throughout most, if not all, of its length (**Figure A-102**). **Table A-21** summarizes the 7-day temperature statistics recorded during the summer of 1999.

---

* Note that the river miles (RM) presented in this report were derived from a 1:5000 stream coverage used for ODEQ modeling purposes and may differ slightly from other sources (such as the Oregon Water Resources Division or USGS river miles).

Image A-39. Dairy Creek at Cornelius-Schefflin Road (River Mile 8.8).
[Temp. Statistic – 67.9*F, Flow – 25.4 cfs, Potential Effective Shade (ES) – 97%, Measured ES – 18%]

Image A-40. Dairy Creek at Susbauer Road (River Mile 6.4).
[Temp. Statistic – 69.1*F, Flow – N/A, Potential Effective Shade (ES) – 96%, Measured ES – 96%]

Image A-41. Dairy Creek at Highway 8 (River Mile 2.2).

[Temp. Statistic – 69.0*F, Flow – 37.7 cfs, Potential Effective Shade (ES) – 92%, Measured ES – 49%]

Figure A-101. Observed Daily Maximum Stream Temperatures for Dairy Creek.

Figure A-102. Observed Maximum 7-Day Temperature Statistics for Dairy Creek.
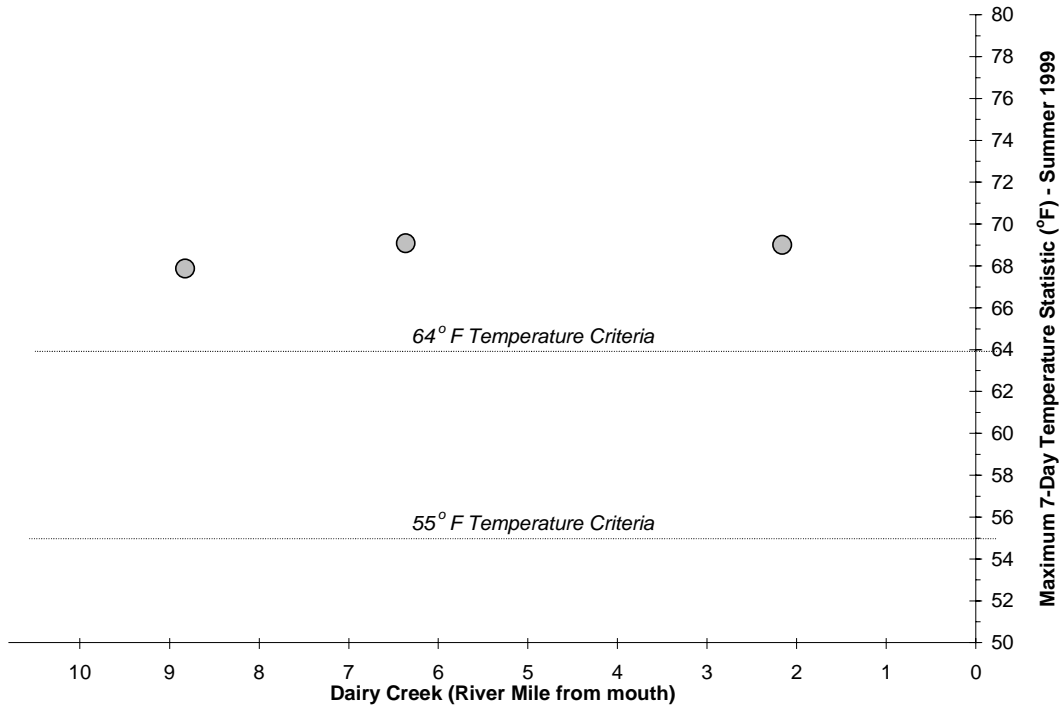
Table A-21. Calculated Stream Temperature Statistics for Dairy Creek						
Temperature Site	Start	End	Max. Daily Temp		Max. 7-Day Statistic	
(RM = River Mile from mouth)	*Date*	*Date*	*Date*	*(^{o}F)*	*Date*	*(^{o}F)*
RM 2.2 Highway 8	6/24/99	9/13/99	8/04/99	70.0	8/26/99	69.0
RM 6.4 Susbauer Road	6/24/99	9/13/99	8/04/99	70.0	8/26/99	69.1
RM 8.8 Cornelius-Schefflin Road	6/24/99	9/13/99	8/10/99	68.9	8/26/99	67.9

The diurnal temperature profiles recorded within Dairy Creek are typical of a deep, slow-moving stream. Notice in **Figure A-103** that the difference between the daily minimum and daily maximum temperatures is not very pronounced. Stream discharge rates for Dairy Creek are displayed in **Figure A-104**. Flows in late July were around 30 cfs.

Dairy Creek was flown for FLIR from the mouth to the forks on July 28, 1999 from 16:49 to 17:02. The FLIR temperature profile is presented in **FigureA-105**. The approximately nine miles of Dairy Creek was 69-70°F at the time of the FLIR flight. These temperatures fall within the sub-lethal temperature range from salmonids (**Table A-22**).

Figure A-103. Diurnal Temperature Trends Observed in Dairy Creek on July 28, 1999.
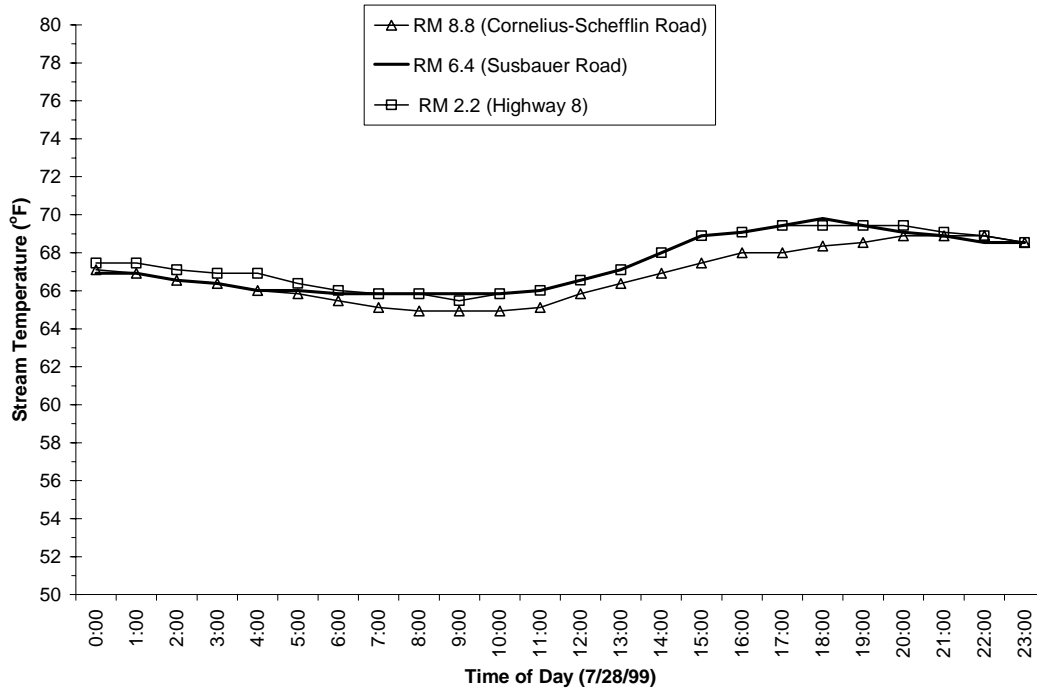
Figure A-104. Stream Flow Observed in Dairy Creek on July 28, 1999.

Figure A-105. Dairy Creek FLIR Temperature Profile (16:49 to 17:02 on 7/28/99)
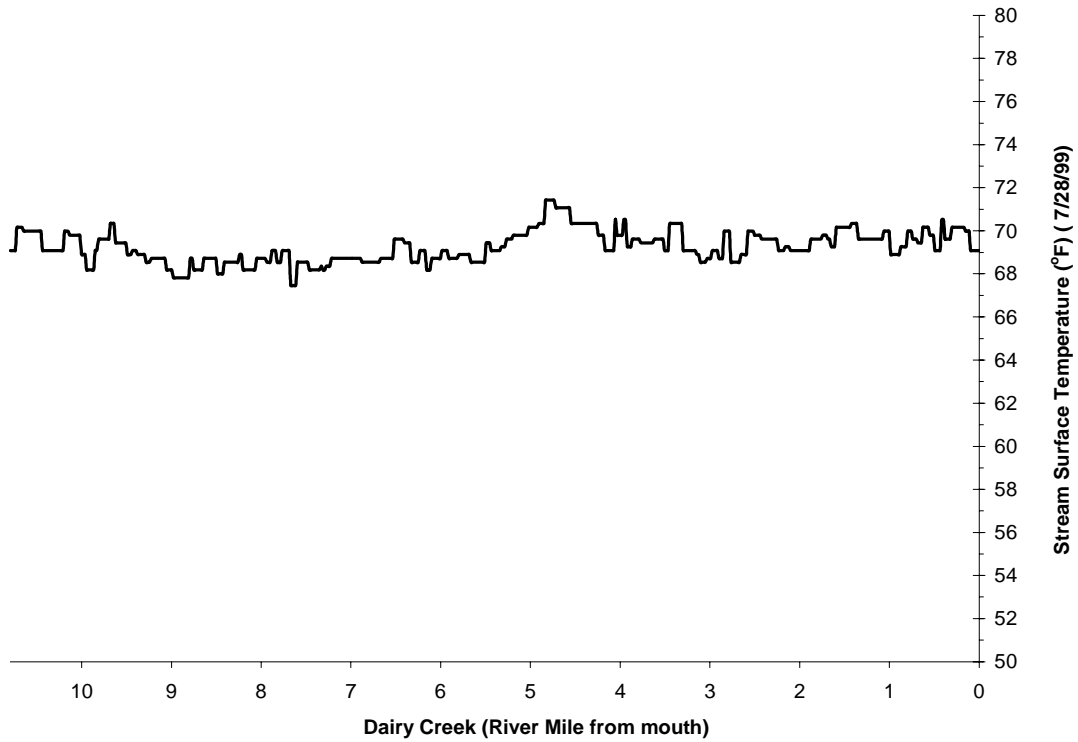
Table A-22. FLIR-derived Water Temperatures in Dairy Creek (7/28/99)			
Temperature (°F)	Distance (miles)	Percent of Total	Mode of Thermal Mortality
Less than 55.0	-	-	
55.0 to 59.5	-	-	
59.5 to 64.0	-	-	
64.0 to 68.5	0.8	9.0%	
68.5 to 73.0	8.1	91.0%	Sub-Lethal Range
73.0 to 77.5	-	-	
Greater than 77.5	-	-	Incipient Lethal Range
Totals	8.9	100.0%	

This section contains some examples of the FLIR images and their corresponding day video images that were recorded on the July 28, 1999 flight. Confluences and different thermal regimes are represented in this selection of images.

Image A-42. Confluence of the Tualatin River and Dairy Creek.
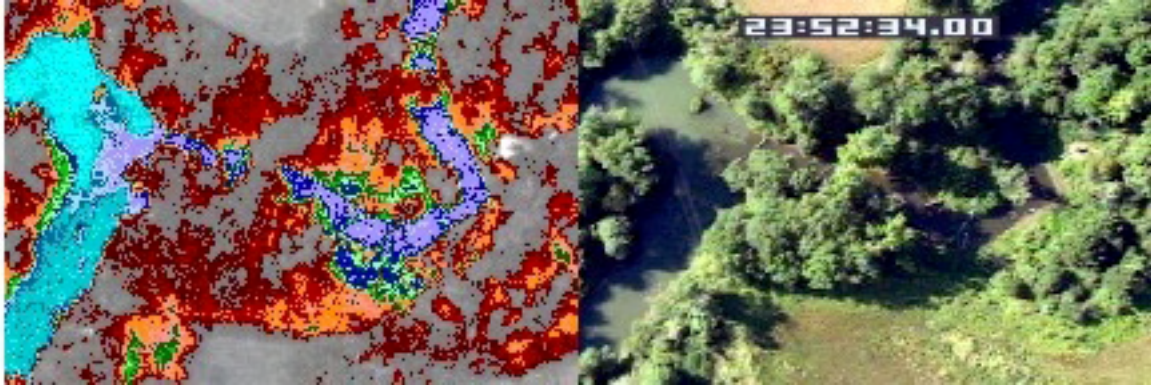
Image A-43. Dairy Creek at McKay Creek. McKay Creek is not visible in the image.
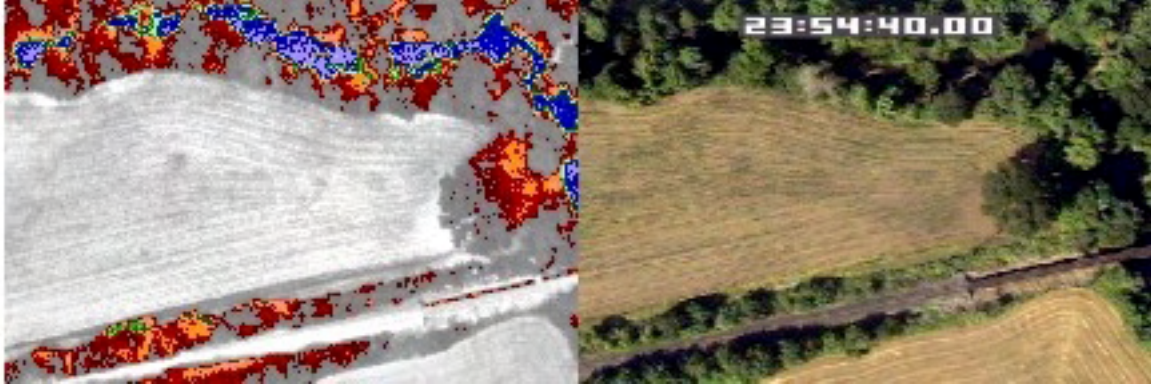
Image A-44. A typical scene along Dairy Creek (river mile 2.8) showing vegetation immediately along the stream bank flanked by agricultural fields and in this case a golf course

* **FLIR Image Temperature Scale (*C)**

Image A-45. Confluence of East Fork and West Fork Dairy Creek. West Fork Dairy Creek flows from right to left in the image while East Fork Dairy flows from the top to the bottom of the image. Trees and other bank side vegetation obscure the confluence.
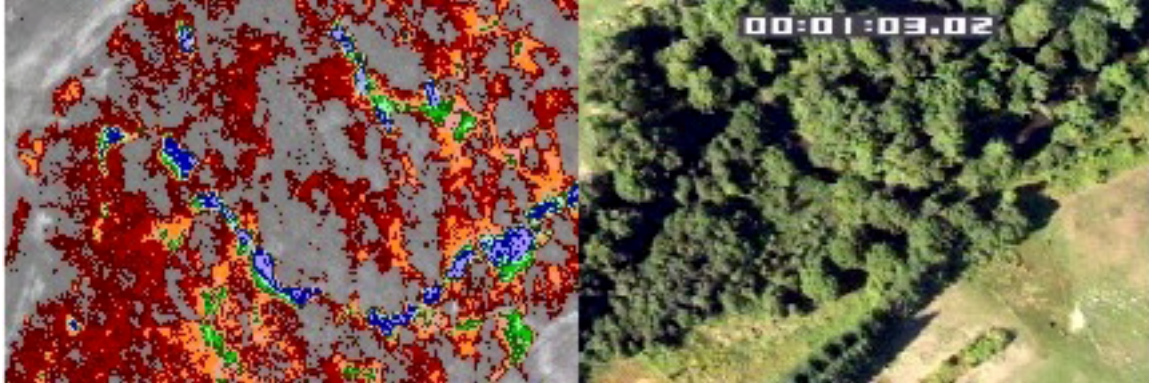
FLIR Image Temperature Scale (°C)

WEST FORK DAIRY CREEK/DAIRY CREEK MODEL INPUT

Dairy Creek and West Fork Dairy Creek were modeled as one continuous system. FLIR temperature data was collected from the mouth of Dairy Creek to the upper West Fork Dairy Creek uninterrupted. The following charts display longitudinal model input data for the Dairy Creek and West Dairy Creek system. River miles 0 through 10.8 are Dairy Creek, while river miles 10.8 through 27.4 are West Fork Dairy Creek.

- Elevation and Gradient (**Figure A-106**)
- Aspect (**Figure A-107**)
- Near Stream Disturbance Zone Widths and Wetted Widths (**Figure A-108**)
- Topographic Shade (**Figure A-109**)
- Vegetation Geometry (**Figure A-110**)
- Flow Volume (**Figure A-111**)
- Flow Velocity (**Figure A-112**)
- Water Column Depth (**Figure A-113**)

Figure A-106. West Fork Dairy/Dairy Creek Elevation and Gradient at Each 100-foot Model Reach.
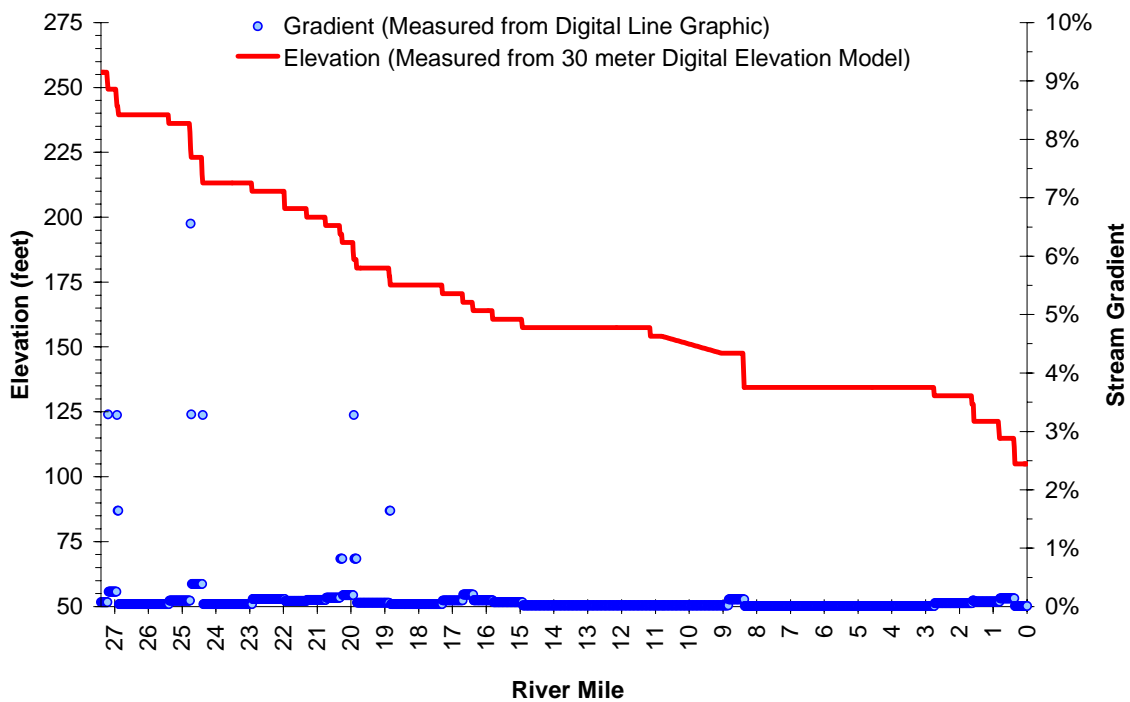
Figure A-107. West Fork Dairy Creek/Dairy Creek Aspect at Each 100-foot Model Reach.
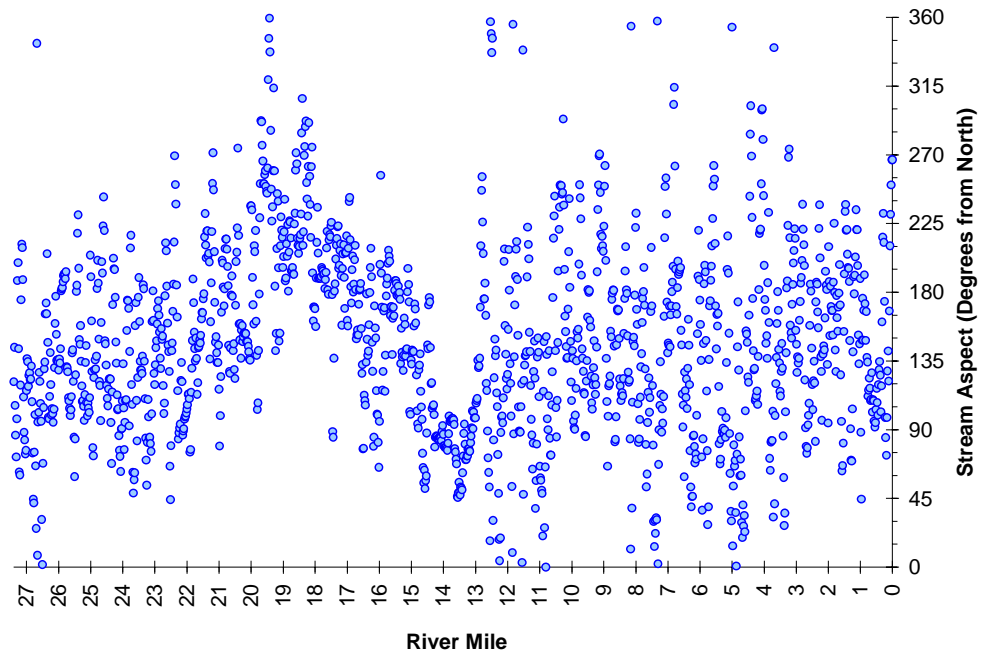
Figure A-108. West Fork Dairy Creek/Dairy Creek Wetted Widths and NSDZ Widths.
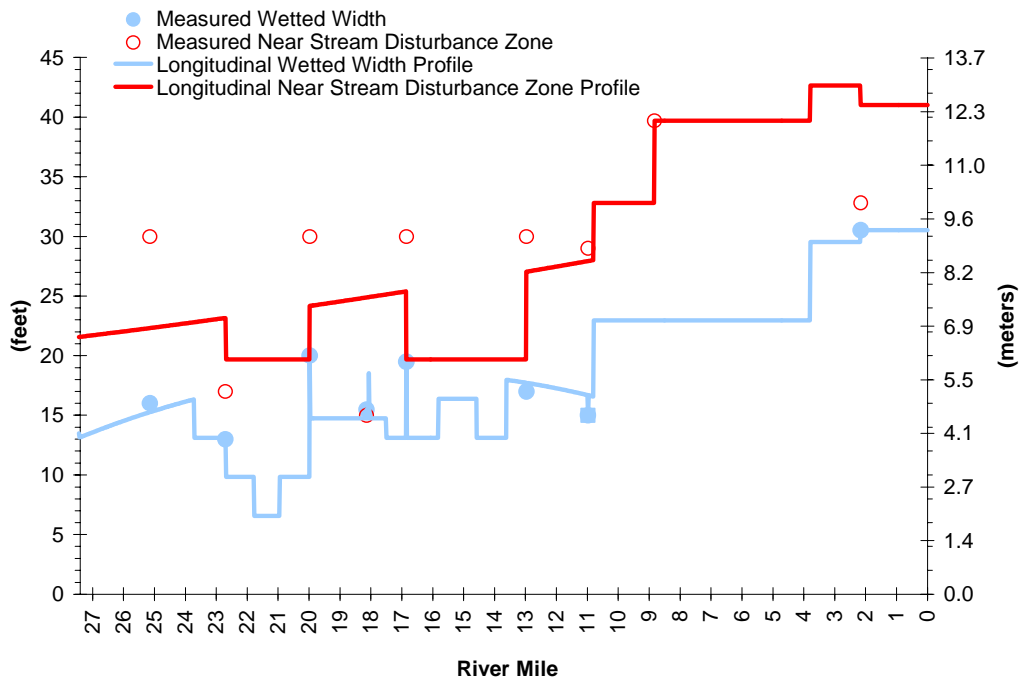
Figure A-109. West Fork Dairy Creek/Dairy Creek Topographic Shade at Each 100-foot Model Reach
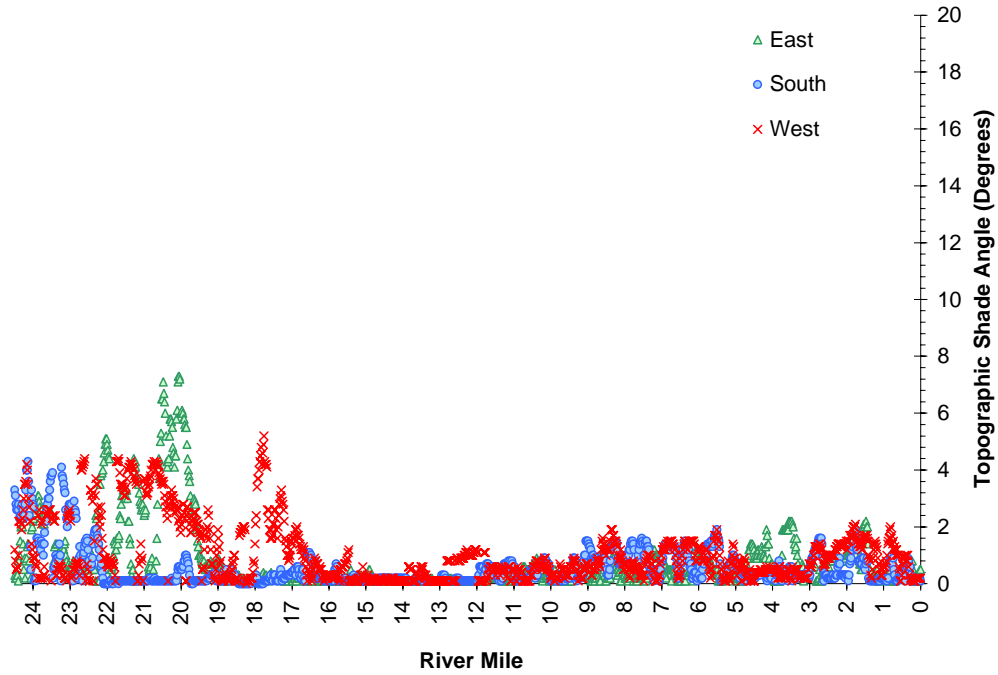
Figure A-110. West Fork Dairy Creek/Dairy Creek Current Vegetation Heights for Each 100-foot Model Reach.
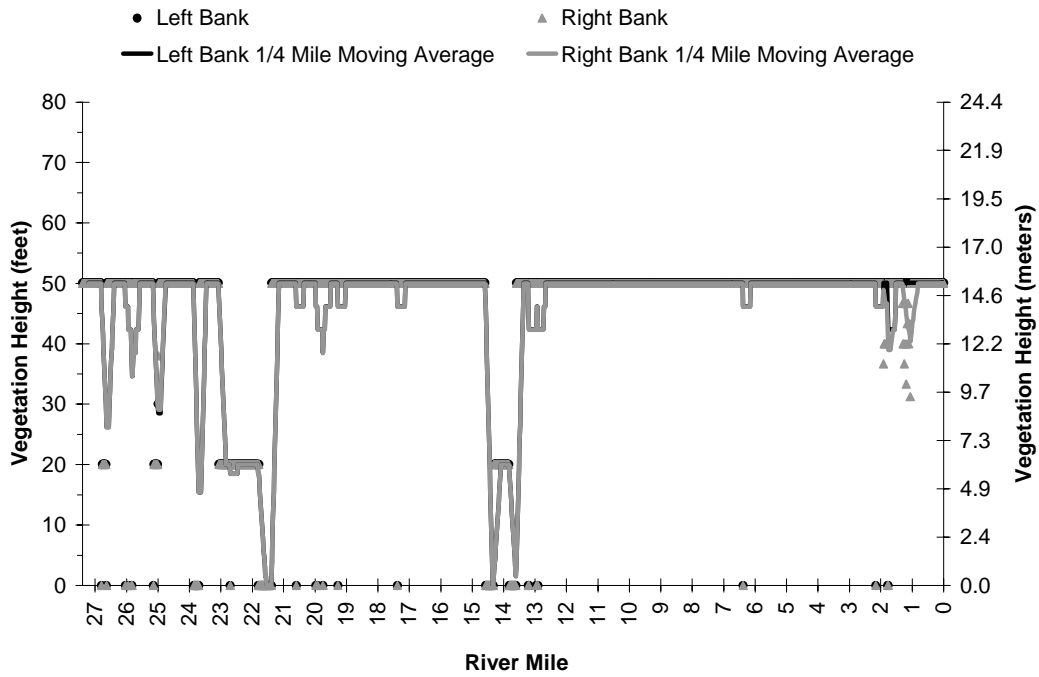
Figure A-111. West Fork Dairy Creek/Dairy Creek Current Vegetation Densities at Each 100-foot Model Reach.
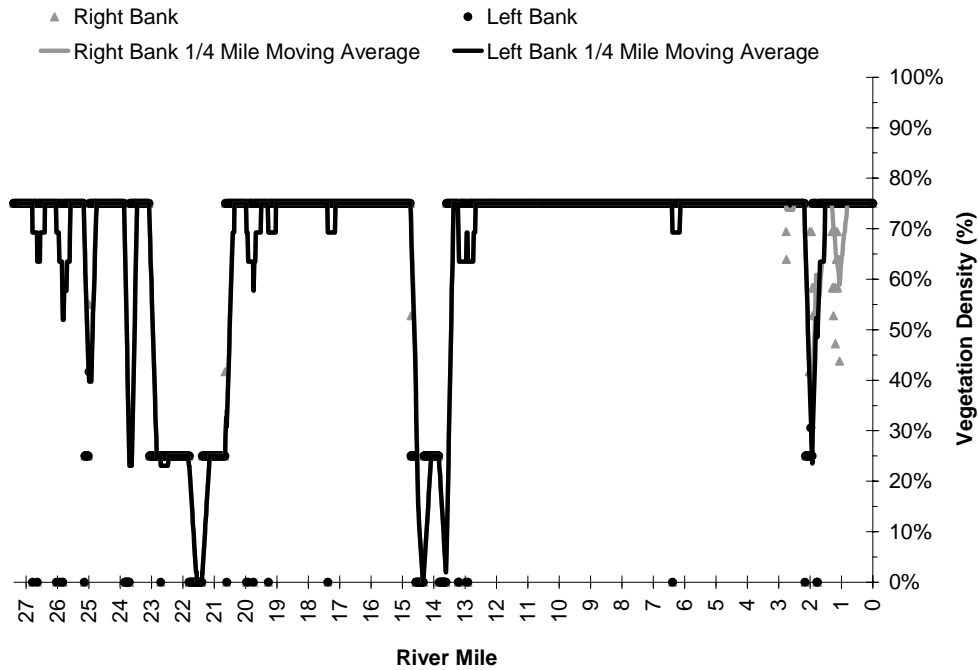
Figure A-112. West Fork Dairy Creek/Dairy Creek Current Vegetation Widths at Each 100-foot Model Reach.
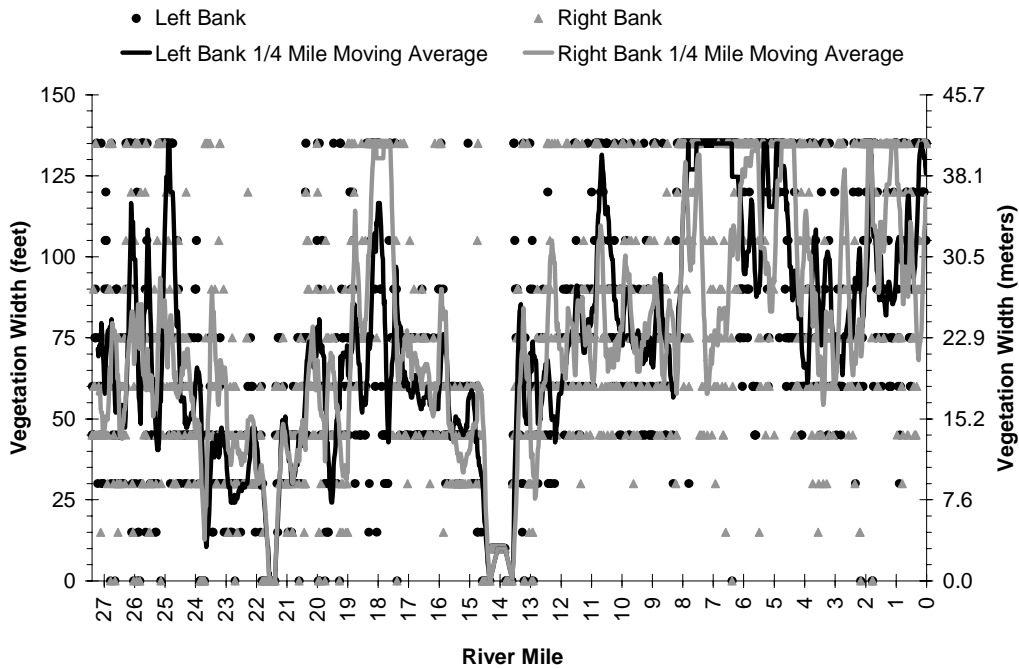
Figure A-113.   West Fork Dairy Creek/Dairy Creek Measured and Interpolated Flow Volume.
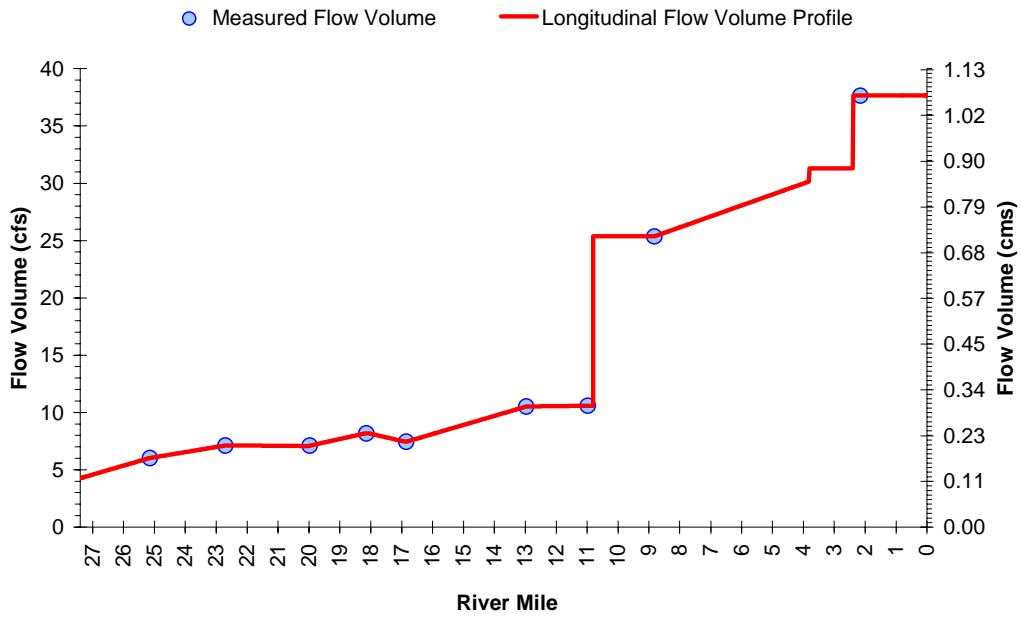
Figure A-114.   West Fork Dairy Creek/Dairy Creek Measured and Mannings Derived Longitudinal Flow Velocities.
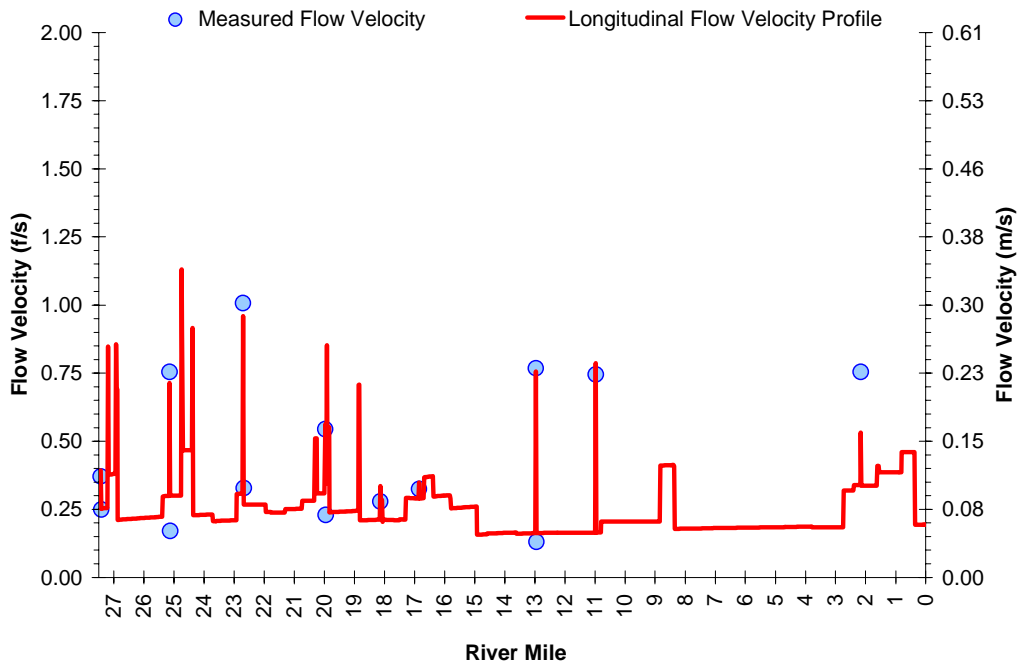
Figure A-115. West Fork Dairy Creek/Dairy Creek Measured and Mannings Derived Longitudinal Water Column Depths.
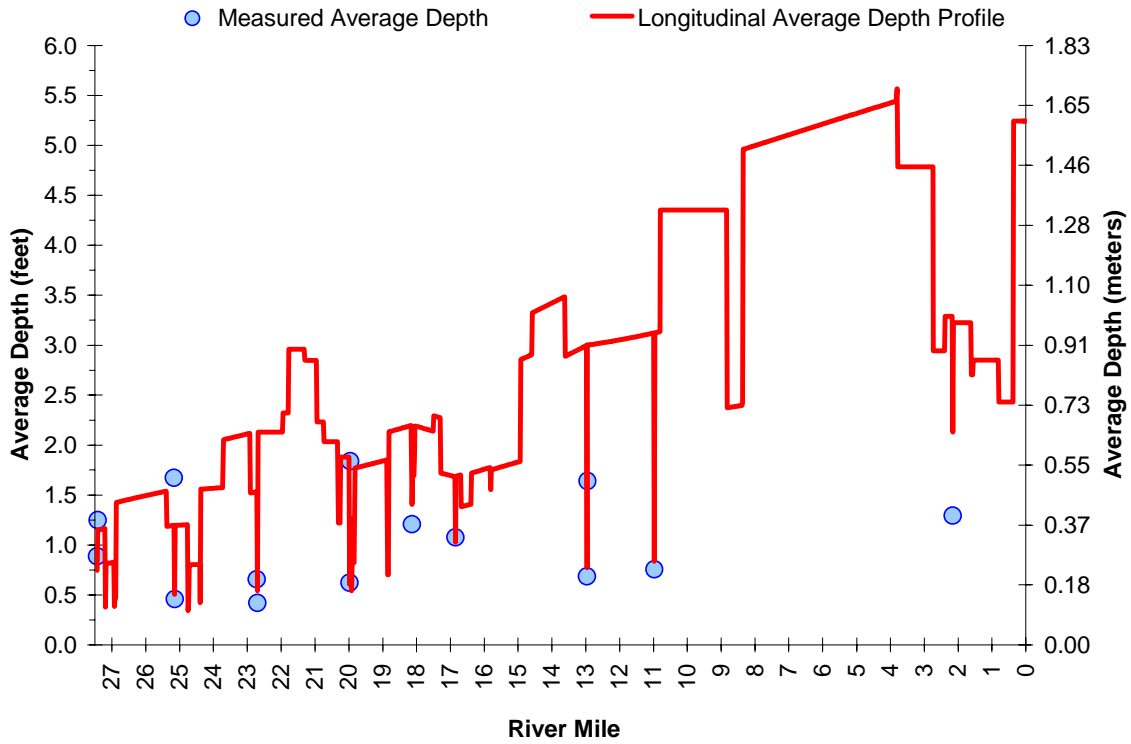
WEST FORK DAIRY CREEK/DAIRY CREEK MODEL RESULTS

Dairy Creek and West Fork Dairy Creek were modeled as a continuous system since FLIR was collected nonstop from the mouth of Dairy Creek to near the headwaters of West Fork Dairy Creek.

This section presents temperature modeling results for West Fork Dairy Creek and Dairy Creek. Graphical and statistical validation of the calibrated model are shown, in addition to temperature predictions for system potential vegetation conditions. Recall that the date modeled was July 28, 1999 and is representative of critical stream temperature, stream flow, and climatic conditions. In other words, this modeling effort has captured the time period in 1999 when stream temperatures were near their peak.

Spatial validation of the calibrated model is presented in **Figure A-116**. The solid line is the calibrated model temperature prediction at 5:00 PM on July 28, 1999, while the dots represent the FLIR-measured temperatures at that same time.

The standard error and average deviation for the spatial data calibration are:

$$Standard\ Error = 0.50^oC\ (0.91^oF)$$

$$Average\ Deviation = 0.13^oC\ (0.24^oF)$$

Figure A-116. West Fork Dairy Creek/Dairy Creek Observed and Predicted Spatial Temperature Data.
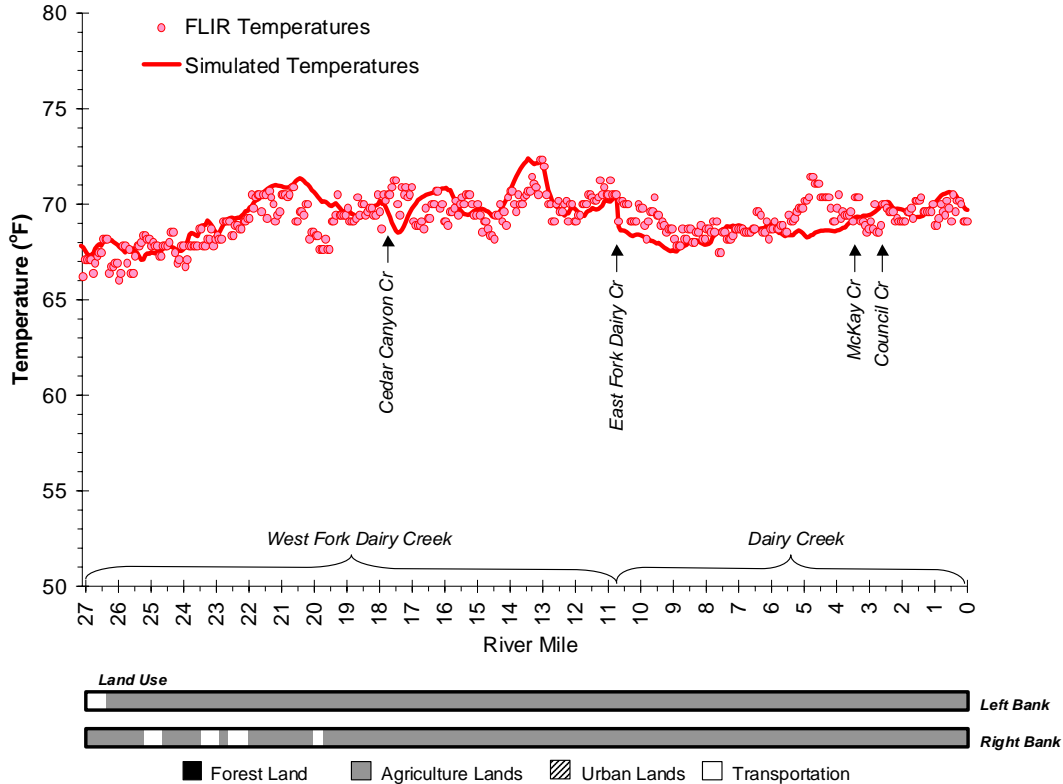
Figure A-117 displays the measured and predicted hourly temperatures at nine continuous temperature monitoring locations on West Fork Dairy Creek and Dairy Creek. Node 1 is the upper boundary condition and remains constant, therefore it is not graphed. Standard errors, and average deviations are presented for each node.

The mean standard error and mean average deviation for the continuous data are:

$$Mean\ Standard\ Error = 0.37^oC\ (0.67^oF)$$

$$Mean\ Average\ Deviation = 0.66^oC\ (1.18^oF)$$

Figure A-117.   West Fork Dairy Creek/Dairy Creek Model Continuous Data Validation.
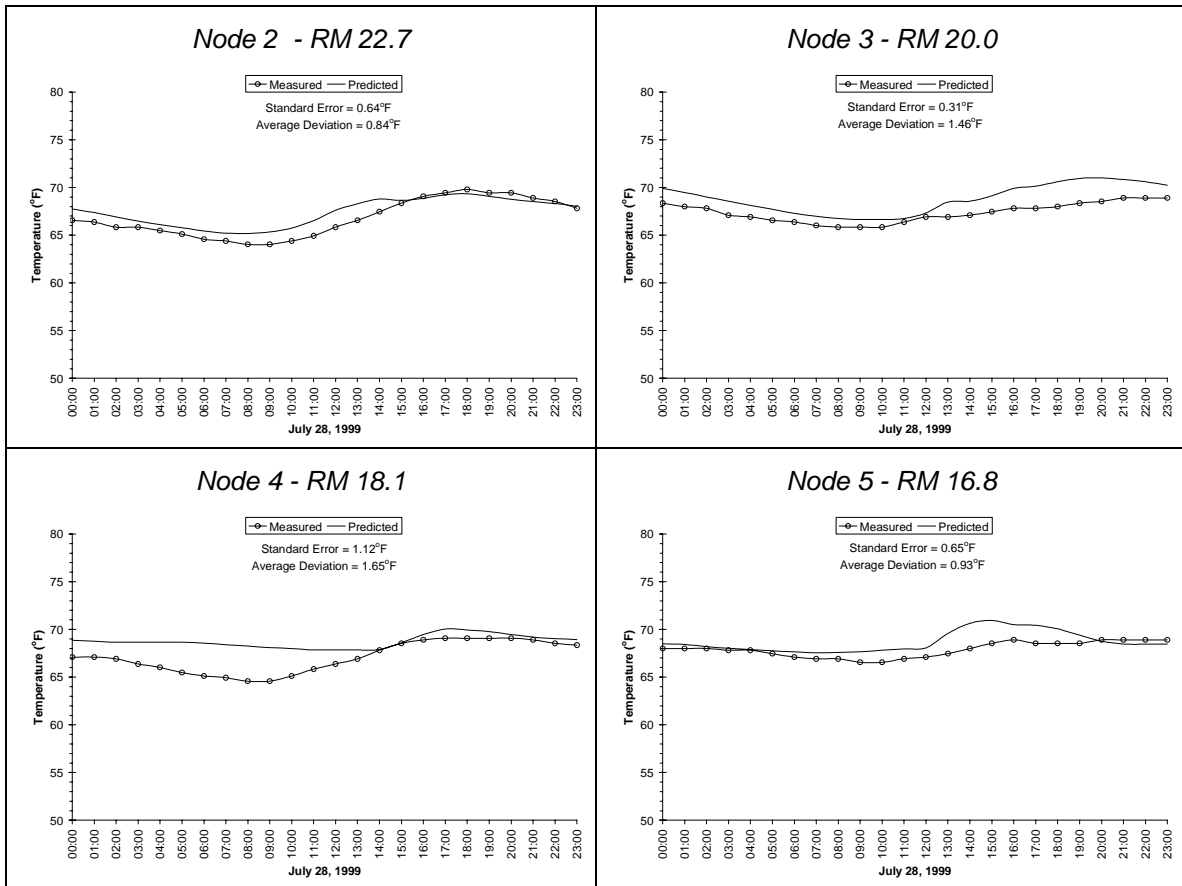
Figure A-117 (Cont'd.). West Fork Dairy Creek/Dairy Creek Model Continuous Data Validation

Loading Capacity - 40 CFR 130.2(f)

Loading Capacity is based on the condition that meets the *no measurable surface water temperature increase resulting from anthropogenic activities*. This condition is termed *System Potential* and is achieved when (1) non-point source solar radiation loading reflects a riparian vegetation condition without human disturbance and (2) point source discharges cause no measurable increases in surface water temperatures.

Solar radiation loading was calculated using system potential riparian vegetation, at current channel and stream aspect conditions. A detailed description of potential vegetation conditions is presented in **Table A-8**. Current and System Potential solar loading for the West Fork Dairy Creek/Dairy Creek are presented in **Figure A-118**. Solar radiation loading for Current Condition and System Potential condition is presented for every 100 meters of modeled stream length. As can be seen in **Figure A-118**, solar radiation loading at System Potential is much less than levels currently observed on West Fork Dairy Creek/Dairy Creek (i.e., Current Condition).

Figure A-118. West Fork Dairy Creek/Dairy Creek Solar Radiation Load at System Potential and Current Conditions
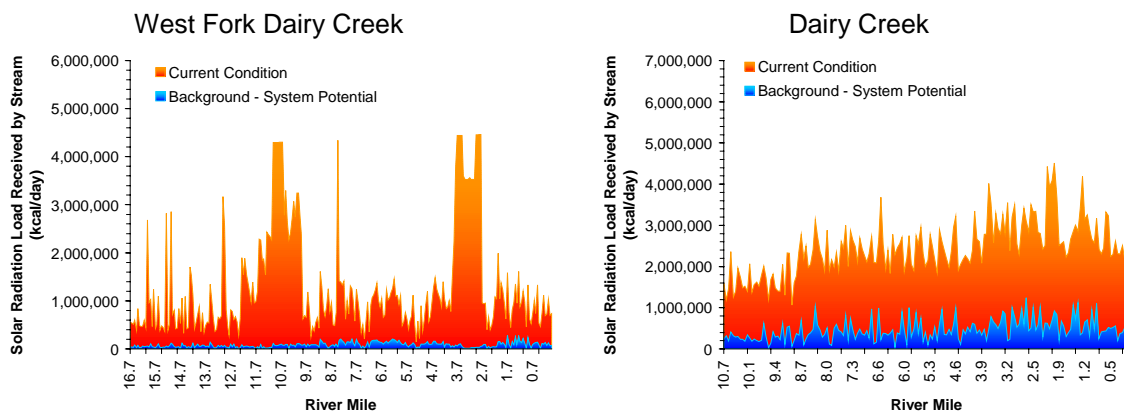
Allocations – 40 CFR 130.2(g) and 40 CFR 130.2(h)

Load Allocations (Non-Point Sources) - The **temperature standard** targets system potential (i.e. no measurable temperature increases from anthropogenic sources). To meet this requirement the system potential solar radiation heat load (Dairy Creek - $1.8 \cdot 10^7$ Kcal/day, and West Fork Dairy Creek - $4.5 \cdot 10^6$ Kcal/day) is allocated to background nonpoint sources. Anthropogenic nonpoint sources are not given a heat load.

Wasteload Allocations (Point Sources) - Surface water discharges into receiving waters have been given a heat load based on the $0.25^{o}F$ allowable increase in the mixing zone as specified in the temperature standard. Heat loads have been converted to allowable effluent temperatures as well. It should be noted that the wasteload allocation is the point source heat load and not the calculated maximum effluent temperatures. There are several options for meeting the allocated heat loads (i.e. passive effluent temperature reductions, changes in facility discharge operation, purchasing instream flows, pollutant trading, etc.).

Temperature Allocation Summary **Non-Point Sources**	
Dairy Creek	
Source	*Loading Allocation* *Allowable Nonpoint Source Solar Radiation Heat Load* *(kcal/day)*
Natural	$1.0 \cdot 10^8$ Kcal/day
Agriculture	$\varnothing$
Forestry	$\varnothing$
Urban	$\varnothing$
Future Sources	$\varnothing$
West Fork Dairy Creek	
Source	*Loading Allocation* *Allowable Nonpoint Source Solar Radiation Heat Load* *(kcal/day)*
Natural	$4.5 \cdot 10^6$ Kcal/day
Agriculture	$\varnothing$
Forestry	$\varnothing$
Urban	$\varnothing$
Future Sources	$\varnothing$

Currently, there are no permitted point sources that discharge into West Fork Dairy Creek or Dairy creek; however, there are two on McKay Creek, a tributary to Dairy Creek.

Surrogate Measures – 40 CFR 130.2(l)

The solar radiation load (Kcal/day) at system potential condition was calculated by multiplying the stream surface area by the solar radiation flux (ly/day). Percent effective shade was used as a surrogate measure of the solar radiation flux calculated at system potential conditions (**Figure A-119**). The individual points in the figure represent the current and allocated conditions for every 100 meters. Accordingly, System Potential heat load condition along West Fork Dairy Creek/Dairy Creek translates into approximately 90% or greater effective shade throughout much of the system.

Figure A-119. West Fork Dairy Creek/Dairy Creek Surrogate Measure for Non Point Sources - Effective Shade.
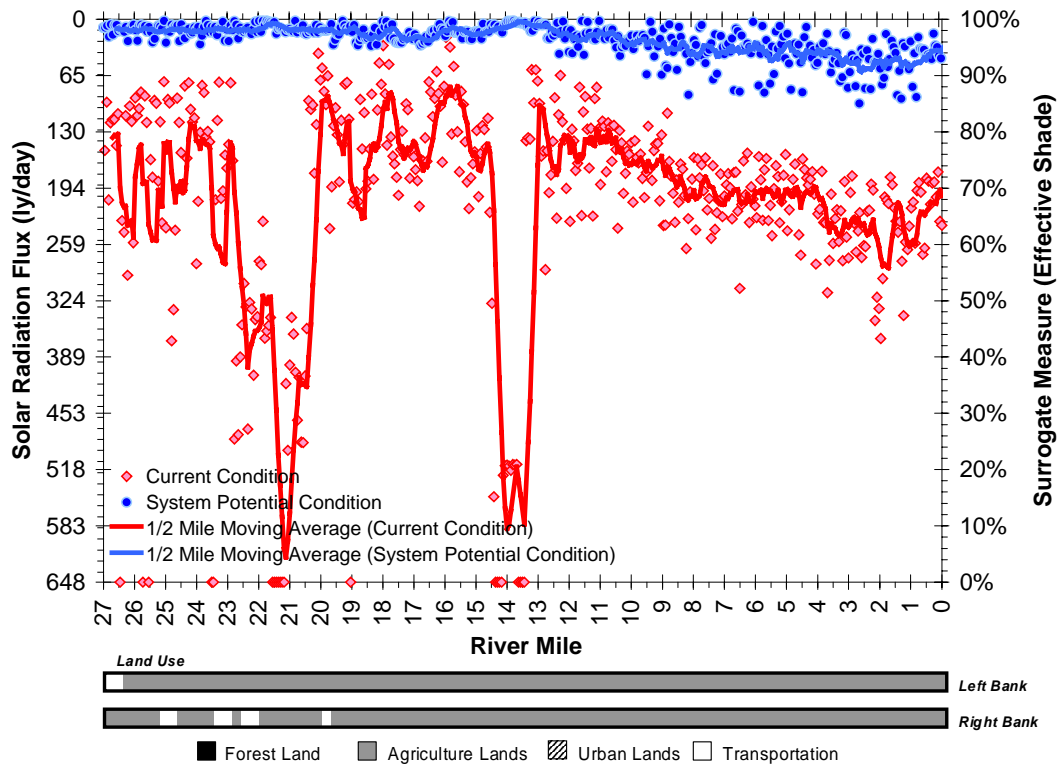
Water Quality Standard Attainment Analysis – CWA §303(d)(1)

Figure A-120 illustrates predicted West Fork Dairy Creek/Dairy Creek temperatures at 5:00 PM on July 27, 1999 with the following scenarios: 1) non-point sources at Load Allocations and point source discharges at current levels, and 2) non-point source at Load Allocation and point source discharges removed. Predicted temperatures in the West Fork Dairy Creek/Dairy Creek system are relatively similar at both Load Allocation scenarios. Point source discharge (into McKay Creek) at current levels only slightly raise stream temperatures under the Loading Allocation.

Figure A-120. WF Dairy Creek/Dairy Creek Longitudinal Temperature Profile - Model Output – 1) Non-Point Source Load Allocation and Current Point Source Discharge, and 2) Non-Point Source Load Allocation and Remove Point Source Discharge – 5:00 PM July 29, 1999.
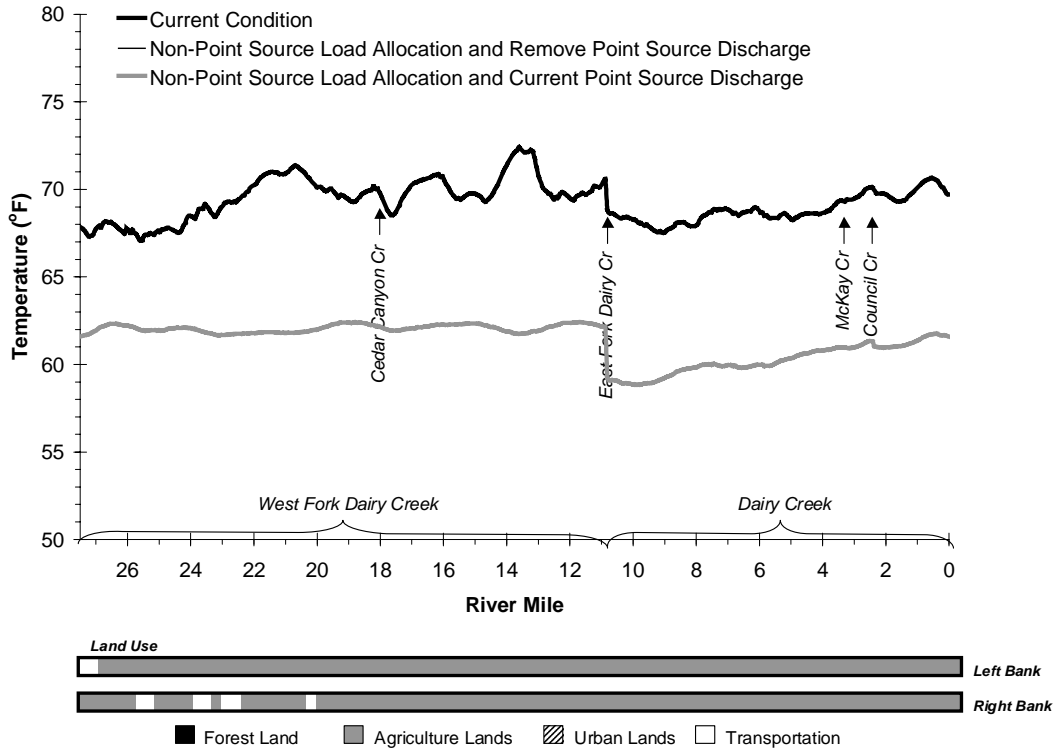
Two scenarios were run in which non-point sources were maintained at current conditions and point source discharge conditions were modified. **Figure A-120** displays predicted West Fork Dairy Creek/Dairy Creek temperatures at 5:00 PM on July 29, 1999 with the following scenarios: 1) non-point sources at Current Conditions and point source discharges removed; and 2) non-point sources at Current Conditions and point sources at Waste Load Allocations. As can be seen in **Figure A-120**, the general temperature profiles were similar between these scenarios and Current Conditions; however, a localized effect downstream of the point source can be observed.

As mentioned above, *System Potential* is achieved when (1) non-point source solar radiation loading reflects a riparian vegetation condition without human disturbance and (2) point source discharges cause no measurable increase in surface water temperature. Accordingly, **Figure A-121** presents predicted West Fork Dairy Creek/Dairy Creek temperatures at a Waste Load Allocation and Load Allocation scenario. **Figure A-122** illustrates that implementing Waste Load Allocations and Load Allocations will drastically reduce temperatures in West Fork Dairy Creek/Dairy Creek.

Figure A-121. West Fork Dairy Creek/Dairy Creek Longitudinal Temperature Profile - Model Output – 1) Non-Point Source Current Condition and Remove Point Source Discharge, and 2) Non-Point Source Current Condition and Point Source Waste Load Allocation – 5:00 PM July 28, 1999.
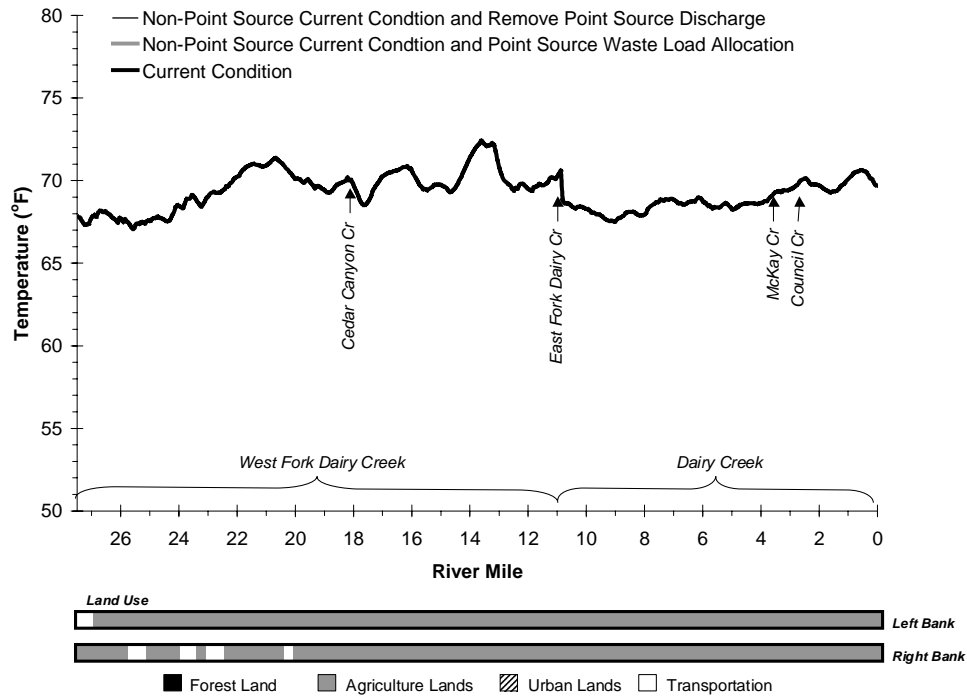
Figure A-122. West Fork Dairy Creek/Dairy Creek Daily Temperature Range for Current Conditions Compared with Allocated Measures - July 28,1999.
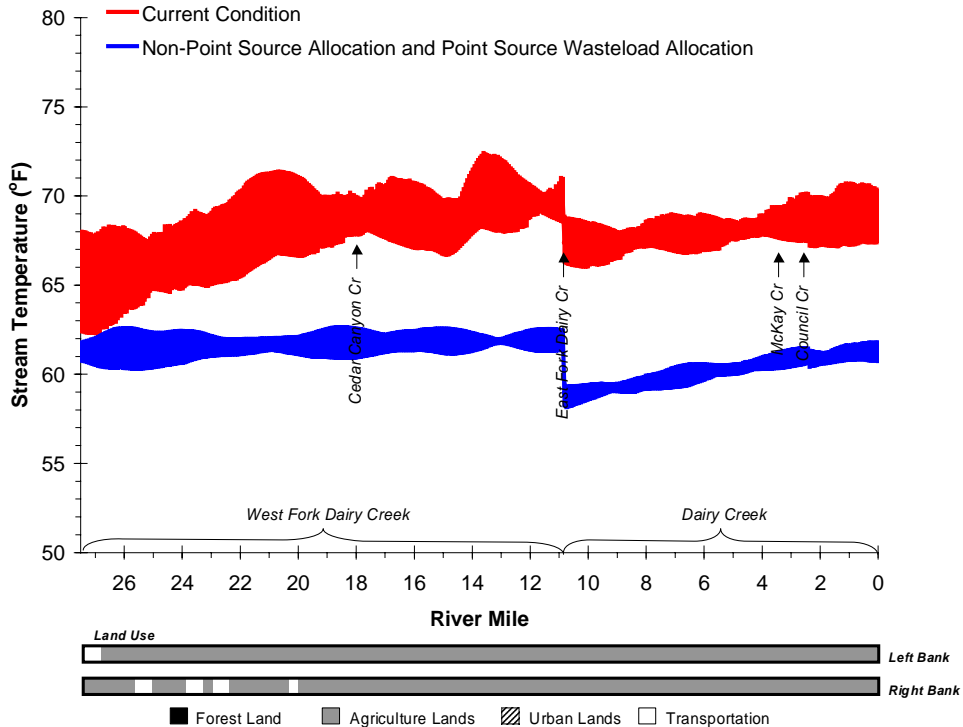
Figure A-123. West Fork Dairy Creek/Dairy Creek Current and Site Potential (Allocated) Temperature Distributions.
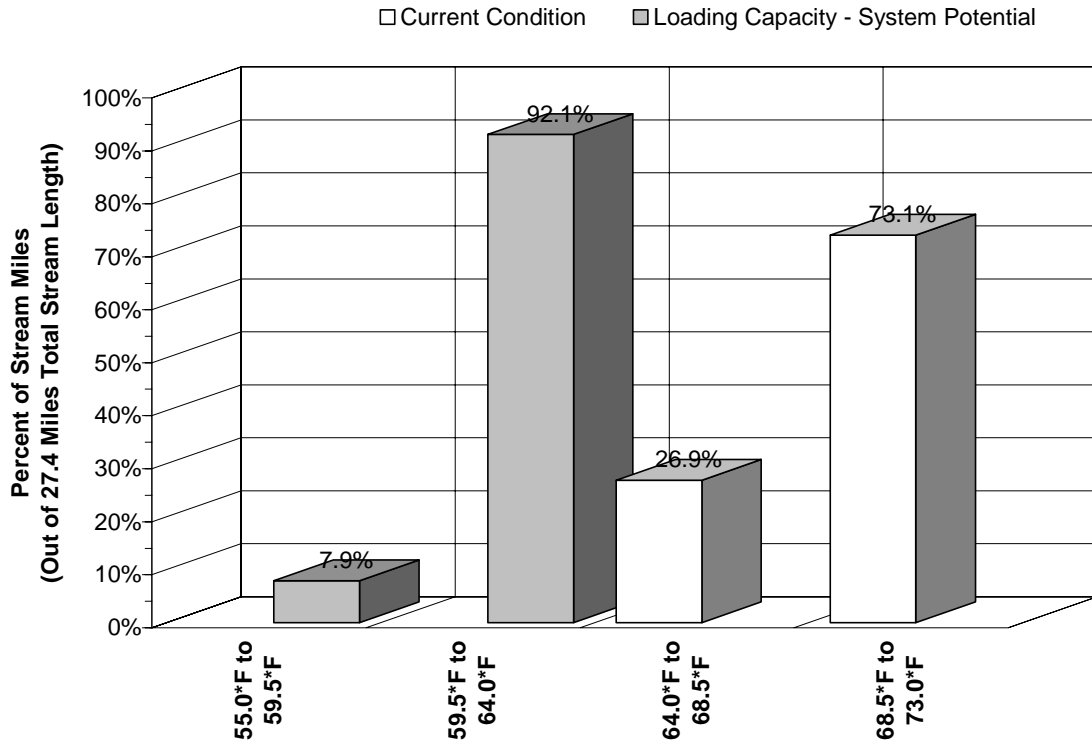
MCKAY CREEK

MCKAY CREEK* CURRENT CONDITION

The Oregon Department of Environmental Quality collected stream temperature, flow, and site descriptions along McKay Creek during the summer of 1999. **Figure A-124** illustrates the location of these sampling sites. Digital photographs taken at several sites are presented in **Images A-46** through **A-47.**

Figure A-124. Water Quality Sampling Locations for McKay Creek During the Summer of 1999.
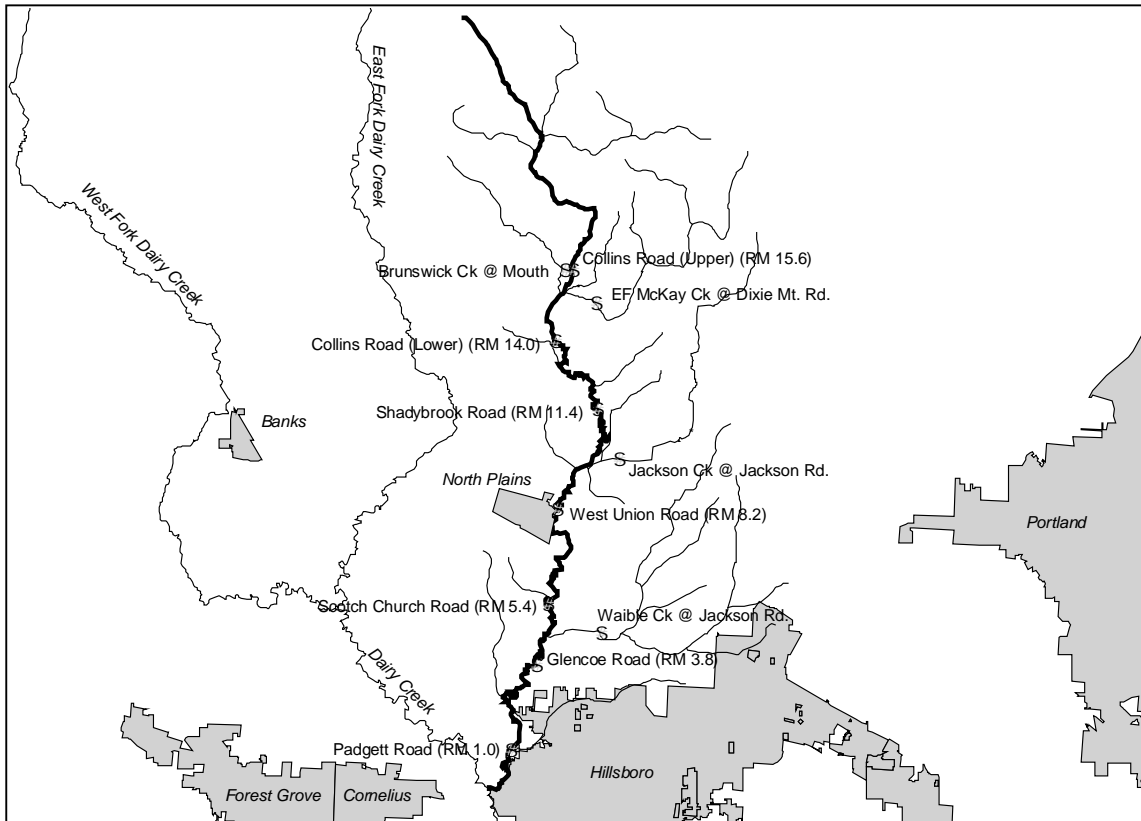
McKay Creek temperatures increase during the summer period, with daily maximums occurring in late July and August (**Figure A-125**). Daily maximum stream temperatures for the summer of 1999 are plotted in **Figure A-126**. Only the uppermost monitoring location had a maximum 7-day statistic that fell below the 64°F temperature criteria (**Figure A-126**). **Table A-23** summarizes the stream temperature statistics for McKay Creek and some of its tributaries.

---

* Note that the river miles (RM) presented in this report were derived from a 1:5000 stream coverage used for ODEQ modeling purposes and may differ slightly from other sources (such as OWRD or USGS river miles).

Image A-46.   McKay Creek at Collins Road (Lower) (River Mile 15.6).
[Temp. Statistic – 66.1*F, Flow – 3.5 cfs, Potential Effective Shade (ES) – 95%, Measured ES – 58%]

Image A-47.   McKay Creek at Padgett Road (River Mile 1.0).
[Temp. Statistic – 68.7*F, Flow – 6.4 cfs, Potential Effective Shade (ES) – 95%, Measured ES – N/A]
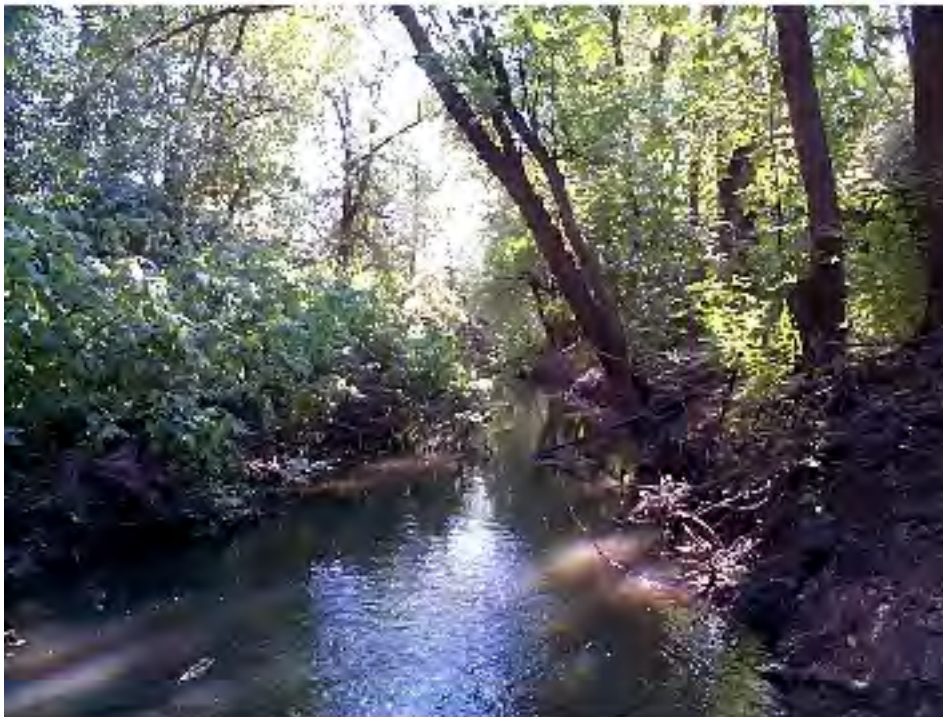
Figure A-125. Observed Daily Maximum Stream Temperatures for McKay Creek.
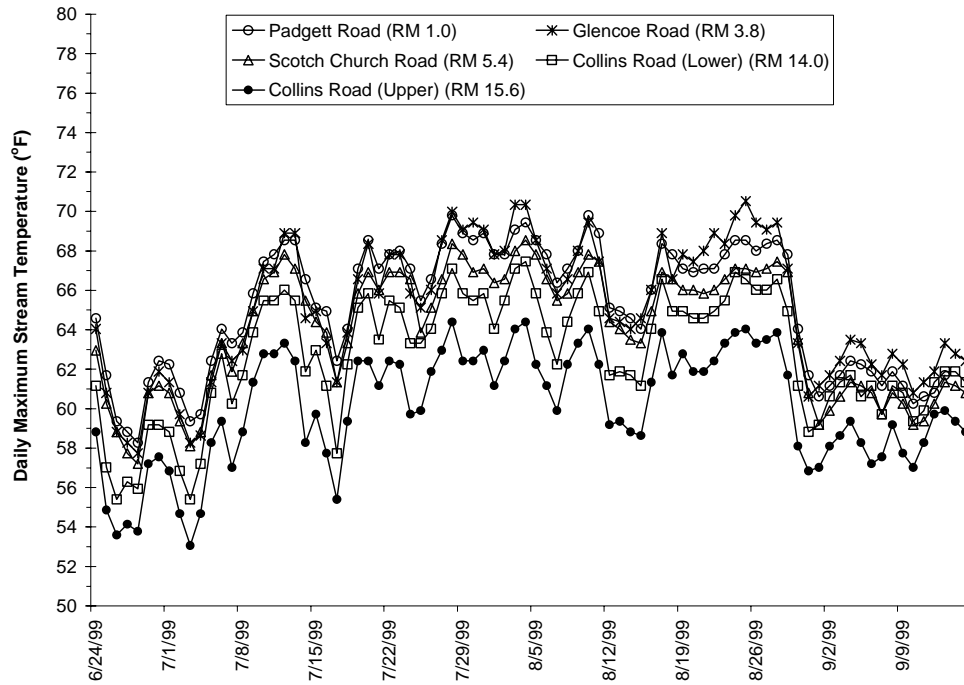
Figure A-126. Observed Maximum 7-Day Temperature Statistics for McKay Creek.
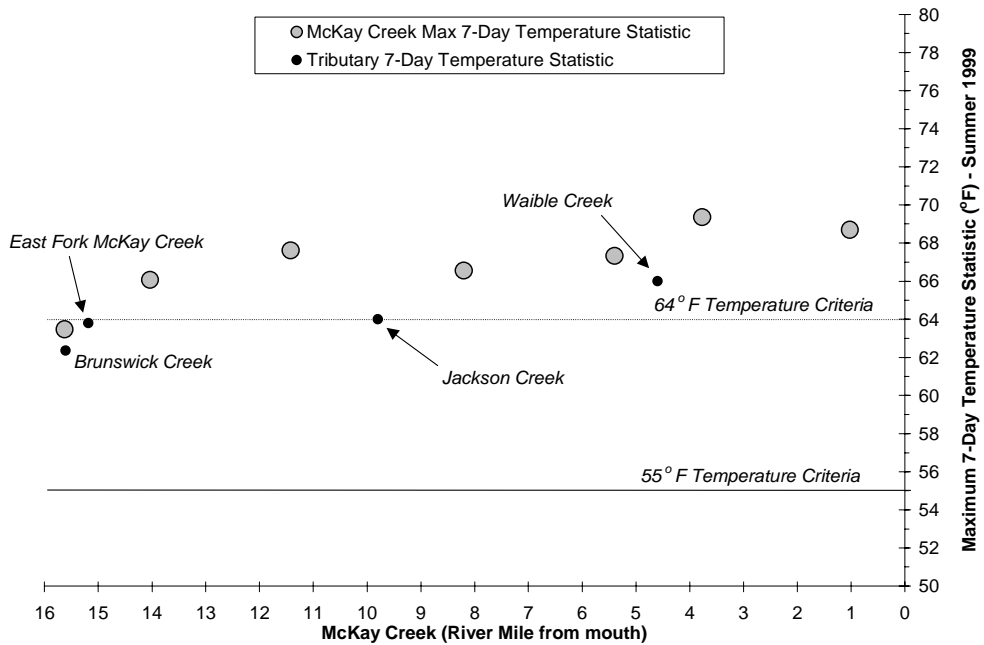
Table A-23. Calculated Stream Temperature Statistics for McKay Creek and Tributaries						
Temperature Site	Start	End	Max. Daily Temp		Max. 7-Day Statistic	
(RM = River Mile from mouth)	Date	Date	Date	(°F)	Date	(°F)
RM 1.0 Padgett Road	6/24/99	9/13/99	8/10/99	69.8	7/31/99	68.7
RM 3.8 Glencoe Road	6/24/99	9/15/99	8/25/99	70.5	8/25/99	69.4
RM 5.4 Scotch Church Road	6/24/99	9/15/99	8/4/99	68.5	8/2/99	67.3
RM 8.2 West Union Road	6/24/99	9/21/99	7/20/99	67.8	8/3/99	66.6
RM 11.4 Shadybrook Road	6/24/99	9/15/99	8/4/99	68.9	8/2/99	67.6
RM 14.0 Collins Road (Lower)	6/18/99	9/15/99	8/4/99	67.5	8/26/99	66.1
RM 15.6 Collins Road (Upper)	6/18/99	9/15/99	8/4/99	64.4	8/25/99	63.5
McKay Creek Tributaries						
Waible Ck at Jackson Road	6/24/99	9/21/99	6/24/99	69.4	6/27/99	66.0
Jackson Ck Jackson School	6/18/99	9/14/99	7/20/99	65.1	7/22/99	64.0
Jackson Ck at J. Quarry Rd	6/18/99	9/14/99	8/17/99	67.5	8/25/99	66.8
Brunswick Ck at Collins Rd	6/18/99	9/15/99	8/17/99	63.3	8/25/99	62.4
EF McKay at Dixie Mtn. Rd	6/18/99	9/15/99	8/28/99	64.4	8/26/99	63.9

Water temperatures in McKay Creek varied through out the course of the day, with maximum temperatures occurring in the late afternoon and minimum temperatures occurring during the early morning hours. Diurnal temperature profiles for McKay Creek on July 29, 1999 are presented in **Figure A-127**. Relatively small diurnal variability was observed McKay Creek, which is typical of a deep, low gradient stream.

Flows were measured throughout the McKay Creek system during the period of FLIR sampling, which also corresponds to the period of summer maximum water temperatures. Flows generally increase in the downstream direction, reaching a maximum value of 6.5 cfs at near the mouth. Tributary flows on this day were much lower than mainstem levels.

Figure A-127. Diurnal Temperature Trends Observed in McKay Creek on July 29, 1999.
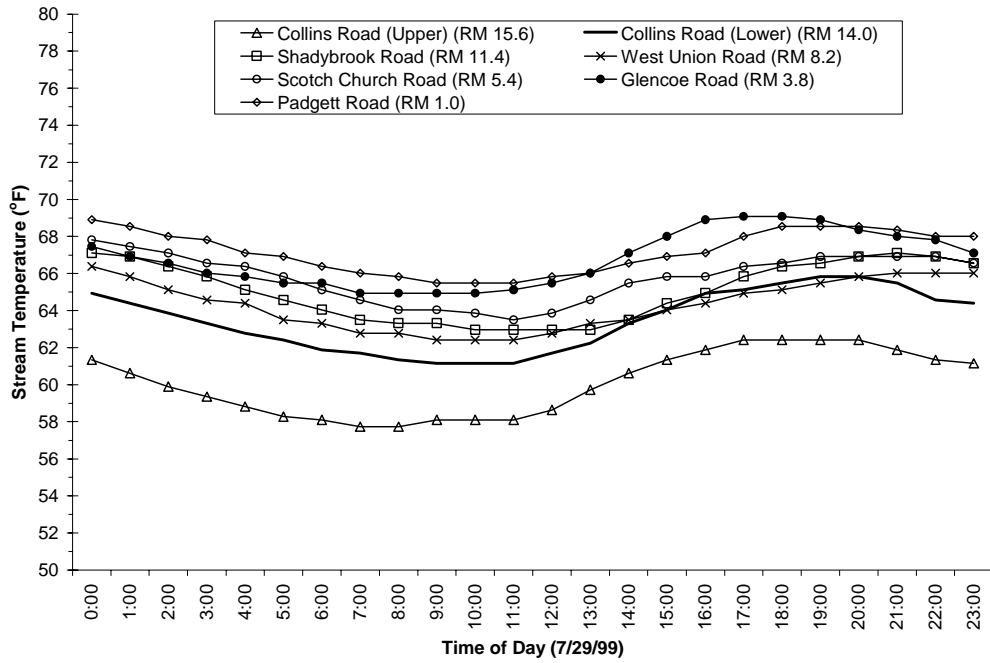
Figure A-128. Stream Flow Observed in McKay Creek on July 29, 1999.
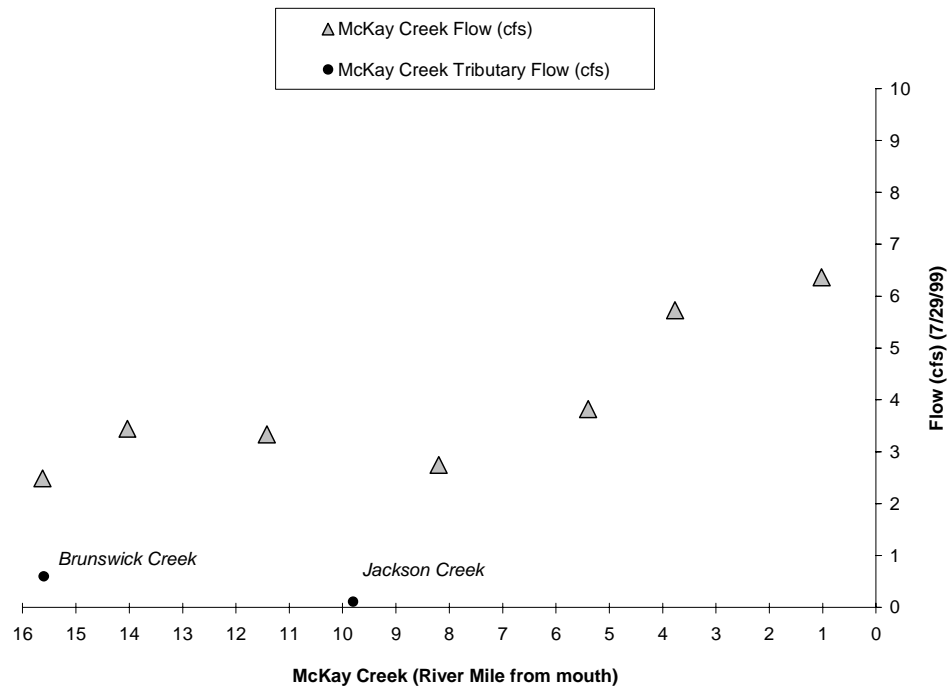
Figure A-129 presents the measured FLIR temperature profile for McKay Creek, which was sampled on July 29, 1999 between 4:16 to 4:48 PM. Several portions of McKay Creek were completely covered by tall deciduous trees and the FLIR camera was unable to see the stream, hence there are gaps in the longitudinal temperature profile. **Table A-24** summarizes the stream temperatures that were recorded with FLIR, and it is readily apparent that most of the stream length flown had temperatures within the sub-lethal temperature range for salmonids.

Figure A-129. McKay Creek FLIR Temperature Profile (16:16 to 16:48 on 7/29/99)
[*Gaps in the profile indicate locations where canopy cover prohibited view of the stream surface.*]
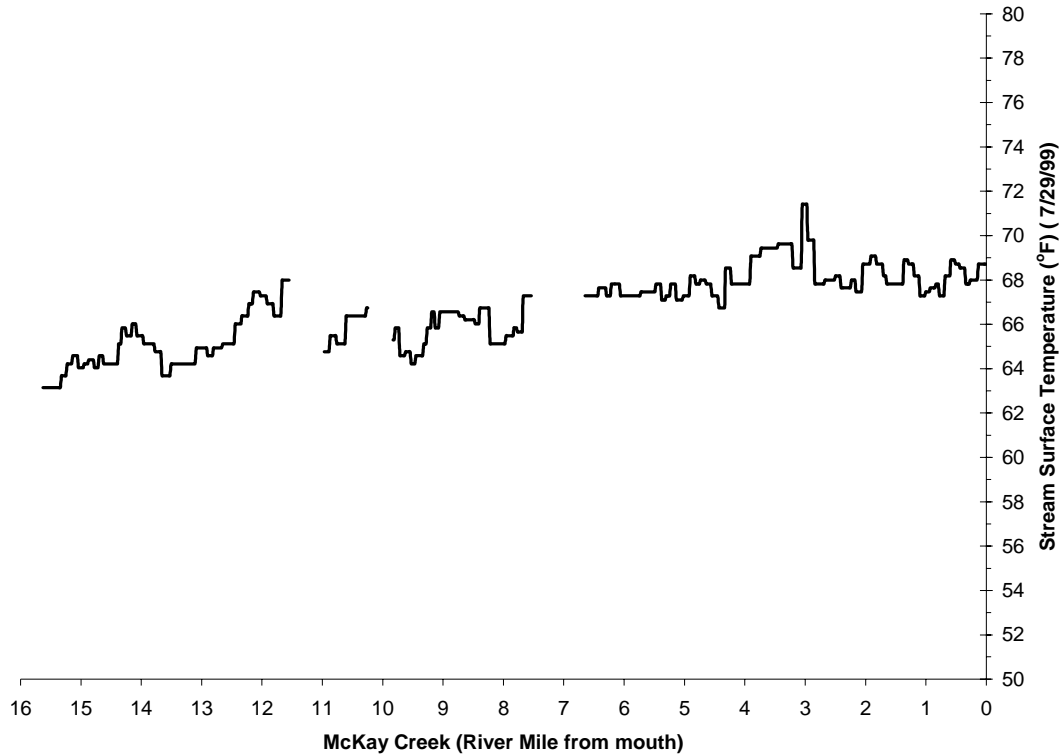
Table A-24. FLIR-derived Water Temperatures in McKay Creek (7/29/99)			
Temperature (°F)	Distance (miles)	Percent of Total	Mode of Thermal Mortality
Less than 55.0	-	-	
55.0 to 59.5	-	-	
59.5 to 64.0	1.6	10.3%	
64.0 to 68.5	14.0	89.7%	
68.5 to 73.0	-	-	Sub-Lethal Range
73.0 to 77.5	-	-	
Greater than 77.5	-	-	Incipient Lethal Range
Totals	15.6	100.0%	

Selected FLIR and video images of McKay Creek show the range of land uses that occur along the stream, including a golf course, agricultural, and forested areas.

Image A-48.   McKay Creek (RM 0.5) as it passes by a golf course.[*]
[*The median surface water temperature is 68.5^{o}F*].
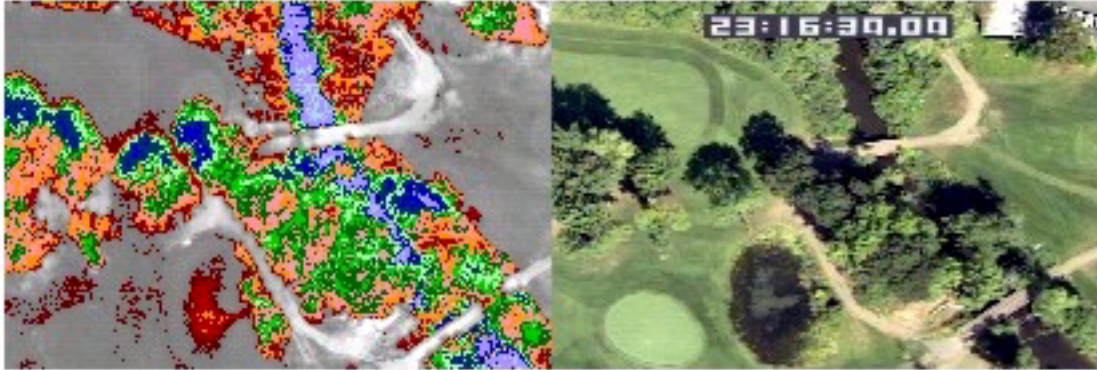
Image A-49.   Thermal microclimate associated with riparian vegetation on McKay Ck (RM 12.9). [*The median surface water temperature is 67.1^{o}F.*]

Image A-50.   The thermal environment within Upper McKay Creek (RM 20.4).
[*The median water temperature is 57.9^{o}F.]*
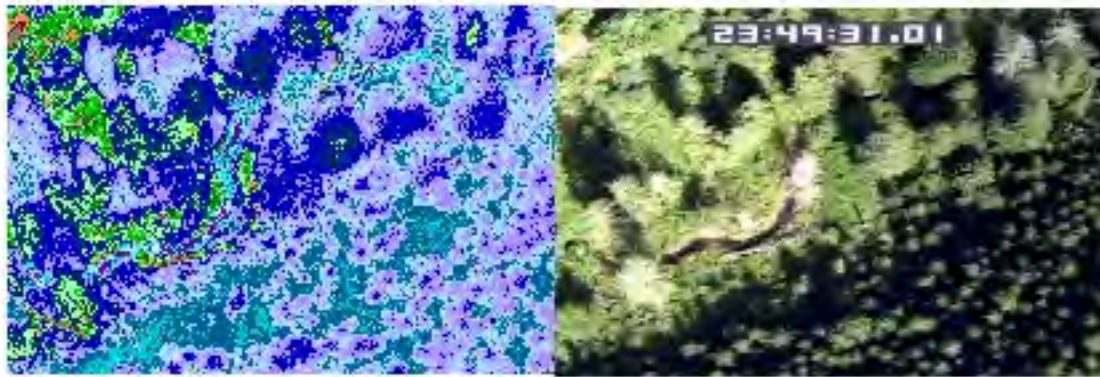
FLIR Image Temperature Scale (*C)[*]

MCKAY CREEK MODEL INPUTS

McKay Creek was modeled from river mile 15.6 to the mouth. This section graphically displays the model input data for each of the 100-foot model segments. Recall that this appendix also describes the various data sources and methodology used to assemble the model input.

Figures 167 through **174** show the following model input data referenced according river mile:

- Elevation and Gradient (**Figure A-130**)
- Aspect (**Figure A-131**)
- Near Stream Disturbance Zone Widths and Wetted Widths (**Figure A-132**)
- Topographic Shade (**Figure A-133**)
- Vegetation Geometry (**Figure A-134**)
- Flow Volume (**Figure A-135**)
- Flow Velocity (**Figure A-136**)
- Water Column Depth (**Figure A-137**)

Figure A-130. McKay Creek Elevation and Gradient at Each 100-foot Model Reach
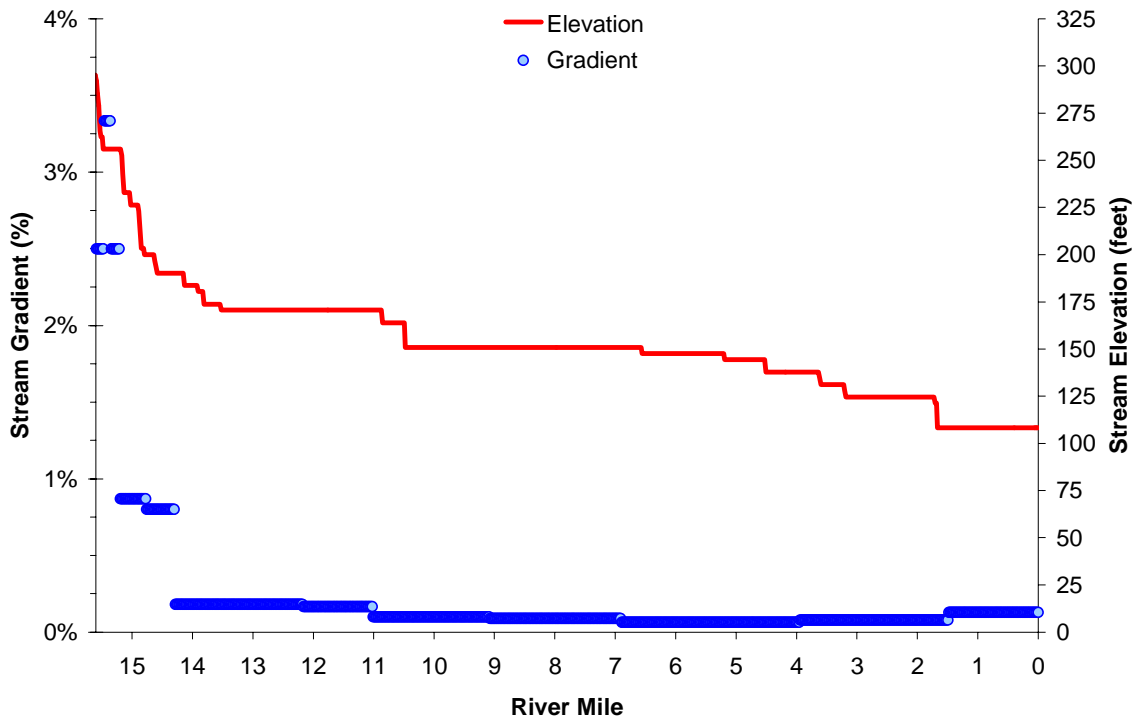
Figure A-131.   McKay Creek Aspect at Each 100-foot Model Reach
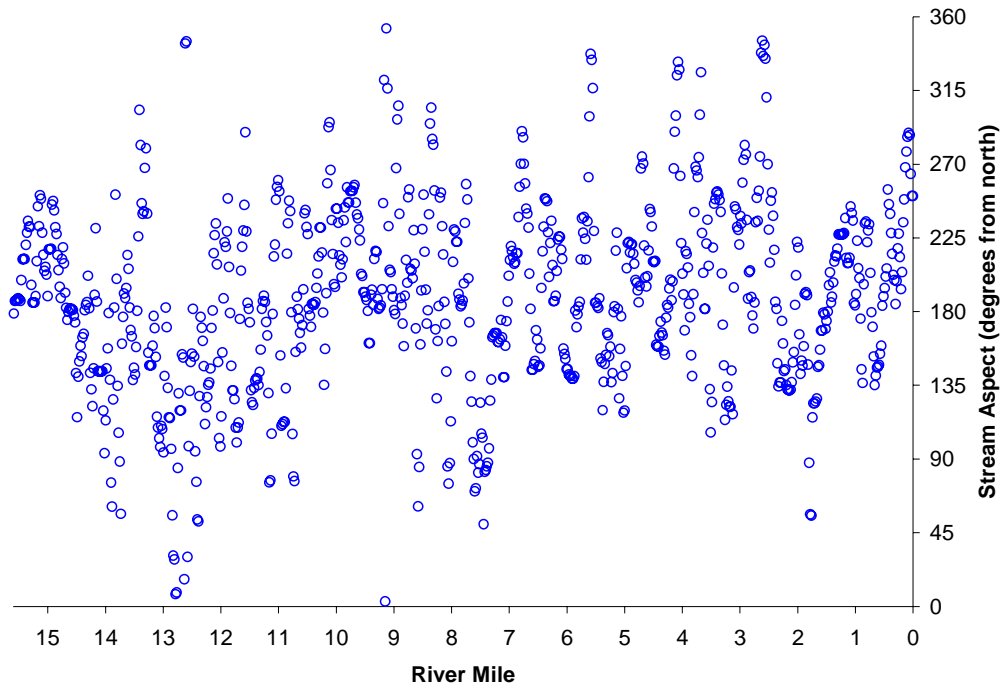
Figure A-132.   McKay Creek Wetted Widths and NSDZ Widths.
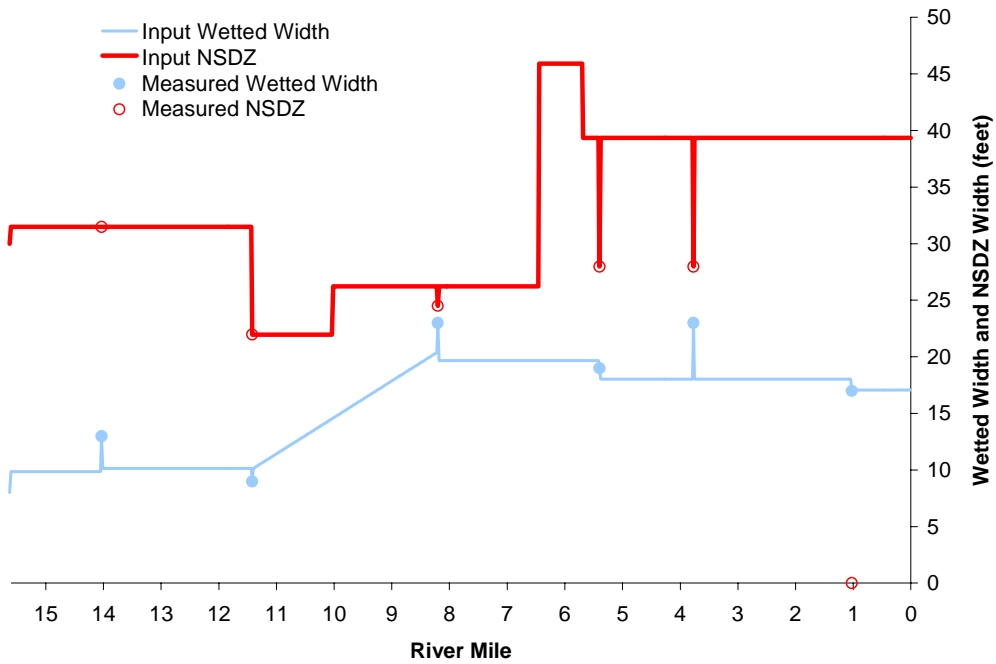
Figure A-133.   McKay Creek Topographic Shade at Each 100-foot Model Reach.
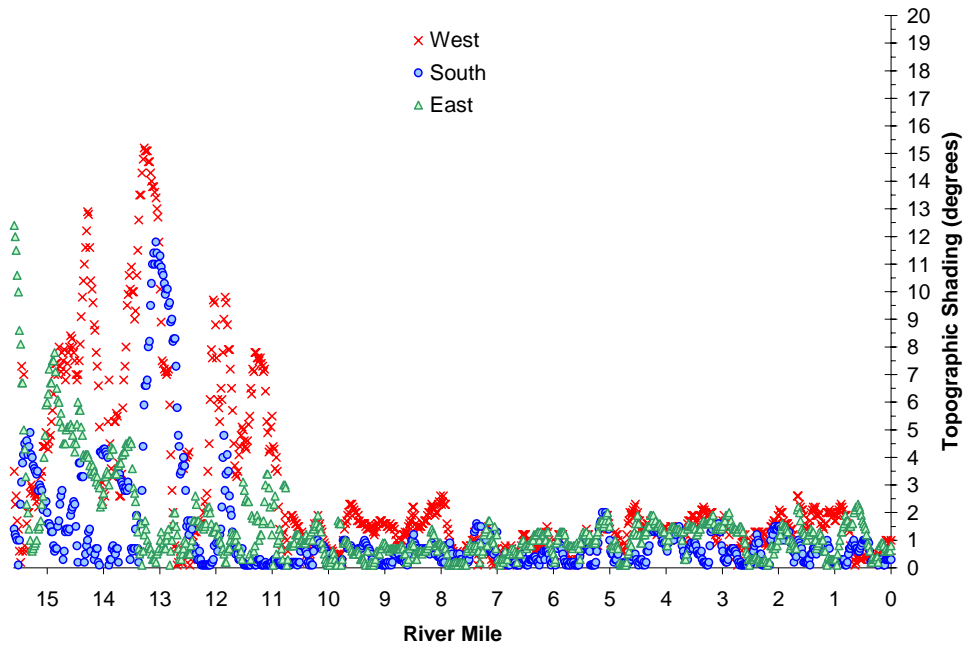
Figure A-134.   McKay Creek Current Vegetation Heights and Widths for Each 100-foot Model Reach.
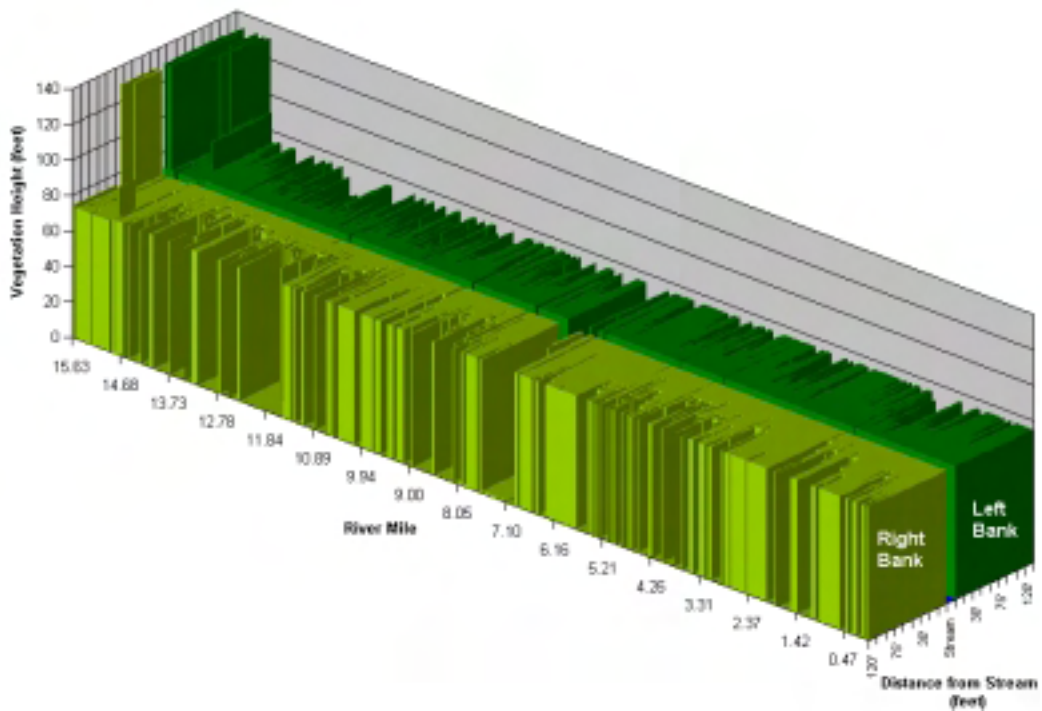
Figure A-135. McKay Creek Measured and Interpolated Flow Volume.
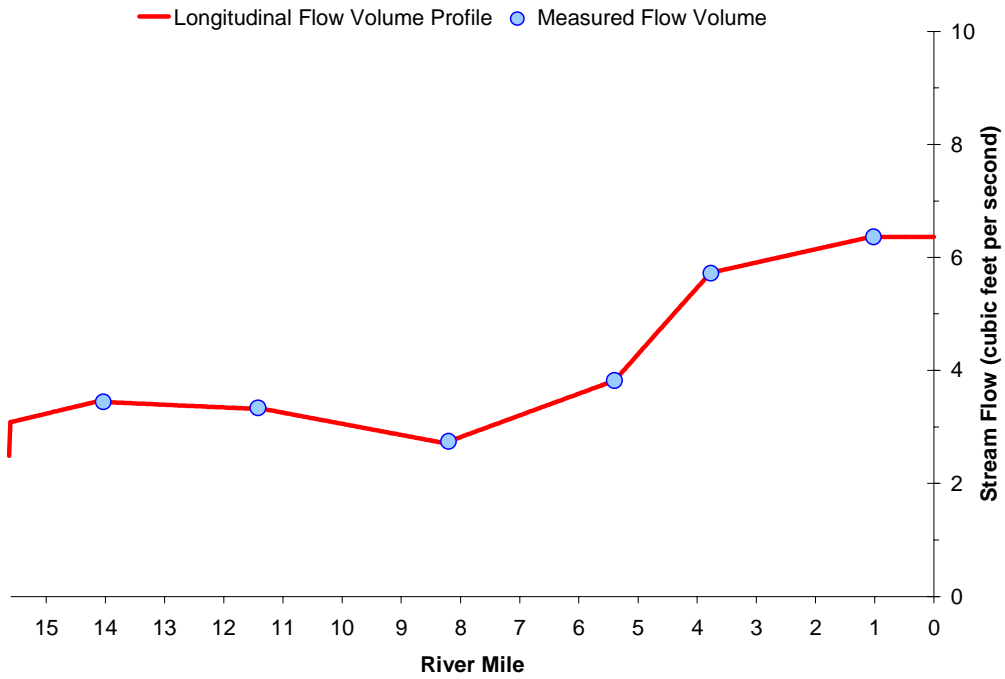
Figure A-136. McKay Creek Measured and Mannings Derived Longitudinal Flow Velocities[13]

---
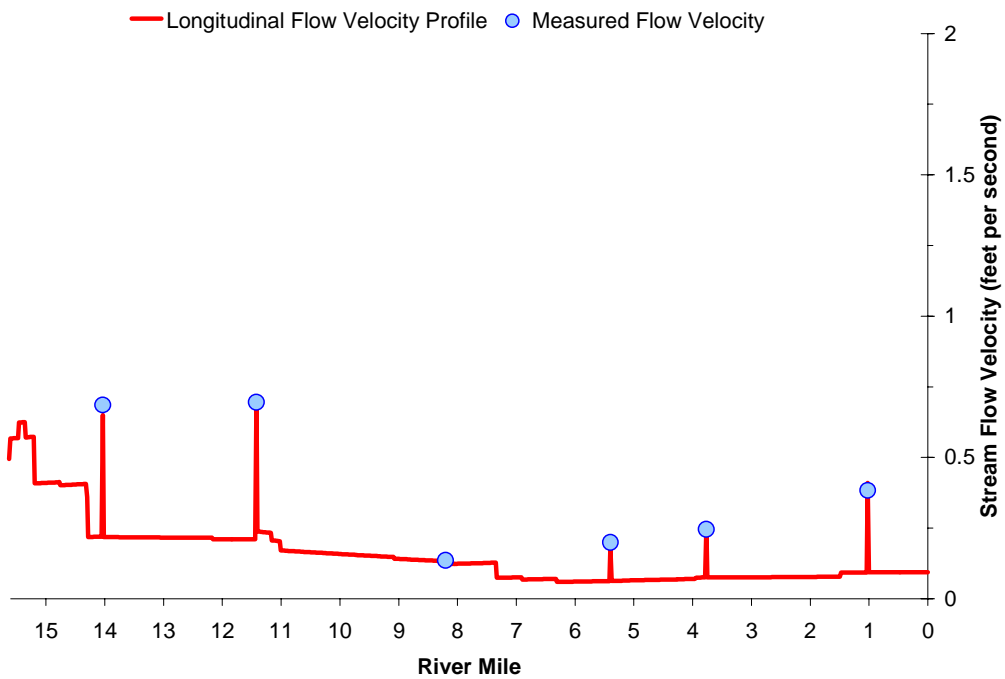
[13] Note that due to the low gradient nature of McKay Creek, DEQ data collection targeted riffles to provide more accurate flow measurements (faster velocities).

Figure A-137. McKay Creek Measured and Mannings Derived Longitudinal Water Column Depths[14]

---
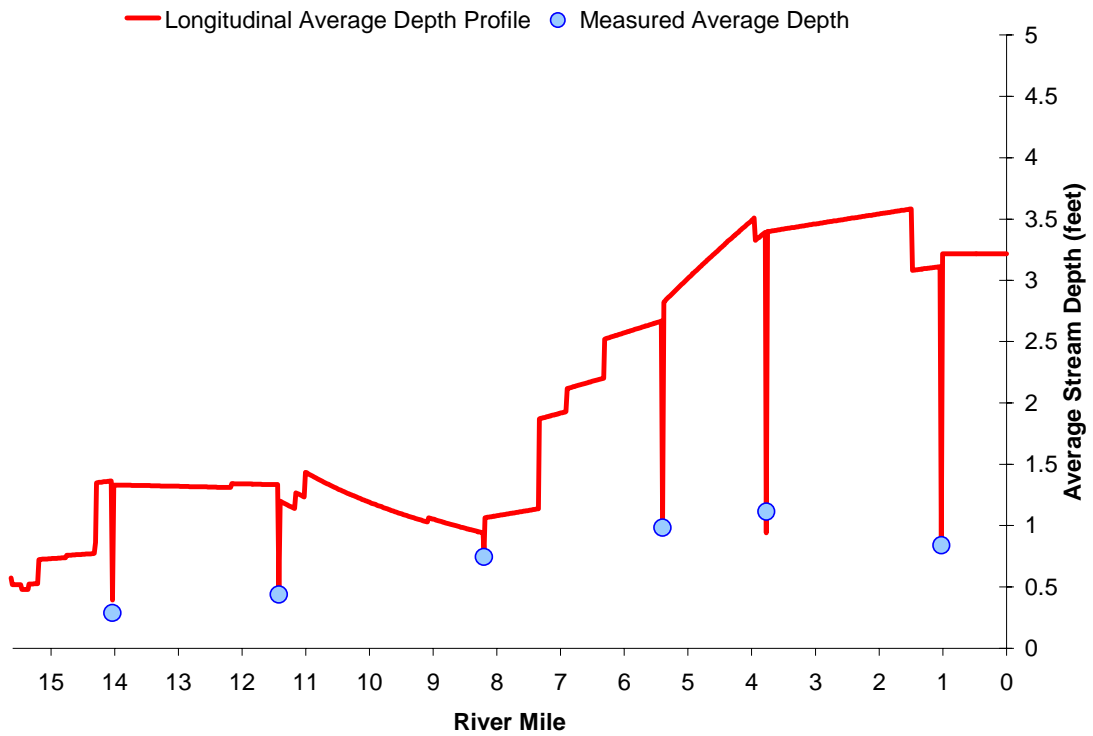
[14] Note that due to the low gradient nature of McKay Creek, DEQ data collection targeted riffles to provide more accurate flow measurements (faster velocities).

MCKAY CREEK MODEL RESULTS

This section presents temperature modeling results for McKay Creek. Graphical and statistical validation of the calibrated model are shown, in addition to temperature predictions for potential vegetation and flow conditions. Recall that the date modeled was July 29, 1999 and is representative of critical stream temperature, stream flow, and climatic conditions. In other words, this modeling effort has captured the time period in 1999 when stream temperatures were near their peak.

Spatial validation of the calibrated model is presented in **Figure A-138**. The solid line is the calibrated model temperature prediction at 4:00 PM on July 29, 1999, while the dots represent the FLIR-measured temperatures at that same time. Notice how McKay Creek temperatures exceeded 64°F for the majority of the river miles modeled.

The standard error and average deviation for the spatial data calibration are:

$$Standard\ Error = 0.59^oC\ (1.07^oF)$$

$$Average\ Deviation = 0.13^oC\ (0.24^oF)$$

Figure A-138.   McKay Creek Observed and Predicted Spatial Temperature Data.
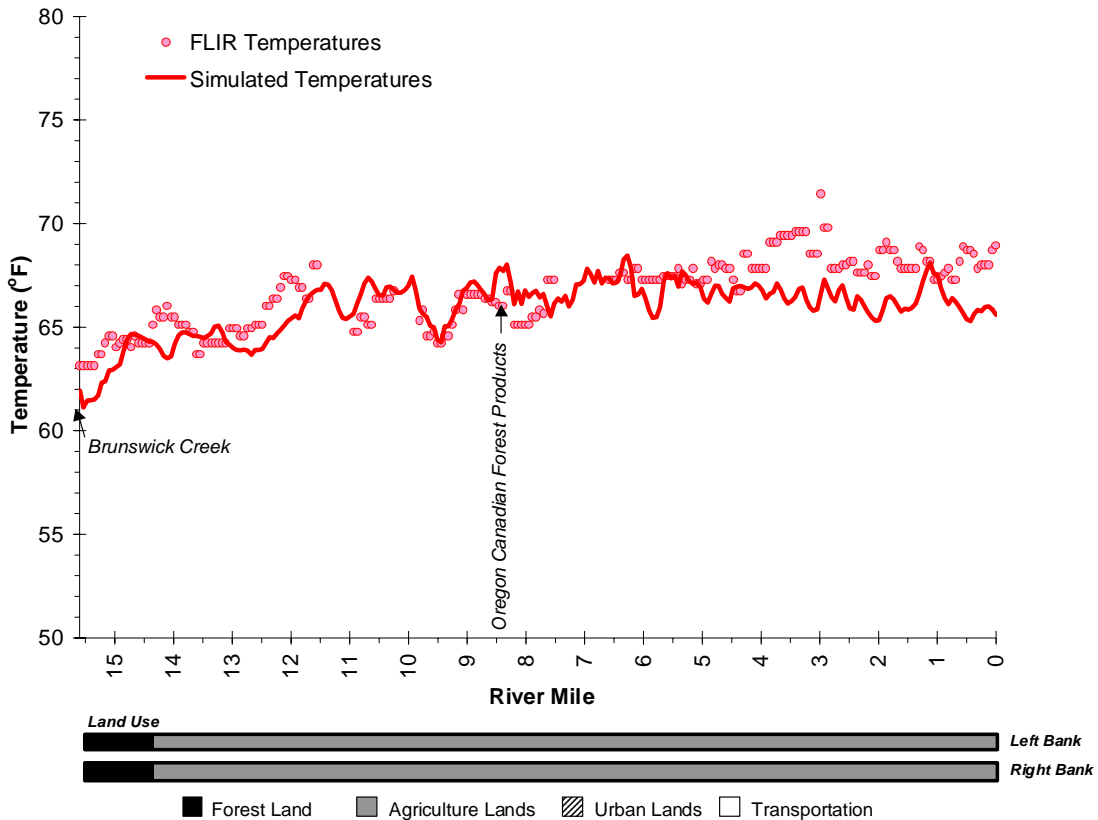
Figure A-139 displays the measured and predicted hourly temperatures at six continuous temperature monitoring locations on McKay Creek. Node 1 is the upper boundary condition and remains constant, therefore it is not graphed. Standard errors, and average deviations are presented for each node.

The mean standard error and mean average deviation for the continuous data are:

Mean Standard Error = 0.51^{o}C (0.91^{o}F)

Mean Average Deviation = 0.88^{o}C (1.59^{o}F)

**Figure A-139.** McKay Creek Model Continuous Data Validation

Loading Capacity - 40 CFR 130.2(f)

Loading Capacity is based on the condition that meets the *no measurable surface water temperature increase resulting from anthropogenic activities*. This condition is termed *System Potential* and is achieved when (1) non-point source solar radiation loading reflects a riparian vegetation condition without human disturbance and (2) point source discharges cause no measurable increases in surface water temperatures.

Solar radiation loading was calculated using system potential riparian vegetation, at current channel and stream aspect conditions. A detailed description of potential vegetation conditions is presented in **Table A-8**. Current and System Potential solar loading for McKay Creek are presented in **Figure A-140**. Solar radiation loading for Current Condition and System Potential condition is presented for every 100 meters of modeled stream length. As can be seen in **Figure A-140**, solar radiation loading at System Potential is much less than levels currently observed on McKay Creek (i.e., Current Condition). Allowable point source heat loading at load capacity conditions are summarized below and described in detail in the main TMDL document.

Figure A-140.   McKay Creek Solar Radiation Load at System Potential and Current Conditions
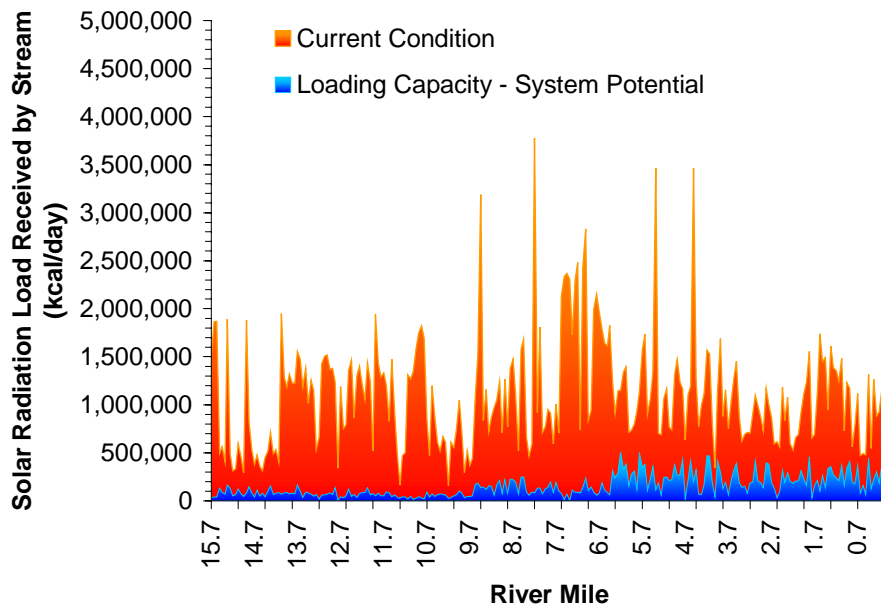
Allocations – 40 CFR 130.2(g) and 40 CFR 130.2(h)

*Load Allocations (Non-Point Sources) - The **temperature standard** targets system potential (i.e. no measurable temperature increases from anthropogenic sources). To meet this requirement the system potential solar radiation heat load (8.7·10[6] Kcal/day) is allocated to background nonpoint sources. Anthropogenic nonpoint sources are not given a heat load.*

Wasteload Allocations (Point Sources) - Surface water discharges into receiving waters have been given a heat load based on the 0.25°F allowable increase in the mixing zone as specified in the temperature standard. Heat loads have been converted to allowable effluent temperatures as well. It should be noted that the wasteload allocation is the point source heat load and not the calculated maximum effluent temperatures. There are several options for meeting the allocated heat loads (i.e. passive effluent temperature reductions, changes in facility discharge operation, purchasing instream flows, pollutant trading, etc.).

Temperature Allocation Summary **Non-Point Sources**	
Source	*Loading Allocation* *Allowable Nonpoint Source Solar Radiation Heat Load* *(kcal/day)*
Natural	3.8·10^7 Kcal/day
Agriculture	∅
Forestry	∅
Urban	∅
Future Sources	∅

Point Sources - Allowable Point Source Effluent Source Heat Loading						
		Q_R	Q_{PS}	T_{PS}	Max T_P	H_{PS}	H_{WLA}
Facility Name	**Rec. Water**	Receiving Water 7Q10 Low Flow (cfs)	Facility Design Flow (cfs)	Point Source Effluent Temp. (°F)	Max Daily Site Potential River Temp. (°F)	Current Point Source Heat Loading on River (kcal/day)	Allowable Point Source Heat Loading in Zone of Dilution (kcal/day)
Oregon-Canadian	McKay Cr. RM - 8.5	0.20	0.33	82.0	57.8	4.3•10^6	1.7•10^4
Henningsen	Council Cr. RM - 10.0	0.15*	0.02	69.0	57.8	7.1•10^5	1.3•10^4

Surrogate Measures – 40 CFR 130.2(I)

The solar radiation load (Kcal/day) at system potential condition was calculated by multiplying the stream surface area by the solar radiation flux (ly/day). Percent effective shade was used as a surrogate measure of the solar radiation flux calculated at system potential conditions (**Figure A-141)**.. The individual points in the figure represent the current and allocated conditions for every 100 meters. Accordingly, System Potential heat load condition along McKay Creek translates into approximately 90% or greater effective shade throughout much of the system.

Figure A-141. McKay Creek Surrogate Measure for Non Point Sources - Effective Shade.
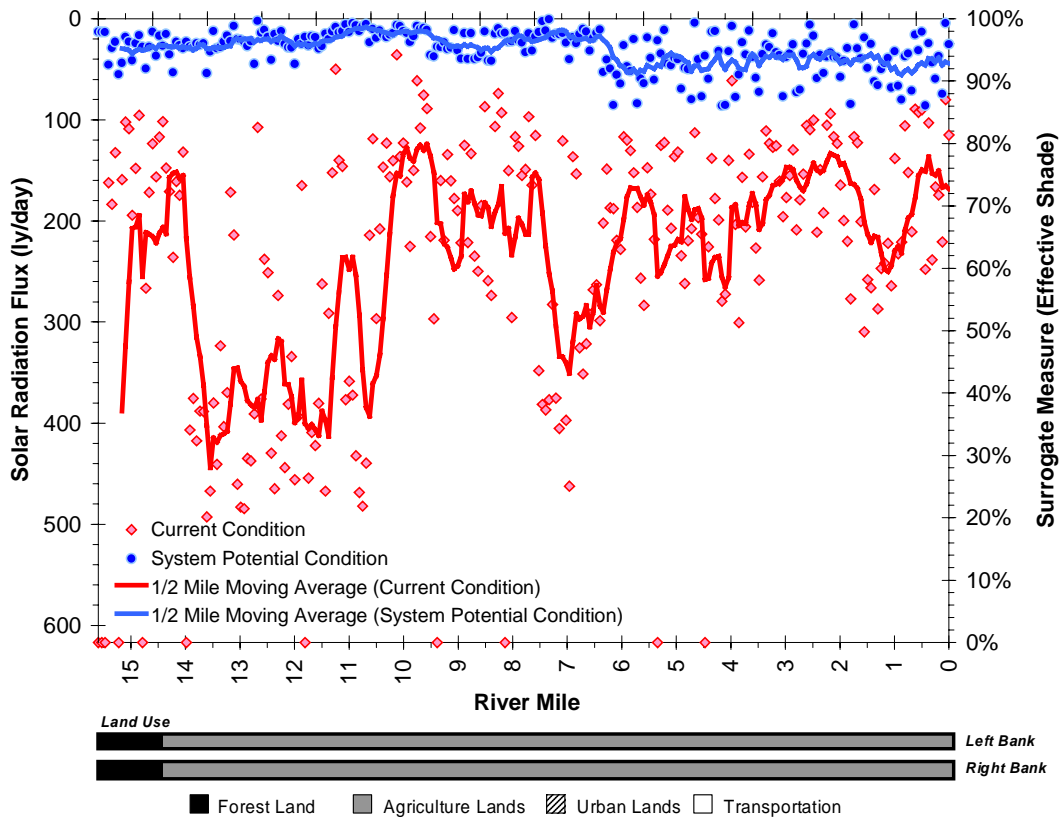
Water Quality Standard Attainment Analysis – CWA §303(d)(1)

Figure A-142 illustrates predicted McKay Creek temperatures at 5:00 PM on July 29, 1999 with the following scenarios: 1) non-point sources at Load Allocations and point source discharges at current levels, and 2) non-point source at Load Allocation and point source discharges removed. Predicted temperatures in McKay Creek are relatively similar at both Load Allocation scenarios. Point source discharge at current levels only slightly raises stream temperatures under the Loading Allocation (approximately river mile 4.0 to river mile 2.0).

Figure A-142. McKay Creek Longitudinal Temperature Profile - Model Output – 1) Non-Point Source Load Allocation and Current Point Source Discharge, and 2) Non-Point Source Load Allocation and Remove Point Source Discharge – 5:00 PM July 29, 1999.
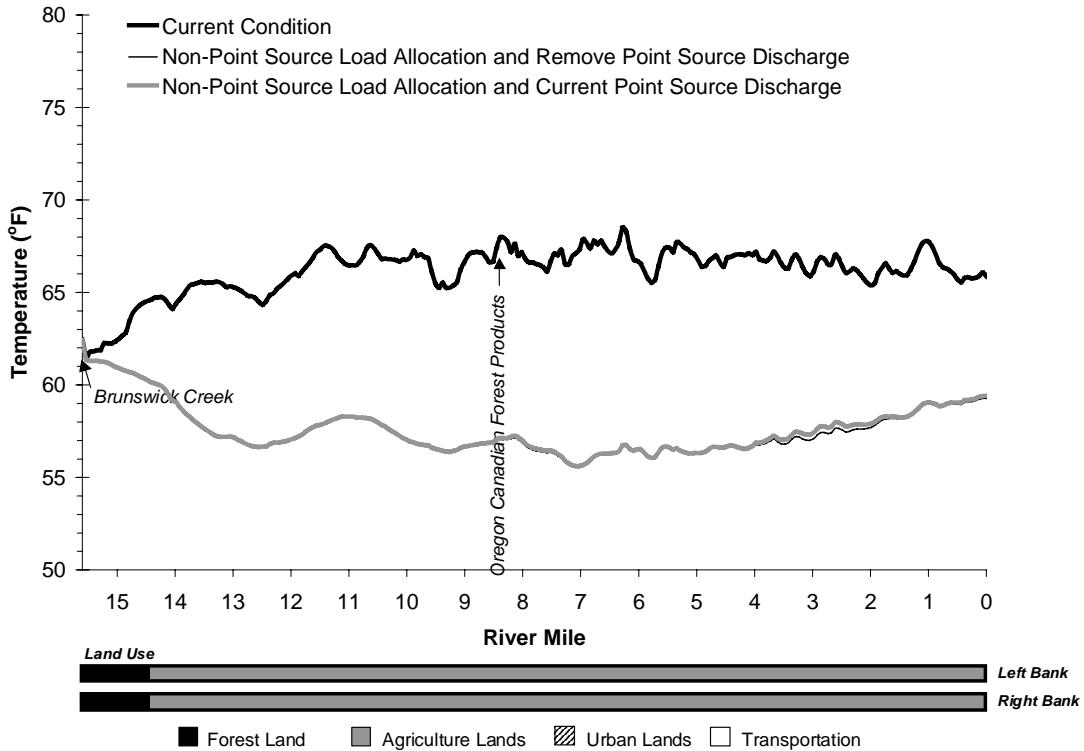
Two scenarios were run in which non-point sources were maintained at current conditions and point source discharge conditions were modified. **Figure A-143** displays predicted McKay Creek temperatures at 5:00 PM on July 29, 1999 with the following scenarios: 1) non-point sources at Current Conditions and point source discharges removed; and 2) non-point sources at Current Conditions and point sources at Waste Load Allocations. As can be seen in **Figure A-143**, the general temperature profiles were similar between these scenarios and Current Conditions; however, a localized effect downstream of the point source can be observed.

As mentioned above, *System Potential* is achieved when (1) non-point source solar radiation loading reflects a riparian vegetation condition without human disturbance and (2) point source discharges cause no measurable increase in surface water temperature. Accordingly, **Figure A-144** presents predicted McKay Creek temperatures at a Waste Load Allocation and Load Allocation scenario. **Figure A-145** illustrates that implementing Waste Load Allocations and Load Allocations will drastically reduce temperatures in McKay Creek.

Figure A-143. McKay Creek Longitudinal Temperature Profile - Model Output – 1) Non-Point Source Current Condition and Remove Point Source Discharge, and 2) Non-Point Source Current Condition and Point Source Waste Load Allocation – 5:00 PM July 29, 1999.
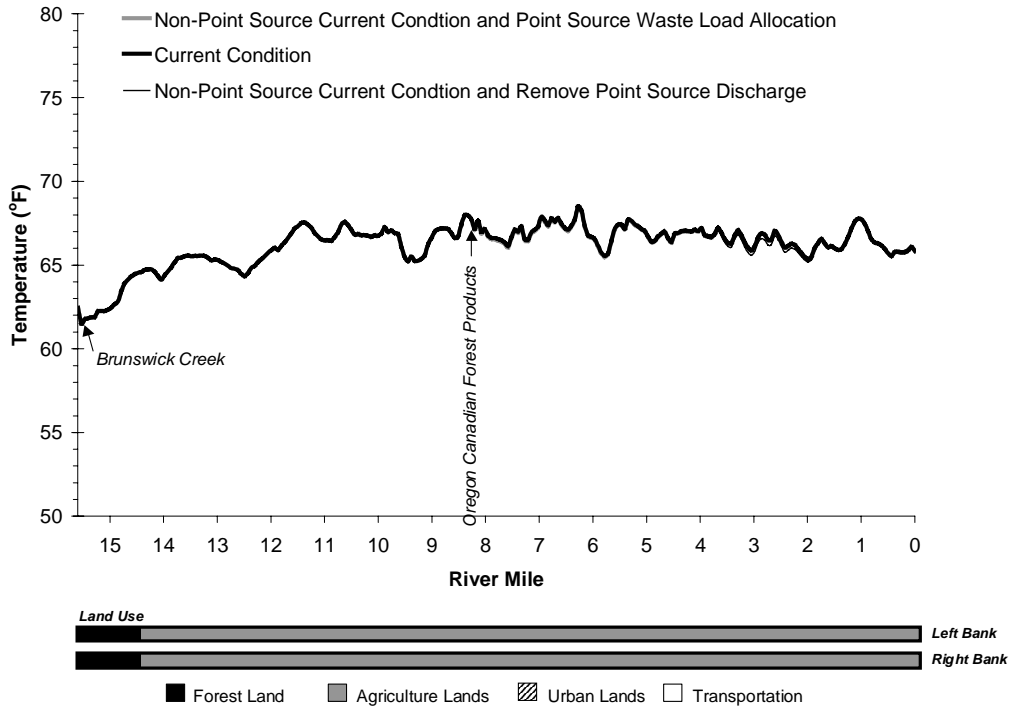
Figure A-144. McKay Creek Daily Temperature Range for Current Conditions Compared with Allocated Measures - July 29, 1999.
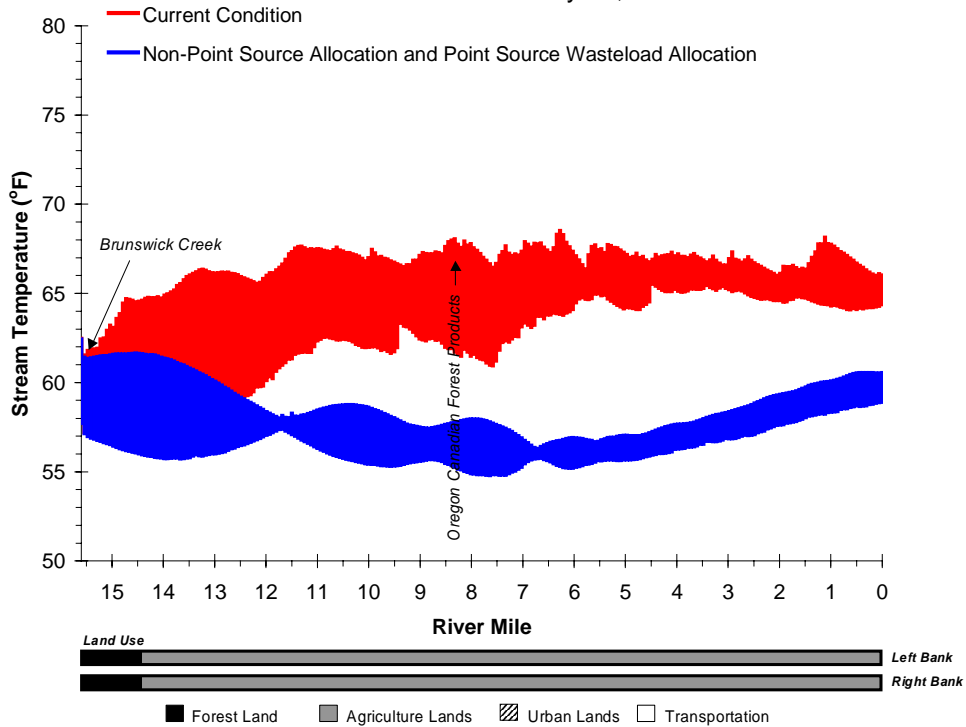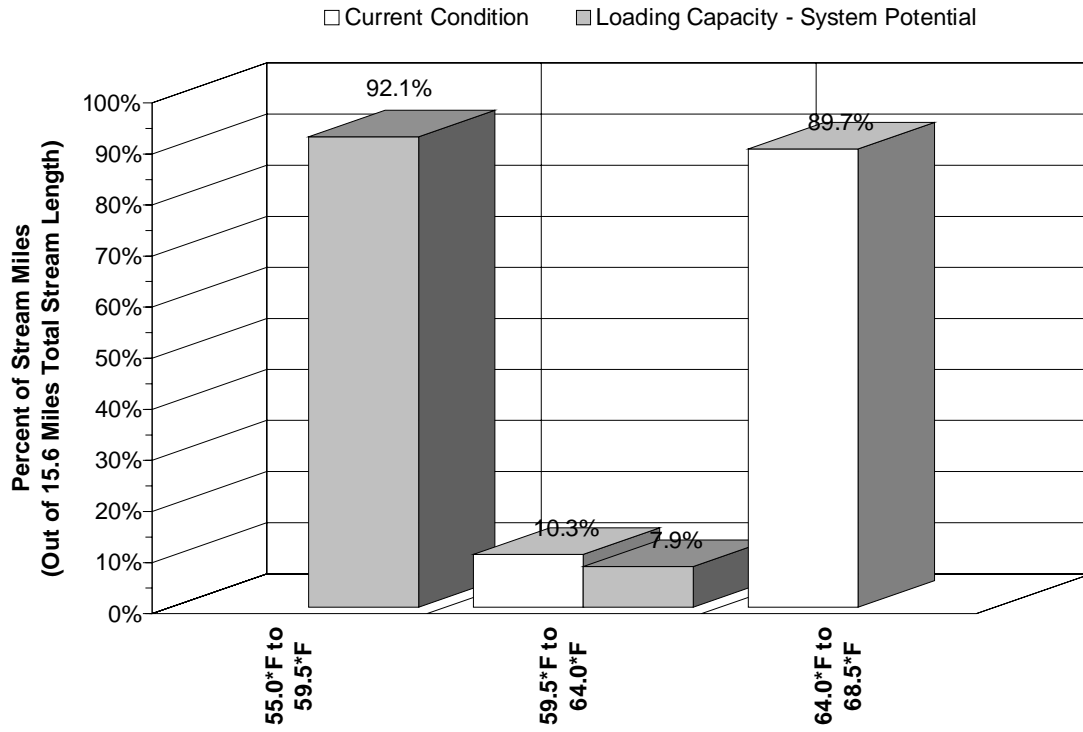
**Figure A-145.** McKay Creek Current and Site Potential (Allocated) Temperature Distributions.

ROCK AND BEAVERTON CREEKS

ROCK CREEK* CURRENT CONDITION

The Oregon Department of Environmental Quality collected water quality data in Rock Creek during the summer of 1999. This effort included the collection of continuous hourly temperature data, FLIR temperature data, flow measurement, and site descriptions. Sampling locations are illustrated in **Figure A-146**. Digital photographs taken at several Rock Creek sampling locations are presented in **Image A-51** through **Image A-52**.

Figure A-146. Water Quality Sampling locations for Rock Creek during the Summer of 1999.
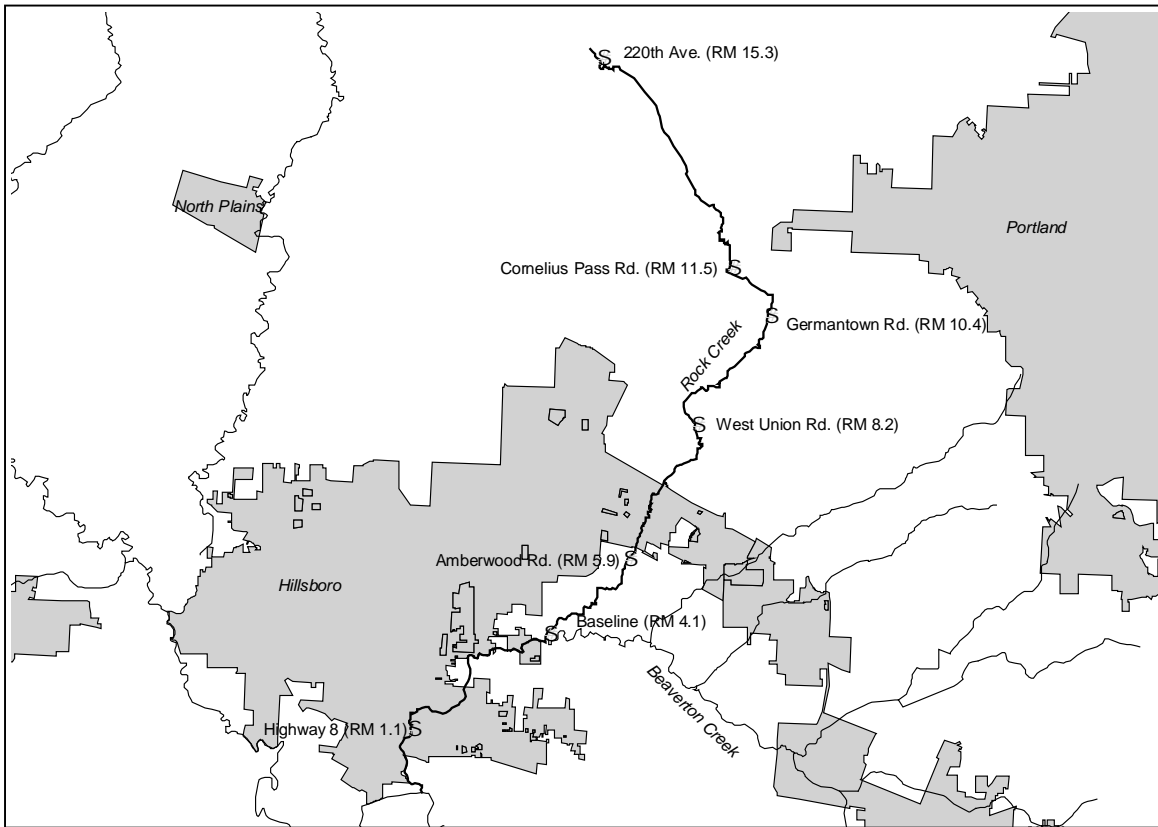
Water temperatures in Rock Creek increase during the summer period, with maximum temperatures occurring in late July. Accordingly, FLIR thermal imagery was collected for Rock Creek on July 30, 1999. In Addition, flow measurements were also collected during this period. The longitudinal profile of the calculated 7-Day temperature statistics for Rock Creek, and several of its tributaries, are presented in **Figure A-147**. Observed 7-day temperature statistics within Rock Creek were all above the 64°F standard in 1999. Calculated 7-day temperature statistics for Rock Creek and tributaries in 1999 are also presented in **Table A-25**.

---

* Note that the river miles (RM) presented in this report were derived from a 1:5000 stream coverage used for ODEQ modeling purposes and may differ slightly from other sources (such as OWRD or USGS river miles).

Image A-51.   Rock Creek at Baseline Road (River Mile 4.1)

[Temp. Statistic – 68.2*F, Flow – 6.9 cfs, Potential Effective Shade (ES) – 68%, Measured ES – 96%]

Image A-52.   Rock Creek at Germantown Road (River Mile 10.4)

[Temp. Statistic – 65.3*F, Flow – N/A, Potential Effective Shade (ES) –98%, Measured ES – N/A]

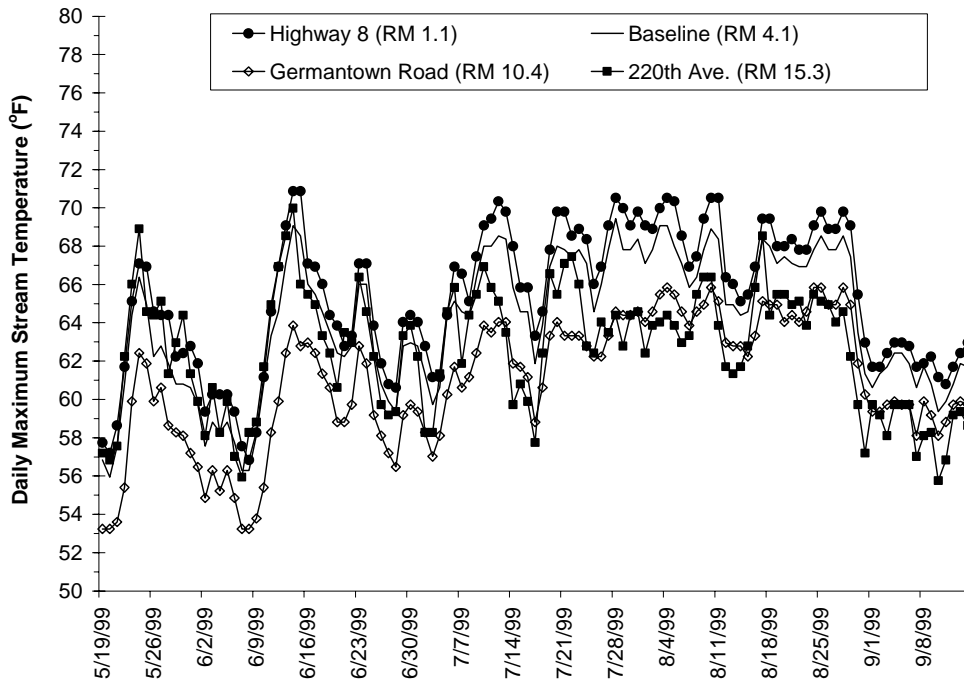**Figure A-147.** Observed daily maximum temperatures for Rock Creek in 1999.

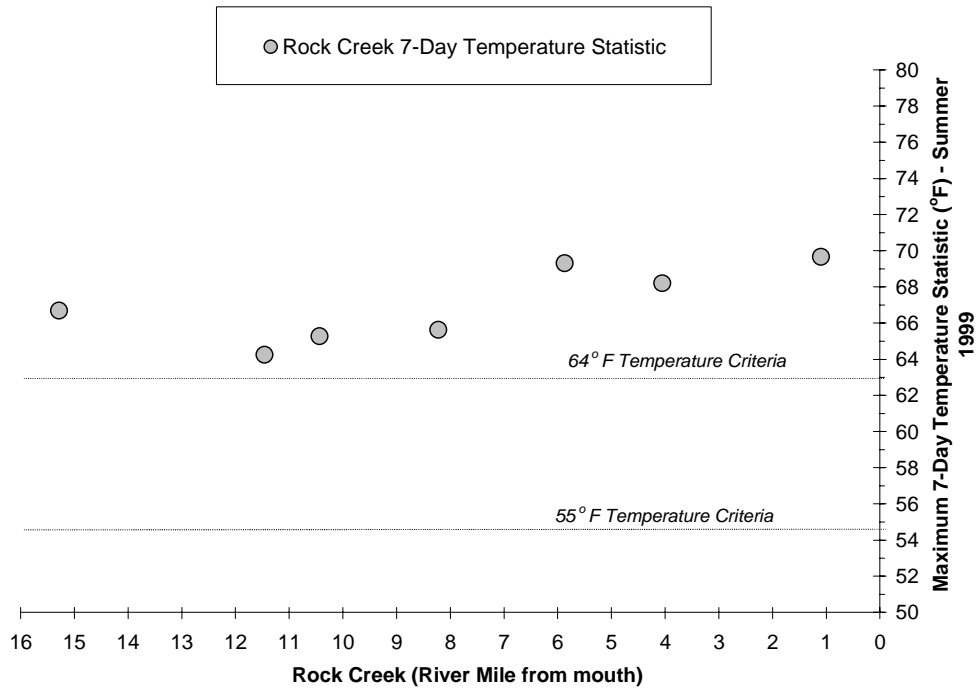**Figure A-148.** Observed 7-Day temperature Statistics for Rock Creek during the summer of 1999.

Table A-25. Calculated 7-Day Temperature Statistics for Rock Creek in 1999.						
Temperature Site (RM = River Mile from mouth)	Start Date	End Date	Max Temp. (Date)	(°F)	7-Day Statistic (Date)	(°F)
Rock Creek at Hwy. 8	5/19/99	9/14/99	6/15/99	70.9	8/02/99	69.7
Rock Creek at Baseline	5/19/99	9/14/99	7/28/99	69.4	7/31/99	68.2
Rock Creek at Amberwood	5/19/99	9/14/99	8/10/99	70.9	7/31/99	69.3
Rock Creek at West Union	5/19/99	9/14/99	8/28/99	66.6	8/25/99	65.6
Rock Creek at Germantown Road	5/19/99	9/21/99	8/28/99	65.8	8/26/99	65.3
Rock Creek at Cornelius Road	6/26/99	9/14/99	7/22/99	66.0	7/09/99	64.2
Rock Creek at 220th	5/19/99	9/14/99	6/14/99	70.0	6/14/99	66.7

Water temperatures in Rock Creek varied through out the course of the day, with maximum temperatures occurring in the late afternoon and minimum temperatures occurring during the early morning hours. Diurnal temperature profiles for Rock Creek on July 30, 1999 are presented in **Figure A-149**. Relatively small diurnal variability was observed Rock Creek, which is typical of a deep, low gradient stream.

Flows were measured throughout the Rock Creek system during the period of FLIR sampling, which also corresponds to the period of summer maximum water temperatures. As can be seen in this **Figure A-150**, Beaverton Creek significantly increases flow conditions in Rock Creek.

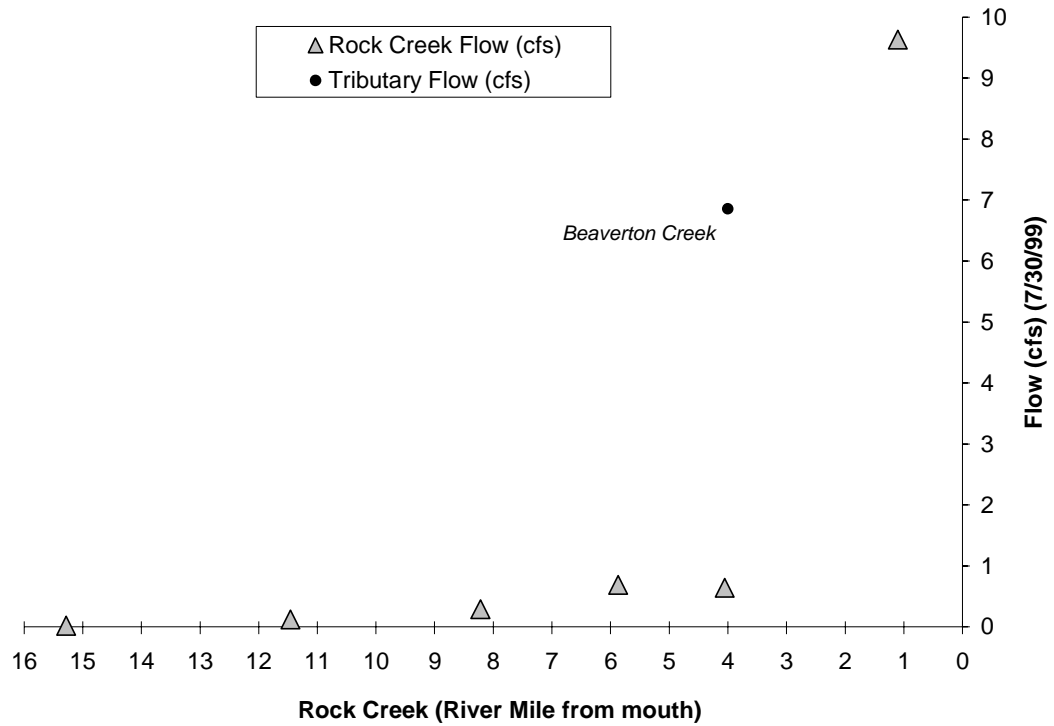**Figure A-149.** Diurnal temperature trends observed in Rock Creek on July 30, 1999.
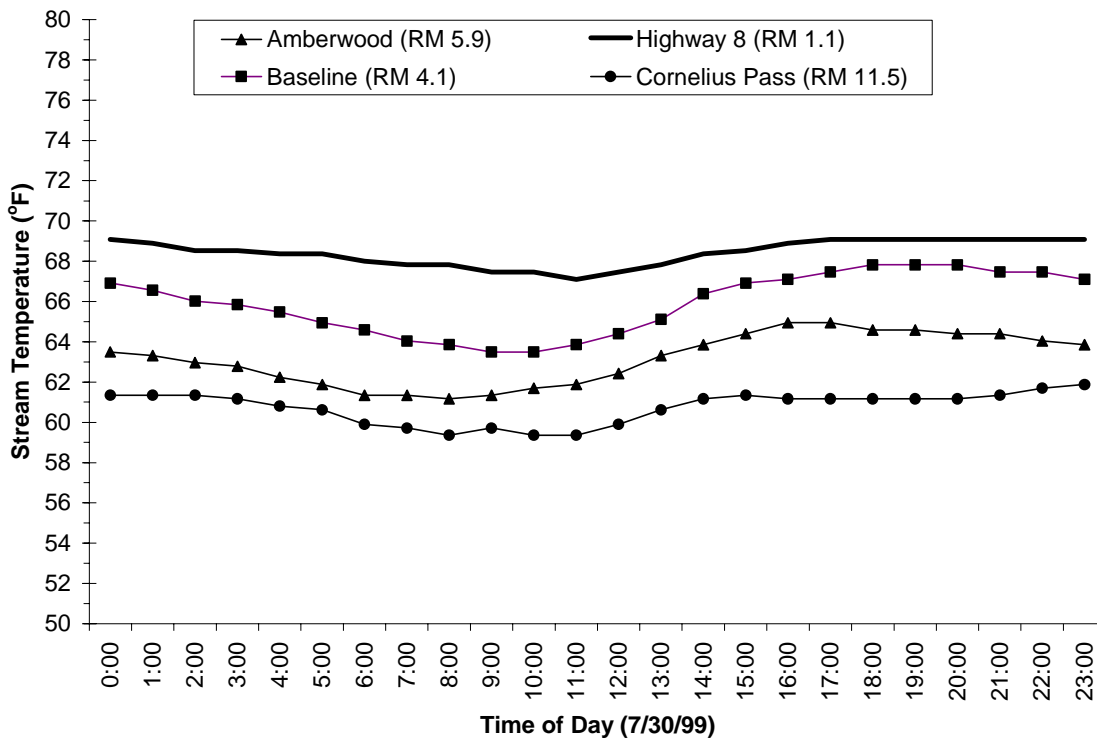
Figure A-150. Water discharge observed in Rock Creek on July 30, 1999.

Rock Creek (River Mile from mouth)

FLIR images were taken of Rock Creek on July 30, 1999. FLIR thermal imagery codes temperatures utilizing a Celsius temperature scale. Note that the 64°F correspond to a Celsius temperature of 17.8°C.

Image A-53. Rock Creek upstream of its confluence with the Tualatin River.
*[Rock Creek is visible in the thermal image and flows from the right to left in the image.]*[*]

---
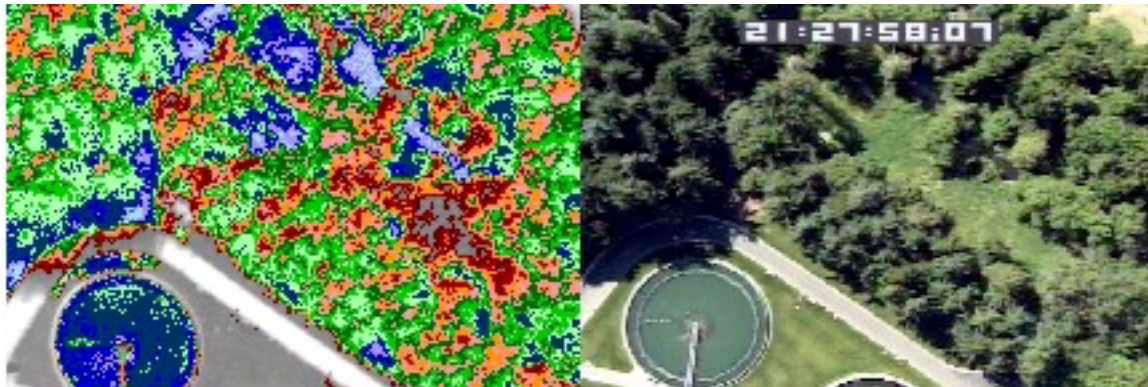
[*] **FLIR Image Temperature Scale (*C)**[*]

BEAVERTON CREEK* CURRENT CONDITION

The Oregon Department of Environmental Quality collected water quality data in Beaverton Creek during the summer of 1999. This effort included the collection of continuous hourly temperature data, FLIR temperature data, flow measurement, and site descriptions. Sampling locations are illustrated in **Figure A-151.** Digital photographs taken at several Beaverton Creek sampling locations are presented in **Image A-54** and **Image A-55**.

Figure A-151.   Water Quality Sampling locations for Beaverton Creek during the Summer of 1999.
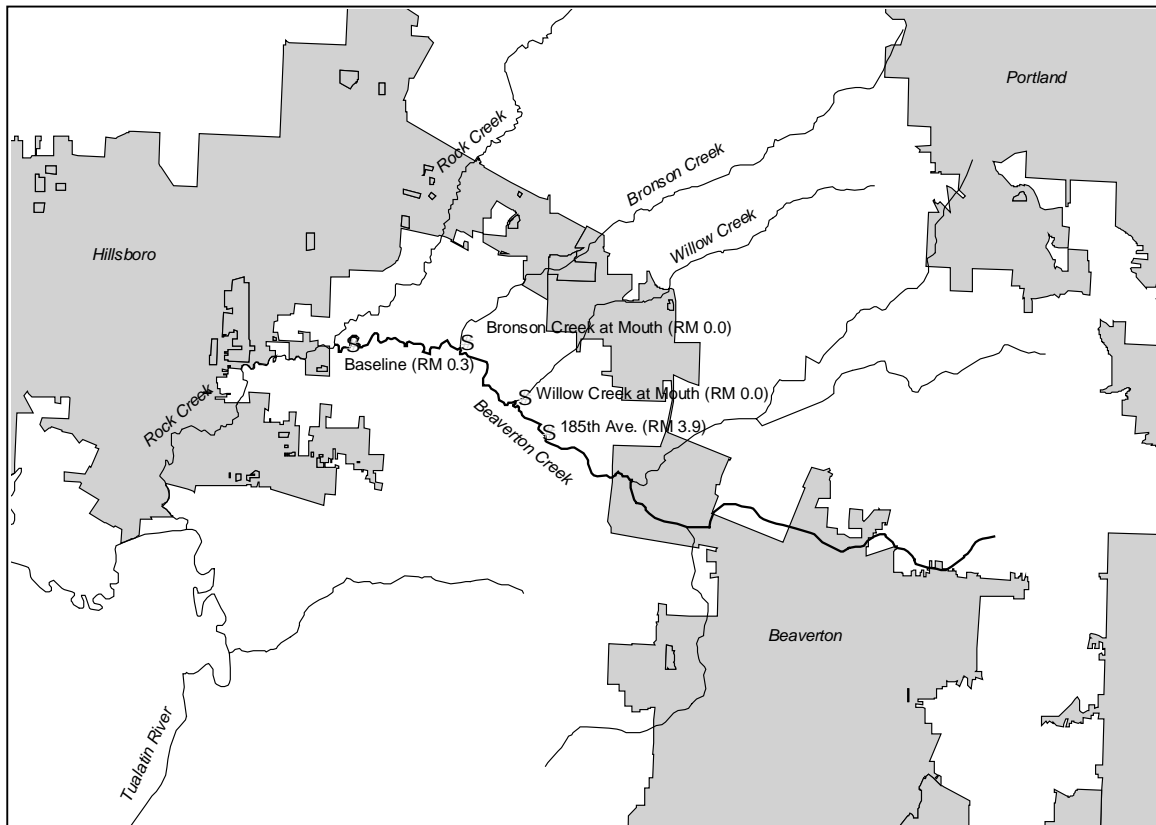
Water temperatures in Beaverton Creek increase during the summer period, with maximum temperatures occurring in late July. Accordingly, FLIR thermal imagery was collected for Beaverton Creek on July 30, 1999. In addition, flow measurements were also collected during this period. The longitudinal profile of the calculated 7-Day temperature statistics for Beaverton Creek, and some of its tributaries, are presented in **Figure A-153**. No observed portion of Beaverton Creek had 7-day temperature statistics recorded below the 64°F standard in 1999. Calculated 7-day temperature statistics for Beaverton Creek and tributaries in 1999 are presented in **Table A-26**.

---

* Note that the river miles (RM) presented in this report were derived from a 1:5000 stream coverage used for ODEQ modeling purposes and may differ slightly from other sources (such as OWRD or USGS river miles).

Image A-54. Beaverton Creek at Baseline Road (River Mile 0.3)
[Temp. Statistic – 71.4*F, Flow – 6.9 cfs, Potential Effective Shade (ES) – N/A, Measured ES – 87%]

Image A-55. Beaverton Creek at SW 185th Avenue (River Mile 3.9)
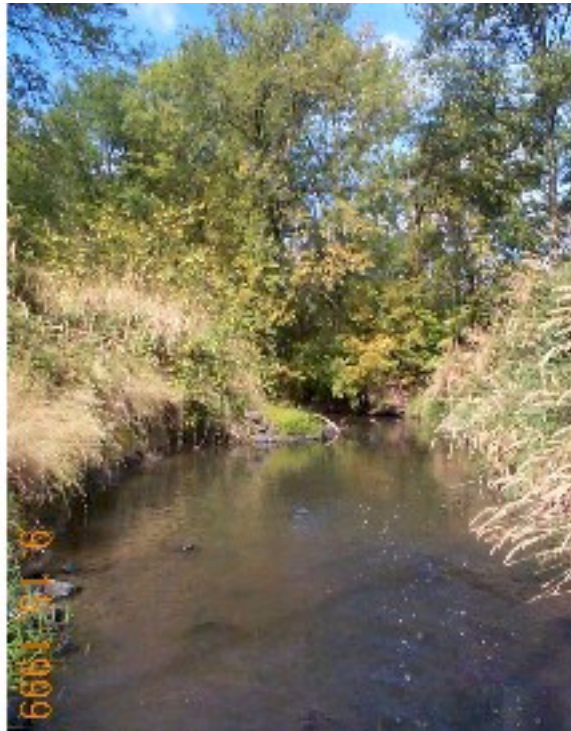[Temp. Statistic – 67.1*F, Flow – 5.9 cfs, Potential Effective Shade (ES) – 98%, Measured ES – 77%]

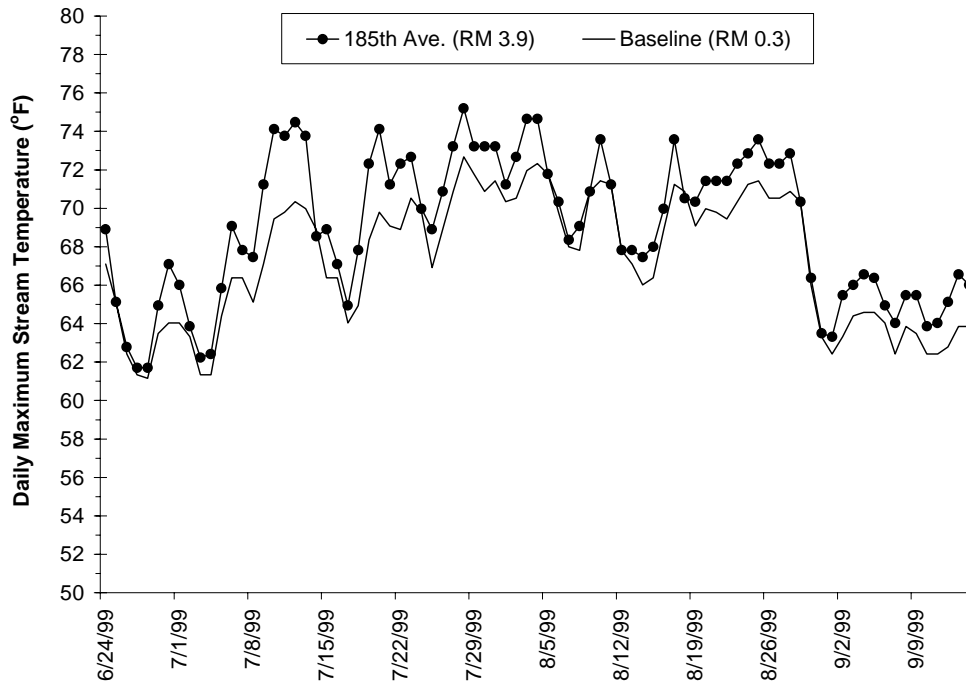**Figure A-152.** Observed daily maximum temperatures for Beaverton Creek in 1999.

Figure A-153. Observed 7-Day temperature Statistics for Beaverton Creek during 1999.
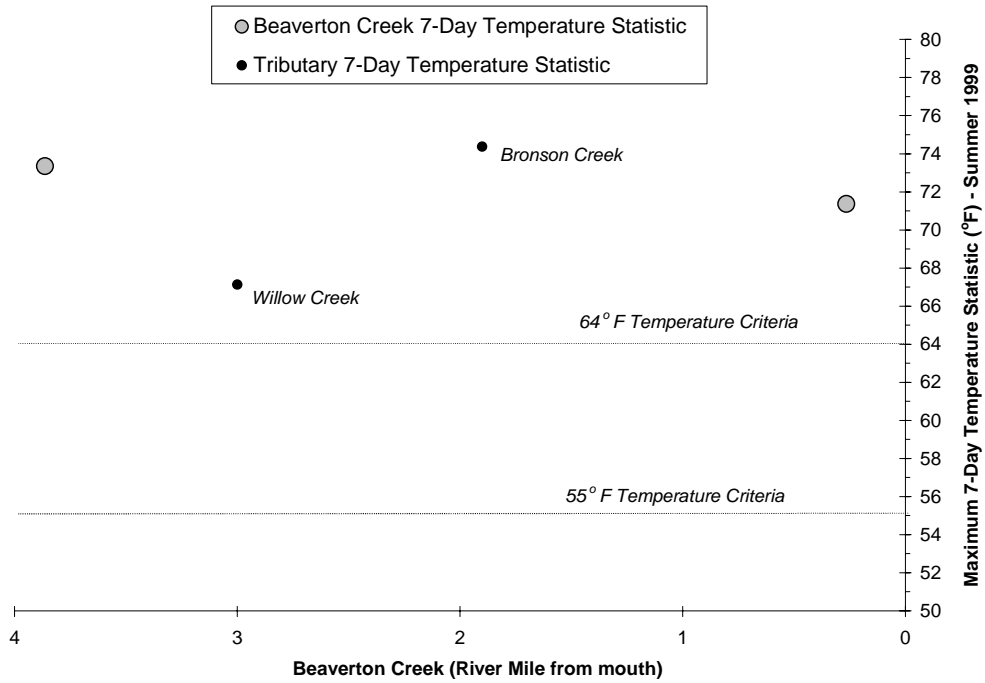
Table A-26. Calculated 7-Day Temperature Statistics for Beaverton Creek in 1999.

Temperature Site (RM = River Mile from mouth)	Start Date	End Date	Max Temp. (Date)	(°F)	7-Day Statistic (Date)	(°F)
Beaverton Creek at Baseline	5/19/99	9/14/99	7/28/99	72.7	7/31/99	71.4
Beaverton Creek at 185th	6/24/99	9/14/99	7/28/99	75.2	7/31/99	73.3
Bronson Creek at Mouth	6/24/99	9/14/99	7/12/99	76.8	7/12/99	74.0
Willow Creek at 185th	6/24/99	9/14/99	8/05/99	67.8	8/03/99	67.1

Water temperatures in Beaverton Creek varied through out the course of the day, with maximum temperatures occurring in the late afternoon and minimum temperatures occurring during the early morning hours. Diurnal temperature profiles for Beaverton Creek on July 30, 1999 are presented in **Figure A-154**. Relatively small diurnal variability was observed Beaverton Creek, which is typical of a deep, low gradient stream. Flows were measured in Beaverton Creek during the period of FLIR sampling, which also corresponds to the period of summer maximum water temperatures (**Figure A-155**). Beaverton Creek discharge was approximately 7 cubic feet per second near its mouth. As can be seen in this **Figure A-156**, observed flows in Beaverton Creek were much higher than levels observed in Willow Creek and Bronson Creek.

Figure A-154. Diurnal temperature trends observed in Beaverton Creek on July 30, 1999.
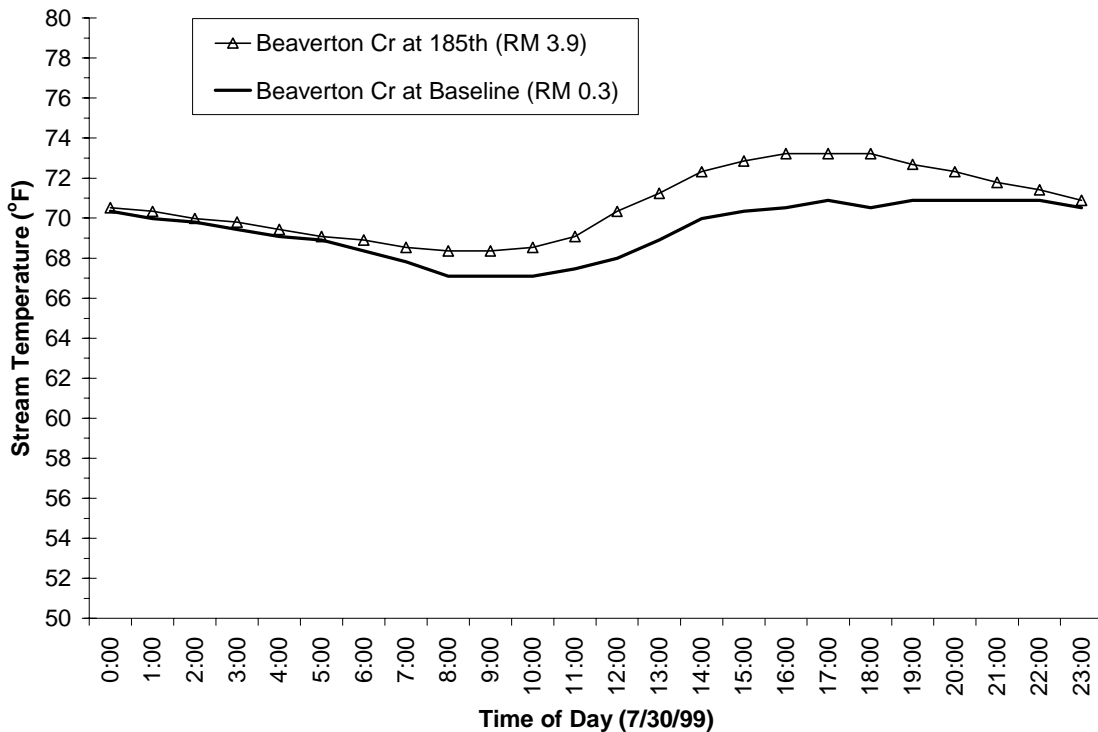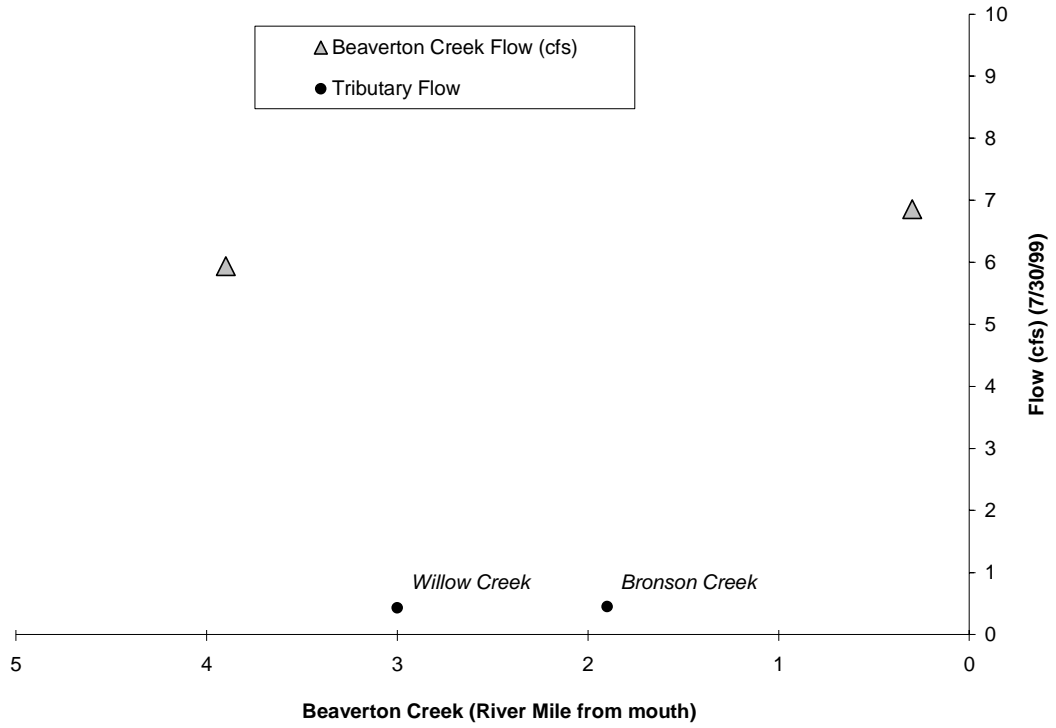
Figure A-155.   Water discharge observed in Beaverton Creek on July 30, 1999.

The following FLIR images were taken of Beaverton Creek on July 30, 1999. FLIR thermal imagery interprets temperatures utilizing a Celsius temperature scale. Note that the 64°F corresponds to 17.8^{o}C.

Image A-56. Beaverton Creek (RM 3.3) illustrating an area of potential thermal stratification. [*Stratification is evidenced by the change from an approximately 2°C rise and then drop in the surface temperature within this frame.*]
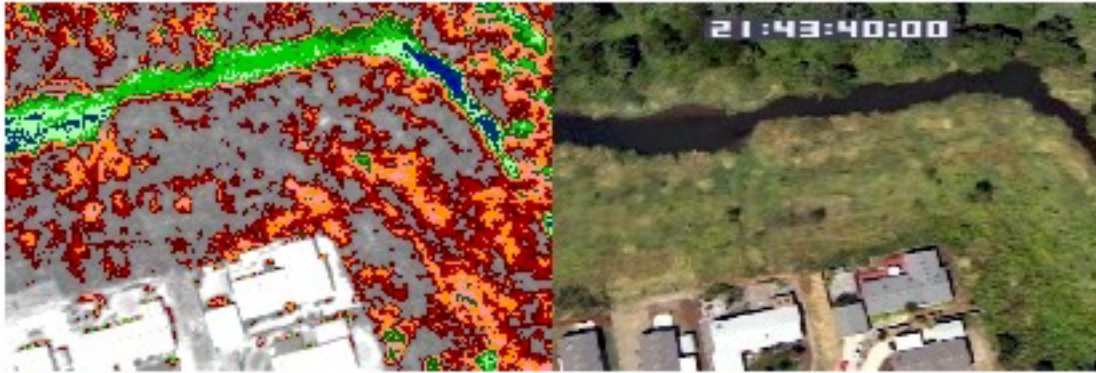
Image A-57. Beaverton Creek (RM 3.8) at SW 185th St Bridge near Aloha. [*The median surface water temperature at this location is 22.0^{o}C.*]
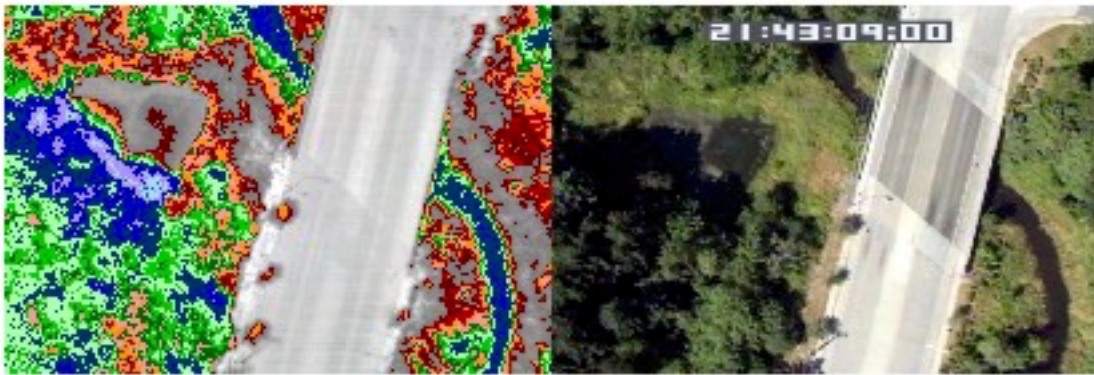
Image A-58. Beaverton Creek (RM 7.6) showing large off channel pond. [*The median surface water temperature in the creek at this location is 19.9^{o}C.*]

FLIR Image Temperature Scale (*C)[*]
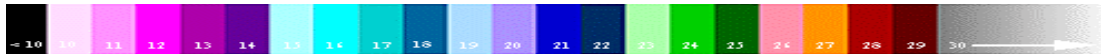
ROCK AND BEAVERTON CREEK MODEL INPUTS

Rock and Beaverton Creek were modeled contiguously, beginning approximately at river mile 4 on Beaverton Creek, and proceeding downstream to the confluence of Rock Creek and the Tualatin River.

This section graphically displays the model input data for each of the 100-foot model segments. Recall that this appendix also describes the various data sources and methodology used to assemble the model input.

- Elevation and Gradient (**Figure A-156**)

- Aspect (**Figure A-157**)

- Near Stream Disturbance Zone Widths and Wetted Widths (**Figure A-158**)

- Topographic Shade (**Figure A-159**)

- Vegetation Geometry (**Figure A-160**)

- Flow Volume (**Figure A-161**)

- Flow Velocity (**Figure A-162**)

- Water Column Depth (**Figure A-163**)

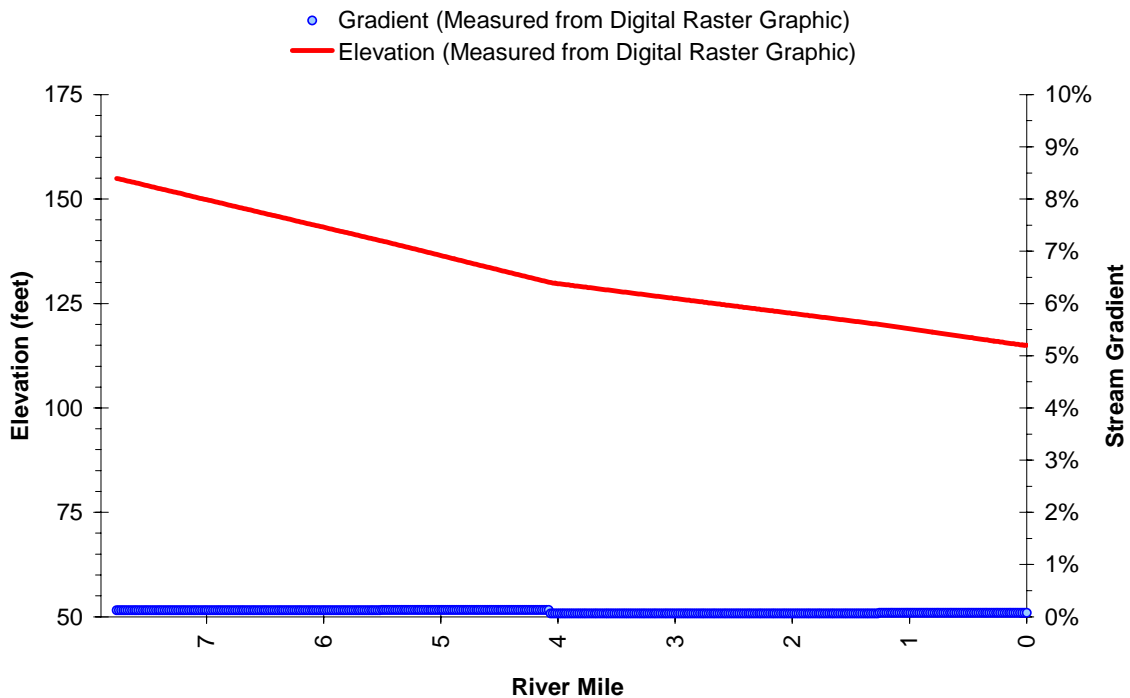**Figure A-156.** Rock and Beaverton Creek Elevation and Gradient at Each 100-foot Model Reach

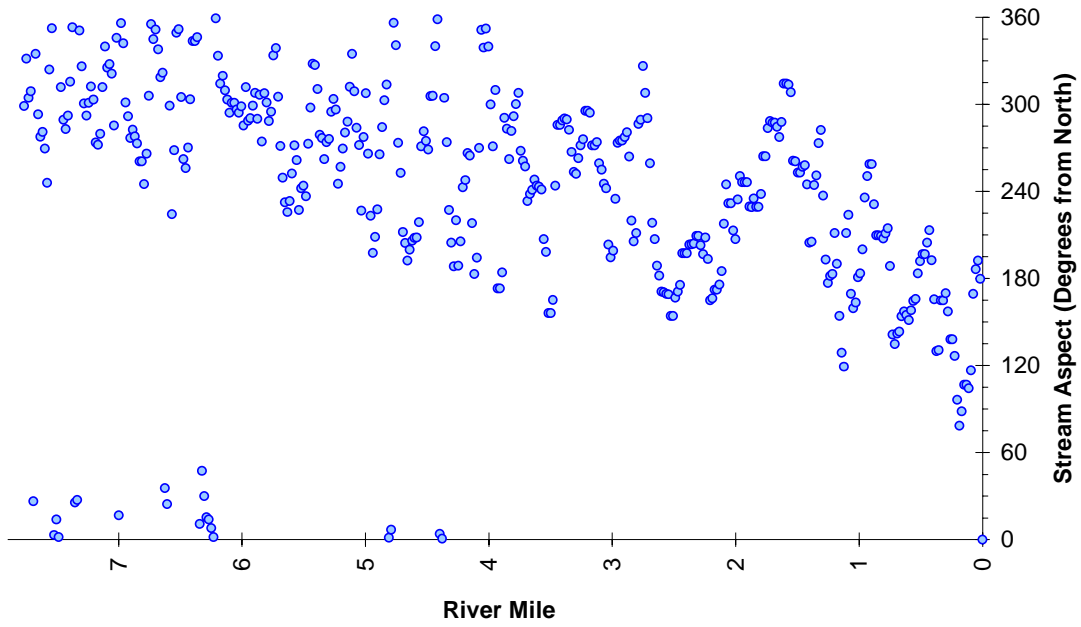**Figure A-157.** Rock and Beaverton Creek Aspect at Each 100-foot Model Reach

Figure A-158. Rock and Beaverton Creek Wetted Widths and NSDZ Widths.
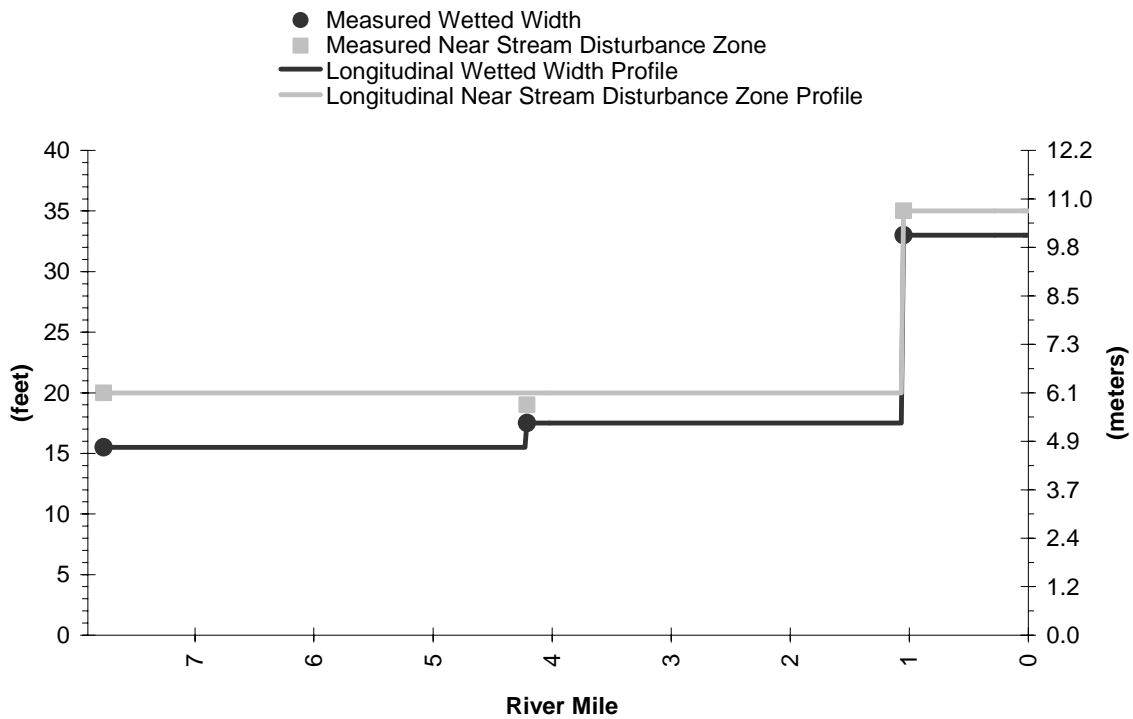
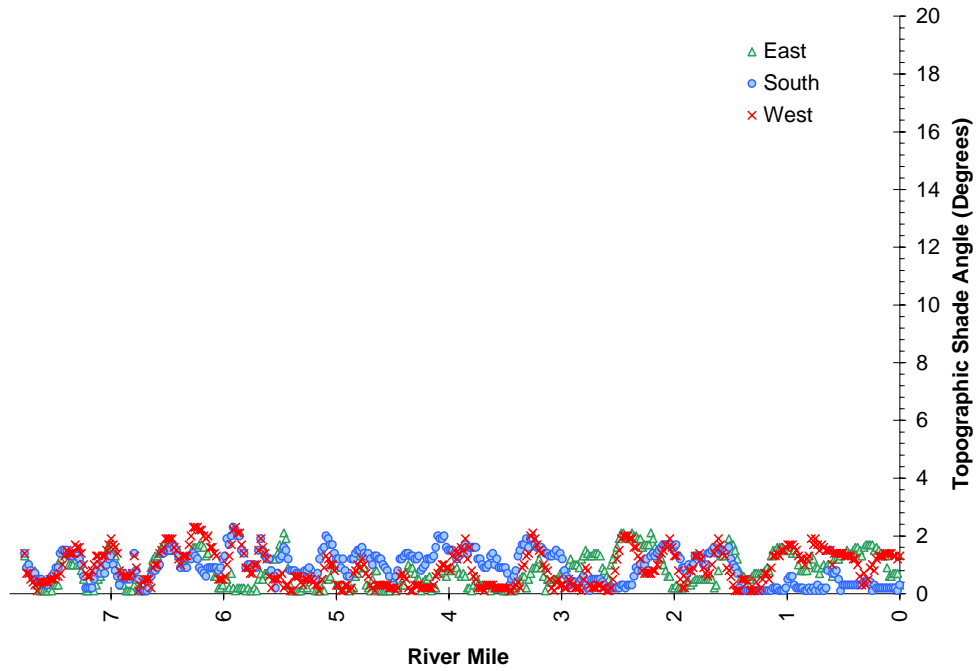**Figure A-159.** Rock and Beaverton Creek Topographic Shade at Each 100-foot Model Reach.

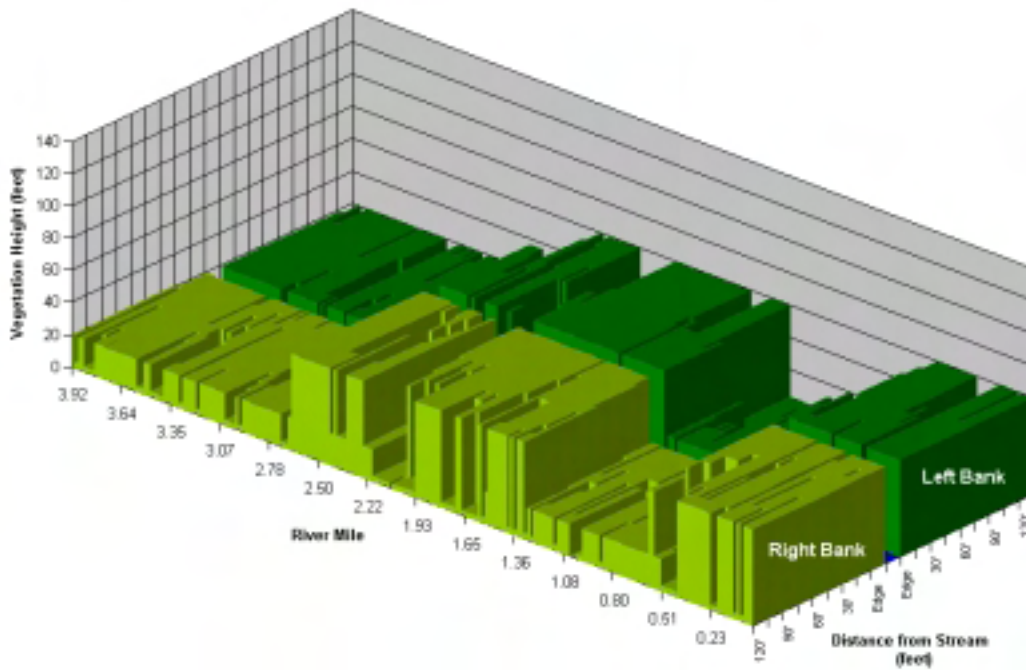**Figure A-160.** Rock Creek Current Vegetation Heights for Each 100-foot Model Reach.

Figure A-161. Beaverton Creek Current Vegetation Heights for Each 100-Foot Model Reach.
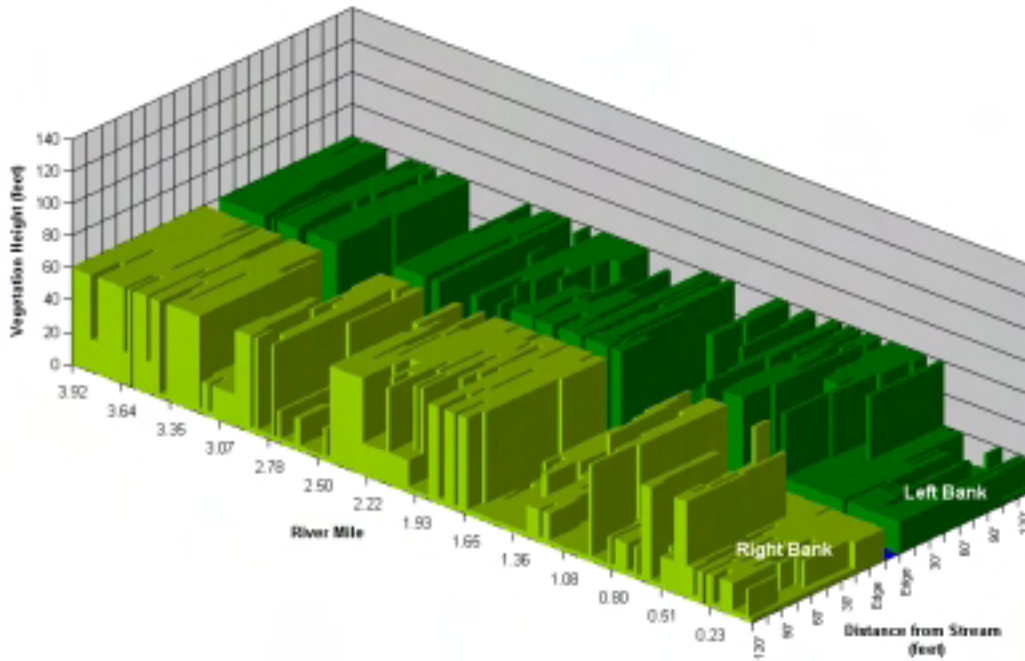

Figure A-162. Rock and Beaverton Creek Measured and Interpolated Flow Volume.
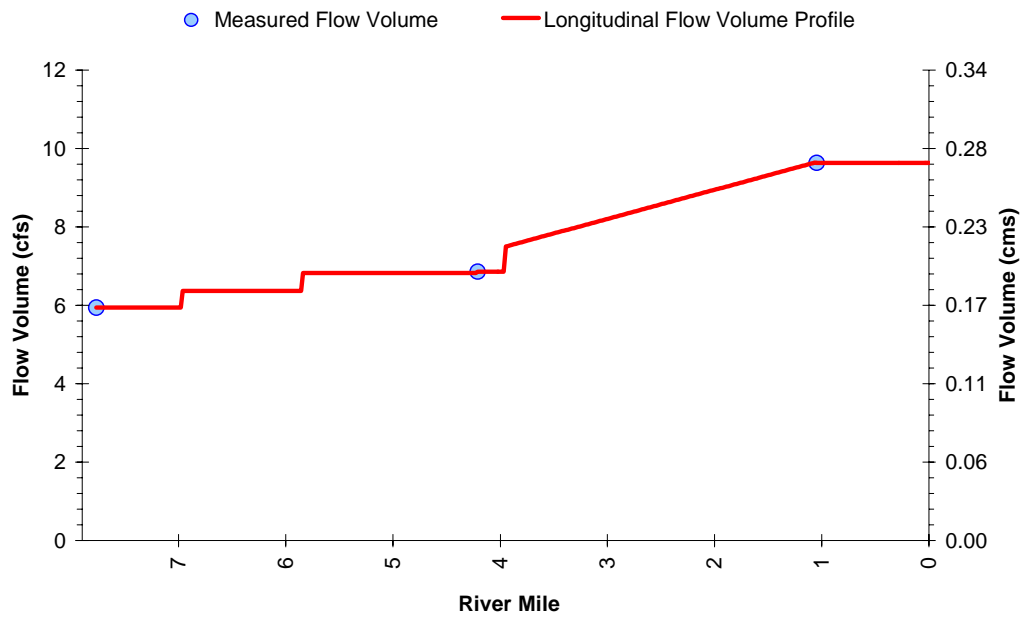
Figure A-163. Rock and Beaverton Creek Measured and Mannings Derived Longitudinal Flow Velocities.
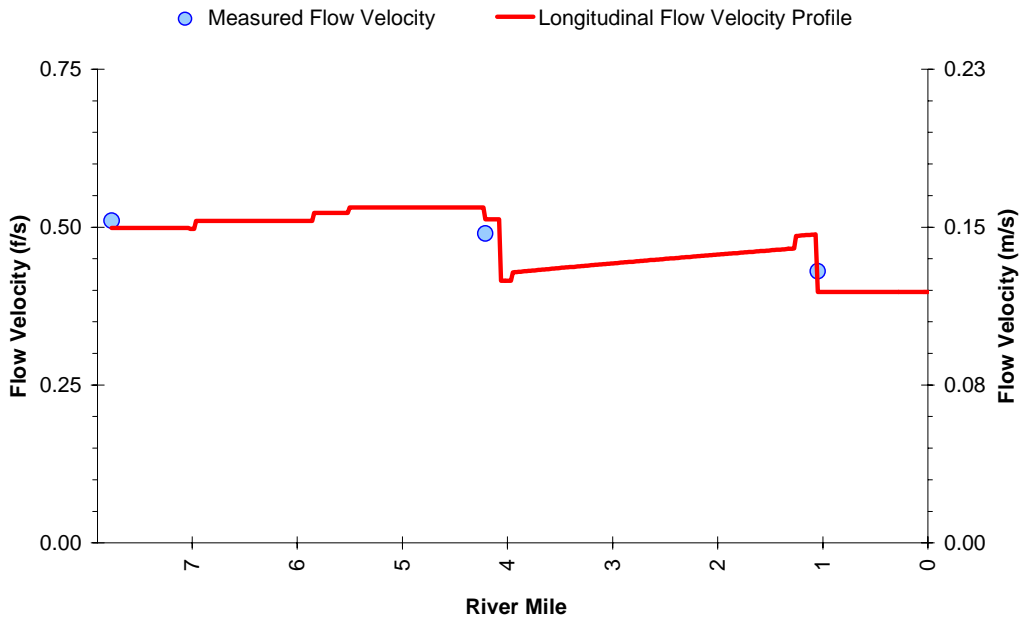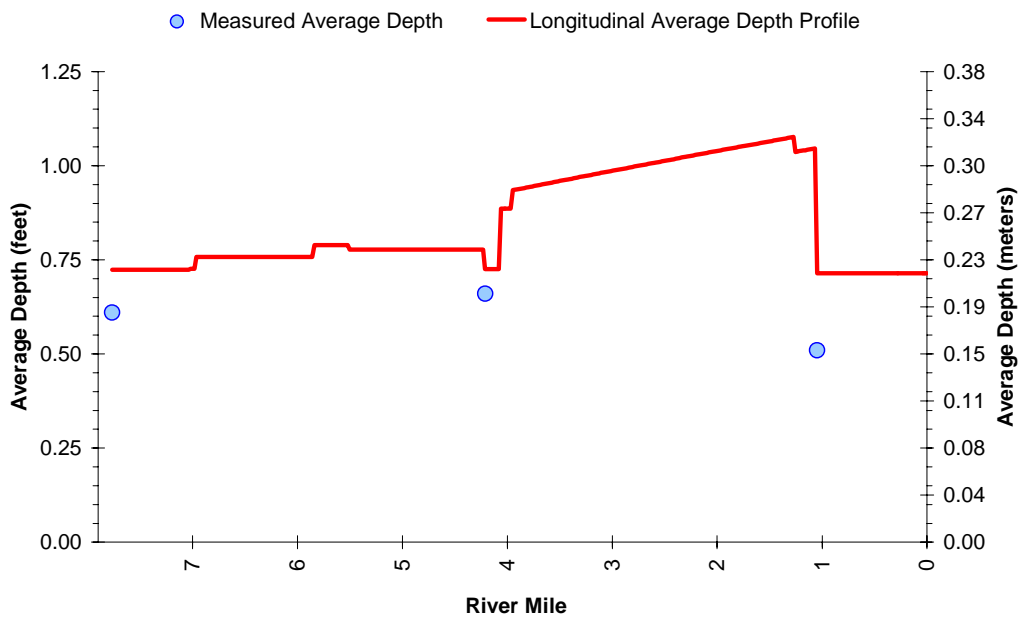

Figure A-164. Rock and Beaverton Creek Measured and Mannings Derived Longitudinal Water Column Depths.
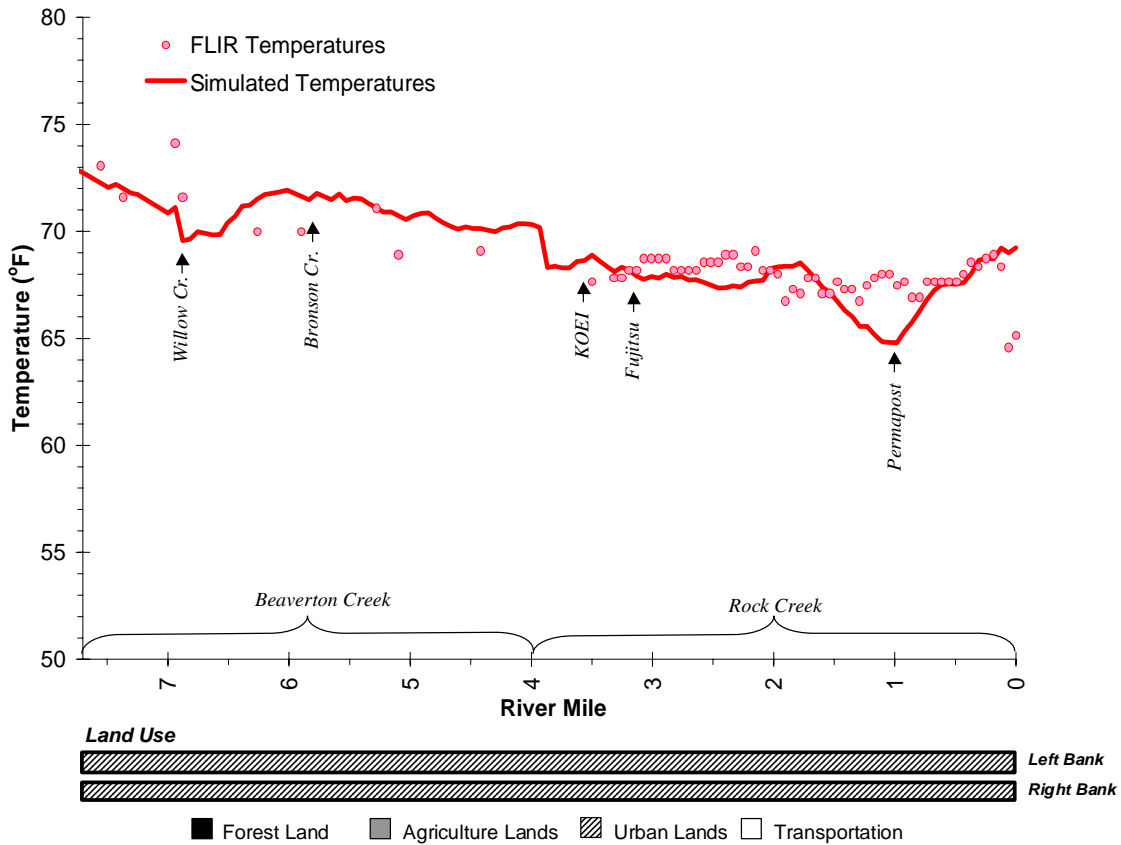
ROCK AND BEAVERTON CREEK MODEL RESULTS

This section presents temperature modeling results for Rock and Beaverton Creeks. Graphical and statistical validation of the calibrated Rock Creek/Beaverton Creek model are shown, in addition to temperature predictions for various scenarios. Recall that the model was calibrated with data collected on July 30, 1999 and thus is representative of critical stream temperature, stream flow, and climatic conditions. In other words, this modeling effort has captured the period when stream temperatures were near their peak. Spatial validation of the calibrated model is presented in **Figure A-165**. The solid line is the calibrated model temperature prediction at 3:00 PM on July 30, 1999 while the dots represent the FLIR-measured temperatures at that same time.

The standard error and average deviation for the spatial data calibration are:

$$Standard\ Error = 0.75^oC\ (1.35^oF)$$

$$Average\ Deviation = 0.11^oC\ (0.20^oF)$$

Figure A-165. Rock and Beaverton Creek Observed and Predicted Spatial Temperature Data.
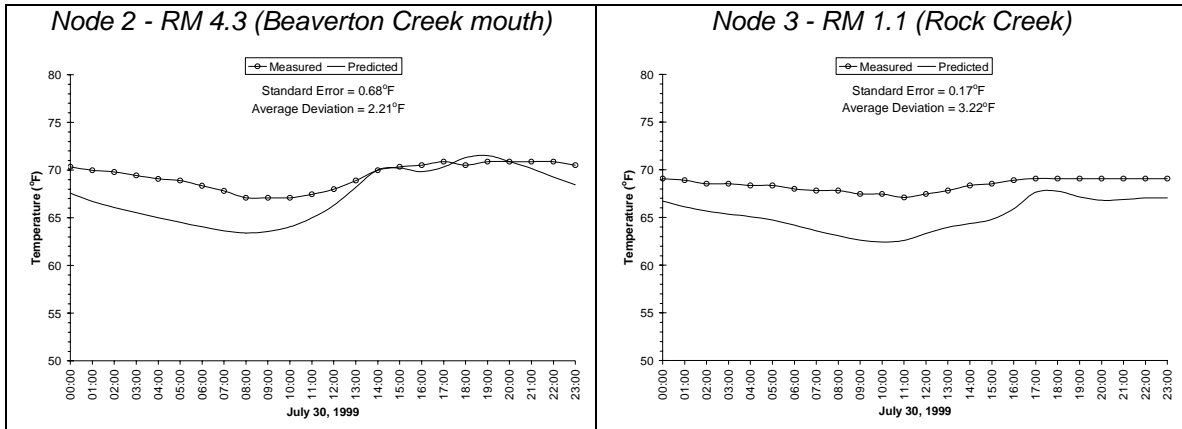
Observed and predicted hourly temperatures at two continuous temperature monitoring locations on Rock and Beaverton Creek are presented in **Figure A-166**. Node 1 is the upper boundary condition and remains constant, therefore it was not graphed. Standard errors and average deviations are presented for each node. The mean standard error and mean average deviation for the continuous data are:

$$Mean\ Standard\ Error = 0.23^{o}C\ (0.42^{o}F)$$

$$Mean\ Average\ Deviation = 1.51^{o}C\ (2.71^{o}F)$$

Figure A-166. Rock and Beaverton Creek Model Continuous Data Validation

Loading Capacity - 40 CFR 130.2(f)

Loading Capacity is based on the condition that meets the *no measurable surface water temperature increase resulting from anthropogenic activities*. This condition is termed *System Potential* and is achieved when (1) non-point source solar radiation loading reflects a riparian vegetation condition without human disturbance and (2) point source discharges cause no measurable increases in surface water temperatures.

Solar radiation loading was calculated using system potential riparian vegetation, at current channel and stream aspect conditions. A detailed description of potential vegetation conditions is presented in **Table A-8**. Current and System Potential solar loading for Rock Creek and Beaverton Creek are presented in **Figure A-48**. Solar radiation loading for Current Condition and System Potential condition is presented for every 100 meters of modeled stream length. As can be seen in **Figure A-48**, solar radiation loading at System Potential is much less than levels currently observed on Rock Creek and Beaverton Creek (i.e., Current Condition). Allowable point source heat loading at load capacity conditions are summarized below and described in detail in the main TMDL document.

Figure A-167. Rock Creek and Beaverton Creek Solar Radiation Load at System Potential and Current Conditions
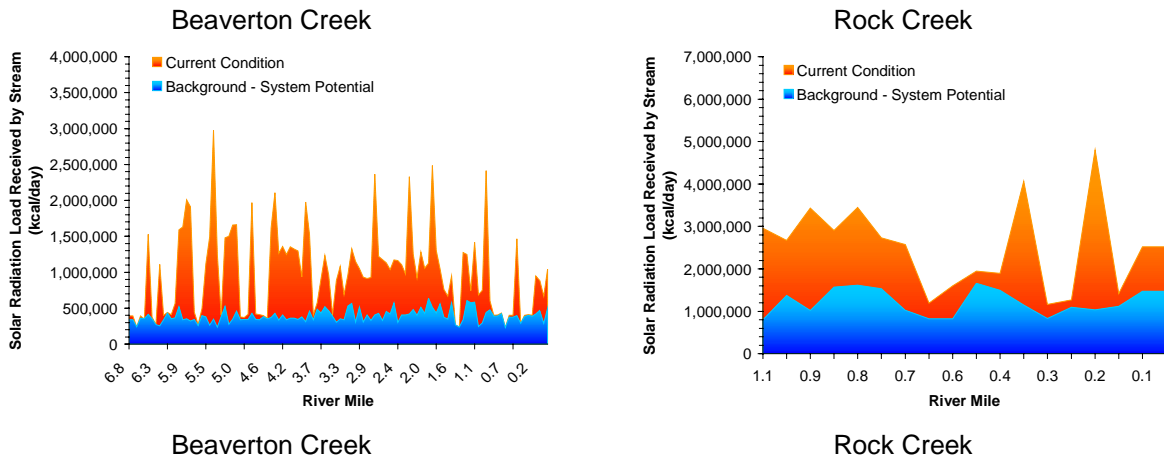
Beaverton Creek

Rock Creek

Allocations – 40 CFR 130.2(g) and 40 CFR 130.2(h)

*Load Allocations (Non-Point Sources) - The **temperature standard** targets system potential (i.e. no measurable temperature increases from anthropogenic sources). To meet this requirement the system potential solar radiation heat load (5.6·10^6 Kcal/day - Rock Creek, and Beaverton Creek – 8.8·10^6 Kcal/day) is allocated to background nonpoint sources. Anthropogenic nonpoint sources are not given a heat load.*

Wasteload Allocations (Point Sources) - Surface water discharges into receiving waters have been given a heat load based on the 0.25^{o}F allowable increase in the mixing zone as specified in the temperature standard. Heat loads have been converted to allowable effluent temperatures as well. It should be noted that the wasteload allocation is the point source heat load and not the calculated maximum effluent temperatures. There are several options for meeting the allocated heat loads (i.e. passive effluent temperature reductions, changes in facility discharge operation, purchasing instream flows, pollutant trading, etc.).

Temperature Allocation Summary Non-Point Sources	
Rock Creek	
Source	*Loading Allocation* *Allowable Nonpoint Source Solar Radiation Heat Load* *(kcal/day)*
Natural	6.5·10^7 Kcal/day
Agriculture	$\varnothing$
Forestry	$\varnothing$
Urban	$\varnothing$
Future Sources	$\varnothing$
Beaverton Creek	
Source	*Loading Allocation* *Allowable Nonpoint Source Solar Radiation Heat Load* *(kcal/day)*
Natural	8.8·10^6 Kcal/day
Agriculture	$\varnothing$
Forestry	$\varnothing$
Urban	$\varnothing$
Future Sources	$\varnothing$

Point Sources - Allowable Point Source Effluent Source Heat Loading						
		Q_R	Q_{PS}	T_{PS}	Max T_P	H_{PS}	H_{WLA}
Facility Name	Rec. Water	Receiving Water 7Q10 Low Flow (cfs)	Facility Design Flow (cfs)	Point Source Effluent Temp. (°F)	Max Daily Site Potential River Temp. (°F)	Current Point Source Heat Loading on River (kcal/day)	Allowable Point Source Heat Loading in Zone of Dilution (kcal/day)
Permapost	Rock Cr. RM - 1.0	4.10	0.11	70.0	60.5	$1.7 \cdot 10^6$	$3.5 \cdot 10^5$
Fujitsu	Rock Cr. RM - 3.2	4.10	0.04	76.0	61.0	$9.8 \cdot 10^5$	$3.5 \cdot 10^5$
KOEI	Rock Cr. RM - 3.6	4.10	0.01	88.0	61.1	$3.7 \cdot 10^5$	$3.5 \cdot 10^5$
Epson	Rock Cr. RM - 7.0	1.02*	0.00	90.0	61.1	$8.2 \cdot 10^4$	$8.2 \cdot 10^4$
Tektronics	Beaverton Cr. RM - 6.7	2.08*	0.02	78.0	61.1	$6.0 \cdot 10^5$	$1.5 \cdot 10^5$
Maxim	Beaverton Cr. RM - 7.0	2.08*	0.03	71.0	61.1	$5.1 \cdot 10^5$	$1.3 \cdot 10^5$

Surrogate Measures – 40 CFR 130.2(I)

The solar radiation load (Kcal/day) at system potential condition was calculated by multiplying the stream surface area by the solar radiation flux (ly/day). Percent effective shade was used as a surrogate measure of the solar radiation flux calculated at system potential conditions (**Figure A-49**). The individual points in the figure represent the current and allocated conditions for every 100 meters. Accordingly, System Potential heat load condition along Rock and Beaverton Creeks translates into approximately 85% or greater effective shade throughout much of the system.

**Figure A-168.** Rock and Beaverton Creek Surrogate Measure for Non Point Sources - Effective Shade.

---
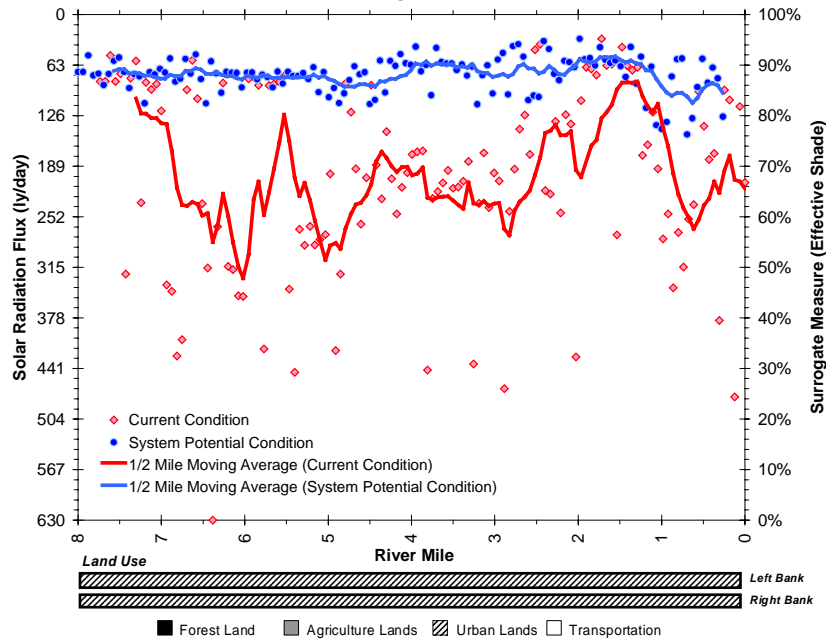
* 7Q10 flows are calculated at nearest stream gage.

Water Quality Standard Attainment Analysis – CWA §303(d)(1)

Figure A-169 illustrates predicted Rock Creek/Beaverton Creek temperatures at 5:00 PM on July 30, 1999 with the following scenarios: 1) non-point sources at Load Allocations and point source discharges at current levels, and 2) non-point source at Load Allocation and point source discharges removed. Predicted temperatures in Rock Creek/Beaverton Creek are relatively similar at both Load Allocation scenarios. Point source discharge at current levels only slightly raise stream temperatures under the Loading Allocation.

Figure A-169. Rock Creek/Beaverton Creek Longitudinal Temperature Profile - Model Output – 1) Non-Point Source Load Allocation and Current Point Source Discharge, and 2) Non-Point Source Load Allocation and Remove Point Source Discharge – 5:00 PM July 30, 1999.
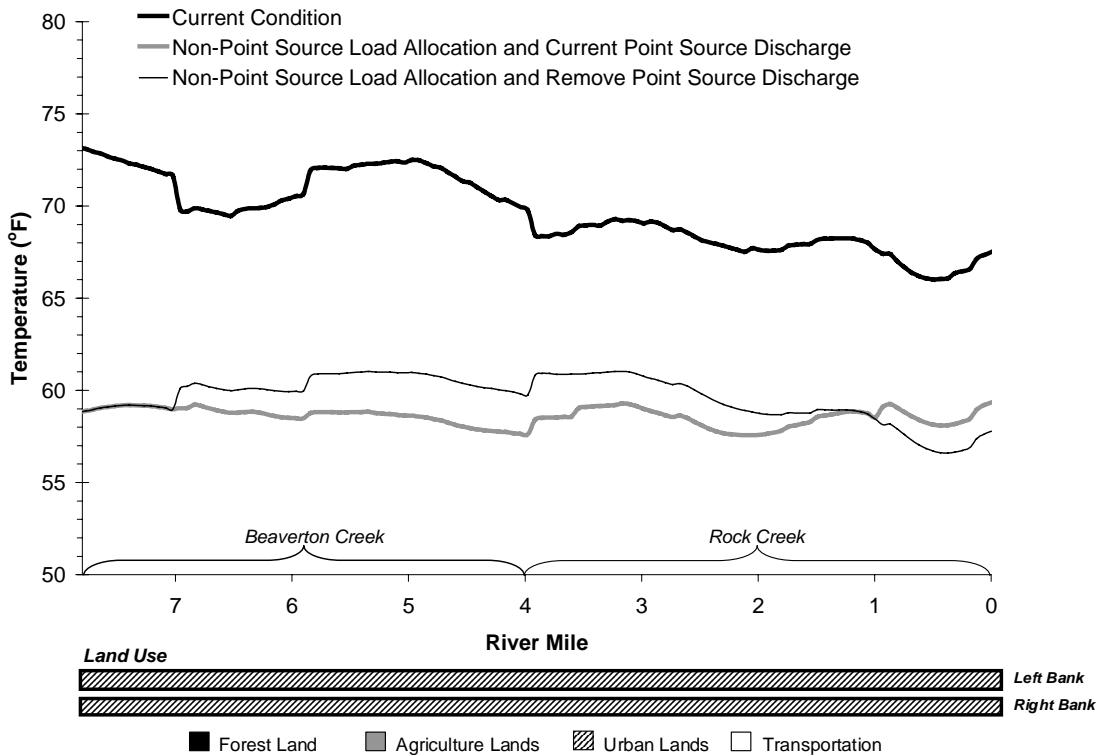
Two scenarios were run in which non-point sources were maintained at current conditions and point source discharge conditions were modified. **Figure 207** displays predicted Rock Creek/Beaverton Creek temperatures at 5:00 PM on July 30, 1999 with the following scenarios: 1) non-point sources at Current Conditions and point source discharges removed; and 2) non-point sources at Current Conditions and point sources at Waste Load Allocations. As can be seen in **Figure A-170**, the general temperature profiles were similar between these scenarios and Current Conditions; however, effects downstream of the point sources can be observed.

As mentioned above, **System Potential** is achieved when (1) non-point source solar radiation loading reflects a riparian vegetation condition without human disturbance and (2) point source discharges cause no measurable increase in surface water temperature. Accordingly, **Figure A-171** presents predicted Rock Creek/Beaverton Creek temperatures at a Waste Load Allocation and Load Allocation scenario. **Figure A-172** illustrates that implementing Waste Load Allocations and Load Allocations will drastically reduce temperatures in Rock Creek/Beaverton Creek.

Figure A-170. Rock Creek/Beaverton Creek Longitudinal Temperature Profile - Model Output – 1) Non-Point Source Current Condition and Remove Point Source Discharge, and 2) Non-Point Source Current Condition and Point Source Waste Load Allocation – 5:00 PM July 30, 1999.
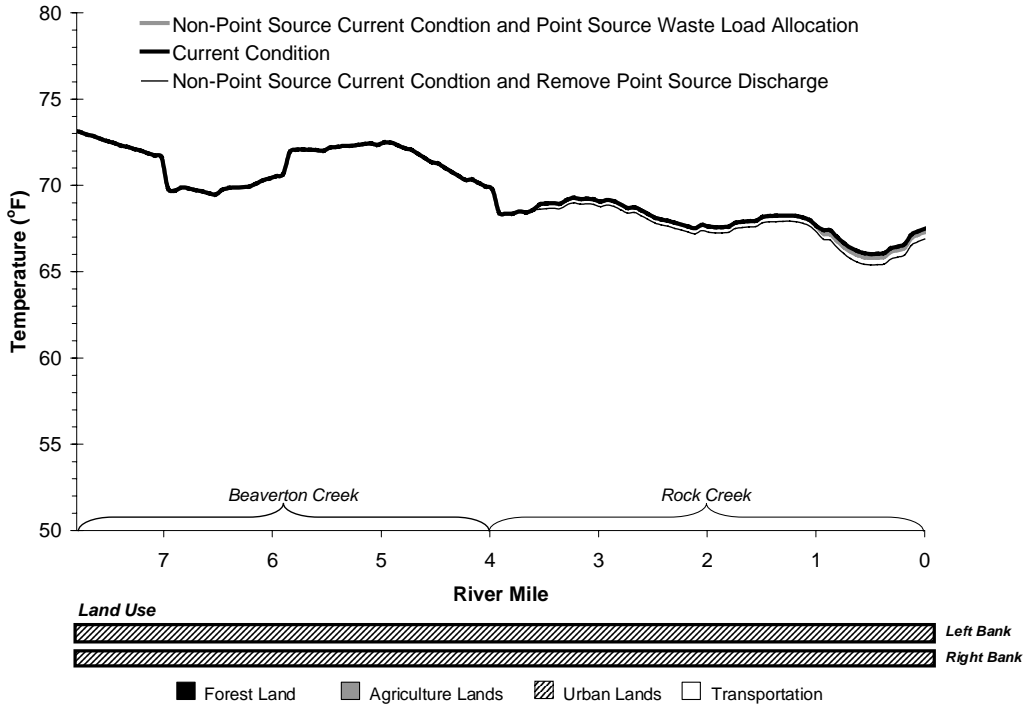

Figure A-171. Rock Creek/Beaverton Creek Daily Temperature Range for Current Conditions Compared with Allocated Measures - July 30, 1999.
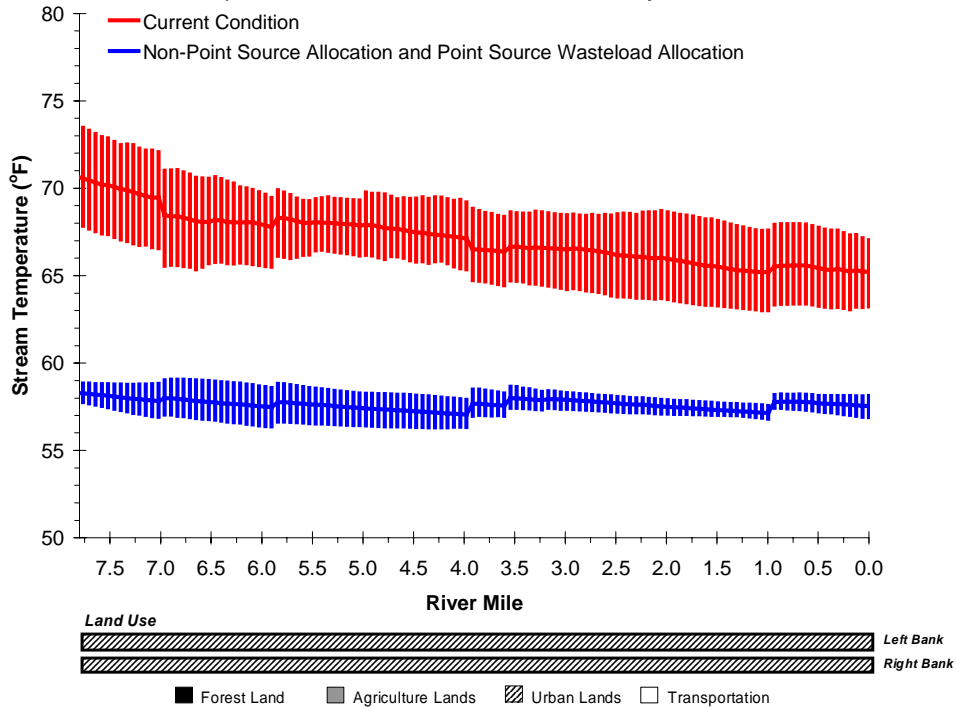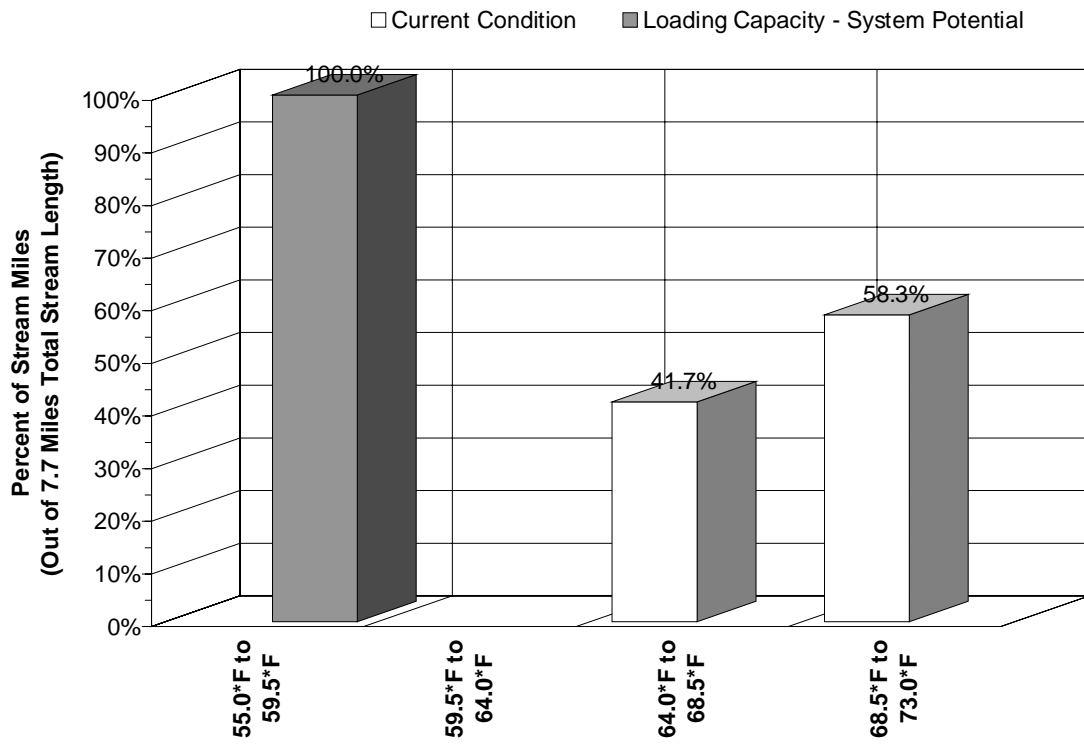
Figure A-172. Rock Creek/Beaverton Creek Current and Site Potential (Allocated) Temperature Distributions.
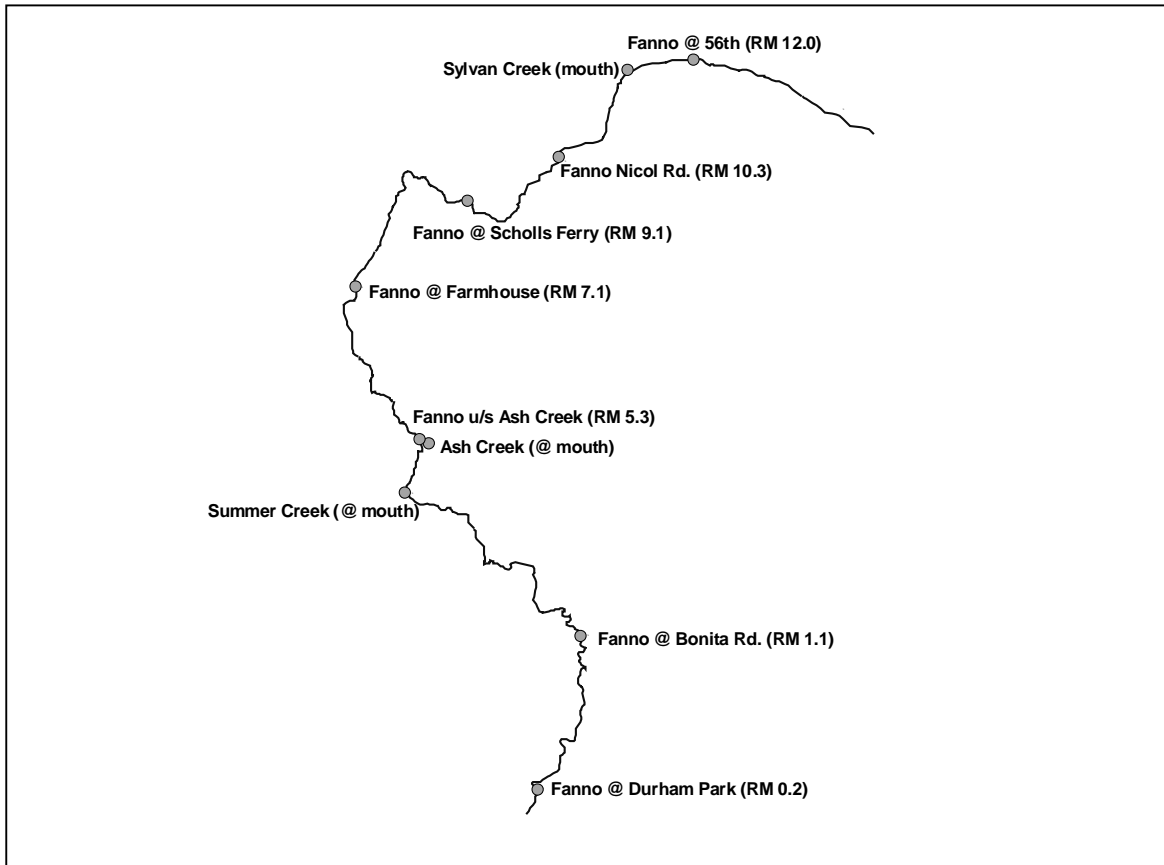
FANNO CREEK

FANNO CREEK* CURRENT CONDITIONS

The Oregon Department of Environmental Quality collected water quality data in Fanno Creek during the summer of 1999. This effort included the collection of continuous temperature data, FLIR temperature data, flow measurement and site descriptions. Sampling locations are illustrated in **Figure A-173**. Digital photographs taken at several Fanno Creek sampling locations are presented in **Image A-59** through **Image A-62**.

Figure A-173. Water Quality Sampling locations for Fanno Creek during the Summer of 1999.

It was determined that water temperatures in Fanno Creek increases during the summer period, with maximum temperatures occurring in late July. Accordingly, FLIR thermal imagery was collected for Fanno Creek on July 29, 1999. It is important to note that flow measurements were also collected during this period. The longitudinal profile of the calculated 7-Day temperature Statistics for Fanno Creek, and several of its tributaries, are presented in **Figure A-175**. No reaches of Fanno Creek were below the 64°F temperature criteria. Observed tributary temperature for Ash and Summer Creek were similar to mainstem temperatures; however, observed Sylvan temperature were well above Fanno Creek temperatures. Calculated water temperature statistics for Fanno Creek and its tributaries in 1999 are presented in **Table A-27**.

---

* Note that the river miles (RM) presented in this report were derived from a 1:5000 stream coverage used for ODEQ modeling purposes and may differ slightly from other sources (such as OWRD or USGS river miles).

Image A-59.   Fanno Creek at Bonita Road.
[Temp. Statistic – 70.0*F, Flow – 4.2 cfs, Potential Effective Shade (ES) – 85%, Measured ES – 26%]

Image A-60.   Fanno Creek upstream of Ash Creek.
[Temp. Statistic – 73.5*F, Flow – 1.2 cfs, Potential Effective Shade (ES) – 90%, Measured ES – XX%]

Image A-61.   Fanno Creek at Nicol Road.

[Temp. Statistic – 68.2*F, Flow – 0.8 cfs, Potential Effective Shade (ES) – 99%, Measured ES – 91%]

Image A-62.   Fanno Creek at 56th Street (Headwaters).

[Temp. Statistic – 66.7*F, Flow – 0.2 cfs, Potential Effective Shade (ES) – 99%, Measured ES – 87%]

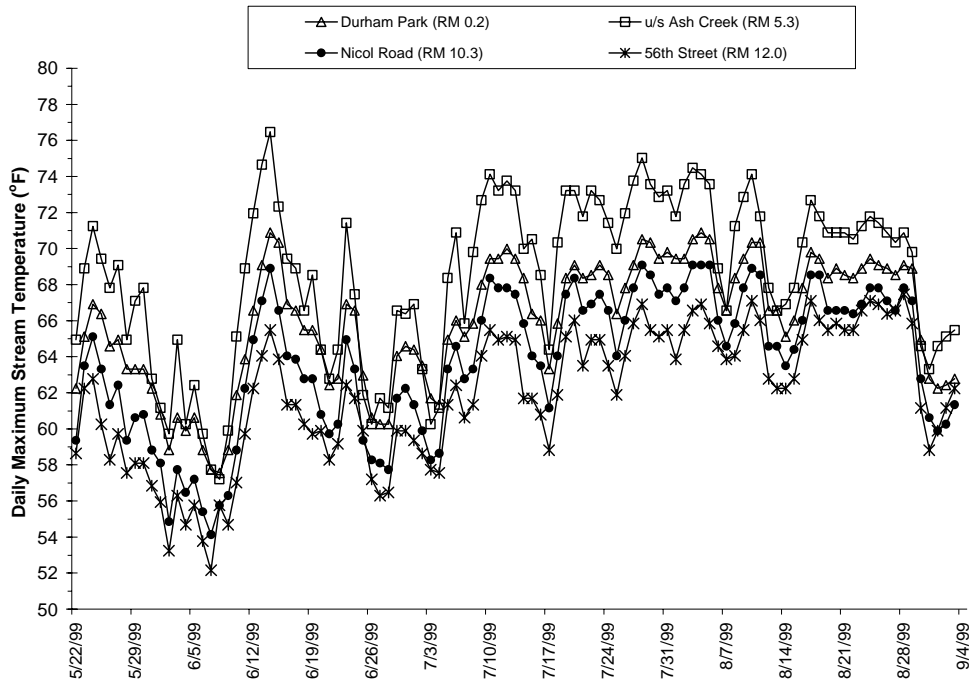**Figure A-174.** Observed daily maximum temperatures for Fanno Creek in 1999.

Figure A-175. Observed 7-Day temperature Statistics for Fanno Creek during the summer of 1999.
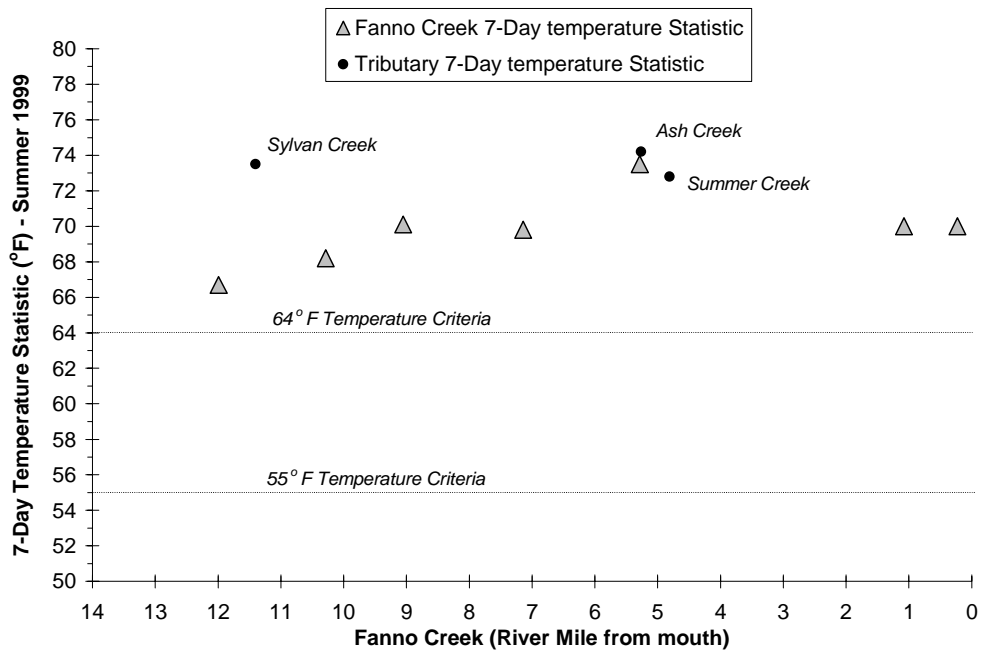
Temperature Site (RM = River Mile from mouth)	Start Date	End Date	Max Temp. (Date)	(°F)	7-Day Statistic (Date)	(°F)
Table A-27. Calculated Water Temperature Statistics for Fanno Creek and tributaries in 1999.						
Fanno Creek						
RM 0.2 (@ Durham Park)	05/15/99	09/06/99	8/04	70.9	8/02	**70.0**
RM 1.1 (@ Bonita Rd)	05/15/99	09/06/99	8/04	70.9	8/02	**70.0**
RM 5.3 (u/s Ash Creek)	05/15/99	09/06/99	6/14	76.5	7/31	**73.5**
RM 7.1 (@ Fanno Farmhouse)	05/19/99	09/06/99	7/28	71.8	7/31	**69.8**
RM 9.1 (@ Scholls Ferry Rd)	05/19/99	09/06/99	7/10	71.4	8/02	**70.1**
RM 10.3 (@ Nicol Road)	05/19/99	09/06/99	8/05	69.1	8/02	**68.2**
RM 12.0 (@ 56th Street)	05/19/99	09/06/99	8/28	67.5	8/26	**66.7**
Fanno Creek Tributaries						
(RM 4.8) Summer Creek @ Mouth	05/15/99	09/06/99	7/31	73.6	7/31	**72.8**
(RM 5.3) Ash Creek @ Mouth	07/27/99	09/06/99	7/28	76.8	7/31	**74.2**
(RM 11.4) Sylvan Creek @ Mouth	05/19/99	09/06/99	6/14	78.6	7/30	**73.5**

Water temperatures in Fanno Creek varied through out the course of the day, with maximum temperatures occurring in the late afternoon and minimums temperature occurring during the early morning hours. The diurnal temperature profile for Fanno Creek on July 29, 1999 is presented in **Figure A-176**. Very little diurnal variability was observed within the upper portion of the basin; however, variability increased dramatically at downstream sites. The greatest diurnal variability was measured at the site located upstream of Ash Creek (River Mile 5.3). It is important to highlight once again that maximum observed water temperatures were observed at this location in Fanno Creek (see **Figure A-175**). Diurnal variability decreased dramatically downstream of this location; however, temperature remain elevated above the standard throughout the course the day. This indicates that the hydrological conditions within these lower reaches are different than upstream conditions.

River discharge was measured throughout the Fanno Creek River system during the period of FLIR sampling, which corresponds to the period of summer maximum water temperatures. Water discharge rates generally increase in a downstream direction, reaching a maximum value of 15.5 cfs in Fanno Creek at Durham Park. Measured flows in Summer Creek, a tributary of Fanno Creek, on this day were similar than mainstem levels. In addition, Ash Creek and Sylvan Creek both had measured flows comparable to Fanno Creek levels.

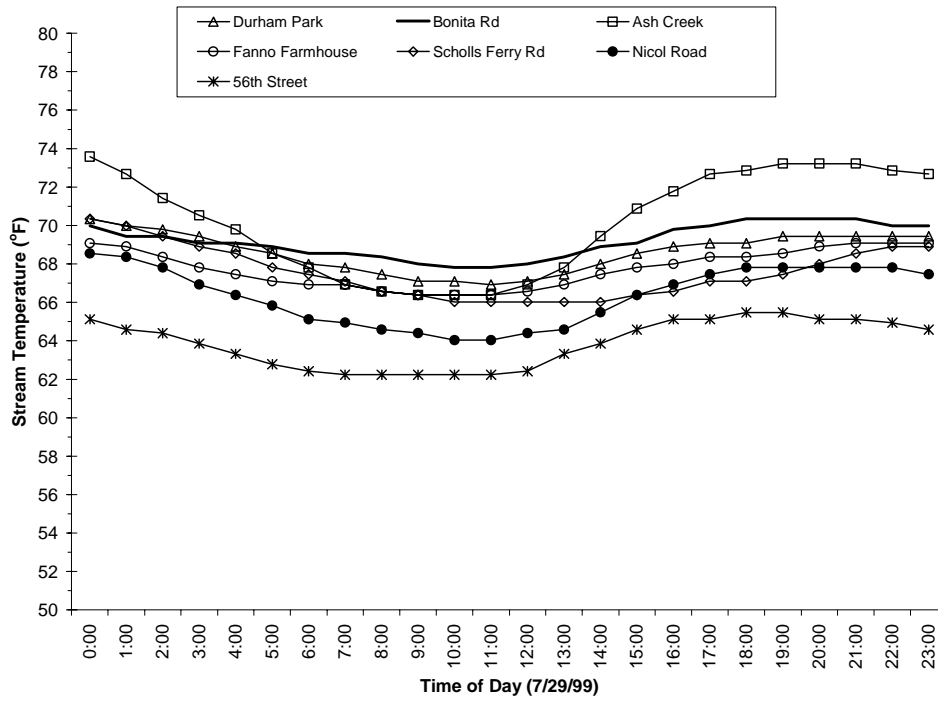**Figure A-176.**   Diurnal temperature trends observed in Fanno Creek on July 29, 1999.

Figure A-177.   Water discharge observed in Fanno Creek on July 29, 1999.
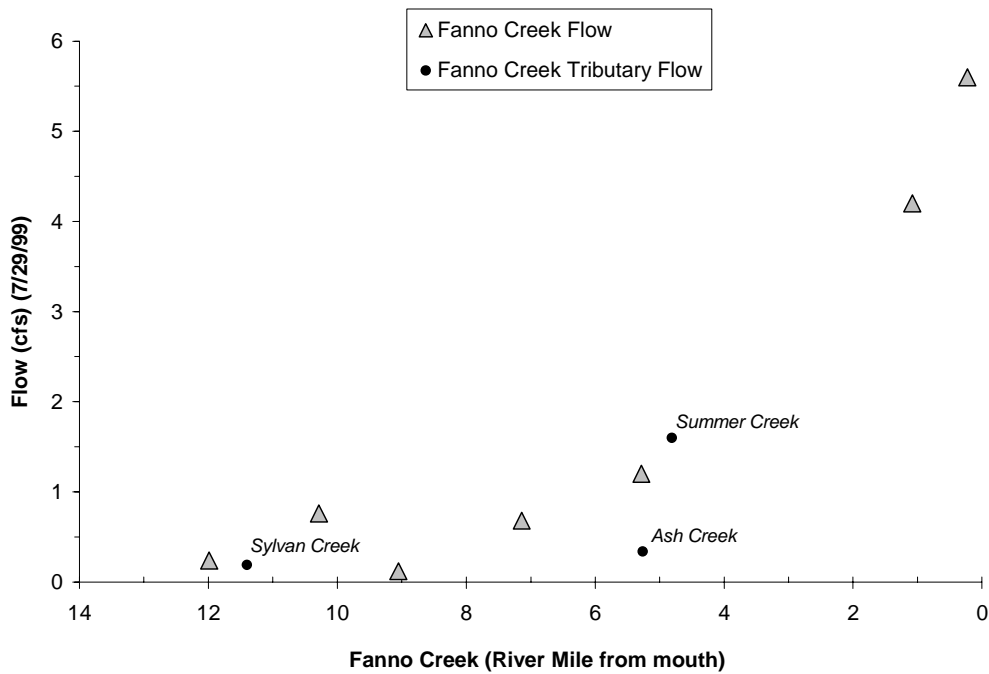
Figure A-178 presents the measured FLIR temperature profile for Fanno Creek, which was sampled on July 29, 1999 between 2:28 to 2:54 PM. As can be seen in this image, all areas of Fanno Creek were above the 64°F criteria during the period of FLIR sampling. **Table A-28** shows that most of Fanno Creek was between 64°F and 73°F in the late afternoon on July 29, 1999.

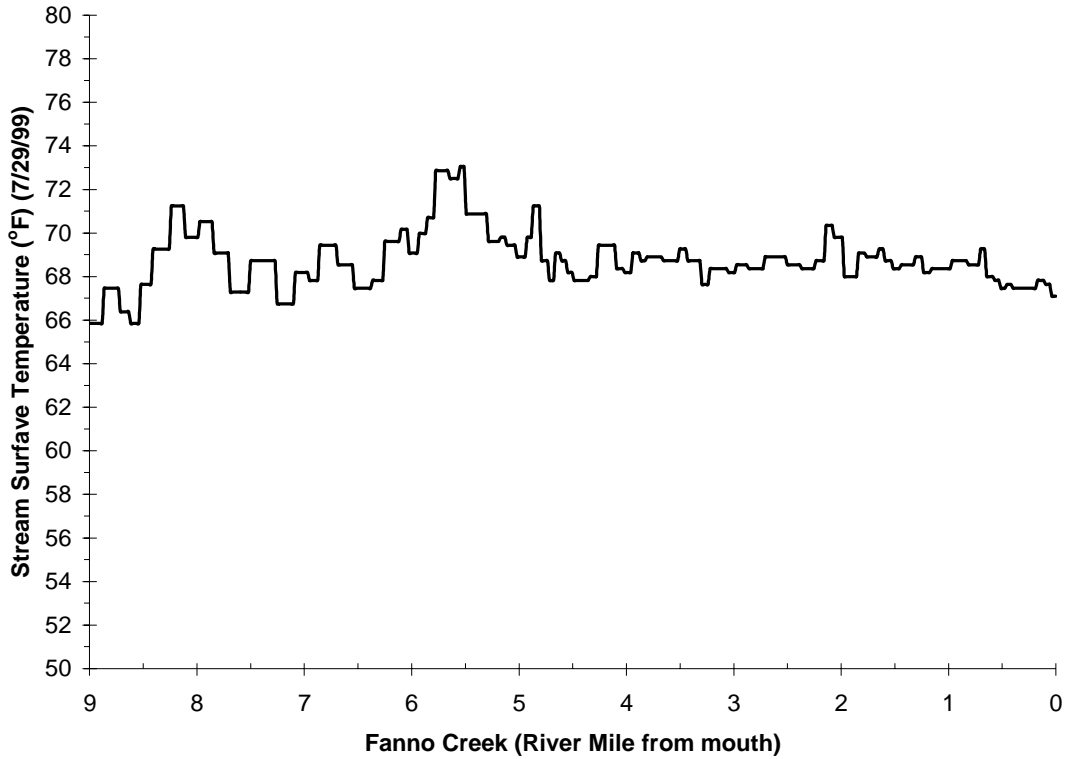**Figure A-178.** Measured FLIR temperature profile for Fanno Creek on July 29,1999.

Table A-28. FLIR Derived Water temperatures in the Fanno Creek (7/29/99)			
Temperature (°F)	Distance (Miles)	Percent of Total	Mode of Thermal Mortality
Less than 55.0	-	-	
55.0 to 59.5	-	-	
59.5 to 64.0	-	-	
64.0 to 68.5	4.0	44.9%	Sub-Lethal
68.5 to 73.0	4.6	51.0%	Limit
73.0 to 77.5	0.4	4.1%	
Greater than 77.5	-	-	Incipient Lethal Limit
Totals	9.0	100%	

The following selected FLIR images were observed in Fanno Creek on July 29, 1999. FLIR thermal imagery codes temperatures utilizing a Celsius temperature scale. Note that the 64°F is equal to a 17.8°C.

Image A-63 presents the temperature condition of Fanno Creek at the confluence with the Tualatin River. Median water temperature of the Tualatin River at the time of FLIR sampling was 20.5°C and Fanno Creek was 19.7°C. Large riparian vegetation stands can be easily observed in the video image.

Image A-64 provides a characteristic view for urban areas of Fanno Creek. Very little riparian vegetation is present at this location. As can be seen in this image, surface temperatures of the urban areas were well above 30°C.

Further upstream, **Image A-65** presents Fanno Creek at an urban region partially obscured by vegetation on the left side of the image. The images show typical urban features mixed with some riparian vegetation.

Image A-66 illustrates Fanno Creek in a typical residential area. Some of these areas contain very little shade producing riparian vegetation.

Image A-67 illustrates that Fanno Creek is in very close proximity to many industrial parking lots such as this one. Run-off from these impermeable surfaces enters directly into the stream. As can be seen in this image, surface temperatures of the urban areas were well above 30°C.

Image A-68 illustrates a "upper" reach of Fanno Creek as it traverses a golf course. Very little shade producing riparian vegetation can be observed in this image.

Image A-63. Surface temperature at the Confluence of Fanno Creek and the Tualatin River.[15]
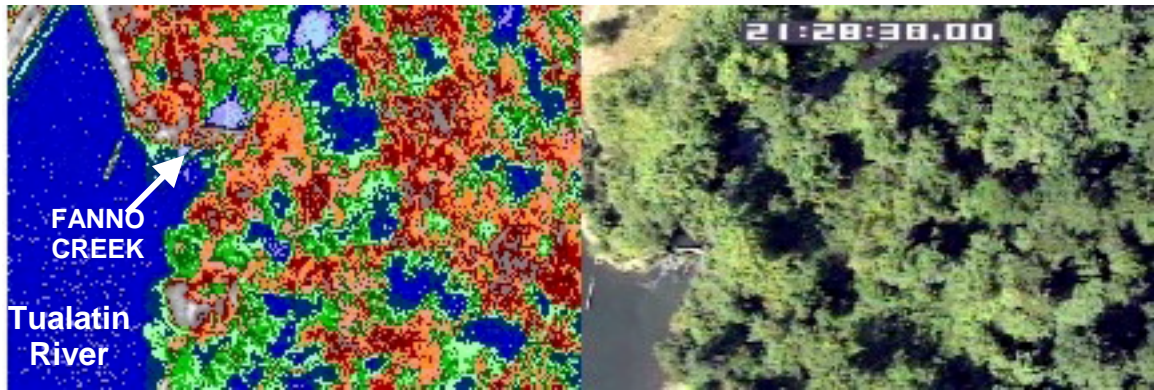

Image A-64. Fanno Creek at a typical urban section.

Image A-65. Fanno Creek at approximate River Mile 4.3.

FLIR Image Temperature Scale (°C)

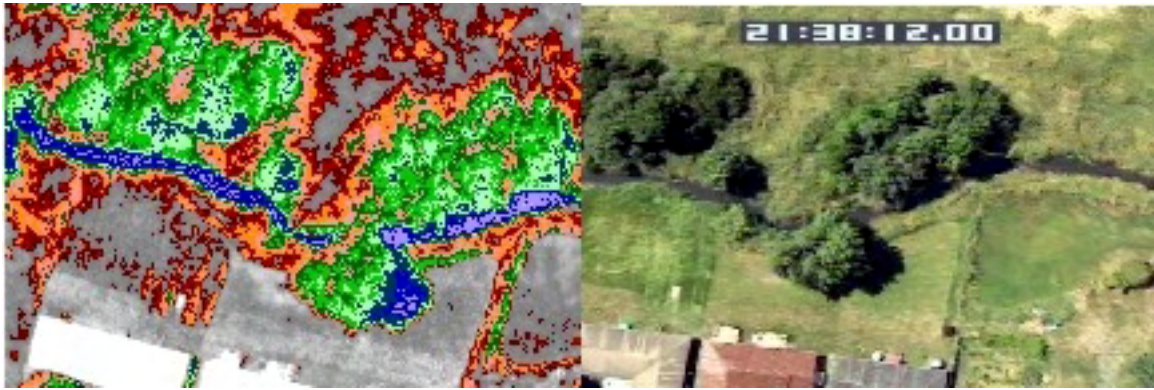**Image A-66.** Fanno Creek at a typical urban residential reach. [16]
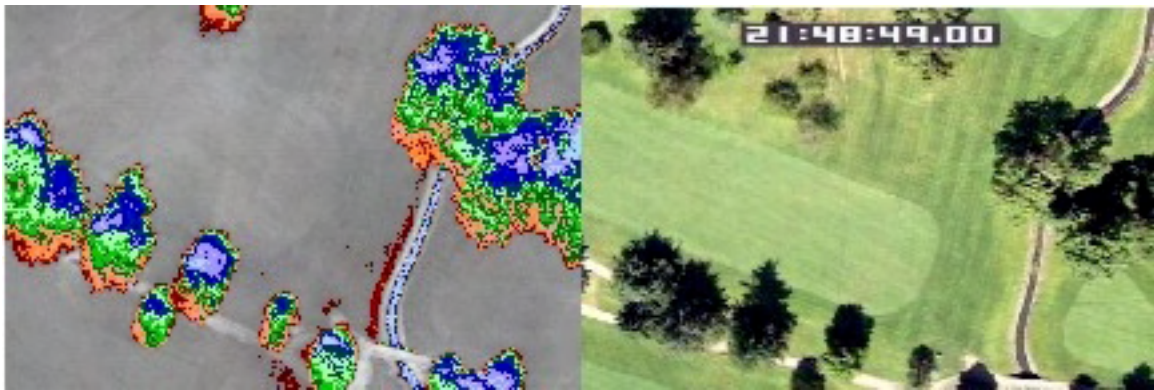

Image A-67. Fanno Creek in close proximity to industrial parking lots.

Image A-68. Fanno Creek as it travels through a golf course.

FLIR Image Temperature Scale (°C)

FANNO CREEK MODEL INPUT DATA

Fanno Creek was modeled from river mile 9.0 to the mouth. Model segment lengths were 100 feet in length. Model input data for each of the 100-foot model segments is graphically presented below. Data sources and methodology used to assemble the model input were presented earlier in this Appendix.

- Elevation and Gradient (**Figure A-179)**
- Aspect (**Figure A-180)**
- Near Stream Disturbance Zone Widths and Wetted Widths (**Figure A-181)**
- Vegetation Geometry (**Figure A-182)**
- Flow Volume (**Figure A-183)**
- Flow Velocity (**Figure A-184)**
- Water Column Depth (**Figure A-185)**

Figure A-179. Fanno Creek Elevation and Gradient at Each 100-foot Model Reach.
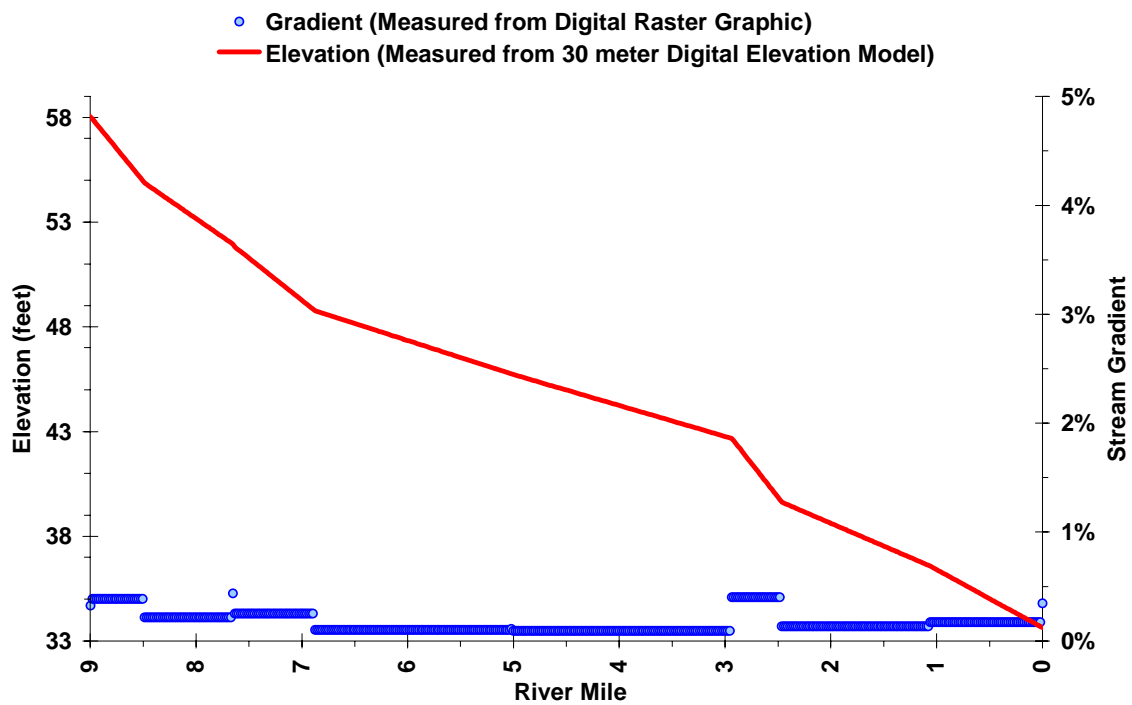
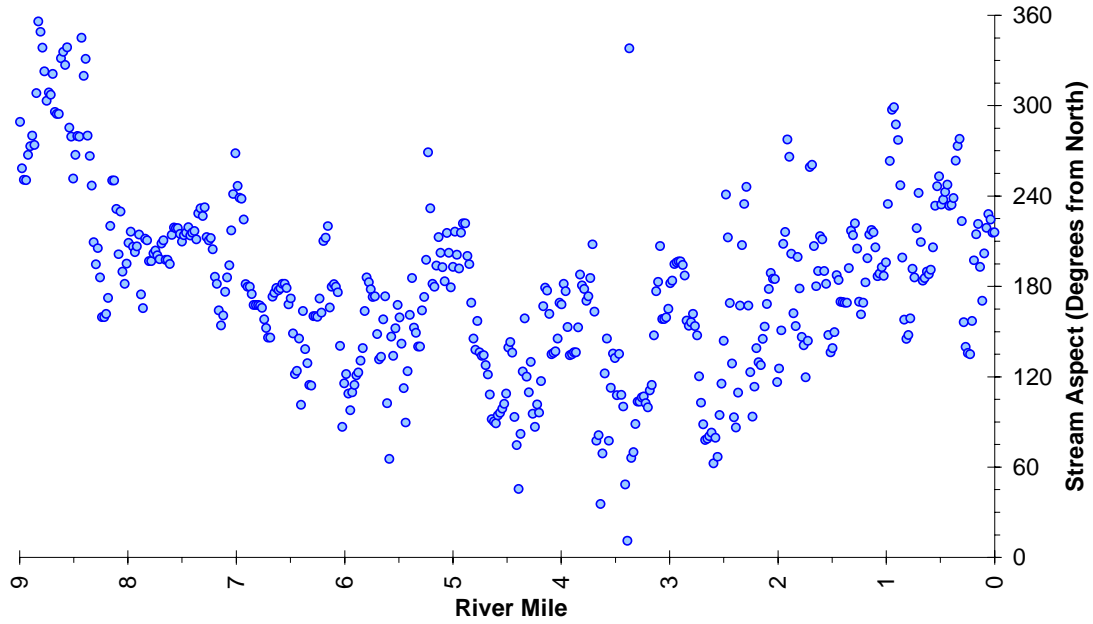**Figure A-180.** Fanno Creek Aspect at Each 100-foot Model Reach.

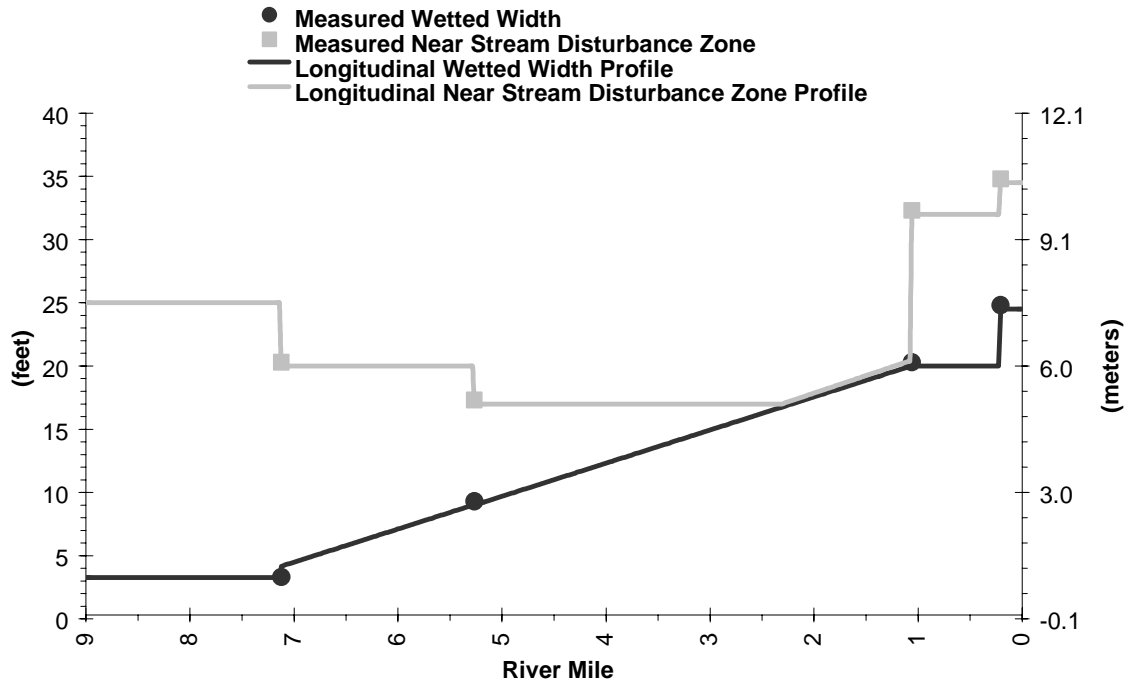**Figure A-181.** Fanno Creek NSDZ and Wetted Widths.

Figure A-182. Fanno Creek Topographic Shade at Each 100-foot Model Reach.
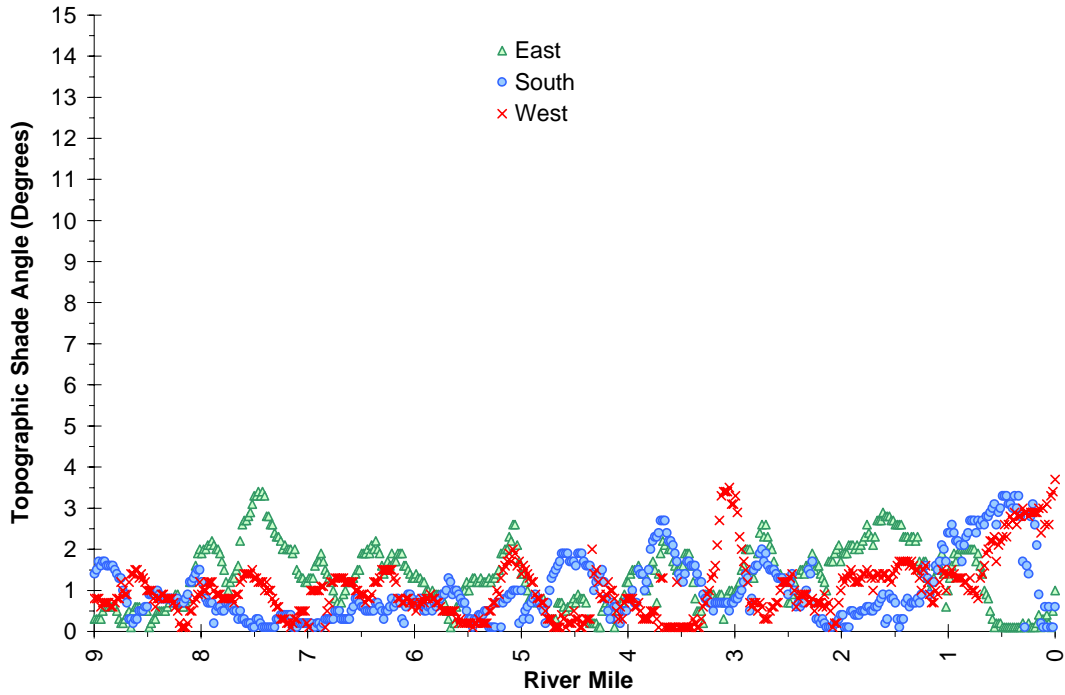

Figure A-183. Fanno Creek Existing Vegetation Heights and Buffer Widths at Each 100-foot Model Reach.
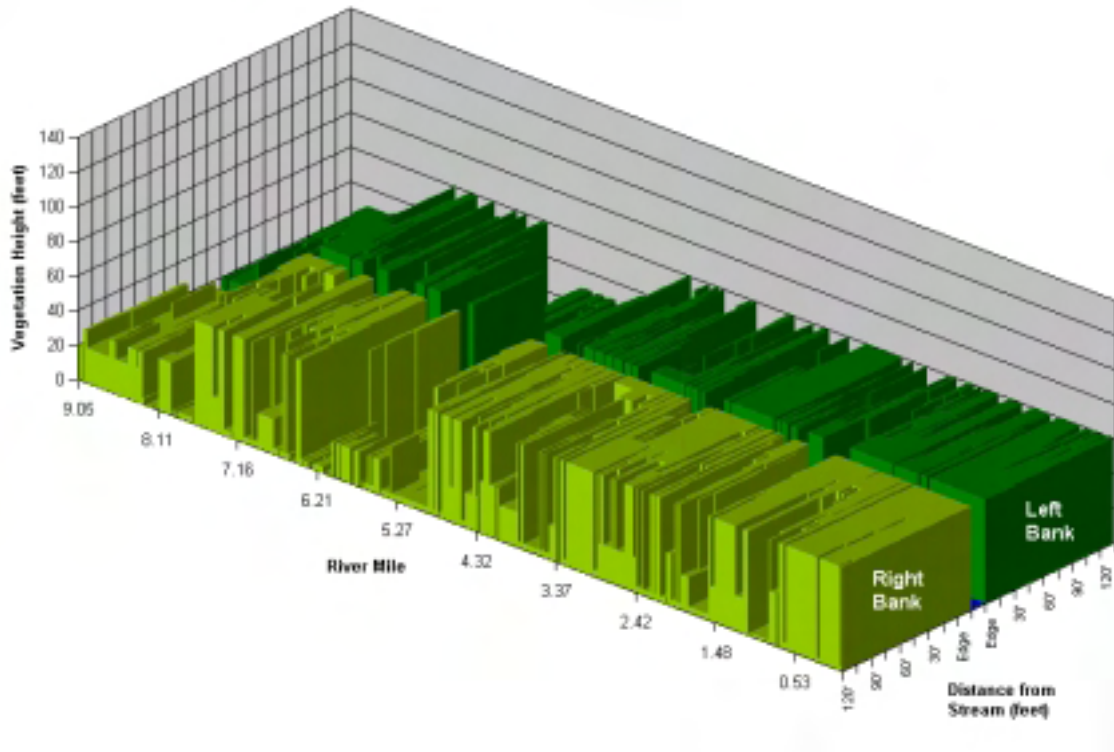
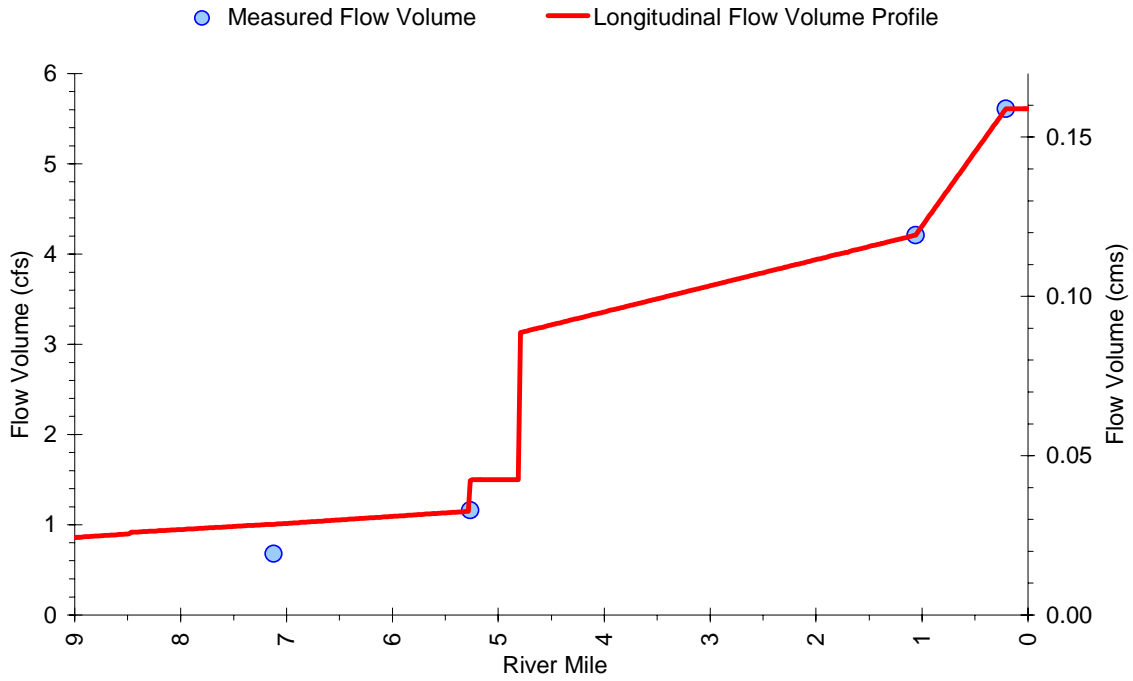**Figure A-184.** Fanno Creek Measured and Interpolated Longitudinal Flow Volume

Figure A-185. Fanno Creek Measured and Mannings Derived Longitudinal Flow Velocities.
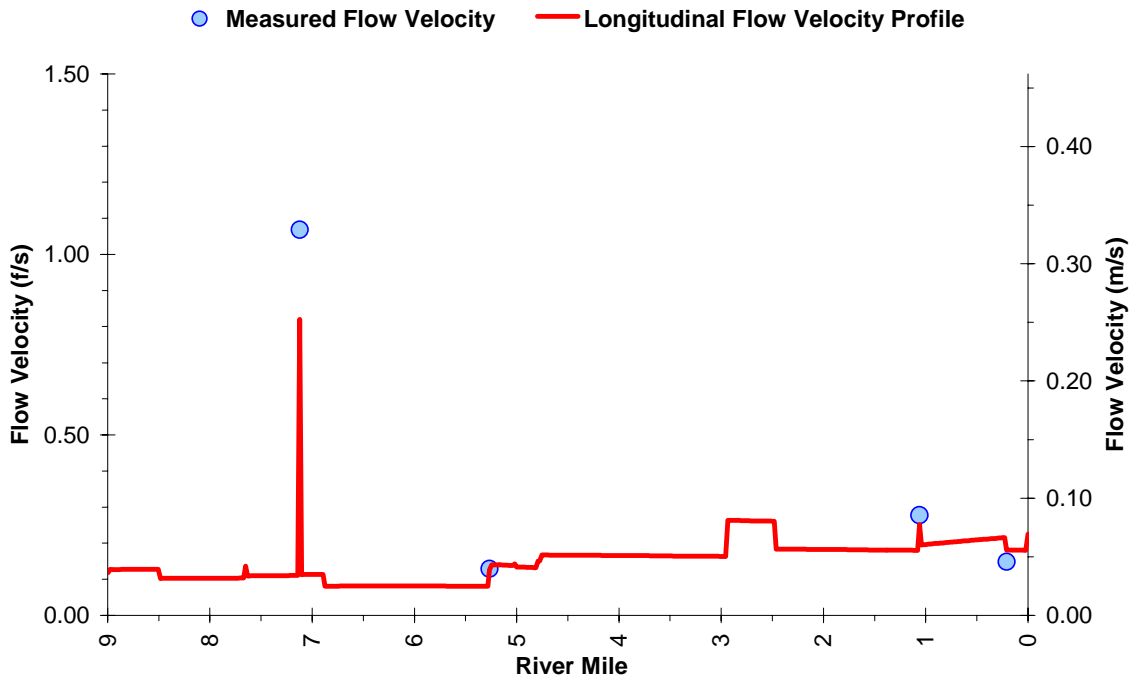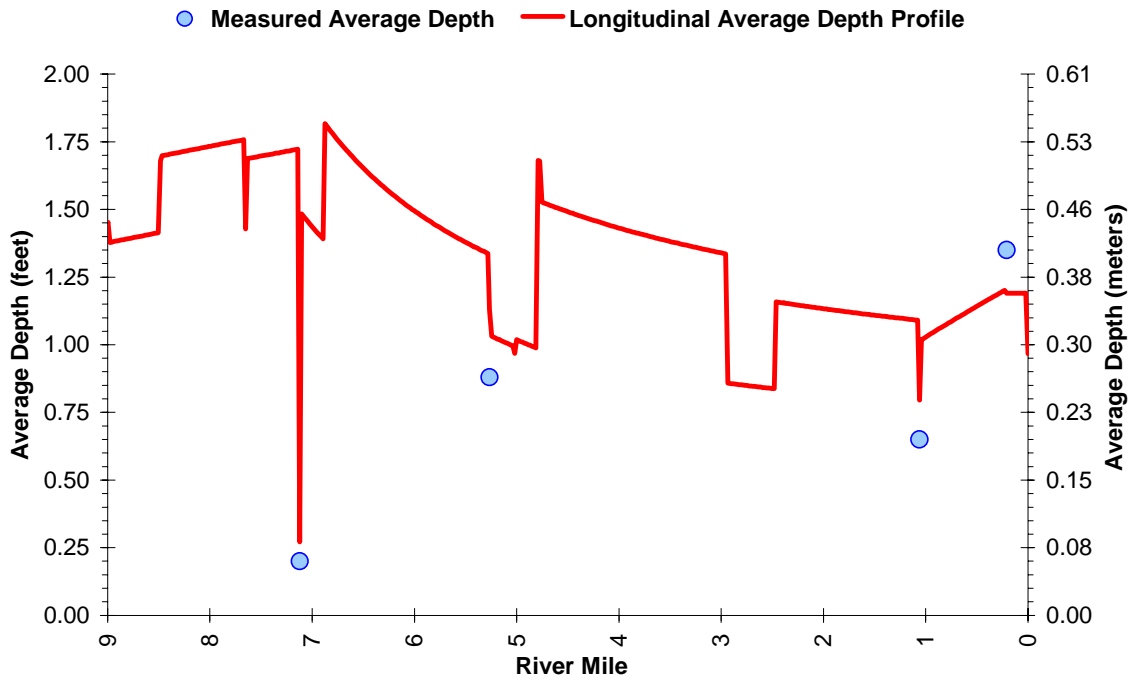
Figure A-186. Fanno Creek Measured and Mannings Derived Longitudinal Water Column Depths

FANNO CREEK MODEL RESULTS

This section presents temperature modeling results for Fanno Creek. Graphical and statistical validation of the calibrated Fanno Creek mainstem model are shown, in addition to temperature predictions for various scenarios. Recall that the modeled was calibrated with data collected on July 29, 1999 and thus is representative of critical stream temperature, stream flow, and climatic conditions. In other words, this modeling effort has captured the period when stream temperatures were near their peak. Spatial validation of the calibrated model is presented in **Figure A-187**. The solid line is the calibrated model temperature prediction at 3:00 PM on July 29, 1999 while the dots represent the FLIR-measured temperatures at that same time.

The standard error and average deviation for the spatial data calibration are:

$$Standard\ Error = 1.09^oC\ (1.97^oF)$$

$$Average\ Deviation = 0.13^oC\ (0.23^oF)$$

Figure A-187. Fanno Creek Observed and Predicted Spatial Temperature Data on July 29, 1999.
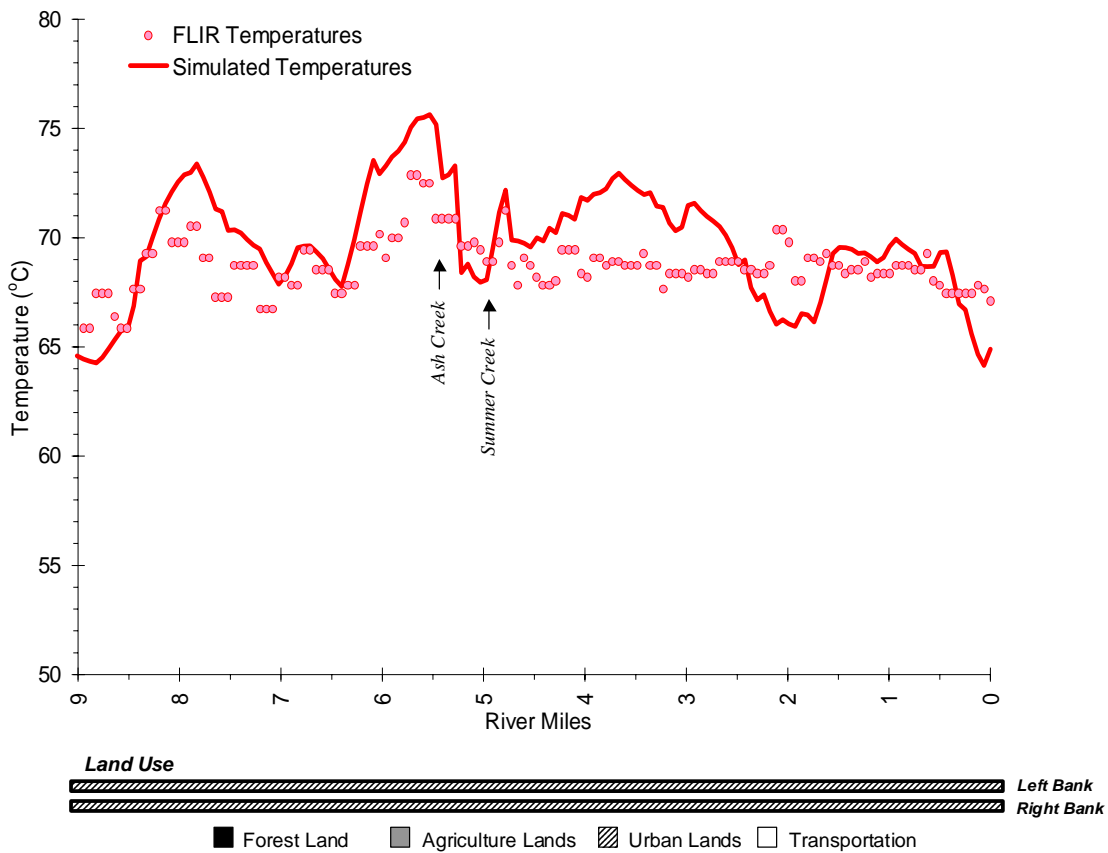
Observed and predicted hourly temperatures at four continuous temperature monitoring locations on Fanno Creek are presented in **Figure A-188**. Node 1 is the upper boundary condition and remains constant, therefore it was not graphed. Standard errors and average deviations are presented for each node. The mean standard error and mean average deviation for the continuous data are:

$$Mean\ Standard\ Error = 0.48^oC\ (0.86^oF)$$

$$Mean\ Average\ Deviation = 1.62^oC\ (2.92^oF)$$

Figure A-188.   Fanno Creek Model Continuous Data Validation

Loading Capacity - 40 CFR 130.2(f)

Loading Capacity is based on the condition that meets the ***no measurable surface water temperature increase resulting from anthropogenic activities***. This condition is termed ***System Potential*** and is achieved when (1) non-point source solar radiation loading reflects a riparian vegetation condition without human disturbance and (2) point source discharges cause no measurable increases in surface water temperatures.

Solar radiation loading was calculated using system potential riparian vegetation, at current channel and stream aspect conditions. A detailed description of potential vegetation conditions is presented in **Table A-8**. Current and System Potential solar loading for Fanno Creek are presented in **Figure A-189**. Solar radiation loading for Current Condition and System Potential condition is presented for every 100 meters of modeled stream length. As can be seen in **Figure A-189**, solar radiation loading at System Potential is much less than levels currently observed on Fanno Creek (i.e., Current Condition). Allowable point source heat loading at load capacity conditions are summarized below and described in detail in the main TMDL document.

Figure A-189. Fanno Creek Solar Radiation Load at System Potential and Current Conditions
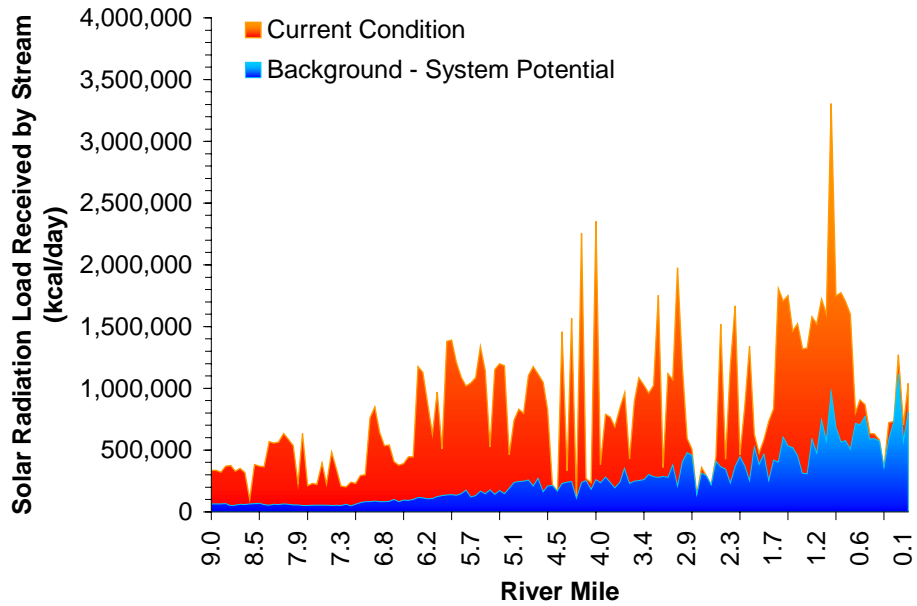
Allocations – 40 CFR 130.2(g) and 40 CFR 130.2(h)

Load Allocations (Non-Point Sources) - The **temperature standard** targets system potential (i.e. no measurable temperature increases from anthropogenic sources). To meet this requirement the system potential solar radiation heat load $(9.2 \cdot 10^6$ Kcal/day) is allocated to background nonpoint sources. Anthropogenic nonpoint sources are not given a heat load.

Wasteload Allocations (Point Sources) - Surface water discharges into receiving waters have been given a heat load based on the $0.25°F$ allowable increase in the mixing zone as specified in the temperature standard. Heat loads have been converted to allowable effluent temperatures as well. It should be noted that the wasteload allocation is the point source heat load and not the calculated maximum effluent temperatures. There are several options for meeting the allocated heat loads (i.e. passive effluent temperature reductions, changes in facility discharge operation, purchasing instream flows, pollutant trading, etc.).
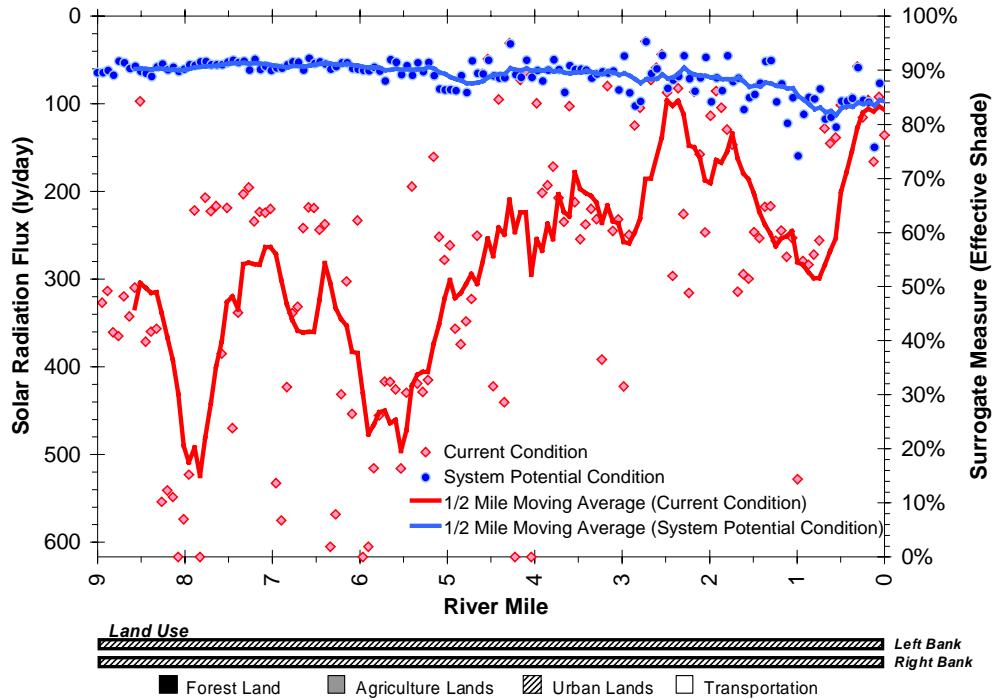
Temperature Allocation Summary **Non-Point Sources**	
Source	*Loading Allocation* *Allowable Nonpoint Source Solar Radiation Heat Load* *(kcal/day)*
Natural	$3.8 \cdot 10^7$ Kcal/day
Agriculture	$\varnothing$
Forestry	$\varnothing$
Urban	$\varnothing$
Future Sources	$\varnothing$

Point Sources - Allowable Point Source Effluent Source Heat Loading						
		Q_R	Q_{PS}	T_{PS}	Max T_P	H_{PS}	H_{WLA}
Facility Name	**Rec. Water**	Receiving Water 7Q10 Low Flow (cfs)	Facility Design Flow (cfs)	Point Source Effluent Temp. (°F)	Max Daily Site Potential River Temp. (°F)	Current Point Source Heat Loading on River (kcal/day)	Allowable Point Source Heat Loading in Zone of Dilution (kcal/day)
Williams	Fanno Cr. RM - 1.5	1.87	0.08	81.0	58.1	$2.6 \cdot 10^6$	$1.6 \cdot 10^5$
Willamette	Fanno Cr. RM - 9.0	0.10	0.04	72.0	60.5	$5.0 \cdot 10^5$	$8.5 \cdot 10^3$

Surrogate Measures – 40 CFR 130.2(I)

The solar radiation load (Kcal/day) at system potential condition was calculated by multiplying the stream surface area by the solar radiation flux (ly/day). Percent effective shade was used as a surrogate measure of the solar radiation flux calculated at system potential conditions (**Figure A-190)**.. The individual points in the figure represent the current and allocated conditions for every 100 meters. Accordingly, System Potential heat load condition along Fanno Creek translates into approximately 85% or greater effective shade throughout much of the system.

Figure A-190. Fanno Creek Surrogate Measure for Non Point Sources – *Effective Shade*

Water Quality Standard Attainment Analysis – CWA §303(D)(1)

Figure A-191 illustrates predicted Fanno Creek temperatures at 5:00 PM on July 29, 1999 with the following scenarios: 1) non-point sources at Load Allocations and point source discharges at current levels, and 2) non-point source at Load Allocation and point source discharges removed. Predicted temperatures in Fanno Creek are rather different at both Load Allocation scenarios. Point source discharge at current levels raise stream temperatures under the Loading Allocation. In Particular, the point source discharge into Ball Creek has a significant warming effect on Fanno Creek under the non-point source load allocation scenario.

Figure A-191. Fanno Creek Longitudinal Temperature Profile - Model Output – 1) Non-Point Source Load Allocation and Current Point Source Discharge, and 2) Non-Point Source Load Allocation and Remove Point Source Discharge – 5:00 PM July 29, 1999.
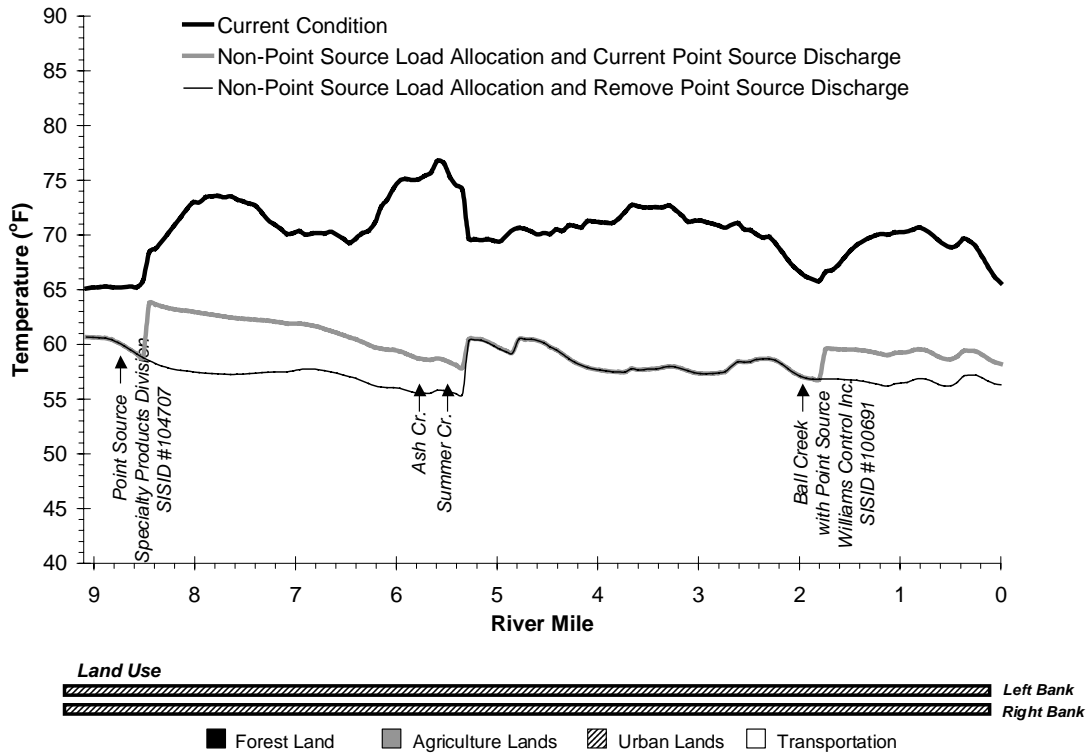
Two scenarios were run in which non-point sources were maintained at current conditions and point source discharge conditions were modified. **Figure A-192** displays predicted Fanno Creek temperatures at 5:00 PM on July 29, 1999 with the following scenarios: 1) non-point sources at Current Conditions and point source discharges removed; and 2) non-point sources at Current Conditions and point sources at Waste Load Allocations. As can be seen in **Figure A-192**, the general temperature profiles were similar between these scenarios and Current Conditions; however, effects downstream of the point sources can be observed.

As mentioned above, *System Potential* is achieved when (1) non-point source solar radiation loading reflects a riparian vegetation condition without human disturbance and (2) point source discharges cause no measurable increase in surface water temperature. Accordingly, **Figure A-193** presents predicted Fanno Creek temperatures at a Waste Load Allocation and Load Allocation scenario. **Figure A-194** illustrates that implementing Waste Load Allocations and Load Allocations will drastically reduce temperatures in Fanno Creek.

Figure A-192. Fanno Creek Longitudinal Temperature Profile - Model Output – 1) Non-Point Source Current Condition and Remove Point Source Discharge, and 2) Non-Point Source Current Condition and Point Source Waste Load Allocation – 5:00 PM July 29, 1999.

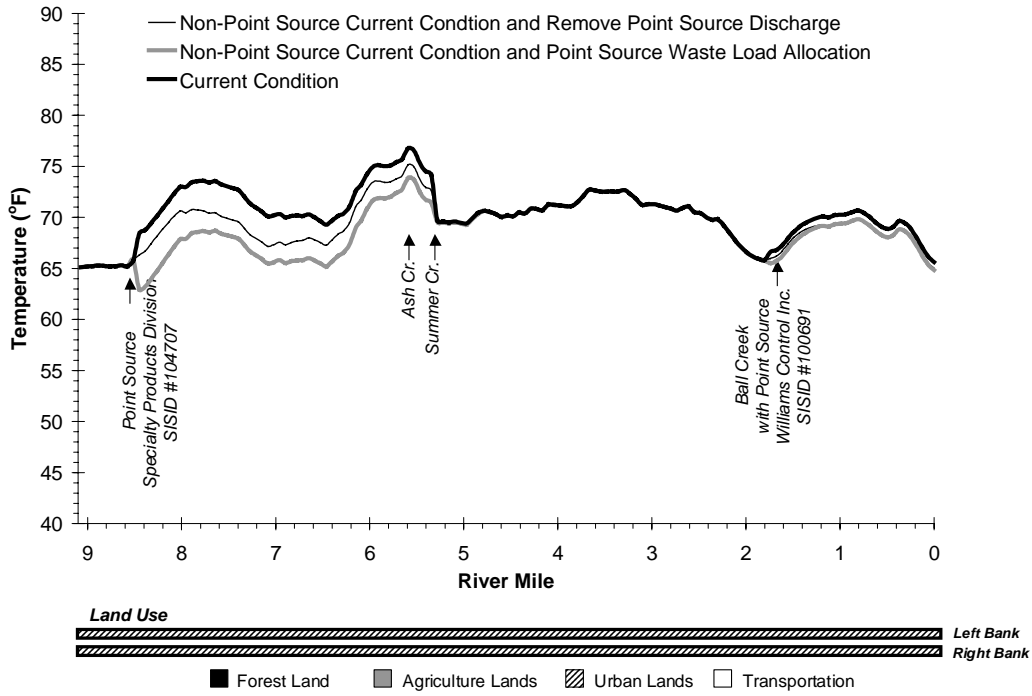**Figure A-193.** Fanno Creek Daily Temperature Range for Current Conditions Compared with Allocated Measures - July 29,1999.
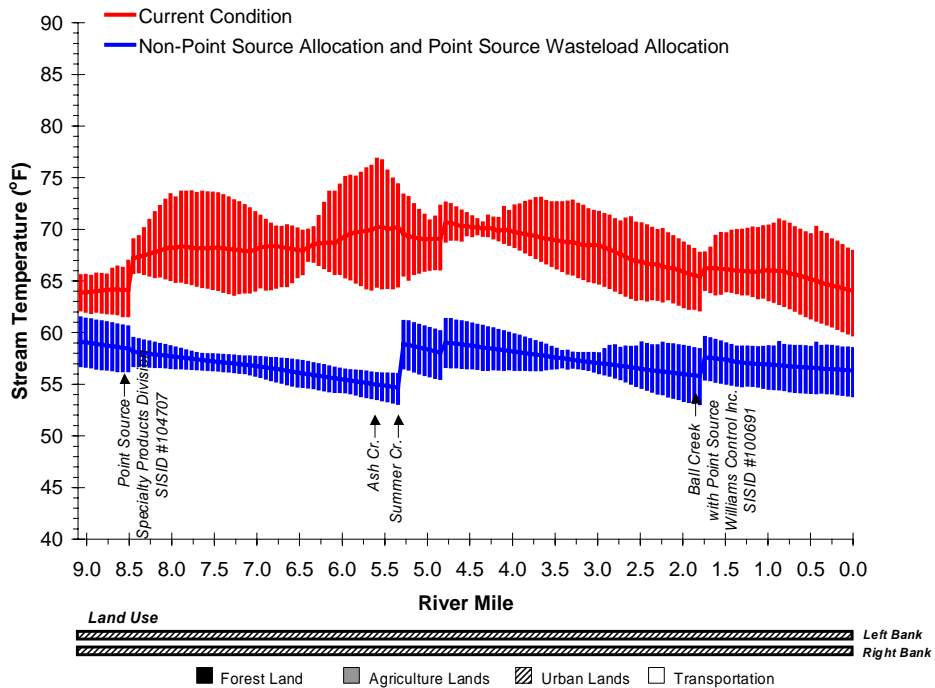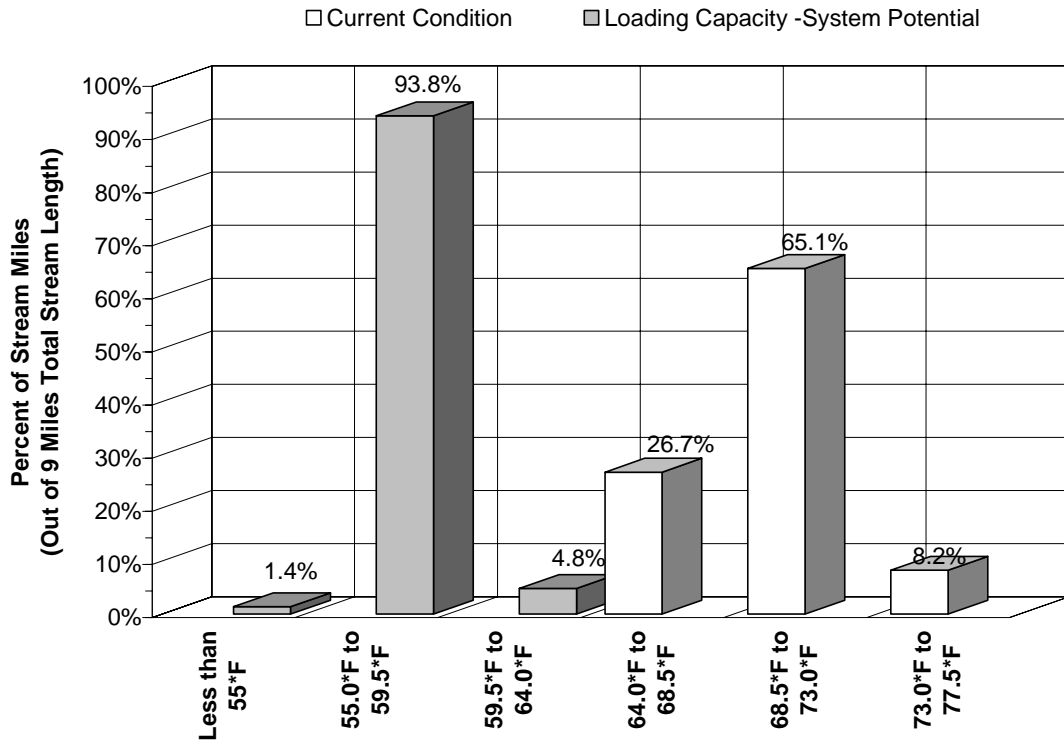
Figure A-194. Fanno Creek Current and Potential (Allocated) Temperature Distributions

This Page is Left Blank Intentionally

A-2: REFERENCES

Bell, M.C. 1986. Fisheries handbook of engineering requirements and biological criteria. Fish Passage Development and Evaluation Program, U. S. Army Corps of Engineers, North Pacific Division. Portland, Oregon, 290 pp.

Beschta, R.L, R.E. Bilby, G.W. Brown, L.B. Holtby, and T.D. Hofstra. 1987. Stream temperature and aquatic habitat: Fisheries and forestry interactions. Pp. 191-232. *In*: E.O. Salo and T.W. Cundy (eds), Streamside Management: Forestry and Fishery Interactions. University of Washington, Institute of Forest Resources, Contribution No. 57. 471 pp.

Beschta, R.L. and J. Weatherred. 1984. A computer model for predicting stream temperatures resulting from the management of streamside vegetation. USDA Forest Service. WSDG-AD-00009.

Beschta, R.L., S.J. O'Leary, R.E. Edwards, and K.D. Knoop. 1981. Sediment and Organic Matter Transport in Oregon Coast Range Streams. Water Resources Research Institute. OSU. WRRI-70.

Bowen, I.S. 1926. The ration of heat loss by convection and evaporation from any water surface. Physical Review. Series 2, Vol. 27:779-787.

Boyd, M.S. 1996. Heat Source: stream temperature prediction. Master's Thesis. Departments of Civil and Bioresource Engineering, Oregon State University, Corvallis, Oregon.

Brett, J.R. 1952. Temperature Tolerance in Young Pacific Salmon, Genus *Oncorhynchus. J. Fish. Res. Bd. Can.*, 9(6):265-323.

Breuner, N. 1998. *Gales Creek Watershed Assessment Project*. Prepared for the Tualatin River Watershed Council. Hillsboro, OR.

Brown, G.W. 1983. Chapter III, Water Temperature. Forestry and Water Quality. Oregon State University Bookstore. Pp. 47-57.

Brown, G.W. 1970. Predicting the effects of clearcutting on stream temperature. *Journal of Soil and Water Conservation.* 25:11-13.

Brown, G.W. 1969. Predicting temperatures of small streams. *Water Resour. Res.* 5(1):68-75.

Brown, L.C. and T.O. Barnwell. 1987. *The enhanced stream water quality models qual2e and qual2e-uncas: documentation and user manual.* U.S. Environmental Protection Agency, Athens, Georgia.

Brown & Caldwell, *et al*. 1998. *Fanno Creek Resource Management Plan.* Prepared for the City of Portland Environmental Services.

Brown & Caldwell, *et al*. 1999. *Beaverton Creek Watershed Management Plan.* Prepared for the Unified Sewerage Agency of Washington County.

Buan, C.M. 1995. *A changing mission: story of a pioneer church.* Washington County Historical Society. Beaverton, OR.

Bureau of Land Management (BLM), 1998. WODIP Guidebook: Western Oregon Digital Image Project. Oregon.

Cass, P.L. and R. Miner. 1993. *The historical Tualatin River subbasin.* Oregon Water Resources Research Institute, Oregon State University. Corvallis, OR.

Chen, D.Y. 1996. Hydrologic and water quality modeling for aquatic ecosystem protection and restoration in forest watersheds: a case study of stream temperature in the Upper Grande Ronde River, Oregon. Ph.D. Dissertation. University, of Georgia. Athens, Georgia.

Chow, V.T. 1959. *Open Channel Hydraulics.* New York: McGraw-Hill Co.

Everest F.H., R.L. Beschta, J.C. Scrivener, K.V. Koski, J.R. Sedell, and D.J. Cederholm. 1987. Fine Sediment and salmonid production a paradox. in *Streamside Management Forestry and Fishery Interactions.* Salo and Cundy Eds. College of Forest Resources. University of Washington, Seattle WA.

Fulton, A.E. 1995. *Banks, a darn good little town*. Washington County Historical Society. Beaverton, OR.

Halliday D. and R. Resnick. 1988. *Fundamentals of Physics.* 3rd Edition. John Wiley and Sons, New York. pp. 472-473.

Harbeck, G.E. and J.S. Meyers. 1970. Present day evaporation measurement techniques. J. Hydraulic Division. A.S.C.E., Prceed. Paper 7388.

Harvey, G.W. 1993. Technical review of sediment criteria. Idaho Department of Health and Welfare, Division of Environmental Quality. Boise, ID.

Hawksworth, J. 1999a. *Dairy-McKay Watershed Analysis*. Prepared for the U.S. Bureau of Land Management. Salem District Office.

Hawksworth, J. 1999b (in print). *Upper Tualatin-Scoggins Watershed Analysis*. Prepared for the U.S. Bureau of Land Management. Salem District Office.

Heath A.G. and G.M. Hughes, 1973. Cardiovascular and respiratory changes during heat stress in rainbow trout *(Salmo gairneri)*. *J. Exp. Biol.*, 59:323-338.

Hogan, J.W. 1970. Water temperature as a source of variation in specific activity of brain acetylcholinesterase of bluegills. *Bull. Environment. Contam. Toxicol.*, 5:347-353.

Hokanson, K.E.F., C.F. Kleiner and T.W. Thorslund. 1977. Effects of Constant Temperatures and Diel Temperature Fluctuations on Specific Growth and Mortality Rates and Yield of Juvenile Rainbow Trout, Salmo gairdneri. J. Fish. Res. Bd. Can., 34:639-648.

Holaday, S.A. 1992. Summertime water temperature trends in Steamboat Cr. Basin, Umpqua National Forest. Master's Thesis. Department of Forest Engineering, Oregon State University, Corvallis, Oregon.

Ibqal, M. 1983. An Introduction to Solar Radiation. Academic Press. New York. 213 pp.

Irving, J.S. and T.C. Bjornn. 1984. Effects of substrate size composition on survival of Kokanee salmon and cutthroat and rainbow trout embryos. Univ. of Idaho Coop. Fish. Res. Unit. Tech. Re., pp. 84-96. Moscow, ID.

Iwamoto R.N., E.O. Salo, M.A. Madej, R.L. McComas. 1978. Sediment and water quality: A review of the literature including a suggested approach for water quality criteria. EPA 910/9-78-048.

Jobson, H.E. and T.N. Keefer. 1979. Modeling highly transient flow, mass and heat transfer in the Chattahoochee River near Atlanta, Georgia. Geological Survey Professional Paper 1136. U.S. Gov. Printing Office, Washington D.C.

Kagan, J.S., R. Morgan, and K. Blakely. 1999. *Tualatin and Willow Creek Basin Assessment for Shrub Steppe, Grasslands, and Riparian Wildlife Habitats.* EPA Regional Geographic Initiative Draft Final Report.

Kagan, J. and S. Caicco. 1992. *Manual of Oregon Actual Vegetation*. Prepared for the Gap Analysis Program, U.S. Fish and Wildlife Service. Portland, OR.

KCM, Inc.. 1996. *Subbasin Strategies Plans for Upper Rock, Bronson and Willow Creeks.* Prepared for the Unified Sewerage Agency of Washington County.

Kurahashi & Associates, Inc.. 1997. *Fanno Creek Watershed Management Plan*. Prepared for the Unified Sewerage Agency of Washington County.

Li, H.W., G.L. Lamberti, T.N. Pearsons, C.K. Tait, J.L. Li, and J.C. Buckhouse. 1994. Cumulative effects of riparian disturbance along high desert trout streams of the John Day Basin, Oregon. *Am. Fish Soc.* 123:627-640.

McIntosh, B.A. 1995. Historical changes in stream habitats in the Columbia River Basin. PhD. Dissertation. Oregon State University. Oregon.

Newcombe C.P. and D.D. MacDonald. 1991. Effects of suspended sediment on aquatic ecosystems. North American Journal of Fishery Management. 11:72-82

Omernik, J.M. and Gallant, A.L., 1986. *Ecoregions of the Pacific Northwest*. EPA/600/3-86/033, United States Environmental Protection Agency, Corvallis, OR.

Oregon Coastal Salmon Restoration Initiative (CSRI). 1997. State Agency Measures.

Oregon Department of Environmental Quality. 1995. 1992-1994 Water Quality Standards Review. DO issue paper.

Pacific Habitat Services, Inc., 1998. *Urban Riparian Inventory & Assessment Guide*. Prepared for Oregon Division of State Lands, Salem, OR.

Park, C. 1993. SHADOW: stream temperature management program. User's Manual v. 2.3. USDA Forest Service. Pacific Northwest Region.

Parker, F.L. and P.A. Krenkel. 1969. Thermal pollution: status of the art. Rep. 3. Department of Environmental and Resource Engineering, Vanderbilt University, Nashville, TN.

Pater, David E. *et al*, **1998.** *Ecoregions of Western Washington and Oregon.* USGS\USEPA, Denver, CO.

Rishel, G.B., Lynch, J.A. and E.S. Corbett.. 1982. Seasonal stream temperature changes following forest harvesting. *J. Environ. Qual.* 11:112-116.

Sattterland, D.R. and P.W. Adams. 1992. *Wildland Watershed Managemet.* 2nd edition. John Wiley and Sons, Inc., New York.

Sellers, W.D. 1965. Physical Climatology. University of Chicago Press. Chicago, IL. 272 pp.

Shively, David D., 1993. *Landscape change in the Tualatin River subbasin following Euro-American settlement.* Oregon Water Resources Research Institute, Oregon State University. Corvallis, OR.

Sinokrot, B.A. and H.G. Stefan. 1993. Stream temperature dynamics: measurement and modeling. *Water Resour. Res.* 29(7):2299-2312.

Stowell, R.A., A. Espinosa, T.C. Bjornn, W.S. Platts, D.C. Burns, and J.S. Irving. 1983. A guide for predicting salmonid response to sediment yields in Idaho batholiths watersheds. Unpubl. Rept. UDS-FS.

Tappel, P.D. 1981. A new method of relating spawning gravel size composition to salmonid embryo survival. MS Thesis, Univ. of Idaho, Moscow, ID.

Tappel, P.D. and T.C. Bjornn. 1993. A new method of relating size of spawning gravel to salmonid embryo survival. *N. Am. Journal Fish Mgmt.* 3:123-135.

Taylor, George H., 1993. Normal Annual Precipitation, State of Oregon, Period 1961-1990. Map. Oregon Climate Service, 326 Strand Ag. Hall, Oregon State University, Corvallis, Oregon.

Torgersen, C.E., D.M. Price, H.W. Li, and B.A. McIntosh. 1995. Thermal refugia and chinook salmon habitat in Oregon: Applications of airborne thermal videography. Proceedings of the 15th Biennial Workshop on Color Photography and Videography in Resource Assessment, Terre Haute, Indiana. May, 1995. American Society for Photogrammetry and Remote Sensing.

U.S. Environmental Protection Agency. 1998. Report of the Federal Advisory Committee on the Total Maximum Daily Load Program. EPA 100-R-98-006.

U.S. Environmental Protection Agency, 1986. Quality Criteria for Water, USEPA Publications.

US Geological Survey, 1999. Modeling discharge, temperature and water quality in the Tualatin River, Oregon. Water-Supply Paper 2465-B. US Geological Survey, US Department of Interior, Reston, VA.

US Geological Survey, 1997. Relations of the Tualatin River water temperatures to natural and human-caused factors. Water-Resources Investigations Report 97-4071. US Geological Survey, US Department of Interior, Reston, VA.

US Geological Survey, 1989. Hydrological unit map, State of Oregon. US Geological Survey, US Department of Interior, Reston, VA.

Waters, T.F. 1995. Sediment in streams: sources, biological effects and control. American Fisheries Society Monograph 7.

Wetzel, G.R. 1983. Limnology. Saunders College Publishing. Fort Worth.

Whitney, S., 1985. *Western Forests.* National Audubon Society Nature Guides, Chanticleer Press, Inc., New York.

Wunderlich, T.E. 1972. Heat and mass transfer between a water surface and the atmosphere. Water Resources Research Laboratory, Tennessee Valley Authority. Report No. 14, Norris Tennessee. Pp 4.20.